

TRANSPORTATION RESEARCH
RECORD

No. 1309

Soils, Geology, and Foundations

Geotechnical Engineering
1991

A peer-reviewed publication of the Transportation Research Board

TRANSPORTATION RESEARCH BOARD
NATIONAL RESEARCH COUNCIL
WASHINGTON, D.C. 1991

Transportation Research Record 1309

Price: \$21.00

Subscriber Category

IIIA soils, geology, and foundations

TRB Publications Staff

Director of Publications: Nancy A. Ackerman

Senior Editor: Naomi C. Kassabian

Associate Editor: Alison G. Tobias

Assistant Editors: Luanne Crayton, Norman Solomon

Graphics Coordinator: Diane L. Ross

Production Coordinator: Karen S. Waugh

Office Manager: Phyllis D. Barber

Production Assistant: Betty L. Hawkins

Printed in the United States of America

Library of Congress Cataloging-in-Publication Data

National Research Council. Transportation Research Board.

Geotechnical engineering, 1991.

p. cm—(Transportation research record, ISSN 0361-1981 ; no. 1309)

Papers presented at the 70th Annual Meeting of the Transportation Research Board, held in Washington, D.C., 1991. ISBN 0-309-05118-5

1. Soils—Testing. 2. Roads—Subgrades—Testing.

3. Engineering geology. I. National Research Council (U.S.). Transportation Research Board. Meeting (70th : 1991 : Washington, D.C.) II. Series: Transportation research record ; 1309.

TE7.H5 no. 1309

[TE208]

388 s—dc20

[625.7'32]

91-35710

CIP

Sponsorship of Transportation Research Record 1309

GROUP 2—DESIGN AND CONSTRUCTION OF TRANSPORTATION FACILITIES

Chairman: Raymond A. Forsyth, Sacramento, California

Soil Mechanics Section

Chairman: Michael G. Katona, Tyndall AFB

Committee on Soils and Rock Instrumentation

Chairman: John L. Walkinshaw, Federal Highway Administration, U.S. Department of Transportation

Loren R. Anderson, Harold E. Beeston, Joseph A. Caliendo, Barry R. Christopher, Brian J. Dawes, Charles N. Easton, John B. Gilmore, Gordon E. Green, William H. Hansmire, Neil F. Hawks, John L. Henkes III, Kenneth A. Jackura, Richard H. Ledbetter, P. Erik Mikkelsen, Dewayne L. Misterek, Soheil Nazarian, Gary W. Rhodes, A. J. Simmonds, Anwar E. Z. Wissa, Duncan C. Wyllie

Committee on Transportation Earthworks

Chairman: Richard P. Long, University of Connecticut

Loren R. Anderson, Thomas A. Bellatty, Jerome A. Dimaggio, Raymond L. Gemme, Robert D. Holtz, J. M. Hoover, Ilan Juran, James E. Kelly, Philip C. Lambe, Richard E. Landau, Robert M. Leary, C. William Lovell, David P. McKittrick, Victor A. Modeer, K. Jeff Nelson, Walter C. Waidelich, David E. Weatherby

Geology and Properties of Earth Materials Section

Chairman: Robert D. Holtz, University of Washington

Committee on Soil and Rock Properties

Chairman: Mehmet T. Tumay, National Science Foundation
Robert C. Bachus, S. S. Bandy, Roy H. Borden, Timothy D. Bowen, William H. Hight, Robert D. Holtz, Richard H. Howe, An-Bin Huang, Steven L. Kramer, Rodney W. Lentz, C. William Lovell, Kenneth L. McManis, Priscilla P. Nelson, Norman I. Norrish, Sibel Pamukcu, Gerald P. Raymond, James J. Schnabel, Kaare Senneset, Robert M. Smith, J. Allan Tice, Recep Yilmaz

G. P. Jayaprakash, Transportation Research Board staff

Sponsorship is indicated by a footnote at the end of each paper. The organizational units, officers, and members are as of December 31, 1990.

Transportation Research Record 1309

Contents

Foreword	v
<hr/>	
Inexpensive Automatic Control System for Soils Testing <i>N. Sivakugan, J. L. Chameau, R. D. Holtz, and A. B. Huang</i>	1
<hr/>	
Use of Voice-Recognition Systems for Atterberg Limit Tests <i>Thomas L. Brandon and Robert A. Stadler</i>	5
<hr/>	
Innovations in Hydraulic-Conductivity Measurements <i>Harold W. Olsen, James D. Gill, Arthur T. Willden, and Karl R. Nelson</i>	9
<hr/>	
Measurement of Shear and Compression Waves During Triaxial Testing <i>Kenneth C. Baldwin, Pedro de Alba, Adam Jones, and Ismail Menguc</i>	18
<hr/>	
Finite Element Analysis of Partially Saturated Seepage Through Compacted Fills <i>Timothy D. Stark and William G. Bixby</i>	25
<hr/>	
Broadening the Specification of Granular Fills <i>M. D. Bolton, R. J. Fragaszy, and D. M. Lee</i>	35
<hr/>	
Application of Continuous Dynamic Compaction Control for Earthworks in Railroad Construction <i>Aris A. Samaras, Rüdiger Lamm, and Joseph Treiterer</i>	42
<hr/>	
Decision Support System for Evaluation and Treatment of Earth Slope Instability <i>Dimitri A. Griovas and John C. Reagan</i>	47
<hr/>	

Correlating Resilient Moduli from Pressuremeter Tests to Laboratory California Bearing Ratio Tests	56
<i>Paul J. Cosentino and Yangting Chen</i>	
Laboratory Correlation Study of Near-Surface Response Parameters	66
<i>David C. Kraft, Raymond K. Moore, and J. Dean Grob</i>	
Prototype Geotechnical Information System	71
<i>Reda M. Bakeer, Tarik Hadj-Hamou, and John L. Niklaus</i>	
Seismic Spectra for Highway Bridges in Washington State	84
<i>George Tsiatas, Karen Kornher, and Carlton Ho</i>	

Foreword

The current decade is bringing many changes and innovations related to all aspects of transportation. The 12 papers included in this Record provide a glimpse of technologies that are on the horizon in geotechnical engineering. The range of topics covered is broad; papers are arranged in three groups.

The first group of four papers is on innovations in geotechnical laboratory measurements. Sivakugan et al. describe an automatic control system comprised of a microcomputer, an analog-digital conversion board, an output relay board, a parallel digital interface, and solenoid valves. The system may be used to control soil testing equipment. Brandon and Stadler used a voice-activated system for acquisition of soil test data as an alternative to keyboard input in a laboratory environment. Olsen et al. report on a new method for measurement of hydraulic conductivity of stress-controlled specimens and a modification of the method to obtain hydraulic conductivity versus effective stress data. Baldwin et al. describe a technique for measurement of shear and compression wave parameters of soils to determine their liquefaction resistance.

The second group of four papers is related to earthworks and their construction. Stark and Bixby report on the use of a microcomputer program to analyze seepage through compacted fills to determine the rate at which a fill becomes fully wetted and undergoes expansion and or hydrocompression. Bolton et al. suggest a flexible specification for granular soils used in fills to include gap-graded and friable material. Samaras et al. report on the results of field implementation of a continuous dynamic compaction control method on a section of earthworks. Grivas and Reagan describe a personal computer-based prototype system for the evaluation and treatment of slope instability.

Two of the four papers included in the third group are on correlation of soil properties determined using different equipment or techniques in the laboratory or field. Cosentino and Chen compared resilient moduli determined using a pressuremeter test with California Bearing Ratio test results, whereas Kraft et al. compared the results obtained using a Clegg Impact Soil Tester and a prototype automated cone penetrometer with California Bearing Ratio test results. Bakeer et al. describe a geotechnical information system that integrates a geotechnical data base of an area into a geographical information system. The paper by Tsiatas et al. is on a base spectrum and soil amplification spectra developed for use in the design of highway bridges.

Inexpensive Automatic Control System for Soils Testing

N. SIVAKUGAN, J. L. CHAMEAU, R. D. HOLTZ, AND A. B. HUANG

An inexpensive automatic control system for soils testing is described. The system comprises a microcomputer, an analog-digital conversion board, an output relay board, a parallel digital interface, and solenoid valves. Minimal programming is involved to set up the system, and the required software is ordinarily provided by the manufacturer at no cost. The system has been successfully used in K_o consolidation and strain-controlled loading of cubical clay specimens in a cuboidal shear device. The system may also be used to control other soil testing equipment.

The advent of microcomputers has had a tremendous impact on laboratory testing of soils. Using microcomputers and other electronic components, it is relatively easy to develop specialized interactive data acquisition and control systems for automation of laboratory tests. The rising costs of wages and the declining cost of microcomputers and other electronic components have resulted in rapid advances in such systems (1-6).

Microcomputers and automatic data acquisition systems have become essential to many laboratory experiments. They reduce operator time significantly because the entire book-keeping (i.e., data recording process) is left to the microcomputer. When several readings are to be taken simultaneously or when high-speed recording is required, such data acquisition systems are almost a necessity. If any feedback or corrective action is required while processing the data, some form of servo-control is essential.

In this paper, an inexpensive but efficient servo-control system using solenoid valves is described. The system has been used successfully for cuboidal shear testing (7,8), and it could as well be used with other testing devices.

SOLENOID VALVES FOR SERVO-CONTROL

Solenoid valves are opened or closed by energizing or de-energizing (or vice versa) the magnetic coil inside the valve assembly. This moves a plunger in the middle of the magnetic coil. Solenoid valves can be either AC or DC operated, two way or three way, and normally open (*N/O*) or normally closed (*N/C*). For example, a two-way, normally open, AC-operated solenoid valve remains open when deenergized. A 115 V AC signal would energize the coil and close the valve.

The schematic diagram of a generic servo-control system is shown in Figure 1. This arrangement may be incorporated with little modification into any testing device such as an oedometer, triaxial equipment, or any other specialized testing apparatus. The solenoid valves can be opened or closed on command by the control system, which consists of a microcomputer, a relay output board, and a parallel input/output (I/O) interface board.

In the example in Figure 1, P_1 , P_2 , and P_3 are the pressures at the pressure source, the controlled device, and the exhaust, respectively. Initially, the *N/O* valve is energized, and the *N/C* valve is deenergized, that is, both valves are closed. The range of values that P_2 will take during the test is known, and P_1 and P_2 are set such that $P_1 > P_2 > P_3$ for the entire test. P_1 and P_3 remain constants and require no adjustment. A momentary deenergizing of the *N/O* valve or energizing of the *N/C* valve would accordingly increase or decrease P_2 . After every adjustment of P_2 , measurements and computations are made, followed by corrective action, if required. This process can be repeated until the desired value of P_2 is reached.

In the system developed at Purdue University, the solenoid valves (two-way, *N/O*, B90A303R; two-way, *N/C*, B90A360R; Spangler Valve Company) are operated by a 24-channel, double-pole-double-throw relay output accessory board (Model ERB-24, MetraByte Corporation). Each relay contains two *N/O* and *N/C* contacts for controlling up to 3 A loads at 120 V AC excitation. The ERB-24 is operated by a 24-bit, parallel digital I/O interface (Model PI012, MetraByte Corporation), which occupies an expansion slot of a microcomputer [IBM personal computer (PC)]. The PI012 is driven by programs written in BASIC. After processing the data (measurements of pressure, displacement, etc.) and making the appropriate decisions, the microprocessor sends instructions to the PI012 interface card, which are passed to the ERB-24 relay card down the line. Then, the relevant relays are activated to perform the desired adjustments.

An eight-channel A/D convertor (Model DASH-8, MetraByte Corporation) was used for data acquisition. For every measurement of pressure or displacement, 100 samples were taken, and the arithmetic average was computed and used. The frequency of measurement depends on the number of samples, number of channels, computations required in each cycle of measurement, efficiency of programming, and the programming language used.

Subroutines written in ASSEMBLY language that interact between the PC and computer boards were provided by the manufacturer at no extra charge. The actual data logging and servo-control programs, which communicate with the

N. Sivakugan, College of Engineering, Sultan Qaboos University, Muscat, Sultanate of Oman. J. L. Chameau, School of Civil Engineering, Purdue University, West Lafayette, Ind. 47907. R. D. Holtz, Dept. of Civil Engineering, University of Washington, Seattle, Wash. 98195. A. B. Huang, Dept. of Civil and Environmental Engineering, Clarkson University, Potsdam, N.Y. 13676.

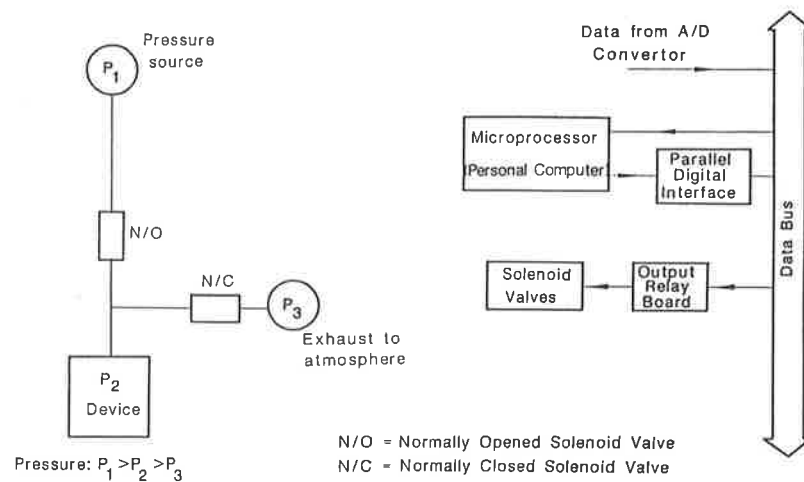


FIGURE 1 Schematic diagram of a generic servo-control system.

computer boards by calling the ASSEMBLY subroutines, can be written in BASIC or any other high-level compilers (e.g., FORTRAN or C). Sample basic programs that encompass a wide variety of applications were also given by the manufacturer. Thus, the actual programming is minimal because it normally involves modifying an existing program to fit a particular application. In addition, commercial data logging software (e.g., DADiSP, LABTECH NOTEBOOK, and ASYSTANT) is also compatible with the system described herein. All such software is menu-driven, which completely eliminates the need for programming. The programs are, however, copyrighted and usually cost more than \$1,000.00.

COST

The two-way *N/O* and *N/C* solenoid valves were priced at \$30.80 and \$24.60, respectively. The relay output accessory board and the interface board were bought for \$97.00 and \$395.00, respectively. A complete IBM-compatible micro-

computer system, which can also be used for other purposes, can be purchased for less than \$1,000.00.

APPLICATIONS

Cuboidal Shear Device

The servo-control device described above, with an automatic data acquisition system, has been successfully employed with a cuboidal shear device built at Purdue. The system is very useful for performing K_o consolidation and strain-controlled loading of cuboidal specimens; predefined stress paths (e.g., a pressuremeter stress path) can also be imposed on a specimen. All can be accomplished without operator assistance during the test (7,8).

The schematic diagram of the servo-control system for the cuboidal shear device shown in Figure 2 is derived from the generic servo system of Figure 1. In the cuboidal shear device,

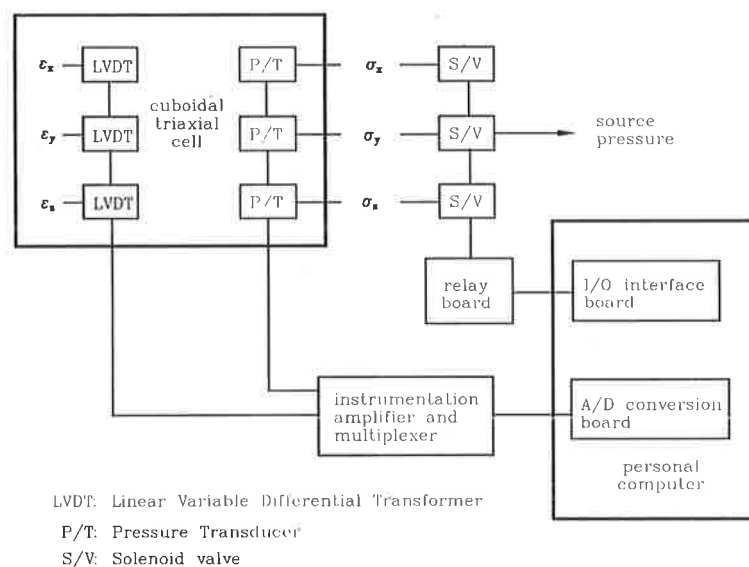


FIGURE 2 Schematic diagram of the servo-control system for the cuboidal shear device.

a 102 mm cubical specimen is compressed by air applied to 6 membranes, 1 on each face of the specimen. The pressure line in each of the three directions is connected to a pair of *N/O* and *N/C* valves (Figure 2). By energizing or deenergizing the appropriate valves, the three principal stresses (σ_x , σ_y , and σ_z) can be regulated to follow the desired stress path. K_o consolidation has been performed with the lateral strain controlled to within ± 0.025 percent. In maintaining essentially zero lateral strain, the two horizontal principal stresses were adjusted repeatedly by opening or closing the solenoid valves while the vertical principal stress was maintained constant. Each cycle of the servo-controlled K_o consolidation consists of the following operations:

- Measure 8 channels of displacements and 4 channels of pressures, each sampled 100 times;
- Display the readings on the monitor and record on the diskette;
- Open/close the solenoid valves; and
- Perform some computations.

Figure 3 shows the flow chart for servo-controlled consolidation. Even with all these operations, a cycle of measurement, calculation, and adjustment takes only 30 sec.

The strain-controlled loading has been performed within ± 5 percent of the specified strain rate. Strain rates were computed continuously with adjustments in pressure after each

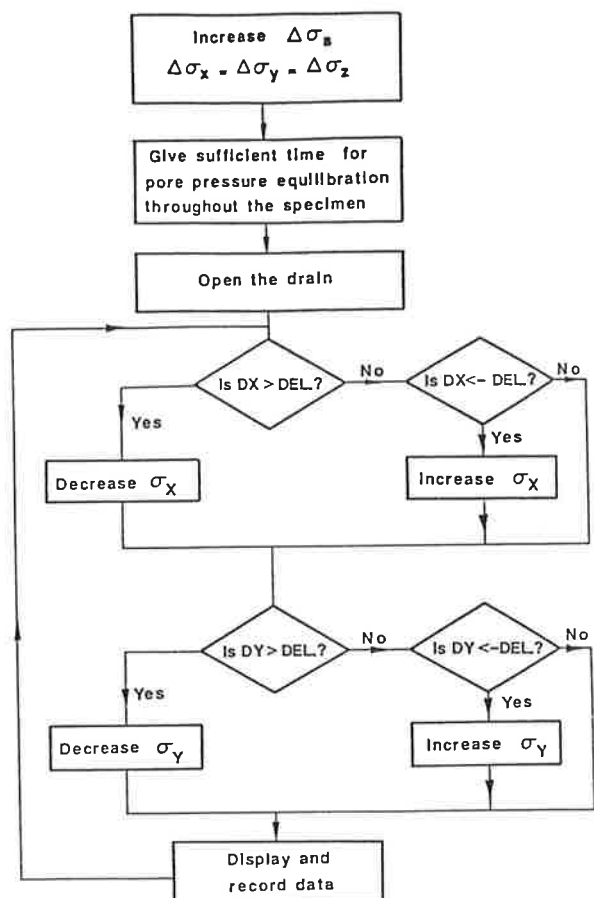


FIGURE 3 Flow chart for servo-controlled K_o consolidation.

measurement. Experimental results obtained using this servo-control system are given elsewhere by Sivakugan et al. (8).

Other Applications

Triaxial Testing

An ideal servo-controlled triaxial apparatus should allow for the following:

- Stress- and strain-controlled loading,
- Drained or undrained loading,
- Anisotropic consolidation and swelling,
- A pre-defined stress path, and
- Automatic data acquisition.

Coatsworth (1) described a computer-controlled triaxial device capable of data acquisition and control. The control was achieved by digital pressure/volume transducers interfaced to the microcomputer. Other possibilities for control include stepper motors, or screw jacks driven by a motor interfaced to a microcomputer. As an alternative, the servo system illustrated in Figure 1 may also be used to achieve all the objectives listed above. For example, K_o consolidation or swelling can be performed in the conventional triaxial cell by adjusting the axial load and the cell pressure.

Oedometer Testing

The use of a microcomputer for data acquisition and control in oedometer testing has been described by Armour and Drnevich (2), Sandbaekken et al. (5), and von Fay et al. (6). The servo system described above can with minor modifications be incorporated to the oedometer to perform conventional stress-controlled tests, constant rate of strain tests, and the like. In a constant rate of strain test, the mechanism would be similar to the strain-controlled loading performed in the cuboidal shear device. In the stress-controlled oedometer tests, the system can be programmed to add the subsequent stress increment at the appropriate time.

CONCLUSIONS

A simple and inexpensive servo-control system using solenoid valves was described. This system can be incorporated to control and at the same time acquire and record test data for most routine and research laboratory soils testing equipment. The efficiency of the system has been evaluated by a series of tests performed with a cuboidal shear device. In those tests, the servo-control system is used to monitor and adjust applied pressures and in turn ensure a desired set of conditions, for example, K_o consolidation, or strain-controlled loading.

ACKNOWLEDGMENTS

The servo-controlled cuboidal shear device developed at Purdue University was supported by the U.S. Air Force Office

of Scientific Research (Grant No. AFOSR-84-0330). This support is gratefully acknowledged.

REFERENCES

1. A. M. Coatsworth. Computer-Controlled Triaxial Soil Testing Equipment in a Commercial Laboratory. *Ground Engineering*, Vol. 17, No. 7, 1984, pp. 19-23.
2. D. W. Armour and V. P. Drnevich. Improved Techniques for the Constant-Rate-of-Strain Consolidation Test. *Consolidation of Soils: Testing and Evaluation*, STP 892, ASTM, Philadelphia, Pa., 1985, pp. 170-183.
3. J. H. Atkinson, J. S. Evans, and C. R. Scott. Developments in Microcomputer Controlled Stress Path Testing Equipment for Measurement of Soil Parameters. *Ground Engineering*, Vol. 38, No. 3, 1987, pp. 15-22.
4. M. Jamiolkowski, C. C. Ladd, G. T. Germaine, and R. Lancellotta. New Developments in Field and Laboratory Testing of Soils. *Proc., 11th International Conference on Soil Mechanics and Foundation Engineering*, San Francisco, Calif., Vol. 1, 1985, pp. 57-153.
5. G. Sandbaekken, T. Berre, and S. Lacasse. Oedometer Testing at the Norwegian Geotechnical Institute. *Consolidation of Soils: Testing and Evaluation*, STP 892, ASTM, Philadelphia, Pa., 1985, pp. 329-353.
6. K. F. von Fay, J. G. Byers, and B. A. Kunzer. Desktop Computer Application for Consolidation Testing and Analysis. *Consolidation of Soils: Testing and Evaluation*, STP 892, ASTM, Philadelphia, Pa., 1985, pp. 217-235.
7. N. Sivakugan. *Anisotropy and Stress Path Effects in Clays*. Ph.D. Thesis. Purdue University, West Lafayette, Ind., 1987.
8. N. Sivakugan, J. L. Chameau, R. D. Holtz, and A. G. Altscheffl. Servo-Controlled Cuboidal Shear Device. *Geotechnical Testing Journal*, ASTM, Vol. 11, No. 2, 1988, pp. 119-124.

Publication of this paper sponsored by Committee on Soils and Rock Instrumentation.

Use of Voice-Recognition Systems for Atterberg Limit Tests

THOMAS L. BRANDON AND ROBERT A. STADLER

The U. S. Army Engineers Ohio River Division (ORD) has incorporated a personal computer (PC)-based voice-recognition system for data acquisition in its geotechnical engineering laboratory. These systems recognize spoken commands as an alternative to keyboard input, which can be a major benefit considering the poor keyboard environment found in many geotechnical engineering laboratories. Voice-recognition systems have several useful implementations for control of simple tests in a production geotechnical engineering laboratory, one of the simplest being Atterberg limit determination. A system developed at the ORD laboratory for this purpose consists of an IBM voice-recognition system installed in a Zenith Z-248 PC. This system is coupled with a Mettler PE-3600 balance having an RS-232 output. The balance is triggered to make a reading by a digital signal produced by the parallel printer port. A computer program has been written to allow hands-off operation for Atterberg limit data acquisition and reduction. The type of system described does not remove the physical effort involved in conducting the test, but removes the need for data sheets and lessens the chance of calculation errors. Voice-recognition systems are being implemented at the ORD lab for visual classification tests.

The U.S. Army Engineers Ohio River Division (ORD) Geotechnical Engineering Laboratory has been incorporating automation and data acquisition techniques for simple, but common, soil index tests. Data acquisition systems are often easily adapted to shear tests (triaxial and direct shear) because the transducers used for measurement of force and displacement produce electrical outputs. With many index tests, however, weight is often the only parameter that is electronically measurable. The remaining parameters are usually alphanumeric and are recorded by technicians on data sheets.

Computer-based data-reduction systems have been in place in geotechnical laboratories for many years. Although these systems have proven to be indispensable in production testing, it is still necessary to enter the data into the computer via the keyboard. Accurate keyboard entry is an acquired skill. The dusty environment of a production geotechnical laboratory is a less-than-ideal environment for keyboard entry.

At the ORD laboratory, a system has been developed to aid data collection and reduction for Atterberg limit determination. This system uses a personal computer (PC)-based voice-recognition system to input the alphanumeric data, and a computer-operated electronic balance to record the weights associated with the Atterberg limits test.

ATTERBERG LIMIT TEST

Atterberg limit determination is perhaps the most common test performed by production geotechnical engineering laboratories. It is also one of the easiest tests to perform, aside from the physical effort required for rolling the thread of soil for the plastic limit test and operating the liquid limit device. The only data acquired are water contents and the number of blows to close the groove. In addition to the information detailing the job and sample, the only data recorded by the technicians are the can or tare names, the tare weight, the weight of the tare and moist soil, the weight of the tare and dry soil, and in the case of the liquid limit test, the number of blows to close the groove cut in the sample.

A common procedure used for Atterberg limit tests is as follows:

1. Tare all cans and record can labels.
2. Conduct liquid limit tests, and record weight of tare plus moist soil.
3. Conduct plastic limit tests, and record weight of tare plus moist soil.
4. Place all cans in an oven.
5. After drying, record the weight of the tare plus dry soil.
6. Perform calculations.

The system described in this paper uses the same procedure, but the data is acquired either by voice input or automatically.

VOICE-RECOGNITION SYSTEMS

Voice recognition systems can be considered as an alternative to keyboard input for microcomputer operation. Compared with keyboard entry, voice recognition systems have the advantage that no specific skills are required to use them.

The basic technology used in voice recognition systems has existed for more than 10 years. Earlier systems were expensive and were predominantly the domain of powerful mini- and mainframe computers. Use of the systems was confined mainly to research laboratories. However, like much existing computer equipment, the price of the hardware involved has decreased drastically over the last few years, and many commercial voice-recognition products are available for microcomputers.

The two basic types of voice recognition systems are speaker-dependent and speaker-independent (*I*). Speaker-dependent systems need to be "trained" before use. Following a user-defined vocabulary, the user must repeat each word into a

T. L. Brandon, Virginia Polytechnic Institute and State University, Blacksburg, Va. 24061-0105. R. A. Stadler, Materials Unit, U.S. Army Corps of Engineers, Ohio River Division Geotechnical Engineering Laboratory, 5851 Mariemont Ave., Mariemont, Ohio 25227.

microphone several times, and each word is digitized by the computer. The computer takes an average voice pattern for the word and stores it on disk. After training, when the user speaks into the microphone, the computer compares the voice pattern measured with those already stored on disk. When an adequate comparison is found, the word is printed on the screen in the same manner as if it were typed on the keyboard.

Speaker-independent systems do not need training. Voice patterns are already stored in the computer for certain words. The technology for these systems has not been developed as fully as speaker-dependent systems, and they are more expensive and less accurate. These systems usually have much smaller vocabularies, and regional accents can cause incorrect words to be interpreted.

ATTERBERG LIMIT TEST SYSTEM

The system used at the ORD laboratory to aid in conducting Atterberg limit tests consists of four components:

- Voice recognition card,
- Electronic balance,
- Automatic balance switch, and
- Microcomputer.

Voice Recognition Card

In this application, an IBM Voice Communication Option board, a speaker-dependent system, was used. This card, coupled with IBM Voice Activated Keyboard Utility software, allows a maximum usable vocabulary of about 160 user-defined words, depending on the amount of disk storage space and random access memory. The memory resident software used with this system translates the spoken words into the proper keystrokes. Although the system will allow up to 160 words, only 60 words were needed in this application.

A utility program supplied with the board is used to "train" the system. The operator has to repeat each vocabulary word into the microphone five times to store the required voice patterns. This process takes about 20 min to complete.

Electronic Balance

A Mettler PE-3600 electronic balance is used for recording the weights. This balance, as well as other commercially available balances, has an RS-232 (serial) output port. When a weight measurement is triggered by pressing a button next to the balance, a character string is sent to the computer via the serial port. The balance is designed such that the character string is only transmitted if there are no fluctuations in the reading.

Automatic Balance Switch

In order to bypass the button to trigger the balance to make a reading, a relay board was constructed. The parallel (printer) port of a microcomputer is an 8-bit digital-output port. A

relay powered from a true bit voltage (4.5 VDC) simulates the pressing of the button on the electronic balance. In this manner, the balance can be triggered to perform a weight reading under software control.

Microcomputer

A Zenith Z-248, an IBM-AT class computer, is used to process the data. The performance of a PC-based voice-recognition system depends on the speed of the personal computer. The Z-248 computer used in this application provides about the minimum acceptable performance for the voice-recognition system described. A hard disk is necessary to store the vocabulary files for all of the users. In addition, a serial port is required to receive the output of the balance, and a parallel port is needed to trigger the balance to make a reading.

Shown in Figure 1 is a schematic of the voice-recognition Atterberg limit system.

SYSTEM OPERATION

A computer program named AUTOBERG was written in Microsoft QuickBASIC to control the operation of the Atterberg limits system. At the start of the program, the user must enter his or her name via the keyboard so that the proper vocabulary file may be loaded. After this, the program is under voice control and the main menu (Figure 2) is displayed. The highlighted words shown on this figure are the key words that control the main menu functions.

The first step in conducting a test is to tare the moisture-content containers. At the ORD laboratory, all of the moisture content tests are named by a letter and two numbers (e.g., A16). The technician first says the main menu command "tare" into the microphone and places an empty container on the balance. The technician then says the name of the container in the standard military verbal alphabet. For the container labeled A16, the technician would say, "alpha-one-six." The program then sends the proper bit sequence out of the parallel port to trigger the balance, and the balance makes the measurement. The output string from the balance is read

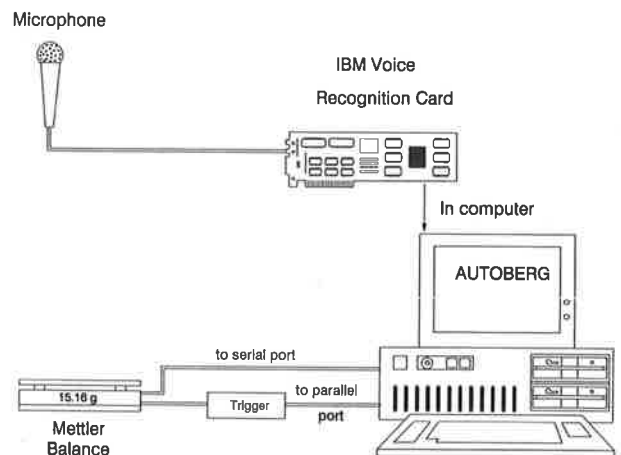


FIGURE 1 Schematic of components used in voice recognition Atterberg limit system.

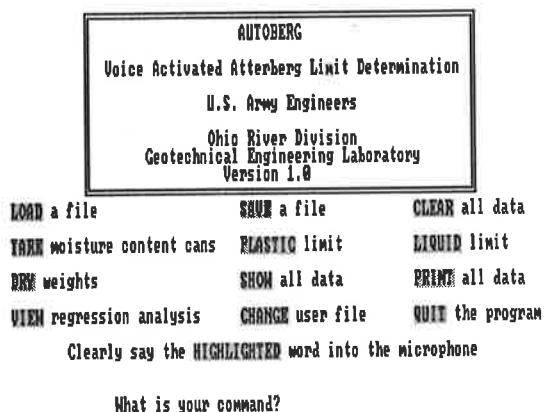


FIGURE 2 Main menu of the computer program AUTOBERG

through the serial port of the computer, and the can name and weight are recorded in a data file. The technician then repeats this process for the tare weight of all the plastic and liquid limit moisture content tins.

The next step is the plastic limit determination. After the 1/8-in. threads of soil are rolled to the proper consistency, the technician places them in a tared moisture content container and places the container on the balance. The technician then says the main menu key word "plastic." The program prompts for the can name, and the technician says the name in the manner as described above. The weight is automatically taken and appended to the data file.

The liquid limit recording procedure is the same as the plastic limit procedure, except after the measurement of the weight of the moist soil and can, the program prompts for the number of blows. Each digit of the number of blows is spoken into the microphone.

To initiate the procedure for recording the final oven-dried weights, the technician says, "dry" into the microphone. The procedure followed is the same as during the initial taring of the cans. For all procedures, the cans may be weighed in any order. The program correctly associates the correct moist and dry weights and tare weights with the type of test performed on the specimen identified by the can label.

Saying the key word "show" displays the data on the screen in tabular form (Figure 3). The data are automatically reduced

Plastic Limit Determination					
Test No.	1	2	3	4	5
Can Name	B16	D22			
Tare Weight	15.61	15.37	0.00	0.00	0.00
Weight of can + moist soil	29.79	30.66	0.00	0.00	0.00
Weight of can + dry soil	19.80	19.77	0.00	0.00	0.00
Water content, w%	21.31	21.19	0.00	0.00	0.00

Liquid Limit Determination					
Test No.	6	7	8	9	10
Can Name	H19	H19	C16		
Tare Weight	15.49	15.42	15.52	0.00	0.00
Weight of can + moist soil	26.16	26.66	26.65	0.00	0.00
Weight of can + dry soil	23.26	23.78	27.05	0.00	0.00
Water content, w%	37.32	35.75	31.25	0.00	0.00
Number of Blows	23	25	30	0	0

Liquid Limit = 35.5 Plastic Limit = 21.3 Plasticity Index = 14.3
Press any key to continue

FIGURE 3 Data displayed on the computer screen by the main menu command "show."

as soon as all of the necessary weights have been taken. The plastic limit given at the bottom of the screen is an average of all of the plastic limit tests made in the test series. The liquid limit is calculated on the basis of a linear regression analysis performed on the data. By saying "print," the technician can receive a copy of the data in this form if a printer is connected to a second parallel port.

The key word "view" plots the logarithm of the number of blows versus the water content for the liquid limit test on the computer screen. The "best fit" line determined from the linear regression analysis and the calculated liquid limit are also shown on the screen.

The program also allows Atterberg limit files to be saved and loaded. The filename may be entered by means of the keyboard, or the filename may be spelled in the same manner as the tare names are entered. The file format created by AUTOBERG is compatible with a companion program, LIMITS, written for the ORD laboratory. This program allows the job name, sample number, boring number, and other descriptive information to be appended to the AUTOBERG file. This program will automatically classify the soil according to the USCS system based on the Atterberg limits, and will generate a hardcopy output similar to the U.S. Army Corps of Engineers ENG Form 3838. Shown in Figure 4 is an example of the hardcopy obtained with LIMITS.

BENEFITS AND LIMITATIONS

The voice-recognition Atterberg limits system described is one of the first attempts at integrating alternative input systems into the ORD geotechnical laboratory. Certain advantages have become apparent with its use:

- The record keeping associated with Atterberg limit tests has been simplified.
- Errors associated with manually recording and reducing the data have been reduced.
- Time is saved in preparation of the final report form.

Although this system has proven to be useful in the ORD laboratory, limitations have also become evident:

- The voice recognition hardware must be used in a relatively quiet environment. Extraneous noise may be interpreted as spoken words by the computer.
- The technician using the system must "train" the computer to understand his or her individual vocabulary. After that time, the technician must always distinctly pronounce each word.
- Constructing such a system involves a relatively high cost. At the time the system was developed (1988), the price of the hardware was approximately \$4,500. The price has decreased somewhat as a result of further developments in voice-recognition systems and computer hardware.

SUMMARY AND CONCLUSIONS

A microcomputer-based voice-recognition system has been developed at the U.S. Army Corps of Engineers ORD Lab-

LIQUID AND PLASTIC LIMIT TESTS						
Project: ATT Region 1 Fairlawn Virginia			Date: 01-29-1990			
Boring No.: B-18			Sample No.: UD-1			
LIQUID LIMIT						
Run Number	1	2	3	4	5	6
Tare Number	H4	H9	CMP6			
Tare plus wet soil, g	26.16	26.66	30.65			
Tare plus dry soil, g	23.26	23.7	27.05			
Weight of water, g	2.89	2.95	3.6			
Weight of tare, g	15.49	15.42	15.53			
Weight of dry soil, g	7.77	8.28	11.51			
Water content (%)	37.32	35.74	31.25			
Number of Blows	23	25	30			
LL = 35.53 PL = 21.25 PI = 14.28 USCS = CL						
PLASTIC LIMIT						
Run Number	1	2	3	4	5	6
Tare Number	B-16	D02				
Tare plus wet soil, g	20.79	20.66				
Tare plus dry soil, g	19.88	19.77				
Weight of water, g	.91	.88				
Weight of tare, g	15.61	15.57				
Weight of dry soil, g	4.26	4.2				
Water content (%)	21.31	21.19				
Remarks:						
Technician:		Computed by: ABERG		Checked by:		

FIGURE 4 Hard copy output of reduced Atterberg limits test results.

oratory to aid in conducting Atterberg limit tests. The controlling computer program, AUTOBERG, is under complete voice control. This system uses an electronic balance to make all weight measurements, and all data are automatically reduced. A companion program, LIMITS, classifies the soil specimen based on the Atterberg limits, and produces a report-quality form similar to the U.S. Army Corps of Engineers Form 3838.

Although care need be exercised when operating the system, it has proven to reduce the time required for data reduction and the chance of operator error. Application of voice-

recognition technology is currently being extended to visual classification procedures.

REFERENCE

1. W. L. Rosch. 1987. Voice Recognition: Understanding the Master's Voice. *PC Magazine*, Vol. 6, No. 8, pp. 261-295.

Publication of this paper sponsored by Committee on Soils and Rock Instrumentation.

Innovations in Hydraulic-Conductivity Measurements

HAROLD W. OLSEN, JAMES D. GILL, ARTHUR T. WILLDEN, AND
KARL R. NELSON

Innovations in laboratory methods for hydraulic-conductivity measurements have been developed by using a flow pump to generate a constant rate of flow through a test specimen and monitoring the hydraulic gradient induced thereby with a differential-pressure transducer. In most applications of this constant-flow method to date, hydraulic-conductivity tests have been conducted on stress-controlled specimens following conventional loading increments in one-dimensional consolidometers and also after increments of three-dimensional consolidation in triaxial cells. Similarly, a constant rate of flow through one end of a test specimen has been generated with a flow pump while flow through the opposite end of the specimen is driven to or from a pressure-controlled reservoir. More recent innovations include a new flow-pump actuator that enables identical flow rates to be infused and withdrawn from opposite ends of a test specimen and the use of additional flow pumps to control the effective stress and volume of a specimen. These innovations provide a convenient approach for obtaining hydraulic conductivity versus effective stress data in triaxial cells on a wide variety of materials, including sandstones and shales that cannot be trimmed and mounted in fixed-ring permeameters or one-dimensional consolidometers. These innovations also provide a means to integrate constant-flow hydraulic conductivity measurements with continuous-loading consolidation tests on fully saturated specimens in both back-pressured consolidometers and in triaxial cells.

Presented in this paper is an overview of the innovations in laboratory methods for hydraulic-conductivity measurements that have been developed using a flow pump to generate a constant rate of flow through a test specimen and monitoring the hydraulic gradient induced thereby with a differential pressure transducer. Experimental data are presented to illustrate how various applications of this constant-flow method can be used to provide more detailed and higher-quality technical information in less time than conventional methods.

The innovations involve applications of the constant-flow method in one-dimensional consolidometers and in conventional triaxial cells. The advantages of these innovations arise because the generation of low flow rates and the measurement of pressures and forces with transducers in the constant-flow method can be accomplished more easily and accurately than the measurement of low flow rates and the control of pressures and forces involved in conventional constant-head and falling-head methods. For example, flow rates as low as 10^{-7} cm³/sec can easily be generated with commercially available flow pumps.

However, the measurement of such flow rates requires long periods of time because the practical resolution of volume-measurement techniques used in geotechnical laboratories is about 10^{-3} cm³ (*I*). Also, fluid pressures are easily measured to 10^{-3} psi with transducers; however, they can only be controlled to about 10^{-1} psi with air-pressure regulators commonly used in geotechnical laboratories.

FLOW PUMPS

The flow pumps that were used are the commercially available pumps shown in Figure 1 from The Harvard Apparatus Co., South Natick, Massachusetts. (Use of trade names in this report is for descriptive purposes only and does not imply endorsement by the U.S. Geological Survey.) These pumps are about 70 cm long, 20 cm wide, and 20 cm tall. One pump has a single carriage in which a cross member, known as a "saddle," moves in either direction by means of a worm gear that is driven by a variable-speed direct-current motor through a transmission box with 12 combinations of gears between the worm gear(s) and the motor. The other pump has two carriages whose worm gears are driven by the same motor and transmission box. In the dual-carriage pump, the saddles move at the same rate in either the same direction or in opposite directions. In both pumps, a speed controller on the direct-current motor governs rotation of the worm gears at speeds between those determined by the gear selector. These features enable the saddles to be advanced or withdrawn at any constant rate ranging from about 10^{-1} to 10^{-6} cm/sec.

These pumps are often called "syringe" pumps because they were initially designed to move the piston of a syringe with the saddle while the syringe barrel was held stationary within the carriage. A syringe of any size can be used, provided that it is not too large for the carriage. Hamilton gas-tight syringes that consist of precision-bore glass barrels and pistons with Teflon seals and stainless-steel syringes fabricated by a local machinist were used. Actuators that have advantages over syringes also were used (Figure 2). The top design (*A*), introduced by Olsen et al. (2), features a stepped shaft that has two diameters so that the flow rate is proportional to the difference between the cross-sectional areas where the diameter changes. With this design, the differential area that generates flow can be much smaller than the area of a piston in a conventional syringe. The middle design (*B*), introduced by Aiban and Znidarcic (3), has a shaft that is sealed in a piston guide block instead of in the cylinder barrel. This design is more rugged and easier to deair than a conventional syringe.

H. W. Olsen, U.S. Geological Survey, Branch of Geologic Risk Assessment, Box 25046, Mail Stop 966, Denver, Colo. 80225. J. D. Gill, Michael W. West and Associates, 8906 West Bowles Ave., Littleton, Colo. 80123. A. T. Willden and K. R. Nelson, Department of Engineering, Colorado School of Mines, Golden, Colo. 80401.



FIGURE 1 Single-carriage (top) and dual-carriage (bottom) flow pumps.

The bottom design (C), introduced here, provides a means to simultaneously infuse and withdraw at identical rates. This design is also rugged and easy to deair. In addition, it provides a means to minimize the force imposed on the saddle from the piston of a conventional syringe when the fluid pressure is elevated. In the bottom design (C) in Figure 2, the force on the saddle is proportional to the difference between the inflow and outflow pressures, which is generally small, on the order of a few psi or less. In contrast, for design B and for

conventional syringes, the force on the saddle is proportional to the pore pressure, which is commonly elevated to 50 psi or greater.

Figure 3 illustrates that flow rates ranging from about 10^{-7} to greater than 10^{-1} cm^3/sec can be obtained with the flow pumps in Figure 1 when equipped with syringes having inside diameters of 0.05 in. (0.127 cm) to 2 in. (5.08 cm). The corresponding range of cross-sectional areas can also be obtained with the actuator designs in Figure 2. The horizontal axis shows transmission gear settings ranging from 1 to 12 and the resulting velocities of the saddle that pushes or pulls a syringe piston. The curves extend to the left of gear setting 12 to the velocity obtained with a gear setting of 12 while the speed controller on the variable speed motor is set at 10 percent of its full range. For each gear setting, the saddle velocity varies directly with the speed controller setting. According to the manufacturer's specifications, the system delivers flow rates accurate to within 2 percent and with a reproducibility of 0.5 percent.

STRESS-CONTROLLED SPECIMENS IN CONSOLIDOMETER AND TRIAXIAL SYSTEMS

The constant-flow method was introduced during the mid-1960s (4-6) in fundamental studies of the laws and mechanisms governing pore-fluid movement in kaolinite. The test cell was a one-dimensional consolidometer wherein the specimen was rigidly confined in a cylindrical sleeve and between two hydraulically controlled pistons.

Beginning in the late 1970s, applications of the constant-flow method for stress-controlled specimens in one-dimensional consolidometers and triaxial cells expanded in both research and practice (2,3,7-14). In most of these applications, a constant rate of flow through one end of a test specimen has been generated with a flow pump while flow through the opposite end of the specimen moved to or from a pressure-controlled reservoir, as illustrated in Figure 4. In both systems a flow pump (P) infuses or withdraws fluid across one end of the specimen (S) while flow across the opposite end moves to or from a pressure-controlled reservoir (R). A differential pressure transducer (M) monitors the induced pressure difference across the specimen. In the consolidometer (top), a linear variable differential transformer (LVDT) (K) monitors the

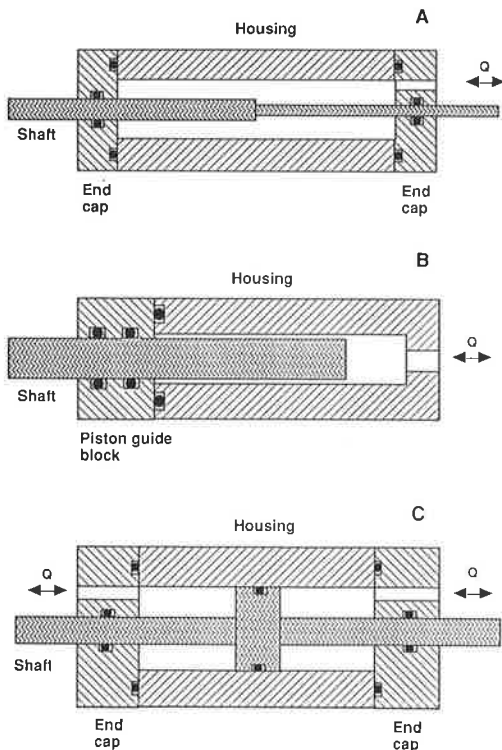


FIGURE 2 Flow pump actuator designs with advantages over conventional syringes: (A) the stepped shaft, (B) the piston guide block, and (C) the symmetry of the shaft and housing on either side of the central part of the shaft that is sealed to the housing with an O-ring.

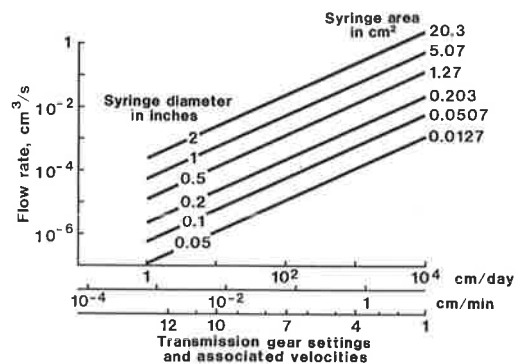


FIGURE 3 Flow rates that can be generated by the flow pumps in Figure 1.

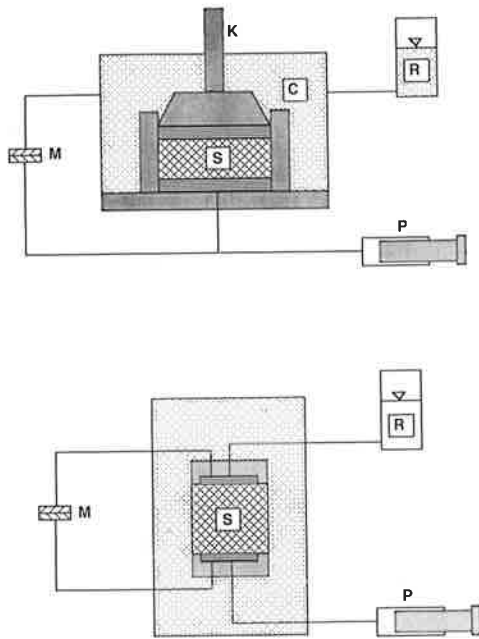


FIGURE 4 Diagrams of a back-pressured one-dimensional consolidometer (top) and a triaxial cell (bottom) equipped for constant-flow hydraulic-conductivity measurements on stress-controlled specimens.

specimen thickness, and flow between the sample (S) and the reservoir (R) passes through the back-pressure chamber (C).

Hydraulic-conductivity measurements have been conducted following increments of one-dimensional consolidation in consolidometers and three-dimensional consolidation in triaxial cells. For these systems, the demonstrated capabilities of the constant-flow method and its advantages over constant-head and falling-head methods are as follows.

Constant-flow test data for sand and silty-clay specimens in a triaxial system (like that illustrated in Figure 4) are shown in Figures 5 and 6. Figure 5 shows that the response time for sand is short and that small head differences across the specimen (on the order of a few centimeters of water or less) can be measured with both high resolution and accuracy, even though some noise appears in the measured head differences as a result of fluctuation in flow rates from mechanical sources within the flow pump. In contrast, Figure 6 shows that the response time for clays can be substantial. Moreover, the measured head difference across a clay specimen includes a small head difference (on the order of a few millimeters of water) which is present during the zero flow condition.

Experience shows that residual head differences are not uncommon and that they can vary somewhat with time. Their causes may include variations in room temperature with time, internal pressure gradients caused by variations in the degree of saturation, and geochemical sources of osmosis within a specimen (15). The practical significance of these small differences is that they can be a source of experimental error that limits the sensitivity of the constant-flow method for low-gradient hydraulic-conductivity measurements on clays. Nevertheless, the constant-flow method allows tests on clays to be run at much lower hydraulic gradients than can be

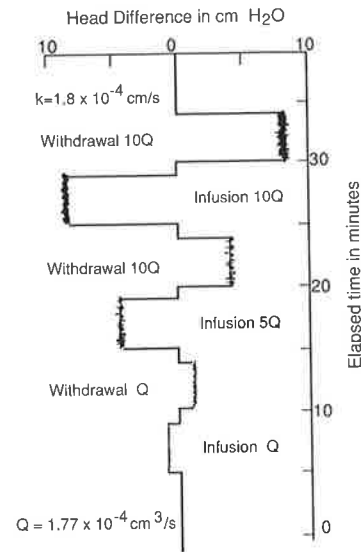


FIGURE 5 Constant-flow hydraulic-conductivity data on a sand specimen under stress control in a triaxial system like that illustrated in Figure 4.

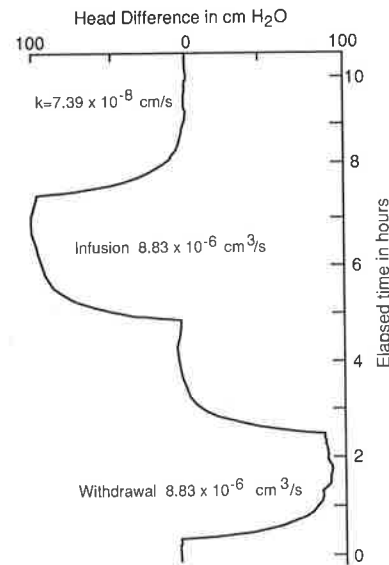


FIGURE 6 Constant-flow hydraulic-conductivity data on a clay specimen under stress control in a triaxial system like that illustrated in Figure 4.

accomplished with conventional constant-head and falling-head methods in a reasonable period of time.

Regarding the response time (the time required to reach steady state after beginning or ending a period of flow through a specimen), its cause was recognized to be seepage-induced consolidation in constant-head tests more than 20 years ago (16-18). For example, Al-Dhahir and Tan (17) showed how Terzaghi's (19) governing equation for one-dimensional consolidation can be used, with analogous heat conduction theory from Carslaw and Jaeger (20), to interpret the coefficient of

consolidation from the initial transient phase of a constant head test. For a constant-flow test, the response time can be similarly described with analytical solutions in work by Carslaw and Jaeger (20), and the coefficient of consolidation can be interpreted therewith on data from either the initial or the final transient phases of a constant-flow test (12,13). However, this approach for interpreting the coefficient of consolidation should be used with caution because undissolved air and other sources of compliance in the specimen and permeant system will be sources of error in the interpretation of the coefficient of consolidation.

The practical significance of the response time is that it is a measure of the time required to carry out a constant-flow hydraulic-conductivity test, and this time is much shorter than that required for conventional constant-head and falling-head tests because the latter depends on the time required for a measurable quantity of flow through the specimen. In addition, because the response time is governed by the consolidation process, it varies with the square of the drainage path and therefore can be shortened substantially by reducing the height of a specimen.

When large gradients are externally imposed or induced across compressible specimens under stress control in consolidometers or triaxial cells, seepage-induced volume changes can be of sufficient magnitude to cause substantial errors in hydraulic-conductivity measurements. Pane et al. (9) summarized the advantage of the constant-flow method for minimizing this error as follows: "In using conventional tests one is faced with a paradox. The use of high gradients reduces the time of testing but introduces substantial errors in the test results. However, the use of low gradients extends the testing time to unacceptable limits. The flow pump test [constant-flow method] solves both these problems."

It should be recognized that although errors from seepage-induced volume changes can be readily minimized with the constant-flow method, they cannot be avoided entirely. Pane et al. (9) concluded, "If the clay is very soft and normally consolidated, even the lowest gradients can cause significant seepage consolidation." They further suggest that to minimize induced errors, "The gradients must be such that the seepage-induced effective stresses are substantially less than the maximum past effective stress." In this regard, recent work by Aiban and Znidarcic (3) is of particular interest because it shows small discrepancies between hydraulic-conductivity values obtained with constant-flow and constant-head methods that are clearly attributable to seepage-induced volume changes even though the magnitudes of the discrepancies are negligible for most practical applications.

CONTROLLED INFLOW AND OUTFLOW RATES IN TRIAXIAL SPECIMENS

Recently the new infuse/withdraw actuator (Figure 2C) has been used in the triaxial systems illustrated in Figure 7. In both systems the infuse/withdraw actuator, which is mounted in a single-carriage flow pump, generates identical flow rates through opposite ends of the specimen while the pressure differences across the specimen and between the pore fluid and chamber fluid are monitored with differential transducers (*M* and *N*). Both systems also have a second single-carriage

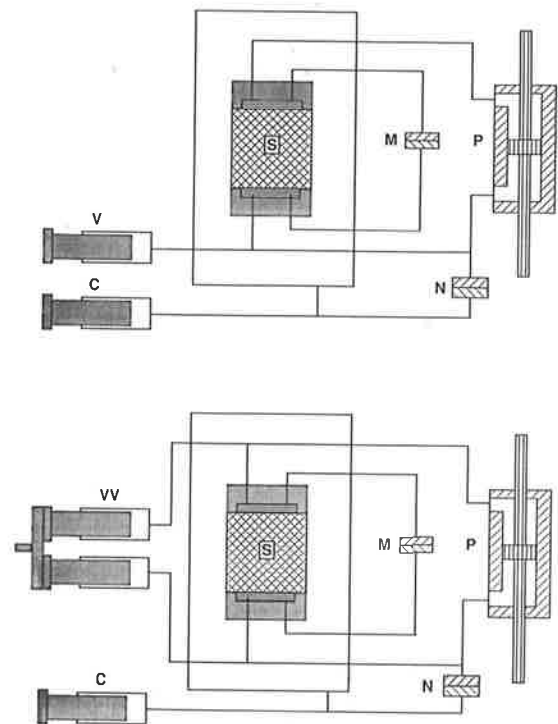


FIGURE 7 Triaxial cells equipped with one flow pump (*P*) that infuses and withdraws identical rates of flow across opposite ends of a specimen (*S*), differential transducers (*M* and *N*) that measure the pressure difference across the specimen (*M*) and the pressure difference between the pore fluid and the chamber fluid (*N*), and additional flow pumps for controlling the chamber fluid pressure (*C*) and the effective stress or the volume of a test specimen (*V* and *VV*).

flow pump (*C*), equipped with a stainless steel syringe, that provides a means to control the chamber fluid pressure. The use of a flow pump for controlling the chamber fluid pressure is an alternative to the bellows and air-pressure regulator that control the chamber fluid pressure in the more conventional triaxial system in Figure 4.

The systems in Figure 7 each have a third flow pump for controlling the volume of pore fluid in the specimens. In the upper system pore fluid is transmitted to or from one end of the specimen with one stainless steel syringe mounted in a single-carriage flow pump. In the lower system, pore fluid is transmitted to or from both ends of the specimen simultaneously with identical stainless steel syringes mounted in a dual-carriage flow pump. In both systems, the third pump provides a means to vary the effective stress or volume of the specimen continuously and to superimpose hydraulic-conductivity measurements on this process. The systems differ in the lengths of their drainage paths for consolidation or rebound of the specimen.

Data obtained with the upper system in Figure 7 on a 2-in. (5.08-cm) diameter by 1-in. (2.54-cm) thick specimen of sandstone from the Michigan Basin are shown in Figure 8. The bottom plot shows the effective stresses applied to the specimen versus time. The middle plot shows the hydraulic conductivity values obtained during each loading step. The

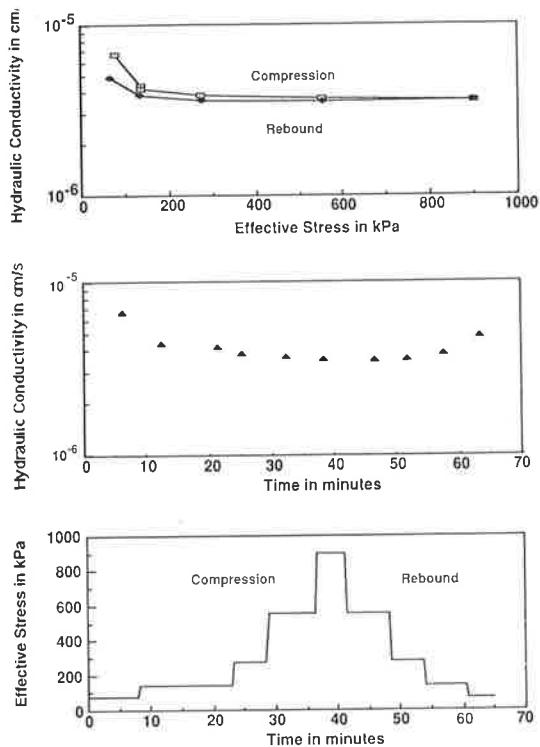


FIGURE 8 Time history of loading (bottom) and hydraulic-conductivity measurements (middle) on a specimen of sandstone from the Michigan Basin in triaxial system illustrated in Figure 7 (top); hydraulic-conductivity versus effective stress relationship from data in the middle and bottom plots (top).

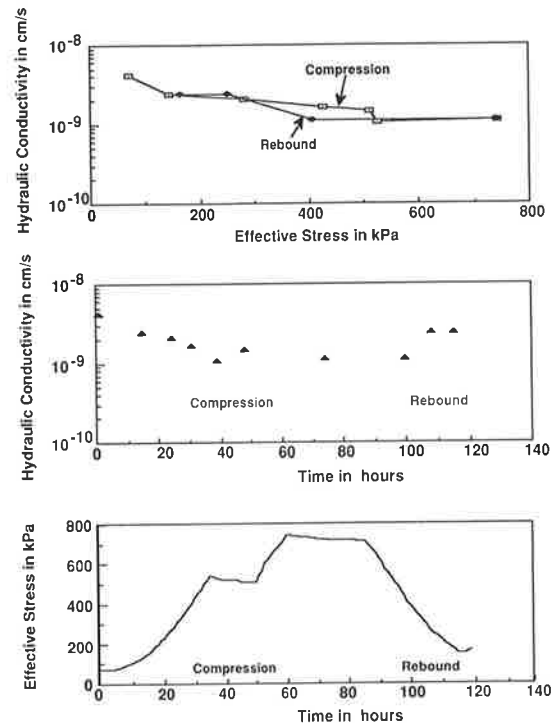


FIGURE 9 Time history of loading (bottom) and hydraulic-conductivity measurements (middle) on a shale specimen in the triaxial system illustrated in Figure 7 (top); hydraulic-conductivity versus effective stress relationship from data in the middle and bottom plots (top).

top plot shows the variation of hydraulic conductivity with effective stress. Ten hydraulic conductivity determinations were obtained after each 9 changes in effective stress in about 1 hr. Note that the hydraulic conductivity is relatively high at low effective stresses, even though the sandstone specimen appeared to be rigidly cemented. The variation of hydraulic conductivity with effective stress in these samples is presumed to reflect the behavior of cracks in the specimen, instead of changes in the permeability of its matrix.

Data obtained with the lower system in Figure 7 on a 4-in. (10.16-cm) diameter by 1-in. (2.54-cm) thick specimen of shale from Oklahoma are presented in Figure 9, using the format in which the data on the sandstone specimen were presented in Figure 8. The bottom plot of Figure 9 shows the effective stress first increased continuously in two steps, each followed by a period of nearly constant effective stress. These steps were accomplished by using the dual-carriage flow pump to withdraw pore fluid from the ends of the specimen at identical rates. During the periods following each step, the flow pump was shut off. Following the latter period, the effective stress was decreased continuously by infusing fluid into the ends of the specimen with the dual-carriage flow pump. The middle plot of Figure 9 shows hydraulic-conductivity measurements obtained both during and between the time intervals when the specimen was being continuously loaded and unloaded.

Finally, the top plot shows the variation of hydraulic conductivity with effective stress derived from the data in the

middle and lower plots. Note that the hydraulic conductivity is extremely low, on the order of 10^{-9} cm/sec, and 10 hydraulic-conductivity measurements were obtained over a range of effective stresses in about 125 hr or 6 days. The response times for the hydraulic conductivity measurements were on the order of 1 to 2 hr. It is noted that high pore fluid pressures were needed to obtain response times of this magnitude. Apparently, the high pressures were needed to drive all the undissolved air in the pore fluid into solution. A flow pump was used to infuse or withdraw fluid from the triaxial chamber, and the plastic cylinder in the triaxial chamber was replaced with a stainless steel cylinder, resulting in pore pressures elevated to more than 300 psi.

VOLUME-CONTROLLED SPECIMENS IN ONE-DIMENSIONAL CONSOLIDOMETERS

Beginning with an Anteus backpressured one-dimensional consolidometer, Gill (21) used two flow pumps to conduct constant-flow hydraulic-conductivity measurements during constant-rate-of-deformation (CRD) consolidation tests, as illustrated in Figure 10. One pump (*F*) transmits fluid to the load pressure chamber (*L*) and thereby provides a means to consolidate a test specimen (*S*) at a constant rate of volume change, which is commonly referred to as a CRD test. The second flow pump (*D*) controls pore-fluid movement across the base of the specimen and thereby provides a means to

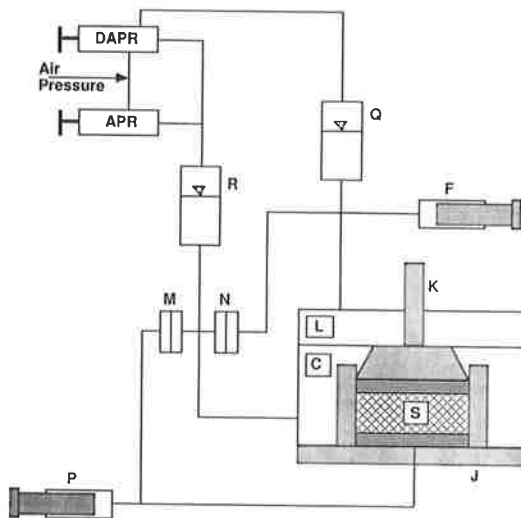


FIGURE 10 Diagram of a back-pressured consolidometer (*J*) equipped for constant-flow hydraulic-conductivity measurements on a volume-controlled specimen (*S*).

conduct constant-flow hydraulic-conductivity tests simultaneously with a CRD consolidation test.

For a conventional CRD test, the second flow pump (*P*) is shut off so as to maintain zero flow across the lower boundary of the specimen while the pore fluid expelled from the sample during consolidation flows into the back-pressure chamber (*R*) and then to the bellofram, where the pressure in the back-pressure chamber (*R*) is externally controlled by the absolute pressure regulator. The sample thickness is monitored with an LVDT (*K*). The effective stress at the top of the specimen, which is proportional to the pressure difference between the load pressure chamber (*L*) and the back-pressure chamber (*R*), is monitored with one differential pressure transducer (*N*). The pore-pressure increase at the base of the specimen resulting from the consolidation process is monitored relative to the back pressure with the other differential pressure transducer (*M*). APR and DAPR are air pressure and differential air pressure regulators, respectively. DAPR and the back-pressure chamber (*Q*) provide a means to apply an initial seating load on the specimen.

The conventional CRD test just described can be modified by periodically using the second flow pump (*P*) to superimpose an arbitrary constant flow rate through the consolidating specimen. Hydraulic-conductivity values are obtained from the components of the pore-pressure difference across the sample that are induced by the superimposed constant-flow rates. Thus, direct measurements of hydraulic conductivity can be obtained during a CRD test.

Data obtained with this approach on an undisturbed specimen of silty clay from Maryland having 30 percent finer than 2μ and a plasticity index (PI) of 33 percent are presented in Figure 11 (21). The specimen was first equilibrated under a small and constant seating load for more than 25 hr. The void ratio initially decreased slightly and then remained almost constant. Hydraulic conductivity was measured periodically by withdrawing pore fluid from the base of the specimen at a constant rate and monitoring the induced pore-pressure

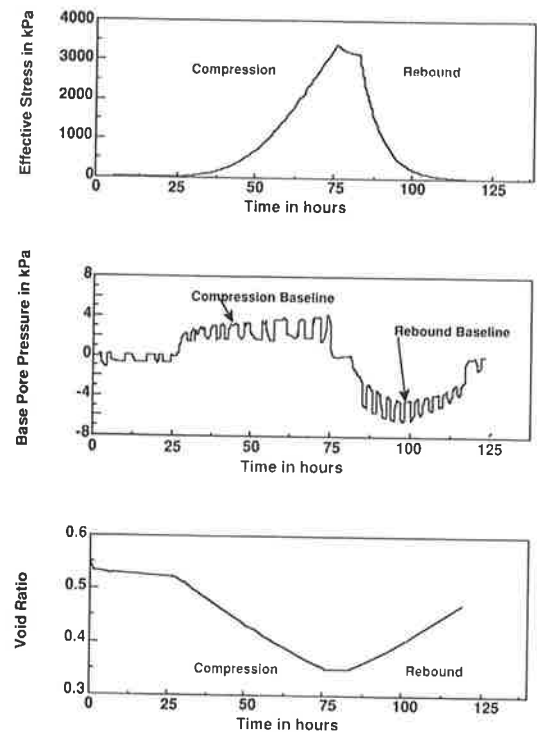


FIGURE 11 Time history of simultaneous constant-flow hydraulic-conductivity and continuous-loading compressibility measurements in the one-dimensional consolidometer illustrated in Figure 10; constant-flow hydraulic-conductivity tests are designated as *k*-tests.

changes at the base of the specimen. Following this initial period of deformation, the specimen was consolidated at a constant rate of deformation until the total elapsed time reached about 75 hr. The top graph shows the buildup of vertical effective stress with time, and the middle graph shows the consolidation-induced pore pressure at the base of the specimen, designated as the "compression baseline." Superimposed hydraulic conductivity tests (*k*-tests) are reflected in periodic changes in base pore pressure from the compression baseline that were induced by withdrawing pore fluid from the base of the sample at a constant rate. When compression was terminated, the base pore pressure returned to zero, and the vertical effective stress decayed somewhat, as a result of secondary compression. During rebound, the effective stress decreased with time [Figure 11 (top)], and the rebound-induced change in base pore pressure, designated as the rebound baseline in Figure 11 (middle), was negative. The changes in base pore pressure induced by superimposed constant-flow hydraulic conductivity tests were clearly evident. Void ratio, specific storage, and hydraulic conductivity versus effective stress relationships are shown in Figure 12 for the test data in Figure 11. Specific storage is a measure of compressibility that is calculated from the slope of the void-ratio versus effective-stress relationship. Specific storage and hydraulic conductivity values were obtained concurrently and independently from direct measurements, whereas, by using conventional consolidation testing methods, hydraulic conductivity can only be obtained indirectly from coefficient-of-consolidation measurements or di-

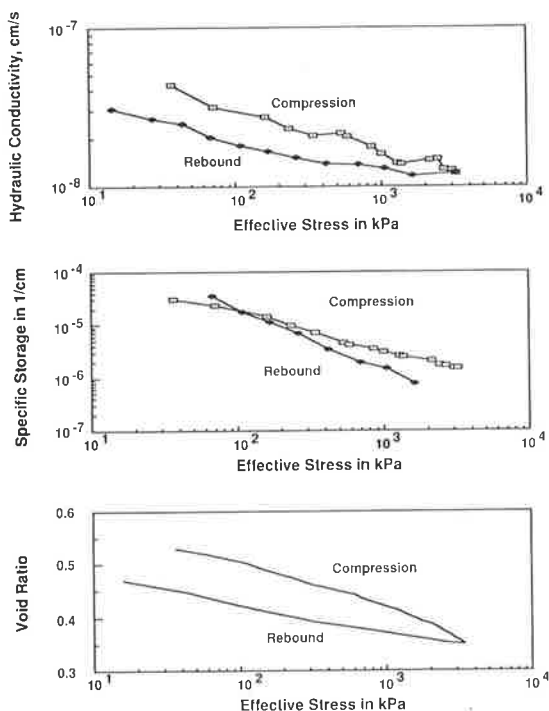


FIGURE 12 Hydraulic conductivity, specific storage, and void ratio versus effective stress for the test data in Figure 11.

rectly between consolidation increments. Finally, note that the duration of the combined test is not affected by the frequency and duration of hydraulic conductivity tests. The total elapsed time is governed solely by the deformation rates used for consolidating and rebounding the specimen.

VOLUME-CONTROLLED SPECIMENS IN TRIAXIAL SYSTEMS

CRD-consolidation and constant-flow hydraulic conductivity tests can also be integrated in the triaxial systems illustrated in Figure 7, provided that the specimens are fully saturated. Volume changes generated by infusing or withdrawing fluid to or from the ends of the specimen can be calculated from the flow rates and time intervals employed. The total specimen volume is not affected by hydraulic conductivity measurements because the inflow and outflow rates are identical. With a system having the capabilities illustrated in Figure 7 (top), the data in Figure 13 were obtained for a specimen of Standard Air Floated (SAF) clay that is marketed by the Georgia Kaolin Company. The specimen was molded from a slurry having a water content of about 110 percent. The slurry was prepared by absorption of distilled and deaired water by dry clay powder under vacuum in a dessicator. To form the specimen, the slurry was poured into a cylinder 5.08 cm in diameter \times 10 cm in length, whose base was capped by a porous stone and submerged under water in a bucket. A porous stone and a piston were placed on the slurry at the top of the cylinder. The entire assembly was mounted in a loading press, where the sample was consolidated slowly at a constant rate of deformation to a predetermined volume that

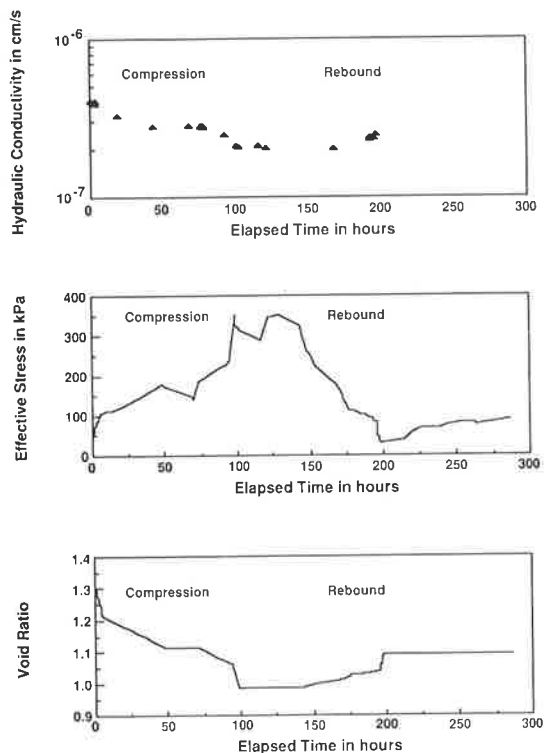


FIGURE 13 Time history of hydraulic conductivity (top), effective stress (middle), and void ratio (bottom) data obtained during simultaneous constant-flow hydraulic-conductivity and continuous-loading compressibility measurements on a kaolinite specimen in the triaxial system illustrated in Figure 7 (top).

would yield a loosely consolidated specimen with sufficient strength to be trimmed and mounted in a triaxial cell. Finally, the material was extruded from the cylinder, cut to a convenient length (about 3 cm), jacketed with impermeable membrane, and mounted in the triaxial cell between the base pedestal and top cap.

The data in Figure 13 show constant-flow hydraulic conductivity and continuous-loading consolidation measurements on a triaxial test specimen. These data are similar to those illustrated for the one-dimensional consolidometer in Figure 11 in that the duration of the combined test is not affected by the frequency and duration of hydraulic conductivity tests. The total elapsed time is governed solely by the deformation rate used for consolidating and rebounding the specimen.

These measurements began after the specimen had been equilibrated to a void ratio of 1.305 under an effective stress of 34.5 kPa. Several flow rates were used to consolidate the specimen with the single-carriage pump, as reflected in different slopes of the void-ratio versus time relationship. This procedure was done to explore the behavior of the experimental system, whereas a constant rate of deformation is needed to obtain consolidation data applicable in practice. The effective-stress values are differences between the chamber pressure and the pore pressure at the base of the specimen. Hydraulic-conductivity measurements were obtained during the course of consolidation or rebound, generated by the

single-carriage pump, by superimposing flow through the specimen with the infuse/withdraw pump and measuring the head difference induced thereby. Some of the relationships that are readily obtained from these data are presented in Figure 14. It should be recognized that the significance of these relationships may be limited because the rate of volume change used to consolidate the specimen was not constant.

SUMMARY AND CONCLUSIONS

The fundamental advantage of the constant-flow method compared with conventional constant-head and falling-head methods is that hydraulic conductivity measurements can be obtained much more rapidly and at substantially smaller hydraulic gradients. This advantage was first exploited in the mid-1960s for fundamental research studies on rigidly confined specimens in one-dimensional consolidometers. Beginning in the late 1970s, applications of the constant-flow method have been expanding in both research and practice. In most applications to date, hydraulic-conductivity tests have been conducted following conventional loading increments in one-dimensional consolidometers and following increments of three-dimensional consolidation in triaxial cells.

More recent innovations include a new flow-pump actuator that enables identical flow rates to be infused and withdrawn across opposite ends of a test specimen and the use of additional flow pumps to control the effective stress or the volume of a test specimen. These innovations provide a convenient

approach for obtaining hydraulic conductivity versus effective stress data in triaxial cells on a wide variety of materials, including sandstones and shales that cannot be trimmed and mounted in either fixed-ring permeameters or one-dimensional consolidometers.

In addition, these innovations provide a means to integrate constant-flow hydraulic conductivity measurements with continuous-loading consolidation tests on fully saturated specimens in both back-pressured consolidometers and in triaxial cells. This combined approach inherits the individual advantages of the constant-flow hydraulic-conductivity and continuous-loading consolidation methods compared with conventional incremental loading, constant-head, and falling-head methods. The hydraulic gradients induced during consolidation and those involved in hydraulic-conductivity measurements are small; a specimen can be consolidated at a constant rate of deformation; and both tests can be run far more quickly than the conventional alternatives. Another advantage of the combined methods is that direct measurements of both hydraulic conductivity and compressibility can be obtained while the specimen is being consolidated at any constant rate of deformation. This avoids the minimum deformation rate required in a CRD test to elevate the pore pressure at one end of the specimen by an amount sufficient for interpreting coefficient-of-consolidation or hydraulic-conductivity values or both. Finally, the time required for a combined test is governed solely by the selected deformation rate; hydraulic-conductivity measurements can be obtained as frequently as desired without affecting the duration of the test.

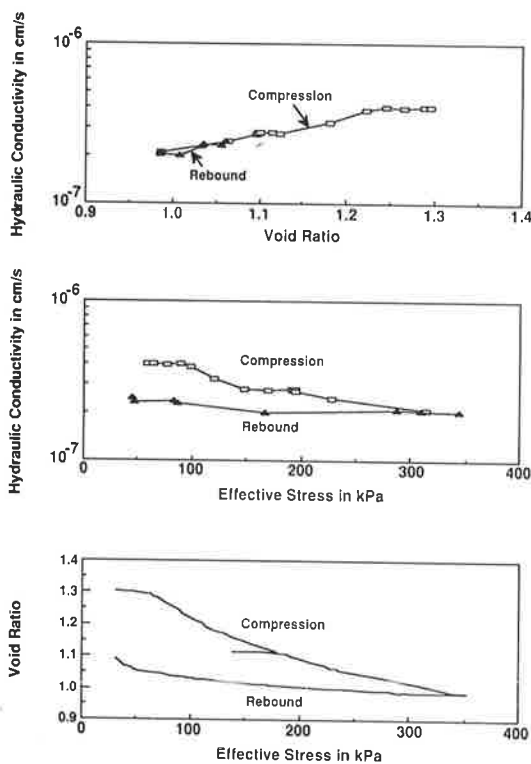


FIGURE 14 Void ratio versus effective stress (bottom), hydraulic conductivity versus effective stress (middle), and hydraulic conductivity versus void ratio (top) relationships for the test data in Figure 13.

REFERENCES

1. J. E. Alva-Hurtado and E. T. Selig. Survey of Laboratory Devices for Measuring Soil Volume Change. *Geotechnical Testing Journal, GTJODJ*, Vol. 4, No. 1, 1981, pp. 11–18.
2. H. W. Olsen, R. W. Nichols, and T. L. Rice. Low-Gradient Permeability Measurements in a Triaxial System. *Geotechnique*, Vol. 35, No. 2, 1985, pp. 145–157.
3. S. A. Aiban and D. Znidarcic. Evaluation of the Flow Pump and Constant Head Techniques for Permeability Measurements. *Geotechnique*, Vol. 39, No. 4, 1989, pp. 655–666.
4. H. W. Olsen. Darcy's Law in Saturated Kaolinite. *Water Resources Research*, Vol. 2, No. 6, 1966, pp. 287–295.
5. H. W. Olsen. Simultaneous Fluxes of Liquid and Charge through Saturated Kaolinite. *Proc., Soil Science Society of America*, Vol. 33, No. 3, 1969, pp. 338–344.
6. H. W. Olsen. Liquid Movement through Kaolinite under Hydraulic, Electric, and Osmotic Gradients. *Bulletin of the American Association of Petroleum Geologists*, Vol. 56, 1972, pp. 2022–2028.
7. D. van Zyl. Design, Construction, and Field Testing of a Heap Leach Clay Pad. *Symposium on Uranium Mill Tailings*, Ft. Collins, Colo., 1982, pp. 521–535.
8. D. van Zyl. Construction and Investigation of a Clay Heap Leach Pad. *Au & Ag Heap and Dump Leaching Practice* (J. B. Hiskey, ed.) . Proc. 1983 Fall Meeting, Society of Mining Engineers, American Institute of Mining, Metallurgical, and Petroleum Engineers, Salt Lake City, Utah, 1984, pp. 59–68.
9. V. Pane, P. Croce, D. Znidarcic, H. Y. Ko, H. W. Olsen, and R. L. Schiffman. Effects of Consolidation on Permeability Measurements for Soft Clays. *Geotechnique*, Vol. 33, No. 1, 1983, pp. 67–72.
10. H. W. Olsen, R. H. Morin, and R. W. Nichols. Flow Pump Applications in Triaxial Testing. *Advanced Triaxial Testing of Soil and Rock* (R. T. Donaghe, R. C. Chaney, and M. L. Silver,

- eds.). *ASTM STP 977*. American Society for Testing and Materials, Philadelphia, Pa., 1988, pp. 68–81.
11. H. W. Olsen, K. R. Nelson, and J. D. Gill. Flow Pump Applications in Geotechnical Measurements. *Proc., 2nd International Symposium on Environmental Geotechnology* (H. Fang and S. Pamukcu, eds.), Tongji University, Shanghai, China, Envo Publishing Company, Inc., Bethlehem, Pa., 1990.
 12. R. H. Morin and H. W. Olsen. Theoretical Analysis of the Transient Response from a Flow-Pump Permeability Test. *Water Resources Research*, Vol. 23, No. 8, 1987, pp. 1461–1470.
 13. R. H. Morin, H. W. Olsen, K. R. Nelson, and J. D. Gill. A Graphical Method for Determining the Coefficient of Consolidation, c_v , from a Flow-Pump Permeability Test. *Geotechnical Testing Journal, GTJODJ*, Vol. 12, No. 4, 1989, pp. 302–307.
 14. D. Znidarcic and S. A. Aiban. Discussion on "Some Measurements of Permeability of Kaolin," by Al-Tabba and Wood. *Geotechnique*, Vol. 38, No. 3, 1988, pp. 453–454.
 15. H. W. Olsen, Osmosis: A Cause of Apparent Deviations from Darcy's Law. *Canadian Geotechnical Journal*, Vol. 22, No. 2, 1985, pp. 238–241.
 16. R. E. Gibson. A Note on the Constant Head Test to Measure Soil Permeability in Situ. *Geotechnique*, Vol. 16, No. 3, 1966, pp. 256–259.
 17. Z. A. Al-Dhahir and S. B. Tan. A Note on One-Dimensional Constant Head Permeability Tests. *Geotechnique*, Vol. 18, No. 4, 1968, pp. 499–505.
 18. W. B. Wilkinson. Constant Head In Situ Permeability Tests in Clay Strata. *Geotechnique*, Vol. 18, 1968, pp. 172–194.
 19. K. Terzaghi. *Theoretical Soil Mechanics*, John Wiley, New York, N.Y., 1943, 510 pp.
 20. H. S. Carslaw and J. C. Jaeger. *Conduction of Heat in Solids*. Oxford University Press, New York, N.Y., 1959, 510 pp.
 21. J. D. Gill. *Simultaneous Measurement of Compressibility and Hydraulic Conductivity Using Volume Controlled Methods*. M.S. Thesis. Colorado School of Mines, Golden, 1989.

Publication of this paper sponsored by Committee on Soils and Rock Instrumentation.

Measurement of Shear and Compression Waves During Triaxial Testing

KENNETH C. BALDWIN, PEDRO DE ALBA, ADAM JONES, AND ISMAIL MENGUC

Researchers at the geotechnical laboratory at the University of New Hampshire have developed a technique for measuring shear (S) and compression (P) wave parameters of triaxial specimens. The triaxial end caps contain S and P wave transducers. Bender bimorphs are used for S waves and thickness expanders are used for P waves. These piezoelectric devices are separated from the triaxial specimen by a flexible window, which protects the transducers from failure due to moisture and allows proper coupling of the acoustic energy. Testing to date has focused on two areas. The first is determining the relationship between the acoustic characteristics of sand and liquefaction resistance. Results indicate that material-dependent one-to-one relationships can be established between S or P wave velocity and liquefaction resistance. Preliminary results from frequency domain measurements related to damping are encouraging as an indicator of sand fabric. The second area is the relationship between shear strength and S or P wave velocity in clays. Staged tests on marine clays indicate the effects of stress history and plasticity on this relationship.

Acoustic waves are transmitted by soils in ways which are characteristic of the particular fabric and density of the material. Thus, nondestructive, low-amplitude, high-frequency waves can be used to characterize individual soils. Based on this premise, the geomechanics group at the University of New Hampshire (UNH) is in the process of developing techniques for reliably measuring acoustic-wave velocities in the laboratory.

The long-term objective of this work is to develop testing methods to compensate for the effects of disturbance in recovering specimens from the field. Measurements of shear (S) and compression (P) wave velocity would be made in the field deposit with an acoustic cone or a closely spaced cross-hole setup. Specimens would be recovered and reconsolidated in a triaxial cell (or other apparatus) equipped with an acoustic measurement system until the in situ wave transmission characteristics were restored in the laboratory. Presumably, at that point the specimen would be restored to its in situ condition and could then be subjected to destructive testing along any desired stress path.

Consequently, the fundamental objective of our research effort was to investigate the potential for establishing correlations between large-strain mechanical properties and S or P wave transmission characteristics for different soils; this in turn has required the development of reliable instrumentation

for generating and receiving acoustic waves in a single triaxial specimen, which is then subjected to large-strain destructive testing under static or dynamic loading.

Presented in this paper is an overview of developments to date, which include the design of small acoustic transducers, capable of generating and receiving S and P waves and small enough to fit into the end caps of the triaxial cell, as well as the configuration of the required measurement system. Selected results from different studies are presented to illustrate the operation of the system.

ACOUSTIC TRANSDUCERS

The transducers generate and receive both S and P waves. Conventional wisdom in the geotechnical community is still that the P wave is carried by the water in saturated soils and thus provides no information on the soil fabric below the water table. However, Ishihara (1) pointed out that P -wave velocity in saturated soil depends essentially on the bulk modulus of the two-phase material and thus will be affected by the soil structure. The effect of soil fabric on the P -wave velocity is smaller than on the S -wave velocity; however, precise P -wave measurements can give much useful information. The use of P waves is most desirable from a practical point of view, because they are easier to generate both in the field and in the laboratory; in the experience of the authors, P waves produce a received signal with a leading edge that is easier to identify than that of S waves, thus greatly facilitating travel-time measurements.

The acoustic transducers, therefore, had to generate low-strain compression and shear disturbances that did not affect the soil fabric, yet provided sufficient signal strength to determine the acoustic parameters. The acoustic transducers had to provide a means of generating and receiving both S and P waves both before and during loading of the triaxial specimen under both static and dynamic conditions.

The underwater acoustics and marine geophysics community has a history of using water-tight acoustic transducers. Compression wave transducers have been routinely deployed for water column and sediment acoustic measurements (2-4). Shirley and Anderson (5,6) developed a corehead velocimeter that successfully deployed compression wave transducers in the cutter of a piston corer. They went on to develop an S -wave transducer for this device using a piezoelectric bender bimorph.

The bender is constructed from two longitudinally expanding piezoelectric ceramics sandwiched together. When a volt-

K. C. Baldwin, Mechanical Engineering Department, University of New Hampshire, Durham, N.H. 03824. P. de Alba, Civil Engineering Department, University of New Hampshire, Durham, N.H. 03824. A. Jones, Northrup, Devine and Tarbell, Inc., Portland, Maine 04103. I Menguc, Kingston-Warren Corp., Newfields, N.H. 03856.

age is applied across the bender, one side expands and the other contracts, resulting in a bending motion (Figure 1). As the voltage is varied sinusoidally, the bender produces a sinusoidally varying mechanical displacement. Conversely, a sinusoidal displacement of the bender causes the piezoelectric elements to produce a sinusoidally varying voltage. Thus, benders can both generate and receive *S* waves. The bender element was chosen because its mechanical impedance closely matched that of the sediment (6).

The design concepts embodied in the transducers used in the UNH research originated with the work of Shirley (7) and Baldwin et al. (4). The transducer has a cylindrical body that houses the piezoelectric elements and fits directly into modified triaxial endcaps. The *S*-wave transducers consist of an array of piezoelectric benders mounted in a base plate in a cantilevered fashion. A four-bender array is used to increase the active area in contact with the specimen. This enhances the ability to couple energy into the specimen. The free end of the benders is encapsulated in a flexible polyurethane window (Figure 2). The array generates and receives *S* waves at its resonant frequency. Similar approaches to piezoelectric *S*-wave transducer design for geotechnical testing using benders have been reported by Brunson and Johnson (8), Horn (9), Schultheiss (10), Strachan (11) and Dyvik and Madshus (12). The *S*-wave transducers involved in all these studies, however, used a single bender element that was not encapsulated but projected up to 10 mm into the specimen. This situation can lead to transducer failure due to mechanical loading, causing

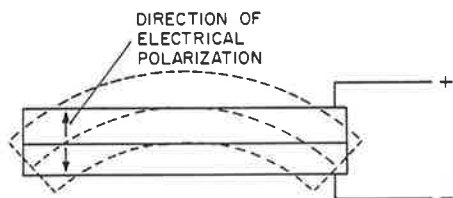


FIGURE 1 Operation of a piezoelectric bender element.

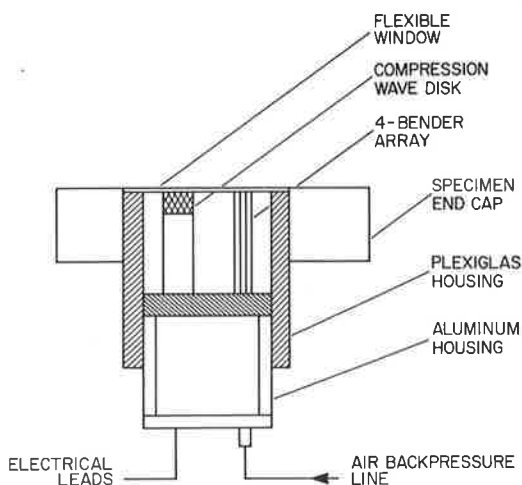


FIGURE 2 End-cap acoustic transducer with *S*- and *P*-wave piezoelectric elements.

undesired bending during insertion as well as short circuits due to moisture effects.

The compression wave transducer uses a thickness-expanding disk. The disk operates at its experimentally determined resonant frequency. The disk is mounted on a pedestal beside the bender array (Figure 2). The free surface of the disk is encapsulated in the flexible window next to the bender array.

The flexible window isolates the piezoelectric elements from the moisture in the soil specimens and provides a surface against which the soil specimens can react and be acoustically coupled to the *S*- and *P*-wave generating elements. The non-wetted side of the window is pressure-compensated to prevent implosion.

The transducer designed shown in Figure 2 was adapted to both 1.4-in.-diameter and 2.8-in.-diameter triaxial specimens. The smaller diameter was used for testing clays in staged triaxial tests, and the larger diameter was used for testing sand in cyclic triaxial liquefaction tests.

MEASUREMENT SYSTEM

The measurement system was configured to determine propagation times for acoustic pulses across a known specimen length. The acoustic travel time was necessary to determine the *P*- and *S*-wave velocities. The pulse-time delay configuration shown in Figure 3 was used to measure the acoustic travel time.

The pulse generator output was a 10 volt peak to peak, 4 cycle, gated sine wave for both *P*- and *S*-wave generation. The frequency was the only parameter that changed; for *P* waves, the frequency was approximately 140 kHz, and for *S* waves, the frequency was approximately 3 kHz. The signal was used to drive the *S*- or *P*-wave transmitting acoustic transducer and to simultaneously trigger the horizontal sweep on the digital oscilloscope, establishing zero time for the travel-time measurement.

The wave was received by the other transducer, and the signal from this receiver was amplified and band-pass filtered before being displayed on the digital oscilloscope. Band-pass

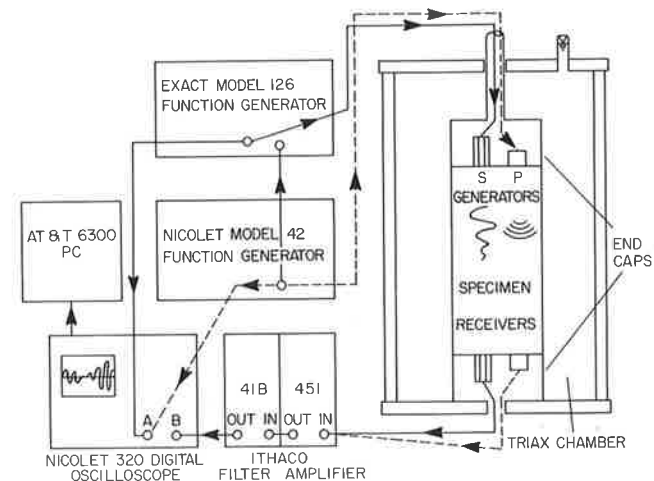


FIGURE 3 Schematic of the acoustic measurement system, transducers, and triaxial chamber.

filtering eliminated noise and passed only those frequencies around the resonant frequency.

The time base on the digital oscilloscope was set to 0.1 $\mu\text{sec}/\text{point}$ for P waves and 2 $\mu\text{sec}/\text{point}$ for S waves to permit the appropriate resolution in the time-delay measurements. The time base increments were selected based on the order of magnitude of the expected acoustic travel times.

The digital oscilloscope provided the time base for digitizing signals and making time-delay measurements. Internal software enabled an operator to create a program that stacked the received signals. Stacking is an averaging technique that has been used successfully in geophysics to enhance the leading edge (first arrival) and minimize noise in received signals. This technique was useful in S -wave velocity measurements and not so critical in P -wave measurements. After the prescribed number of received signals were stacked, the resulting signal was transferred to a personal computer using the WAVEFORM BASIC software package. The signals were stored on floppy disks for future analysis.

ACOUSTIC PARAMETERS

Two basic acoustic parameters, wave velocity and quality factor (Q), were determined using the data acquired with the transducer and measurement system. The wave velocity is related to the inherent stiffness, and Q is related to the inherent damping in the soil specimen.

Wave-velocity measurements were readily made from the acoustic time delay defined by the leading edge of the received signal. Both P - and S -wave velocities were determined by dividing the specimen length by the acoustic time delay. Of the two types of waves, the S -wave signal required more careful consideration because the leading edge was not always obvious.

The S - and P -wave velocities are important data in characterizing a soil, but alone they do not provide a distinctive characterization. In a study of the dynamic behavior of sands, (13), it was determined that characteristic relationships can be established between S - or P -wave velocity and liquefaction resistance, but the range of velocity change that covers the range of sand densities studied was relatively small. It was therefore desirable to extract additional information from the received signals, which would define other characteristic transmission parameters.

Q was borrowed from vibration and electrical circuit analysis. It is a frequency-domain parameter that is related to the center frequency of a signal's spectrum and the frequencies of the half-power points. A graphical representation is shown in Figure 4 (14). The simple expression defining Q from the spectrum is:

$$Q = \frac{f_{\text{center}}}{f_{\text{upper}} - f_{\text{lower}}}$$

where f_{center} is the resonant frequency and f_{upper} and f_{lower} are the upper and lower half power frequencies, respectively. From vibration theory Q is defined as follows (2):

$$Q = \frac{1}{2\zeta} \cong \frac{\pi}{\delta}$$

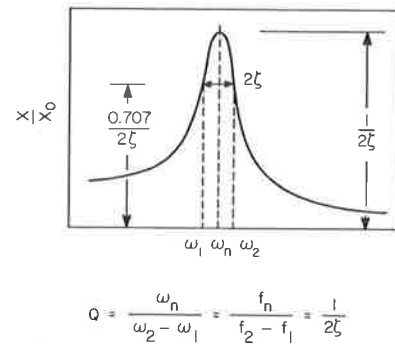


FIGURE 4 Generic spectrum level versus frequency plot indicating the parameters required to determine Q (14).

where ζ is the damping factor in the system and δ (≤ 0.3) is the logarithmic decrement (14).

There are two approaches to determining Q , but regardless of the approach used it is imperative that the transducer response be flat in the frequency band of interest. The measurement must display amplitude versus frequency variations that are indicative of the soil response, not the inherent transducer response.

The straightforward way to determine Q is to drive the transducer with a constant amplitude signal while varying the frequency and noting the changes in received amplitude with frequency. This is done using prescribed frequency increments over a frequency band in which the inherent transducer response is ± 0.5 dB. This method requires many signals to generate the desired result.

The second approach uses the spectrum calculated from the Fast Fourier Transform (FFT) of the stacked received signals. The FFT is the key to this method. It is important in Fourier analysis to define the maximum and minimum frequencies in the band of interest, but because the signals are band-pass filtered, these are known. Sampling the time series or the stacked acoustic signals to avoid aliasing requires sampling at the Nyquist frequency as a minimum. The period of the sampling frequency or digitizing rate is set by the time base on the digital oscilloscope. The time per point or digitizing rate for P - and S -wave data acquisition far exceeds the Nyquist condition.

PRELIMINARY RESULTS

Sands

The first application of the measurement system was to investigate whether unique relationships could be defined between liquefaction resistance and S - or P -wave velocities in the laboratory (13). For this purpose, cyclic triaxial liquefaction tests were carried out on several different sands; Figures 5 and 6 present results from this study for three uniform materials. Wave velocities, S and P , measured immediately before undrained cyclic loading are plotted against the normalized cyclic stress ratio, τ/σ' , required to cause liquefaction in 10 cycles, where τ is the applied cyclic shear stress and σ' is the initial effective confining pressure. These figures indi-

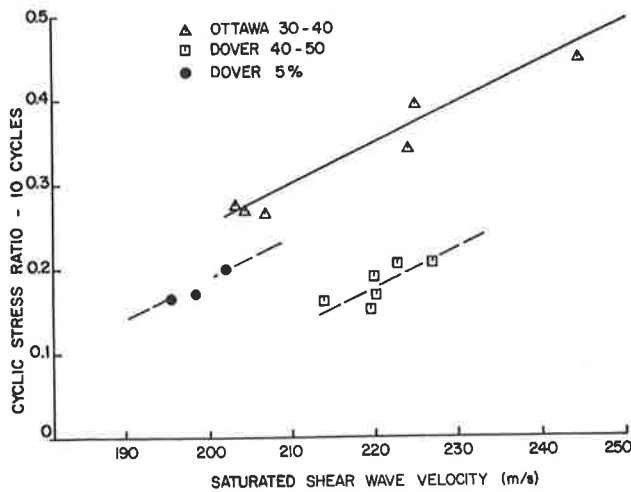


FIGURE 5 S-wave velocity versus liquefaction resistance for three uniform sands.

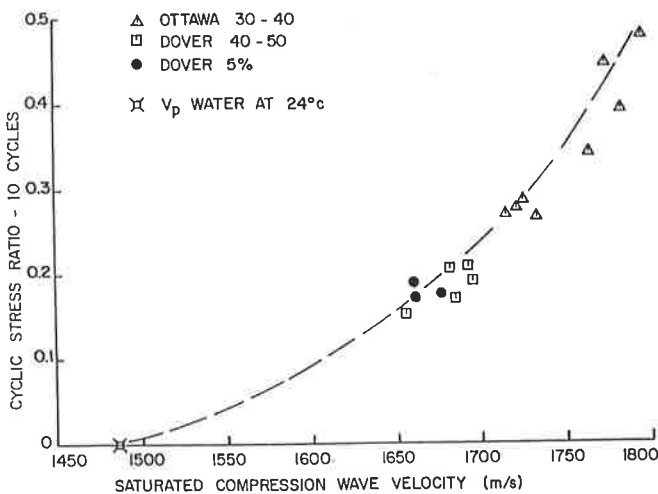


FIGURE 6 P-wave velocity versus liquefaction resistance for three uniform sands.

cate that the different materials display characteristic, individual trends, but that the velocity range for the relative density range studied in each material (roughly 55 to 80 percent) is perhaps 5 to 20 percent for *S* waves and 2 to 5 percent for *P* waves. The problem of detecting the leading edge of the acoustic signal also made the technique significantly operator dependent. Consequently, further studies were carried out to reduce operator-dependency in determining the wave velocities and to attempt to define other acoustic wave properties, which could be used to characterize the depositional state of a sand.

In the study of *S*-wave velocity and *Q* in sands by Menguc (15), the *S*-wave signals were amplified 70 dB and filtered in a band between 2.5 and 4.0 kHz. This resulted in an improved signal as seen in Figure 7a and b. The remaining noise on the leading edge was minimized by stacking as shown in Figure 7c. If an infinite number of signals were stacked, then the noise would be zero for the assumed zero-mean process

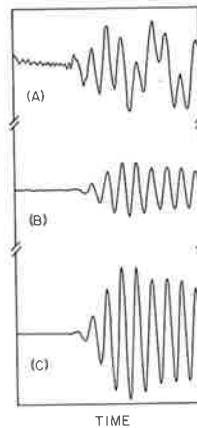


FIGURE 7 Received shear wave signals: (a) unprocessed, (b) filtered, and (c) filtered and stacked.

(16). The “infinite” amount of signals translated to 100 in this case. These improvements, coupled with a fast digital oscilloscope, enhanced the leading edge definition and the velocity determination.

The major concern in this effort was the frequency domain measurements to determine *Q*. The transducers were determined to possess a flat response, ±1 dB, in a band from 1.8 to 4.05 kHz. This information helped establish the bandwidth of the filter defined previously. The stacked signals were demeaned and smoothed by applying a cosine taper to the 5 percent of the time series at each end of the series. This minimizes the energy in side lobes when performing an FFT (16).

Fast Fourier transforms were performed on the signals. The resulting amplitude versus frequency plots were normalized relative to the amplitude at the resonant peak. The normalization was

$$dB = 10 \log \frac{A(f)}{A(f_{res})}$$

where *A*(*f*) is the amplitude at any frequency in the frequency band, and *A*(*f*_{res}) is the resonant frequency amplitude. The peak was at 0 dB, and all other amplitudes were down (or negative) dB's. This presentation facilitated finding the -3 dB points required to define *Q*. The results for dry-pluviated specimens of a uniform medium sand (Holliston 00) are shown in Figure 8 and summarized in the following table.

Relative Density (percent)	Quality Factor	Log Decrement
53.5	2.25	1.395
66.2	2.47	1.272
70.5	2.57	1.222
72.7	3.00	1.046

Quality factor increases with increasing relative density (*Dr*). This implies that the specimens with high *Dr* have narrow bands, (*f_u* - *f_l*), and have less damping. This is indicated in the data in the table, where the log decrement is also presented. This result is reinforced by an observation made on the nonnormalized FFT results. The amplitude of the signal at higher *Dr* is higher for the same level of excitation. This indicates that less acoustic energy is dissipated in the speci-

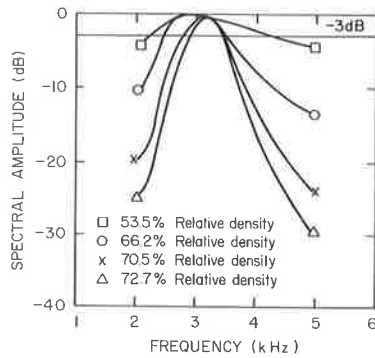


FIGURE 8 S-wave spectral amplitude (dB) plots for various relative densities.

men, that is, looser fabrics attenuate more readily than denser fabrics.

It should be noted that Q shows a 33 percent variation over the restricted relative density range studied for this material, a uniform sand with a D_{50} of 0.5 mm. Thus, these preliminary results suggest that Q may be a sensitive indicator of soil fabric.

Clays

A collateral study to those previously described was carried out to determine the relationship between undrained shear strength in marine clays and S or P -wave velocity, using a measurement system analogous to that developed for sands (17,18). Preliminary results are reported here for four clay samples, two from the Canadian Beaufort Sea, and two from an exposed marine clay deposit near Portsmouth, New Hampshire.

Staged triaxial tests were performed on each sample following the procedure suggested by Nambiar et al. (19). Further, since the Beaufort material was overconsolidated to a degree that was only approximately known, it was further decided to combine the staged test with the SHANSEP procedure (20), in which samples would first be consolidated to stress levels in excess of the maximum past pressure and then rebounded to obtain known degrees of overconsolidation. This procedure would have the additional important advantage of minimizing the effects of sample disturbance. Analogous tests were carried out in the Portsmouth material, to validate the technique for a deposit with known properties (21).

Staged test results are reported for two Beaufort Sea samples, C3 and D4, and two Portsmouth samples, P1 and P2. The four samples were all consolidated beyond their maximum past pressure into the normally consolidated range, as previously described.

It is interesting to remark that all samples clearly exhibited normalized behavior as defined by Ladd and Foote (20) with the undrained strength (S_u) following a relationship for overconsolidated materials of the form

$$\frac{S_u}{\sigma'} = S(\text{OCR})^m$$

where

σ' = effective consolidation stress,
 $S = S_u/\sigma'$ ratio for normally-consolidated material, and
 OCR = overconsolidation ratio.

The values of (m) varied from about 0.79 for the Beaufort clays to 0.88 for the Portsmouth material. These are within the range reported by Olsen et al. (22) for marine clays. This behavior suggests that the combined stage testing-SHANSEP procedure gives reasonable results. This is further confirmed by the effective-stress friction angle of 21 degrees obtained for the normally consolidated Portsmouth clay, which compares well with that reported by Ladd (21) for this material.

Figure 9, from Baldwin et al. (18), shows the variation in S -wave velocity (V_s) with consolidation stress (σ'), for all consolidation stages including the shear tests. Two trends can clearly be discerned; one defined by samples P1 and P2, both of which have a plasticity index (PI) of about 15, and the other by the more plastic C3 and D4, which have PI values of 27 and 35 respectively. Curves fitting the general trends indicated are shown in the figure; in both cases, V_s increase with confining pressure follows an exponential law of the form

$$V_s = K(\sigma)^n$$

where $n = 0.219$ for the P1 and P2 set; and 0.194 for the C3 and D4 data. These values compare well with $n = 0.25$, which was proposed for clays by Hardin and Drnevich (23).

Figure 10 shows the values of S -wave velocity (V_s) obtained immediately before shear testing, plotting against the undrained shear strength (S_u) for the various materials. Although each material is seen to behave slightly differently, for purposes of discussion, two general behavior trends may be imposed on the data: one for the more plastic Beaufort materials and the other for the Portsmouth clays. Within each trend, the tests on the normally consolidated material are seen to define a different branch from those on overconsolidated material. The data further suggest that V_s may be a sensitive indicator of undrained strength change; for example, for the P1 and P2 data, the slope of the normally consolidated branch is about 1.3 kPa/(m/sec), and for C3 and D4 it is approximately 2.8 kPa/(m/sec).

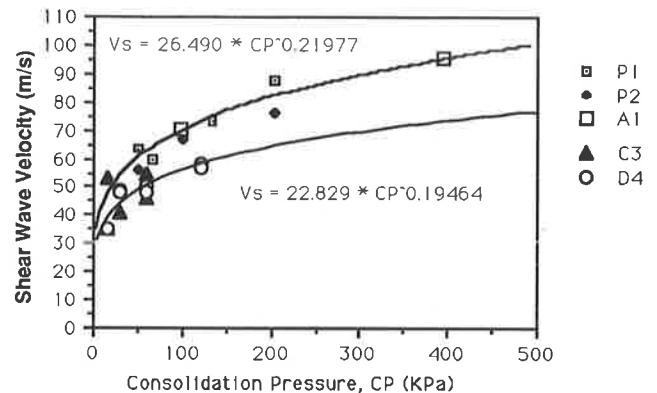


FIGURE 9 Consolidation pressure versus S -wave velocity for two marine clays (18).

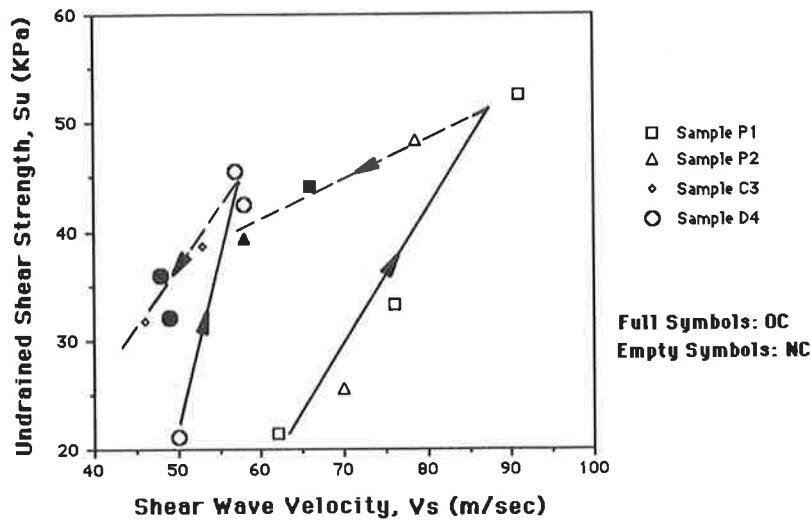


FIGURE 10 S-wave velocity versus undrained shear strength for two marine clays (18).

Figure 11 shows analogous results for P-wave velocities (V_p) versus undrained shear strength for the same materials. In this case, each material defines a unique trend; an interesting feature of this plot is that the normally consolidated branches of the V_p-S_u relationships have similar slopes.

As for sands, V_s is seen to be a more sensitive indicator than V_p ; the slopes of the normally consolidated branches for V_p in Figure 11 range from about 0.4 to 0.7 kPa/(m/sec), which is roughly half the values obtained for V_s and, perhaps more importantly, the velocity change over the range of undrained shear strength studied is on the order of 13 to 47 percent of the lowest value measured in the case of V_s , and only 2 to 3 percent for V_p .

SUMMARY

A system has been developed and tested that has the capability of measuring P- and S-wave parameters in triaxial spec-

imens, which are then subjected to large-strain destructive testing under static or dynamic loading. It is obvious that definite conclusions cannot be reached on the basis of the limited data available, yet general trends may be noted:

- As expected, V_s is a more sensitive indicator of large-strain behavior than V_p ; however, given the relative ease of generating and receiving P waves in the field and in the laboratory, precise V_p measurements can be a useful auxiliary indicator.

- For both sands and clays, each soil seems to follow a characteristic relationship between large-strain strength properties and S- and P-wave velocity. Consequently, in order to relate S- or P-wave measurements in the field to large-strain strength behavior, the characteristic relationship for that particular deposit must be established.

- In clays, stress history is important; the same clay in an overconsolidated state will follow a different S_u-V_s or S_u-V_p relationship than in a normally consolidated state. The

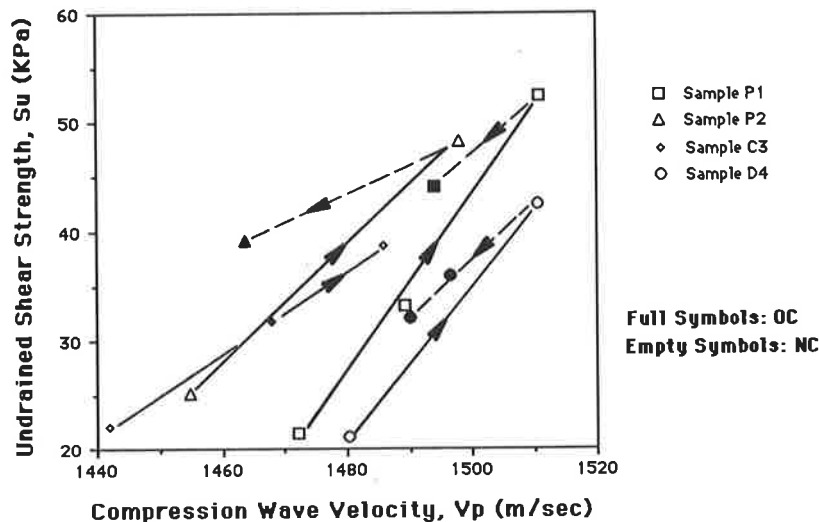


FIGURE 11 P-wave velocity (V_p) versus undrained shear strength (S_u) for two marine clays.

SHANSEP procedure may be useful in removing disturbance effects and developing the S_w -wave velocity relationships in clays that exhibit normalized behavior.

• In sands, laboratory testing has shown that unique relationships can be distinguished between liquefaction resistance and V_s or V_p for different sands prepared by the same procedure or between series of samples of the same sand prepared by different procedures. The Q -factor has been seen to be a sensitive indicator of material density for specimens prepared by the same method. All these results suggest that acoustic measurements are sensitive to all factors (including stress history) that affect sand fabric, so that field specimens reconstituted in the laboratory to their field V_s , V_p and Q -factor values may exhibit large-strain behavior similar to that of the undisturbed field material.

ACKNOWLEDGMENTS

This work was funded in part by the Geological Survey of Canada, the UNH/UMO Sea Grant Program, the UNH Hubbard Fund, and the UNH Eliot Fund, and for their respective contributions the authors are thankful.

REFERENCES

1. K. Ishihara. Propagation of Compressional Waves in a Saturated Soil. *Proc., International Symposium on Wave Propagation and Dynamic Properties of Earth Materials*, University of New Mexico Press, Albuquerque, 1968, pp. 195–206.
2. E. L. Hamilton. Sound Velocity and Related Properties of Marine Sediments, North Pacific. *Journal Geophysical Research*, Vol. 75, 1970, pp. 4423–4446.
3. M. L. Silver and C. A. Moore. Shipboard Measurement of Acoustic Velocities in Sediment Cores. Paper OTC 1546. *Proc., 4th Off-shore Technology Conference*, 1972.
4. K. C. Baldwin, B. Celikkol, and A. J. Silva. Marine Sediment Acoustic Measurement System. *Ocean Engineering*, Vol. 8, No. 5, 1981, pp. 481–488.
5. D. J. Shirley and A. L. Anderson. *Compressional Wave Profiler for Deep Water Measurements*. Technical Report ARL-TR-74-5. Applied Research Laboratories, University of Texas at Austin, 1974.
6. D. J. Shirley and A. L. Anderson. *Acoustic and Engineering Properties of Sediments*. Report ARL-TR-75-58. Applied Research Laboratory, University of Texas at Austin, 1975.
7. D. J. Shirley. An Improved Shear Wave Transducer. *Journal of the Acoustical Society of America*, Vol. 63, No. 5, 1978, pp. 1643–1645.
8. B. A. Brunson and R. K. Johnson. Laboratory Measurements of Shear Wave Attenuation in Saturated Sand. *Journal of the Acoustical Society of America*, Vol. 68, No. 5, 1980, pp. 1371–1375.
9. I. W. Horn. Some Laboratory Experiments on Shear Wave Propagation in Unconsolidated Sands. *Marine Geotechnology*, Vol. 4, No. 1, 1980, pp. 31–54.
10. P. J. Schultheiss. Simultaneous Measurement of P and S Wave Velocities During Conventional Laboratory Testing Procedures. *Marine Geotechnology*, Vol. 4, No. 4, 1981, pp. 343–367.
11. P. Strachan. An Investigation of the Correlation Between Geophysical and Dynamic Properties of Sand. *Proc., Oceans 81, Vol. 1, Publication No. 81CH1685-7 of the Institute of Electrical and Electronic Engineers Council on Ocean Engineering*, Boston, Mass., 1981, pp. 399–403.
12. R. Dyrvik and C. Madshus. Lab Measurements of G_{max} Using Bender Elements. *Advances in the Art of Testing Soils Under Cyclic Conditions*, ASCE, 1985.
13. P. de Alba, K. C. Baldwin, V. Janoo, G. Roe, and B. Celikkol. Elastic-Wave Velocities and Liquefaction Potential. *Geotechnical Testing Journal*, GTJODJ, Vol. 7, No. 2, ASTM 1984, pp. 77–87.
14. W. Thomson. *Theory of Vibration with Applications*, Prentice-Hall, Inc., 1981.
15. I. Menguc. A Study of the Experimental Evaluation of Shear Wave Characteristics in Saturated Sands. M.S. thesis. University of New Hampshire, Durham, 1986.
16. J. S. Bendat and A. G. Piersol. *Random Data Analysis and Measurement Procedures*. Wiley-Interscience, 1971.
17. A. Jones. Measurements of Acoustic Properties of Marine Clays in Triaxial Tests, Project paper for the M.S. University of New Hampshire, Durham, 1989.
18. K. C. Baldwin, P. de Alba, and A. N. Jones. Relationship Between Acoustic and Mechanical Properties of Two Marine Clays. *Shear Waves in Marine Sediments* (in press), 1991.
19. M. R. M. Nambiar, G. V. Rao, and S. K. Gulhati. Multistage Triaxial Testing: A Rational Procedure. *Strength Testing of Marine Sediments: Laboratory and In-Situ Measurements* (R. C. Chaney and K. R. Demars, eds.). ASTM STP 883. Philadelphia, Pa., 1985, pp. 274–293.
20. C. C. Ladd and R. Foote. New Design Procedures for Stability of Soft Clays. *Journal of the Geotechnical Engineering Division*, ASCE, Vol. 100, No. GT7, 1974, pp. 763–786.
21. C. C. Ladd. Test Embankment on Sensitive Clay. *ASCE, SMFD Specialty Conference on Performance of Earth and Earth Supported Structures*, Purdue University, 1972, pp. 101–129.
22. H. W. Olsen, T. L. Rice, P. W. Mayne, and R. D. Singh. Piston Core Properties and Disturbance Effects. *Journal of the Soil Mechanics and Foundation Division*, ASCE, Vol. 112, No. 6, 1986, pp. 608–625.
23. B. O. Hardin and V. P. Drnevich. Shear Modulus and Damping in Soils: Measurement and Parameter Effects. *Journal of the Soil Mechanics and Foundation Division*, ASCE, Vol. 98, No. SM6, 1972, pp. 603–624.

Publication of this paper sponsored by Committee on Soils and Rock Instrumentation.

Finite Element Analysis of Partially Saturated Seepage Through Compacted Fills

TIMOTHY D. STARK AND WILLIAM G. BIXBY

An extensive two-dimensional finite element seepage analysis was conducted to study the parameters affecting the wetting-induced behavior of compacted fills. The results showed that decreasing the placement water content increases the initial suction pressures, which increases the time required for hydrocompression and the magnitude of hydrocompression. The analysis also showed that the time required for hydrocompression increased almost linearly with fill depth. The surface infiltration was found to migrate unevenly through the fill material, resulting in an uneven dissipation of the suction pressures and thus differential ground movements. Because the suction pressures had to be dissipated before a drain could be functional, the installation of a canyon drain or side drain or both did not reduce the amount of hydrocompression or the time required for hydrocompression. However, the drains did cause the wetting front to migrate through the fill in a more uneven pattern than without a drain. To reduce the amount of infiltration and thus hydrocompression, the site should be carefully graded to promote runoff and drains should be installed beneath the irrigation points to intercept the infiltration. If water is allowed to infiltrate the fill, the pavements and structures should be designed for the differential ground movements estimated from the procedure described herein.

Most transportation and residential and commercial construction in southern California involves sites composed of hills and canyons. A typical development consists of grading the site by excavating the hillsides and filling the canyon with the spoils. The depths of the compacted fills are steadily increasing with some in excess of 50 m. Previous research by Nwabukei and Lovell, (1), Brandon et al., (2), and Lawton et al., (3) has shown that compacted soil undergoes a softening when the fill becomes soaked or wetted. The soaking removes the initial suction pressures in the soil, which results in a decrease in effective stress and thus soil modulus. This phenomenon is known as hydrocompression and has resulted in surface deformations that have exceeded tolerable limits. The amount of hydrocompression that occurs depends on the placement water content and relative compaction. In general, the amount of hydrocompression increases with decreasing placement water content, decreasing relative compaction, and increasing overburden pressure.

If expansive soils are incorporated into the fill, the fill behavior and thus the surface deformations become even more complex. As the upper portion of the fill becomes wetted, the soil will expand as a result of the small vertical stresses

applied near the fill surface. As the wetting front moves deeper into the fill, the vertical stresses become large enough to resist the soil expansion, and the compacted soil will hydrocompress. Therefore, if expansive soils are placed in a fill, the compacted soil will swell at shallow depths and compress at deeper depths as a result of the differences in the applied vertical stress.

From a series of laboratory oedometer tests in which compacted specimens are inundated at various overburden stresses, a relationship between fill depth or overburden stress and axial strain, such as that shown in Figure 1, can be obtained. From such a relationship the amount of swell or hydrocompression at various depths in the fill and the depth at which the soil changes from an expansive behavior to a hydrocompression behavior can be easily determined. Figure 1 can also be used to estimate the net movement of the ground surface by (a) dividing the fill into sublayers, (b) calculating the fill depth at the mid-point of each sublayer, (c) estimating the axial strain of each sublayer using Figure 1 and the fill depth at the mid-point of each sublayer, (d) multiplying the appropriate axial strain by the initial thickness of the sublayer, and (e) summing the swell or hydrocompression of all the sublayers to estimate the net ground surface movement. The differential settlement between any two points is estimated from the difference of the net ground surface movement at each of the points. These calculations are analogous to those used for the estimation of consolidation settlements.

The major element missing in this analysis is the time rate of the surface movement, which is controlled by the time rate of wetting of the fill. Because most, if not all, of the infiltration is due to surface irrigation, the wetting front usually migrates from the top to the bottom of the fill. As a result, the upper portion of the fill usually undergoes expansion or hydrocompression before the bottom of the fill becomes wetted. This uneven wetting of the fill led to the following questions concerning the wetting-induced behavior of compacted fills:

1. What is the time required for compacted fills to become fully wetted and undergo expansion or hydrocompression?
2. At what time should distressed pavements and structures be repaired?
3. What is the effect of placement water content on the rate of wetting?
4. What is the effect of drains placed at various locations in the fill on the migration of the wetting front through the fill?

T. D. Stark, Department of Civil Engineering, University of Illinois, Urbana, Ill. 61801. W.G. Bixby, BSI Consultants, 16880 West Bernardo Drive, San Diego, Calif. 92127.

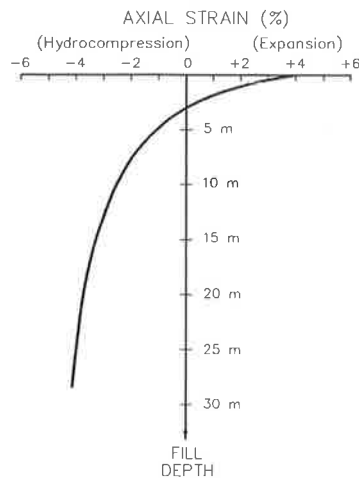


FIGURE 1 Axial strain after inundation as a function of fill depth.

The results of an extensive two-dimensional finite element seepage analysis that was conducted to clarify these aspects of the wetting-induced behavior of compacted fills are described in this paper.

CANYON GEOMETRIES AND SOIL PROPERTIES USED IN ANALYSIS

A confined canyon with 2.5 to 1 side slopes and a bottom width of 10 m was analyzed. Because of the uncertainties involved in modeling the contact between the compacted fill and the formational material of the canyon, the canyon boundaries were assumed to be impermeable. For the shallower depths (5, 10, 16.7, and 25 m) the effect of a canyon drain was investigated by analyzing each depth with and without a drain located at the center of the canyon bottom. For the deeper fills (30 and 50 m) the effects of placing drains at various locations along the canyon walls were also investigated. The effect of placement water content, 2 percent dry versus 2 percent wet of optimum, was investigated using a fill depth of 5 m.

Because of its availability, the Stadium Conglomerate Formation has been used in a large number of fills in the San Diego area. The conglomerate formation is classified as a silty gravel (GM) according to the Unified Soil Classification System, with particle sizes ranging more than 40 mm to less than 0.001 mm. To simulate typical fill operations, a relative compaction of 90 percent based on the Modified Proctor Compaction test (ASTM Standard D1557-78) was used throughout the laboratory testing and finite element analysis.

Cedergren (4) and Carey et al. (5) have shown that the permeability of soils is extremely sensitive to the quantity, character, and distribution of the finest fractions. Their test results on gravelly soils showed that the fines filled the voids and controlled the permeability of the soil. As a result, it was decided that the fine-grained particles of the Stadium Conglomerate would also control the seepage characteristics. Because the ASTM Standard (D2325-81) for the determination of the capillary-moisture relationship using the porous plate

apparatus requires the use of soil passing the No. 10 sieve, all of the laboratory tests were conducted on the minus No. 10 material. The minus No. 10 material makes up approximately 50 percent by weight of the Stadium Conglomerate and classifies as a silty sand (SM).

The optimum water content and maximum dry density, obtained from five Modified Proctor Compaction tests using Method A and the minus No. 10 material, are approximately 10 percent and 19.3 kN/m^3 , respectively. Based on the results of four falling head permeability tests, the average steady-state permeability of the minus No. 10 material compacted at 2 percent wet of optimum was measured to be $2.3 \times 10^{-3} \text{ m/day}$. The average steady-state permeability at 2 percent dry of optimum was obtained from the results of 3 falling head tests and was measured to be $3 \times 10^{-3} \text{ m/day}$. Both of the measured permeabilities are in good agreement with values reported by Sherard et al. (6) and Stark and Duncan (7) for similar soils and were also in excellent agreement with the permeability of $2.85 \times 10^{-3} \text{ m/day}$ measured by Sorben and Sherrod (8) for a local fill composed of Stadium Conglomerate. Based on data presented by Sherard et al. (6), the horizontal permeability was estimated to be four times the vertical permeability.

The drying portion of the volumetric water content and suction pressure relationship, also referred to as the characteristic curve, was obtained from the results of capillary-moisture tests performed using a porous-plate apparatus. The wetting portion of the characteristic curve was estimated using the measured drying curve and data presented by Liakopoulos (9) and Croney and Coleman (10). The relationship between permeability and suction pressure was estimated using the Green and Corey (11) analytical procedure. A number of researchers, such as Elzeftawy and Cartwright (12) and GEOSLOPE (13), have presented data that show that the Green and Corey method provides an excellent estimate of the relationship between permeability and suction pressure. An extensive parametric study revealed that the analytical results were not sensitive to the shape of the characteristic curve or the permeability-suction pressure relationship. The parametric study also showed that the main parameter affecting the analytical results is the steady-state permeability and the initial suction pressure heads.

To determine the initial suction pressures, 20 oedometer tests were conducted using specimens compacted at 2 percent wet (volumetric water content of 0.214) and 2 percent dry (volumetric water content of 0.144) of optimum and a Modified Proctor relative compaction of 90 percent. From these tests the relationship between volumetric water content and fill depth or overburden stress was obtained for both placement water contents. This relationship was confirmed by field testing in which moisture content samples were obtained from two 1-m-diameter bucket-auger borings that were drilled immediately after completion of a 24-m-deep Stadium Conglomerate fill. The moisture content samples were carefully excavated from the wall of the boring every 0.3 m for the entire fill depth. The volumetric water content for each sample was plotted versus fill depth; the resulting relationship was in excellent agreement with the laboratory relationship.

Using the verified relationship between volumetric water content and fill depth and the previously determined characteristic curve, the initial suction pressure at any fill depth

could be obtained. As a result, the fact that the volumetric water content increased with depth was incorporated into the analysis. The final soil parameters used in the seepage analysis of the Stadium Conglomerate at 2 percent wet of optimum are summarized below. The steady-state permeability properties were as follows:

- Vertical permeability = $K_v = 2.3 \times 10^{-3}$ m/day,
- Horizontal permeability = $K_h = 9.2 \times 10^{-3}$ m/day,
- $K_h = 4K_v$, and
- K_h is inclined 0° to the horizontal.

The pressure versus K_h properties are summarized in the following table.

Suction Pressure (kPa)	K_h (m/day)
0	9.2×10^{-3}
-6.2	3.7×10^{-3}
-8.4	2.0×10^{-3}
-10.6	9.8×10^{-4}
-13.8	4.2×10^{-4}
-17.3	1.5×10^{-4}
-32.0	3.4×10^{-5}
-62.5	4.9×10^{-6}

The pore-water storage properties are summarized in the following table.

Volumetric Water Content	Suction Pressure (kPa)
0.35	0
0.33	-3
0.30	-6
0.26	-10
0.24	-20
0.23	-40
0.22	-60
0.21	-80

The soil parameters used in the seepage analysis of the Stadium Conglomerate at 2 percent dry of optimum are summarized below. The steady-state permeability properties were as follows:

- Vertical permeability = $K_v = 3.0 \times 10^{-3}$ m/day,
- Horizontal permeability = $K_h = 1.2 \times 10^{-2}$ m/day,
- $K_h = 4K_v$, and
- K_h is inclined 0° to the horizontal.

The pressure versus K_h properties are presented in the following table.

Suction Pressure (kPa)	K_h (m/day)
0	1.2×10^{-2}
-2.15	2.02×10^{-3}
-3.7	5.15×10^{-4}
-7.1	8.61×10^{-5}
-38	5.16×10^{-6}
-96	1.26×10^{-6}
-156	3.92×10^{-7}
-216	7.97×10^{-8}

The pore-water storage properties are summarized in the following table.

Volumetric Water Content	Suction Pressure (kPa)
0.31	0
0.28	-2
0.24	-5
0.225	-10
0.22	-20
0.214	-40
0.20	-80
0.142	-246

FINITE ELEMENT SEEPAGE PROGRAMS AND APPLIED BOUNDARY CONDITIONS

PC-SEEP, developed by GEOSLOPE (13), was used for this study because of its capability of producing graphical input and output. Before selecting PC-SEEP, pressure heads were calculated for a number of fill geometries and material properties using PC-SEEP and UNSAT1, developed by Neuman (14). The calculated pressure heads from both programs were in good agreement. It should be noted that both programs assume constant total volume and volume change due to hydrocompression and expansion, which is not taken into account in the analysis.

The effects of precipitation and irrigation were simulated by applying an influx at irrigation locations along the top of the fill. The irrigation pattern shown in Figure 2 was determined from surveying a number of typical commercial building sites. It can be seen that a 30-m-wide irrigated strip usually separates the lots or acts as a buffer between the adjacent street, and a 30-m-wide parking lot is provided for each build-

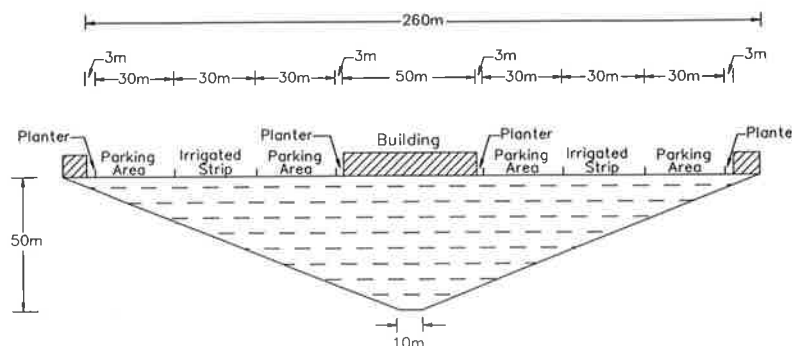


FIGURE 2 Typical irrigation pattern for a 50-m-deep canyon fill.

ing. A 3-m-wide irrigated planter was usually found immediately adjacent to the buildings. The ratio of irrigated area to fill surface was measured to be approximately 25 percent. Based on data presented by Sorben and Sherrod (8), an infiltration rate of 0.46 m/year was used in the irrigation pattern.

Extensive seepage analyses showed that the full canyon geometry, shown in Figure 2, could be modeled using half of the canyon and designating the centerline of the canyon as a no-flow boundary. Thus, the pressure head contours presented here only illustrate half of the canyon.

CALIBRATION OF SOIL PROPERTIES

To investigate the accuracy of the seepage parameters previously described, the measured time rate of settlement of a local fill was compared with the time calculated for migration of the wetting front through the fill. The Villa Trinidad subdivision in San Diego County experienced settlements in excess of 0.3 m due to hydrocompression in the 22-m-deep fill. Brandon et al. (2) reported that the average placement water content of the fill was approximately 0.6 percent wet of optimum and the Modified Proctor relative compaction was at or near 90 percent throughout the fill. Therefore, the settlement was attributed to hydrocompression and not variations in the placement conditions.

Brandon et al. (2) also presented settlement survey data which showed that hydrocompression was completed after approximately 10.1 years of irrigation. Because the fill material was predominantly Stadium Conglomerate, it was decided to use this case history to compare the measured time rate of settlement with that estimated using PC-SEEP and the previously described soil parameters for a placement water content of 2 percent wet of optimum. However, the initial suction pressures were based on a water content of 0.6 percent wet of optimum.

After approximately 8.8 years of irrigation, the calculated wetting front had passed through the entire fill and reached the bottom of the 22-m-deep fill. As a result, the majority of the suction pressures had been dissipated, and thus the majority of the fill would have undergone hydrocompression after 8.8 years of irrigation. The calculated time was approx-

imately 1.5 years faster than the measured time. Soil classification tests of the Villa Trinidad fill material showed that 75 percent of the fill material classified as a clayey sand (SC), and the remaining 25 percent classified as an SM. In addition, the placement water content varied from -2 to $+2$ percent of the optimum, with the average placement water content being approximately 0.6 percent wet of optimum. The slightly lower average placement water content will cause higher initial suction pressures and thus a lower permeability. Therefore, the difference in the measured and calculated hydrocompression times was attributed to the slight difference in the placement water content and the difference in seepage characteristics of a clayey-sand and silty-sand. However, the good agreement between the measured and calculated times for the Villa Trinidad fill provides a good indication that the seepage parameters used for the Stadium Conglomerate are reasonable and can be used to estimate the hydrocompression times for the other fill depths.

SEEPAGE CHARACTERISTICS IN 5-m-DEEP COMPACTED FILL

Figures 3 through 6 show the behavior of the pressure head contours in the 5-m fill without a canyon drain and the Stadium Conglomerate compacted at a water content 2 percent wet of optimum. Because 25 percent of the ground surface is irrigated, only an irrigation strip at the centerline of the canyon was used in the 5 meter deep fill (Figure 3). The figure shows the pressure head contours, in meters, after one day of irrigation. Placement of the Stadium Conglomerate at 2 percent wet of optimum results in suction pressures of almost -7.4 m at the surface of the fill and -7.2 m near the bottom of the fill. Therefore, the entire fill is partially saturated and susceptible to swell or hydrocompression. After one day of irrigation, the infiltration has started to dissipate the suction pressures and a -7 m pressure head contour has appeared beneath the irrigation strip. After 1 year of irrigation the infiltration has caused a large dissipation of the suction pressures near the centerline of the fill (Figure 4). The zero pressure head contour, shown in Figure 4 as a dashed line, is

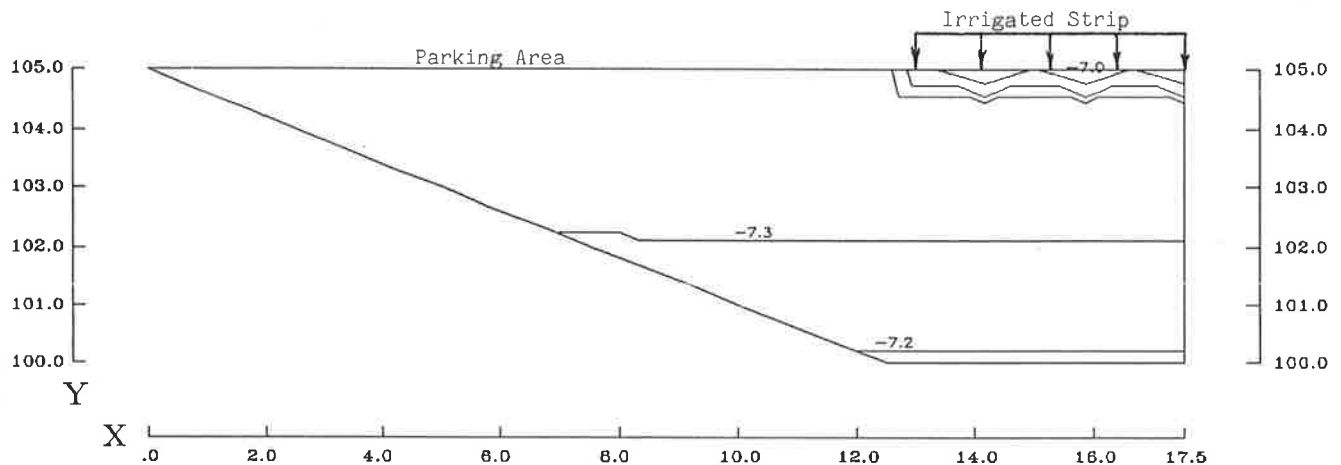


FIGURE 3 Pressure head contours after 1 day of irrigation for the 5-m-deep fill placed at 2 percent wet of optimum.

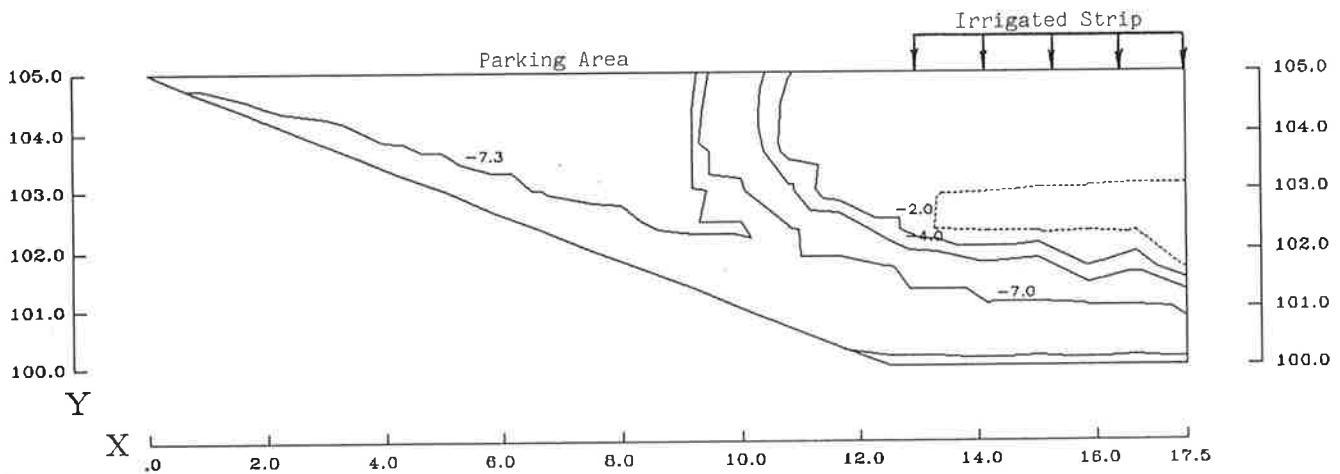


FIGURE 4 Pressure head contours after 1 year of irrigation for the 5-m-deep fill placed at 2 percent wet of optimum.

approximately 2 to 3 m below the ground surface. The zero pressure head contour or wetting front delineates the boundary between partially saturated and fully soaked conditions, the soil that has and has not undergone hydrocompression.

After an elapsed irrigation time of about 1.5 years the wetting front has reached the impermeable boundary at the bottom of the canyon fill (Figure 5). The suction pressures in the shallow portion of the fill continue to dissipate as a result of horizontal seepage, whereas the deeper portion of the fill has already undergone hydrocompression. Before, a drain installed at the bottom center of the canyon would not have functioned because of the existence of suction pressures, and thus a lack of "free" water. Once the wetting front reached the bottom of the canyon and dissipated the suction pressures, the canyon drain could become operational and remove any free or excess water. Therefore, to accurately simulate the influence of a canyon drain in subsequent analyses of the 5-m-deep fill, the drain was not activated until the wetting front reached the canyon bottom, that is, after 1.5 years of irrigation.

After approximately 4 years of irrigation a steady-state seepage condition is reached with the long-term zero pressure

head contour or phreatic surface rising to the ground surface (Figure 6). This is due to the impermeable canyon walls preventing water from leaving the fill. The final location of the phreatic surface will depend on the actual permeability of the canyon walls, and whether a canyon drain is installed.

The results of falling-head permeability and oedometer tests revealed that the degree of saturation of the test specimens after a steady-state seepage condition was obtained ranged from 90 to 98 percent. Therefore, the time required for full hydrocompression is the time necessary to remove the majority of the suction pressures and not necessarily obtain a fully saturated condition. In the 5-m-deep fill, approximately 2.5 years was required for the entire fill to become fully soaked and thus undergo hydrocompression.

The effects of different irrigation patterns on the hydrocompression of the fill were also studied by varying the location of the irrigation strip. Figure 7 shows the behavior of the pressure head contours with the irrigation strip moved to the left side of the canyon instead of at the center. It can be seen that after 2 years of irrigation the wetting front has descended along the canyon wall and has reached the canyon bottom. Therefore, the shallow portion of the fill has under-

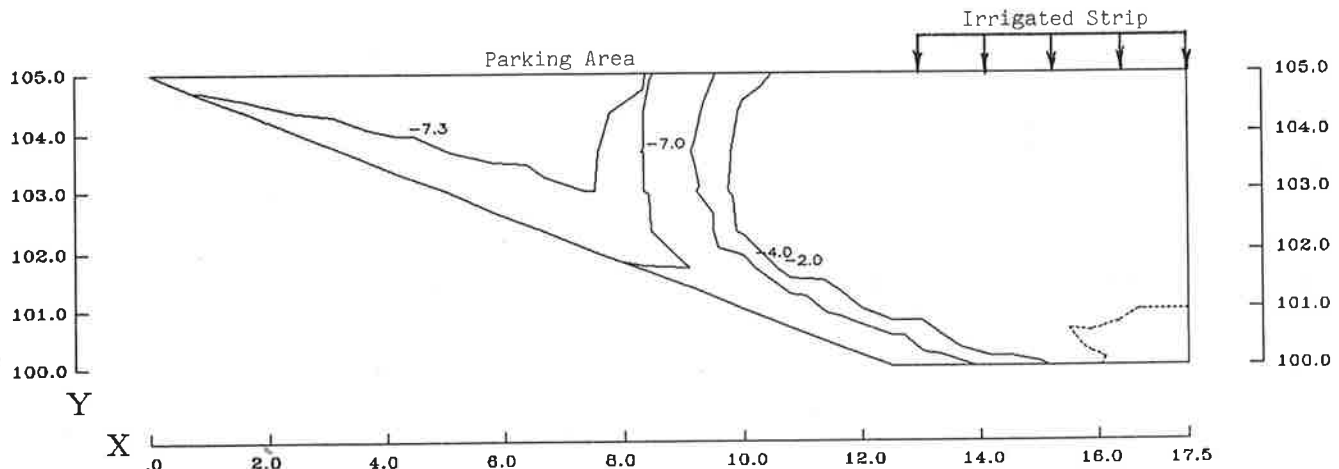


FIGURE 5 Pressure head contours after 1.5 years of irrigation for the 5-m-deep fill placed at 2 percent wet of optimum.

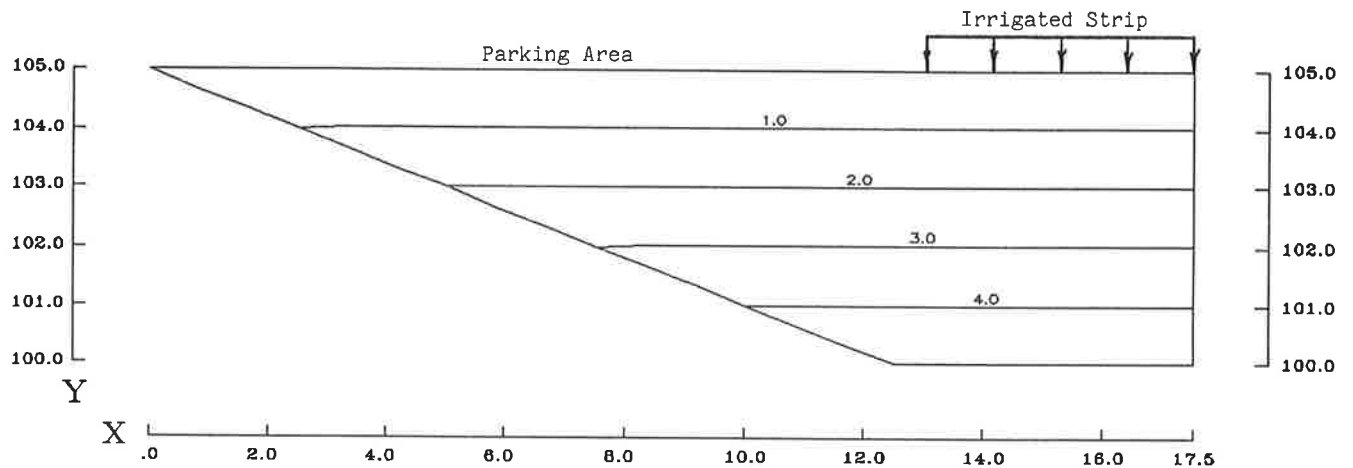


FIGURE 6 Pressure head contours after 4 years of irrigation for the 5-m-deep fill placed at 2 percent wet of optimum.

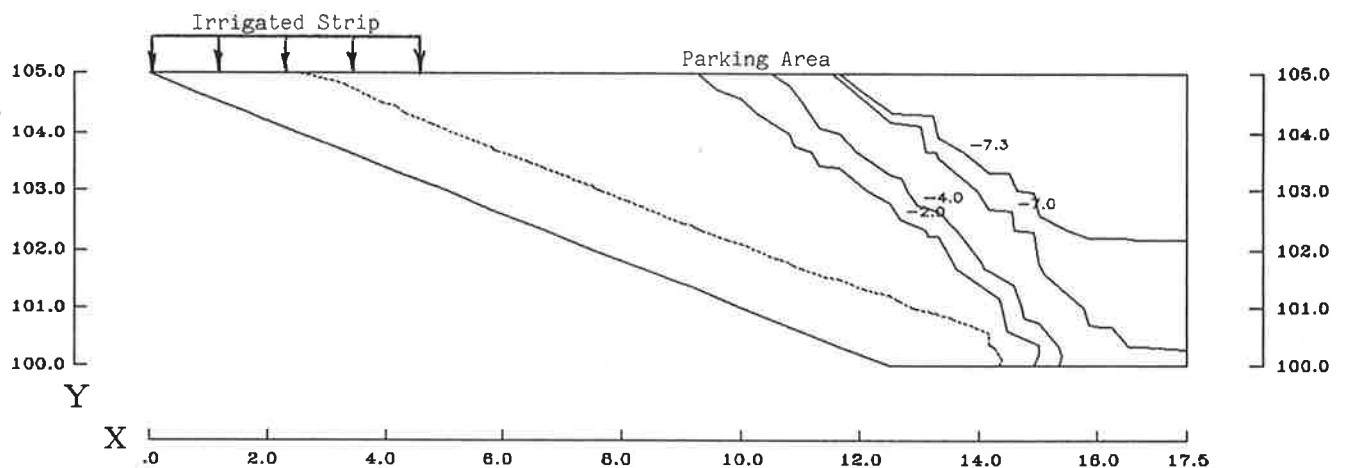


FIGURE 7 Pressure head contours after 2 years of irrigation in the shallow portion of the 5-m-deep fill placed at 2 percent wet of optimum.

gone hydrocompression or expansion or both while the suction pressures in the middle of the fill are still dissipating. In the previous case, after 1.5 years of irrigation the center portion of the canyon had undergone full soaking and thus hydrocompression (Figure 5). Therefore, differences in irrigation patterns will result in different migration patterns of the wetting front and thus hydrocompression.

After 5.3 years of irrigation, the long-term phreatic surface returned to the ground surface, just as it did in Figure 6, and a steady-state seepage condition was achieved. This is approximately 1.3 years longer than was required for the previous case, in which the irrigation strip was located at the centerline of the fill. During the analysis it was found that the irrigation was ponding because of the shallow fill depths below the irrigation strip. Because ponding was not allowed in the analysis, this loss of irrigation contributed to the additional 1.3 years required for a steady-state seepage condition.

From this comparison it can be concluded that the irrigation pattern will affect the time required for hydrocompression to occur and the pattern of differential settlements. If an infinitely wide and deep homogeneous fill is irrigated uniformly,

the wetting front should migrate uniformly through the fill. This should result in a uniform hydrocompression or expansion or both. However, the irrigation pattern, fill geometry, and soil properties are rarely homogeneous, and the infiltration migrates unevenly through the fill, especially in the non-irrigated areas. This causes deformations to occur at different times and locations. These results show that irrigation patterns as well as soil variability contribute significantly to the development of differential settlements. The location of the irrigation areas should be carefully selected and the building sites or roadway easements carefully graded to minimize the amount of infiltration. The installation of drains beneath the irrigation areas may aid in reducing the amount of infiltration and thus surface deformation that occurs.

Because the time required for a steady-state condition is shorter when the irrigation strip is placed at the centerline of the fill, this was considered to be the worst case, and the remaining analyses were conducted with the largest irrigation strip placed at the centerline of the canyon.

Figure 8 shows the behavior of the pressure head contours in the 5-m-deep fill placed at 2 percent dry of optimum. It can be seen from Figure 8 that the initial suction pressures

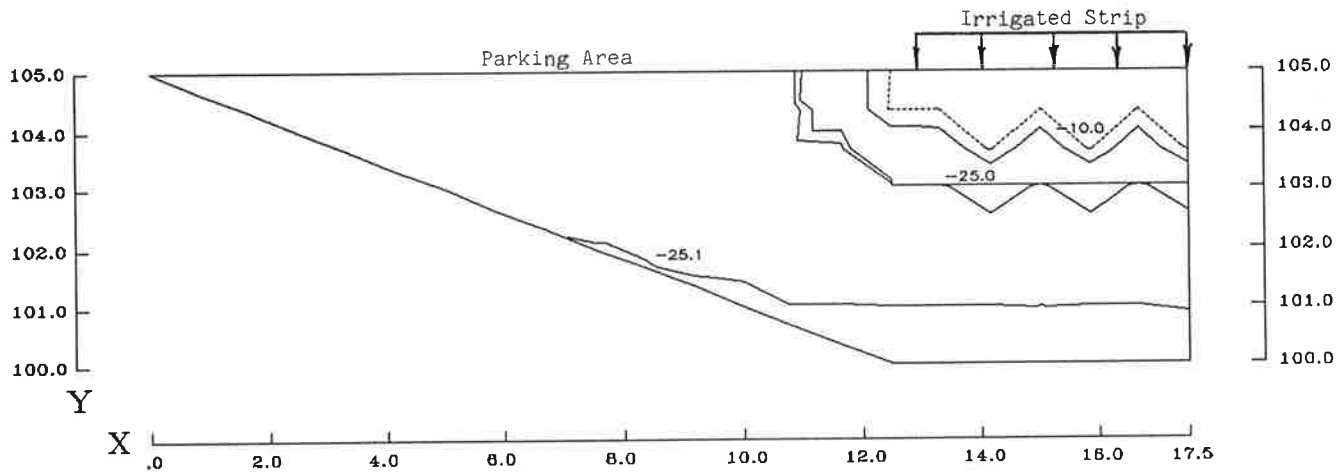


FIGURE 8 Pressure head contours after 4 years of irrigation in a 5-m-deep fill placed at 2 percent dry of optimum without a canyon drain.

ranged from -25 to -25.1 m, which is significantly higher than the -7 to -7.3 m suction pressures observed for a placement water content 2 percent wet of optimum. After approximately 4 years of irrigation the suction pressures have only dissipated to a depth of 1.5 meter (Figure 8). In the 2 percent wet of optimum case, a steady-state condition was reached after 4 years (Figure 6). This is due to the large initial suction pressures and the accompanying decrease in permeability. After almost 14 years of irrigation, the 5-m-deep fill with a placement water content 2 percent dry of optimum reached a steady-state seepage condition with the phreatic surface at or near the ground surface, shown previously in Figure 6.

Figure 9 shows the behavior of the pressure head contours in the 5-m fill with a canyon drain installed at the centerline of the canyon and a placement water content of 2 percent wet of optimum. Canyon drains are usually installed to remove any water that is encountered during the canyon "clean-out" and seepage that migrates through the fill after construction. As noted earlier, the drain will not begin to function until the surrounding suction pressures have been dissipated. As a result, the canyon drain was activated 1.5 years after the start of irrigation, which was the time required for the

wetting front to reach the bottom of the canyon (Figure 5). Approximately 3 years after the drain began to function (4.5 years after the start of irrigation) the steady-state condition shown in Figure 9 was reached. Despite the existence of a free-flowing drain, the continued irrigation at the canyon centerline caused the long-term phreatic surface to rise above the canyon bottom. From this study it was estimated that a 1-m-wide drain has a radius of influence of 1 to 3 m. However, the canyon drain does prevent the wetting front from rising to the ground surface, as shown previously in Figure 6. It is important to note that the installation of a canyon drain does not reduce the amount of hydrocompression that takes place near the center of the fill. The differential settlement may be even greater in fills that have a canyon drain because the wetting front migrates more unevenly through the fill when a drain is installed (Figure 9).

SEEPAGE CHARACTERISTICS IN 50-m-DEEP COMPACTED FILL

Figures 10 and 11 illustrate the behavior of the pressure head contours in the 50-m-deep fill with only a canyon drain

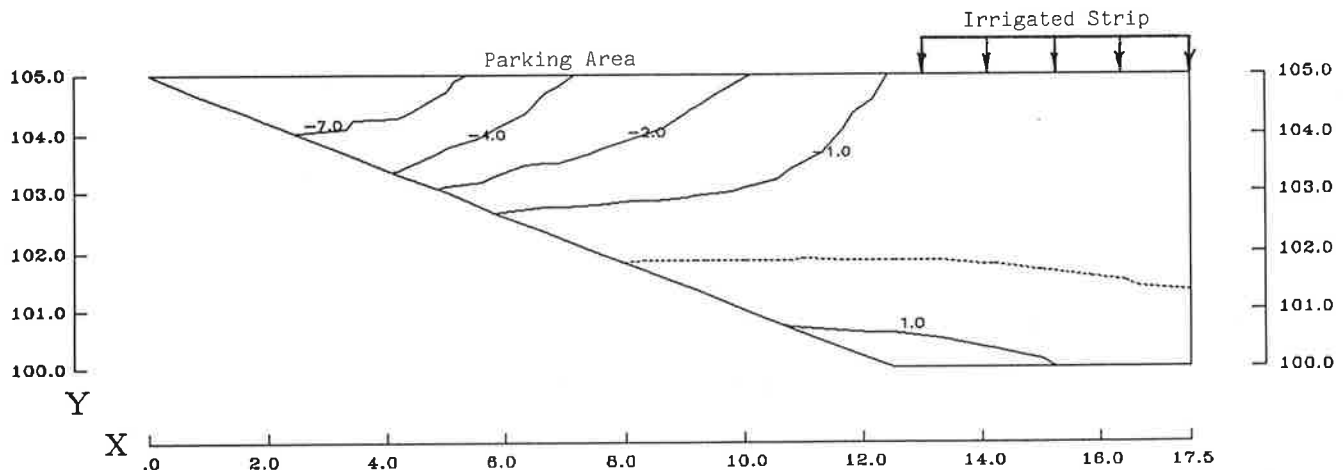


FIGURE 9 Pressure head contours after 4.5 years of irrigation in a 50-m-deep fill placed at 2 percent wet of optimum with a canyon drain.

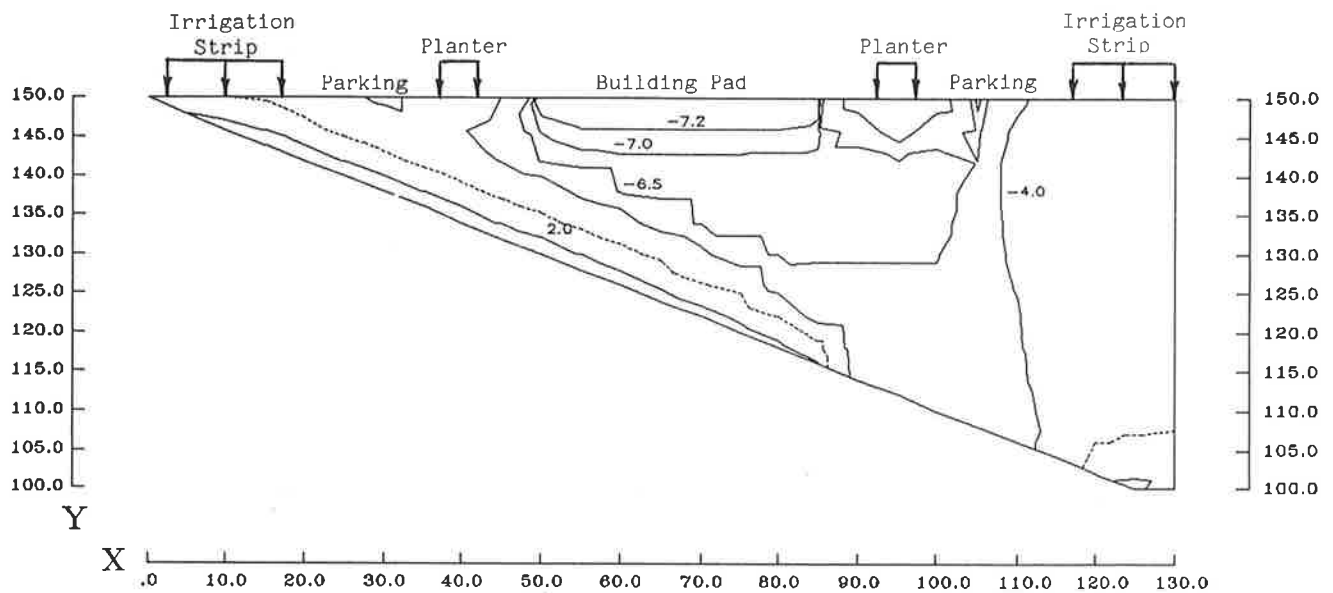


FIGURE 10 Pressure head contours after 14.8 years of irrigation in a 50-m-deep fill placed at 2 percent wet of optimum with a canyon drain.

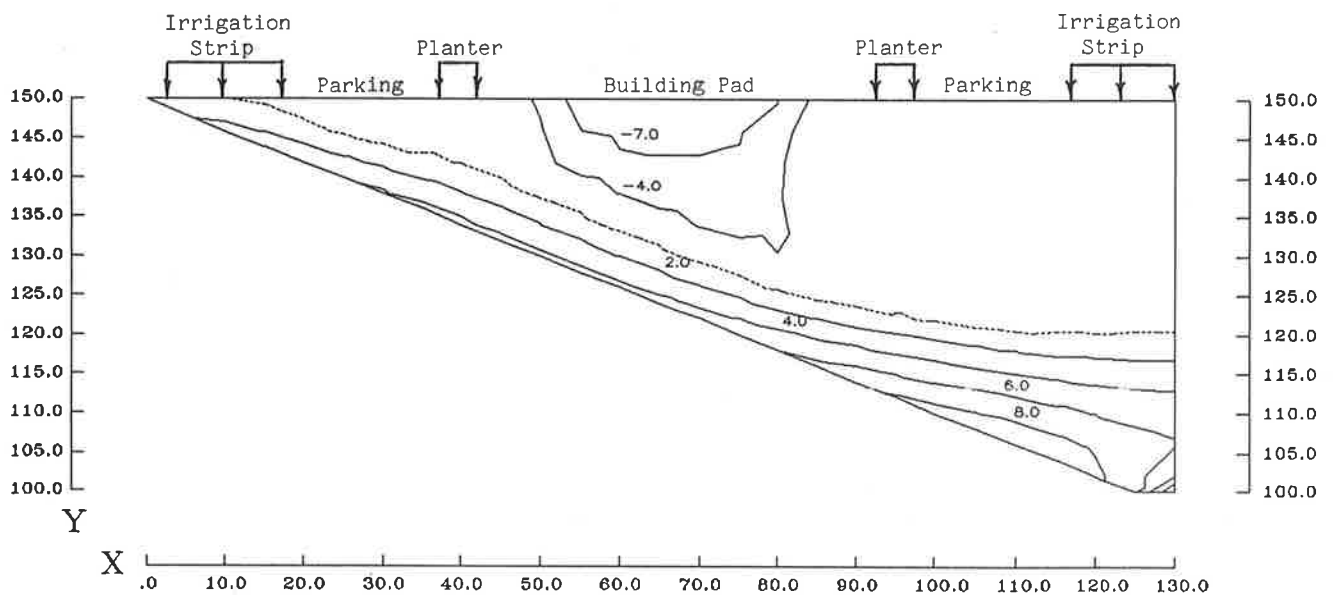


FIGURE 11 Pressure head contours after 30.7 years of irrigation in a 50-m-deep fill placed at 2 percent wet of optimum with a canyon drain.

installed at the centerline of the canyon. The placement conditions are a water content 2 percent wet of optimum and a Modified Proctor relative compaction of 90 percent. The irrigation pattern shown in Figure 2 was used for the 50-m-deep fill. After 14.8 years of irrigation the wetting front beneath the irrigation strip at the centerline of the fill reached the canyon bottom and the canyon drain began to function (Figure 10). It can be seen that the initial suction pressures of -7.2 m were still present below the building pad. The irrigation at the shallow end of the fill resulted in a wetting front that developed and descended along the canyon wall. After 30.7 years of irrigation, or 16 years after the canyon drain began functioning the two wetting fronts have joined

and a steady-state condition is achieved (Figure 11). The long-term phreatic surface remains about 30 m below the surface because of the installation of a canyon drain, which dissipates the positive pressure heads in the fill. It can also be seen that the majority of the suction pressures in the fill have been dissipated except underneath the building pad. The initial suction pressure of -7.2 m has dissipated unevenly underneath the building pad, which will probably result in differential soil expansion or hydrocompression or both.

Figure 12 shows the behavior of the pressure head contours in the 50-m fill with a canyon drain and drains installed in the canyon wall directly below the 3 irrigated strips. The first side drain, located at an x coordinate of 10 m, began functioning

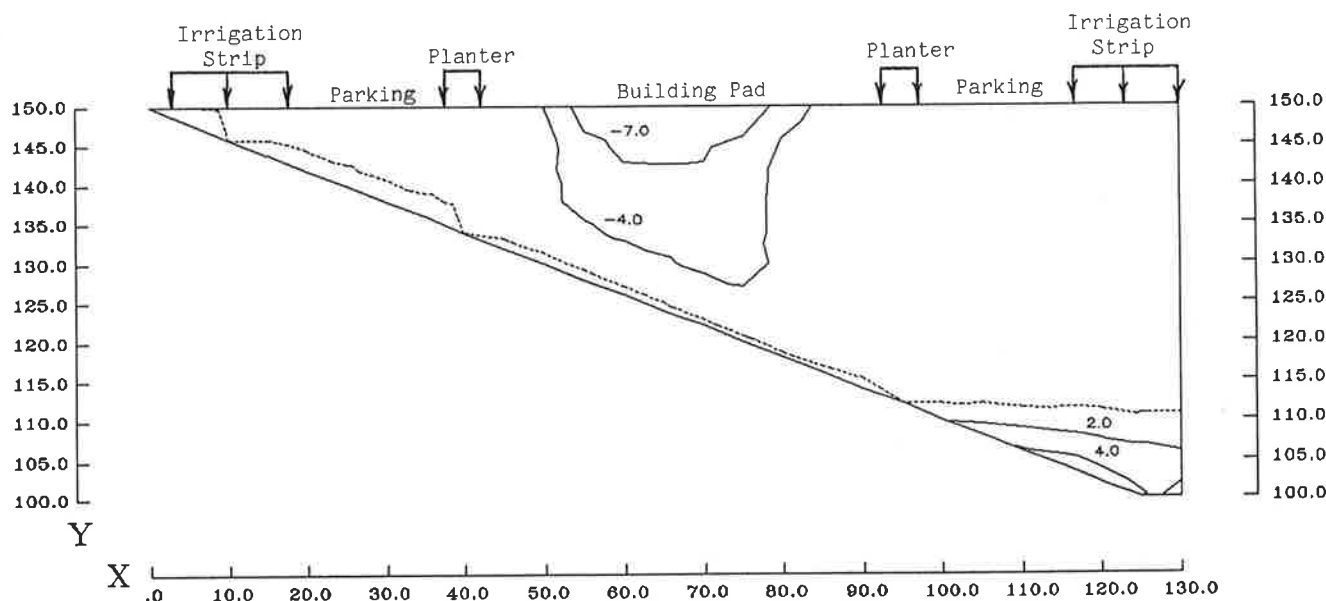


FIGURE 12 Pressure head contours after 37.7 years of irrigation in a 50-m-deep fill placed at 2 percent wet of optimum with canyon and side drains.

after approximately 2.4 years of irrigation. This is the time required for the first wetting front to reach this location and dissipate the surrounding suction pressure. Approximately 10.7 years after irrigation began, the wetting front had migrated along the canyon wall and reached the location of the second side drain, which is directly below the planter at an *x* coordinate of 40 m. Approximately 14.8 years after irrigation began, the wetting front reached the canyon bottom. This is the same amount of time that was required for the wetting front to reach the canyon bottom in the 50-m fill with only a canyon drain. This reaffirms the conclusion that drains have a limited zone of influence. After 33.8 years of irrigation, the wetting front had descended along the canyon wall and reached the location of the final side drain at an *x* coordinate of 95 m. After 37.7 years of irrigation the steady-state seepage condition shown in Figure 12 was achieved. The long-term phreatic surface parallels the canyon wall except where it intersects the three side drains. At the deepest part of the fill, the phreatic line remains approximately 10 m above the canyon drain as a result of the limited influence of the canyon drain.

CONCLUSIONS

The extensive finite element seepage analysis described herein showed that the most important parameter affecting the time required for hydrocompression is the placement water content. If the Stadium Conglomerate is placed at a water content of 2 percent wet of optimum and a Modified Proctor relative compaction of 90 percent, the initial suction pressures are approximately -7.4 m at the fill surface. If the Stadium Conglomerate is placed at a water content of 2 percent dry of optimum, the initial pressure heads exceed -25 m at the fill surface. The finite element analysis showed that approximately 2.5 and 14 years of irrigation are required to complete hydrocompression in a 5-m-deep compacted fill with place-

ment water contents of 2 percent wet and 2 percent dry of optimum, respectively. This substantial time difference is due to the larger initial suction pressures and thus the lower permeability associated with the 2 percent dry of optimum water content. A lower placement water content will also cause a larger amount of hydrocompression or expansion or both as a result of the larger initial suction pressures.

The time required for hydrocompression was also a function of the fill depth. It can be seen from Figure 13 that without canyon or side drains installed in the fill, the time required for hydrocompression increased almost linearly with fill depth. In all of the cases shown in Figure 13, 25 percent of the fill surface was irrigated at a rate of 0.46 m/year, on the basis of data presented by Sorben and Sherrod (8).

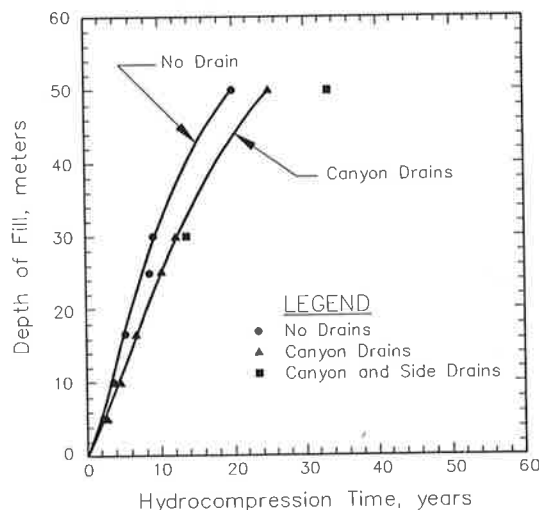


FIGURE 13 Time required for hydrocompression of Stadium Conglomerate fills placed at 2 percent wet of optimum and a Modified Proctor relative compaction of 90 percent.

It can also be seen from Figure 13 that the installation of a canyon drain resulted in hydrocompression times that were slightly longer than the no-drain case. The drains also caused the wetting front to migrate through the fill in a more uneven pattern than the no-drain case. Therefore, it was concluded that the installation of canyon or side drains or both may increase the amount of differential settlement because the fill undergoes a more uneven wetting pattern.

Because the canyon boundaries were assumed to be impermeable, the steady-state phreatic surface was located at or near the ground surface if a canyon drain was not installed. The installation of a canyon drain prevented the phreatic surface from rising to the surface of the fill by dissipating some of the positive pressure heads. If a canyon drain was installed, the steady-state phreatic surface was located at a depth of 0.5 to 0.7 times the depth of the fill.

Based on the analytical results, it was also concluded that the canyon drain did not become operational until the suction pressures around the drain were dissipated. Once the suction pressures were dissipated, "free" water could flow to the drain, which would remove the excess water from the fill. Because the fill material must become soaked or wetted before the canyon and side drains will function, the installation of drains will not reduce the amount of hydrocompression and expansion that will occur.

The seepage analysis also showed that typical surface irrigation patterns will result in an uneven migration of the wetting front through the fill material. The actual migration pattern of the wetting front depends on the location and number of irrigation points and drains installed in the fill. Uneven migration of the wetting front will result in hydrocompression occurring at different times and at different locations in the fill. If expansive soils are incorporated into the fill, the ground movements will become even more complex because some of the fill will be swelling while other portions are hydrocompressing. It is anticipated that this uneven wetting contributes significantly to the differential settlements observed in roadways and structures built on compacted fills. To reduce the amount of differential settlement due to seepage, the fill should be carefully graded to reduce the amount of infiltration. Drains can be installed underneath the irrigation points to intercept the infiltration. If drains are not installed, the fill should be irrigated as evenly as possible so that the wetting front will migrate as uniformly as possible through the fill. If water is allowed to infiltrate the fill, the pavements and structures should be designed for the movements estimated using the procedures described herein.

ACKNOWLEDGMENTS

The authors express their appreciation to Geocon, Inc. of San Diego, California, for providing financial support and the

Stadium Conglomerate samples tested herein. The authors wish to thank in particular Jim Likins, Tom Langpap, Mike Hart, and John Hoobs of Geocon, Inc. for their helpful suggestions during the course of this study. Joe Vettel and Dan Diehr, research assistants at San Diego State University, performed the laboratory tests and assisted with the finite element analyses, respectively.

REFERENCES

1. S. O. Nwabuokei and C. W. Lovell. Compressibility and Settlement of Compacted Fills. *Consolidation of Soils: Testing and Evaluation*. ASTM STP 892. ASTM, Philadelphia, Pa., 1986, pp. 184–202.
2. T. L. Brandon, J. M. Duncan, and W. S. Gardner. Hydrocompression Settlement of Deep Fills. *Journal of Geotechnical Engineering*, ASCE, Vol. 116, No. 10, 1990, pp. 1536–1548.
3. E. C. Lawton, R. J. Fragaszy, and J. H. Hardcastle. Collapse of Compacted Clayey Sand. *Journal of Geotechnical Engineering*, ASCE, Vol. 115, No. 9, 1989, pp. 1252–1267.
4. H. R. Cedergren. *Seepage, Drainage and Flow Nets* (4th ed.). John Wiley and Sons, Inc., New York, N.Y., 1988.
5. A. S. Cary, B. H. Walter, and H. T. Harstad. Permeability of Mud Mountain Dam Core Material. *Transactions*, ASCE, Vol. 108, 1943, pp. 719–728.
6. J. L. Sherard, R. J. Woodward, S. F. Giziensk, and W. A. Clevenger. *Earth-Rock Dams*, John Wiley and Sons, Inc., New York, N.Y. 1963, 725 pp.
7. T. D. Stark and J. M. Duncan. Mechanisms of Strength Loss in Stiff Clays. Geotechnical Engineering Research Report GT 87-5. Virginia Polytechnic Institute, Blacksburg, 1987.
8. D. R. Sorben and K. L. Sherrod. Groundwater Occurrence in the Urban Environment: San Diego, California, *Proc. San Diego Association of Geologists*. Geology of Southwestern San Diego County, California and Northwestern Baja California, G.T. Farsard, ed. 1977, pp. 67–74.
9. A. C. Liakopoulos. *Theoretical Solution of the Unsteady Unsaturated Flow Problems in Soils*. International Association of Scientific Hydrology, The Netherlands, Vol. 10, 1965.
10. D. Croney and J. D. Coleman. Soil Structure in Relation to Soil Suction (pF). *Journal of Soil Science*, Vol. 5, No. 1, 1954, pp. 75–84.
11. R. E. Green and J. C. Corey. Calculations of Hydraulic Conductivity: A Further Evaluation of Some Predictive Methods. *Proc., Soil Science Society of America*, Vol. 35, 1971, p. 308.
12. A. Elzeftawy and K. Cartwright. Evaluating the Saturated and Unsaturated Hydraulic Conductivity of Soils. *Unsaturated Hydraulic Conductivity of Soils*. STP 746, ASTM, Philadelphia, Pa. 1981, pp. 168–181.
13. GEOSLOPE Programming, Ltd. *PC-SEEP, A Finite Element Program for Seepage Analysis*. Canada, 1987.
14. S. P. Neuman. *UNSAT1—A Finite Element Program for Flow in Saturated/Unsaturated Porous Media*. Research Report. Israel Institute of Technology, Haifa, Israel, 1972.

Broadening the Specification of Granular Fills

M. D. BOLTON, R. J. FRAGASZY, AND D. M. LEE

Triaxial tests have been carried out on unconventional fills. The shear strengths of gap-graded fills, with 15 and 30 percent of large particles in a fine matrix of sand, were compared with the matrix alone at a range of relative densities. It was found that when present at 30 percent, the large particles provide additional strength, whereas at 15 percent, they have an adverse effect. Possible mechanisms for these phenomena are discussed. Strength enhancement was still available when the large particles were of poor quality, friable limestone. These laboratory trials suggest that a more flexible specification for fill could lead to significant economies, but further tests will be required for confirmation.

In the United Kingdom, materials for use as backfill to retaining structures and as general fill are specified in the *Specification for Highway Works*, which was compiled by the Department of Transport in 1986 (1). This serves mainly as a guide for structures of moderate size (less than 15 m), typical of the requirements for road embankments. The specification allows particle sizes up to 75 mm to be used behind retaining structures (Figure 1) and up to 500 mm for general fills. It is apparent that the physical dimension of these large particles poses some difficulties in laboratory testing, which will be discussed in this paper.

Granular soils comprising sound particles with sizes distributed on smooth grading curves and a high uniformity coefficient (C_u) have generally been employed as backfill. A uniformity coefficient of 5 is thought to be the minimum required to obtain high dry density under mechanical compaction. Particle soundness is generally assessed by the 10 percent fines method (BS812 1975, Part 3, Method 8), which measures the load in static compaction on a sample of circa 10-mm-diameter particles, such that 10 percent by weight of particles finer than 2.4 mm are produced.

In the wider context of ascribing material parameters to soils containing large particles, it is of interest to explore whether their specification can be broadened to include certain granular fills that would be regarded as unconventional. Unconventional fills can be placed in two categories. The first contains fills with unconventional size distributions, for example, a fill with either a discontinuous gradation or an excessive proportion of fine particles. Granular soils obtained from breaking down rock masses frequently give rise to a gap-graded size distribution, containing a small portion of much larger pieces. These pieces may be left out or subjected to additional crushing. Furthermore, in areas undergoing redevelopment, cheap granular materials are always in abun-

dance in the form of slag, broken brick, or concrete. In such a case, it is possible to introduce these materials, in a controlled quantity, into imported high quality sand. In view of the environmental benefits of avoiding dumps and restricting new quarries, and for economic reasons, the inclusion of these waste materials is an option that should be explored. The second category contains materials that are prone to brittle fracture under moderate stress levels or when being compacted or sheared.

The angle friction, ϕ'_{crit} , for soil shearing at constant volume (in a critical state), has been found to be approximately invariable with density and stress level for a particular soil aggregate. Peak angles of shearing resistance ($\phi'_{max} > \phi'_{crit}$) are associated with dilatancy and depend on initial density and a moderate stress level. The stress (p'_{crit}) necessary to eliminate dilatancy and thereby force soil to contract toward its critical state apparently depends on its initial relative density (I_D) (2).

The reduction of ϕ'_{max} toward ϕ'_{crit} as a result of grain crushing has limited the use of such low-grade granular fill as weakly cemented calcareous limestone and chalk, even in small soil structures. A rare example was the use of soft reef limestone used in the Evretou Dam in Cyprus (3). However, if crushable materials are present in a controlled quantity within a sound material, the mixture may at least be as strong as the sound material alone at the same relative density.

GRAIN FRACTURE

A particle fragmentation test (PFT) was used to give the fracture strength of individual particles over a range of size. An Instron loading frame was used to provide a uniaxial force to crush each particle separately between two smooth platens. The diameter (d) of a particle was taken as the mean of the longitudinal and lateral dimensions. Particles with an aspect ratio close to 1 were chosen and soaked for 24 hr. In the test, the first major drop in the applied load usually signifies the first fracture along the axial direction, which can also be detected visually.

The fracture force depends on the size of the particles and their strength. The relationship can be represented after the Brazilian test for the tensile strength of concrete, by

$$P_f \propto \sigma_f \cdot d^2 \quad (1)$$

where P_f is the fracture force and σ_f is the tensile strength of the material.

Figure 2 shows that P_f/d^2 and d can be related by linear

M.D. Bolton and D.M. Lee, Department of Engineering, University of Cambridge, Trumpington Street, Cambridge. CB2 1PZ England. R.J. Fragaszy, GeoSyntec Consultants, Norcross, Ga. 30093.

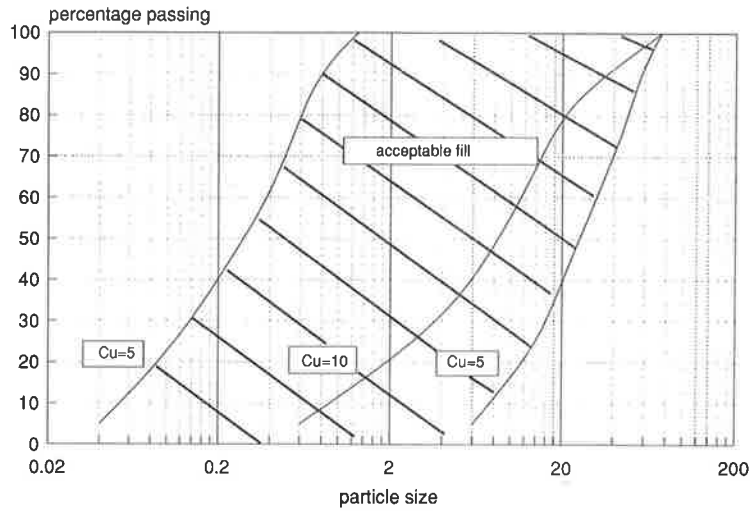


FIGURE 1 Acceptable fills for structures.

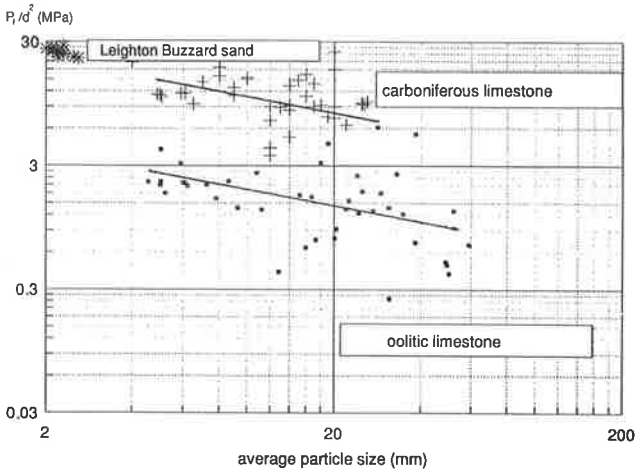


FIGURE 2 Particle strength.

regression lines on logarithmic scales. An empirical relationship can be written as follows:

$$\frac{P_f}{d^2} = K \cdot d^b \quad (2)$$

where K is a material constant and b represents the slope of the plot, which is negative.

This leads to the following equation:

$$\sigma_f \propto d^b \quad (3)$$

This equation implies that a material with a slope of zero on the logarithmic plot ($b = 0$) will be “perfect” material, for which strength does not deteriorate with particle size. Brittle materials such as soil usually have a negative value of b . As a result of crack propagation from internal flaws, if the flaw size is proportional to the particle size, Griffith (4) implies the following:

$$\sigma_f \propto d^{-0.5} \quad (4)$$

A number of materials had been tested, and three were chosen for this study—Leighton Buzzard sand, oolitic limestone, and carboniferous limestone (Figure 2). The limestones gave $b \approx -0.3$.

MATERIAL PROPERTIES

The regression lines in Figure 2 show that Leighton Buzzard sand has a similar fracture strength tendency to the carboniferous limestone, whereas the oolitic limestone is approximately 5 times weaker, size by size. Large carboniferous limestone particles could therefore be treated as sound inclusions in a matrix of sound Leighton Buzzard sand, whereas oolitic limestone inclusions can be treated as friable and low grade.

Grain properties of the three materials are presented in Table 1. The values for roundness and sphericity were assigned according to tables constructed by Krumbein (5) and Rittenhouse (6), respectively.

MATERIAL GRADATION

This gradation of samples for the triaxial tests was chosen under two conditions. The first condition concerns the maximum particle size to be included. A minimum value of 10 for the ratio (r) of sample diameter to particle size was recommended by Bishop and Henkel (7). However, lower values, such as 6 and 4, had been used by other researchers [Siddiqi (8), Marachi et al. (9), al-Hussaini (10), and Su (11)].

TABLE 1 GRAIN PROPERTIES OF MATERIALS

	Leighton Buzzard sand	oolitic limestone	carboniferous limestone
specific gravity	2.664	2.710	2.729
gradation mm	0.1-2	3.35-5.6	3.35-5.6
surface texture	smooth	very rough	rough
sphericity	0.87	0.75	0.69
roundness	0.6	0.4	0.3

It can be concluded that as the value of r becomes smaller than six, the strength and stiffness are somewhat enhanced as possible ruptures are impeded. In this study, the maximum particle size used was 5.6-mm in 70-mm-diameter triaxial samples. In addition, it was decided to simulate a gap-graded soil mixture. The Leighton Buzzard sand was chosen as the sound matrix material with sizes from 0.1 to approximately 2 mm. Both limestones were used as the large content with sizes from 3.35 to approximately 5.6 mm. Fills *A* and *B* contained the matrix with 15 percent by weight of oolitic and carboniferous limestones, respectively, and Fills *C* and *D* contained the matrix with 30 percent of oolitic and carboniferous limestone particles (Figure 3). In this way, the strength characteristic of the mixtures can be compared with that of the matrix alone.

TRIAXIAL TESTS

The triaxial apparatus used in Cambridge was first assembled by Houlsby (12). Various modifications have been made since. The current set-up consists of a Geonor cell unit with a rotating bush that reduces the ram friction. The cell pressure is provided by a mercury pot system capable of providing 650 kPa. A GDS pressure controller is used to provide the back pressure for the drained tests, as well as for measuring the volume change of the sample. The test progress is computer controlled, and measurements of axial load, volume change, and axial strain are logged and stored in disk files for post processing. The magnitudes of cell pressure and pore pressure are also monitored in all tests.

All samples were 70 mm in diameter. Greased rubber discs were used to minimize the end friction imposed by the platens. As a result of using fee ends, "dead-ends" are effectively eliminated, and samples of aspect ratio 1 can be used. All tests conducted here were drained with fully saturated samples, achieved by first flushing carbon dioxide through the sample before introducing de-aired water under a small pressure head. Skempton's parameter B was checked in all samples to demonstrate a value of at least 0.95.

All tests were conducted with a cell pressure of 60 kPa. Each material was tested over a range of relative density in order to establish a correlation between ϕ'_{max} and I_D . The test

program and part of the results are presented in Table 2. Typical plots of mobilized ϕ' versus axial strain (ϵ_1) and volumetric strain (ϵ_v) versus ϵ_1 are shown in Figures 4 and 5.

DENSITY CORRECTION METHOD

Fragaszy et al. (13) discussed the behavior of sound granular fills containing various proportions of large, well-rounded, smooth particles. It was found, for smaller proportions in which the large particles could be considered to be "floating" in a finer matrix, that the strength of the total soil could be estimated as that pertaining to the matrix material remote from the large particles, discounting the looser matrix material in the zone of disturbance around each large particle. The objective of that study was to permit the modeling of the total soil aggregate by deducing an appropriate density in which to test a scalped sample of matrix material after the larger particles were removed. Because the objective here is simply to report on certain parameters affecting the strength of the total soil, no equivalent modeling criteria will be introduced to deal with these more complex materials. If the present results are considered promising, further work on the modeling of field compaction would prove desirable. Tests on fills with genuinely large particles, even maximum density tests, are difficult to achieve and validate.

TEST RESULTS

For compacted fills, the mobilized peak strength ϕ'_{max} is always used for stability or earth pressure calculations. In Figures 6

TABLE 2 SUMMARY OF TEST PROGRAM AND RESULTS

Test	Consolidated			ϕ'_{max} (deg)	ϕ'_{crit} (deg)
	ρ_{dry}	$v = 1 + e$	I_D		
matrix: $\rho_{max} = 1.931$ $\rho_{min} = 1.660$					
M15	1.740	1.531	32.8	38.80	38.4
M40	1.802	1.478	56.2	40.63	39.9
MM40	1.818	1.465	61.9	41.19	38.4
M60	1.882	1.410	84.1	43.16	38.6
M80	1.910	1.395	93.3	44.03	38.5
Fill A 15% oolitic limestone: $\rho_{max} = 1.976$ $\rho_{min} = 1.670$					
O15	1.824	1.464	54.5	39.31	37.4
O40	1.867	1.431	68.1	40.59	37.5
O50	1.901	1.405	78.1	42.05	*
O60	1.931	1.383	87.3	43.27	38.6
Fill B - 15% carboniferous limestone: $\rho_{max} = 2.017$ $\rho_{min} = 1.740$					
C20	1.835	1.457	37.7	39.05	38.5
C30	1.891	1.414	58.1	41.00	*
C40	1.935	1.382	73.4	42.26	38.1
C60	1.959	1.365	81.4	43.85	38.2
Fill C - 30% oolitic limestone: $\rho_{max} = 2.014$ $\rho_{min} = 1.710$					
O40-P30	1.860	1.440	53.4	41.78	40.20
O80-P30	1.931	1.387	75.8	45.46	41.30
Fill D - 30% carboniferous: $\rho_{max} = 2.091$ $\rho_{min} = 1.800$					
C40-P30	1.968	1.364	61.3	42.60	40.21
C80-P30	2.010	1.335	75.1	45.56	40.87

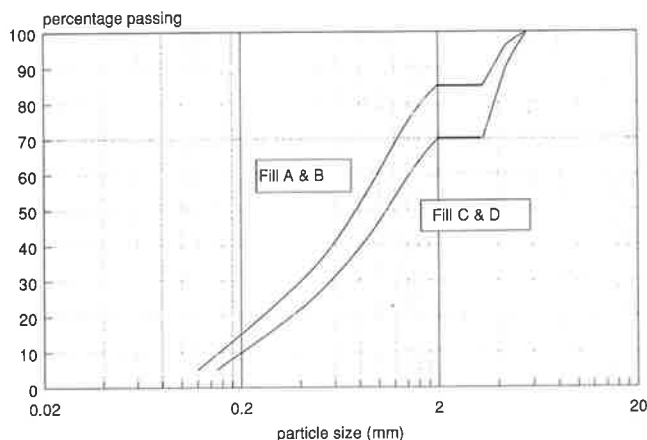


FIGURE 3 Tested unconventional fills

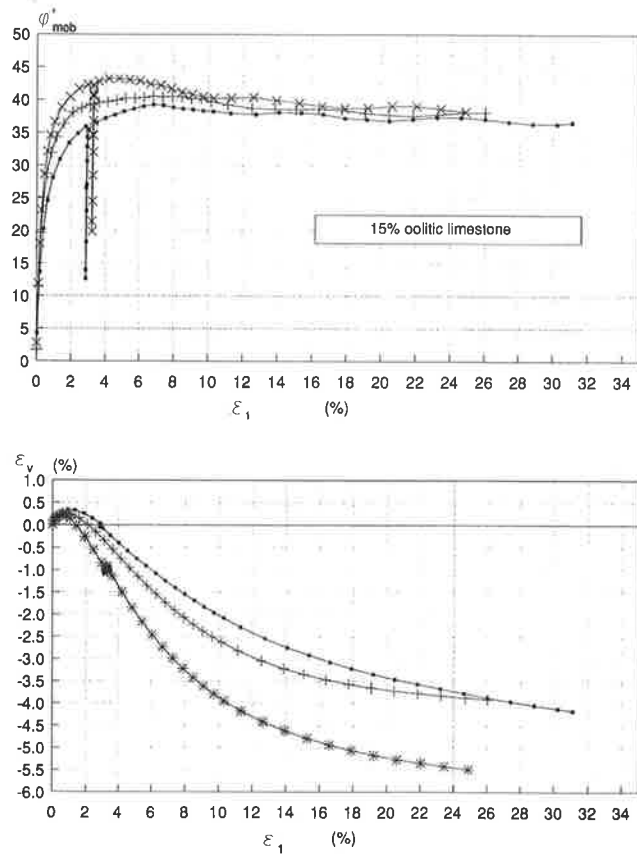


FIGURE 4 Axial strain versus mobilized strength (top) and volumetric strain (bottom) for Fill A.

and 7, values of ϕ'_{max} are plotted against the relative density of the corresponding soil mixture. For this purpose, the maximum and minimum dry densities were determined following ASTM methods. The data for the matrix are plotted as a bilinear line and are treated as a norm, against which to compare other data.

It is found from the plots that ϕ'_{max} varies approximately linearly with the relative density (I_D) for each material, at least when values I_D are greater than 50 percent. When the large particle content is at 15 percent, it is observed that the rates of increase of ϕ'_{max} , with respect to I_D for the matrix, for fills A and B are all similar. However, when the large particle content is at 30 percent, the rates of increase of ϕ'_{max} for fills C and D are much higher than for the matrix.

However, perhaps more significantly, it is observed that the absolute values of ϕ'_{max} for the fills with respect to those of the matrix do not follow the same trend when the proportion of large particles is different. For fills C and D, it is found that, for values of I_D greater than 50 percent, their strengths are always higher than those of the matrix alone at the same relative density ($\sim +3^\circ$ at $I_D = 70$ percent). It is believed that the large particles, when present in a significant quantity, act as discrete tensile reinforcing elements. This self-reinforcing effect is analogous to the enhancement of strength of triaxial samples due to rough platens.

When the amount of large particles is reduced, as in fills A and B, it might be anticipated that the reinforcing effect

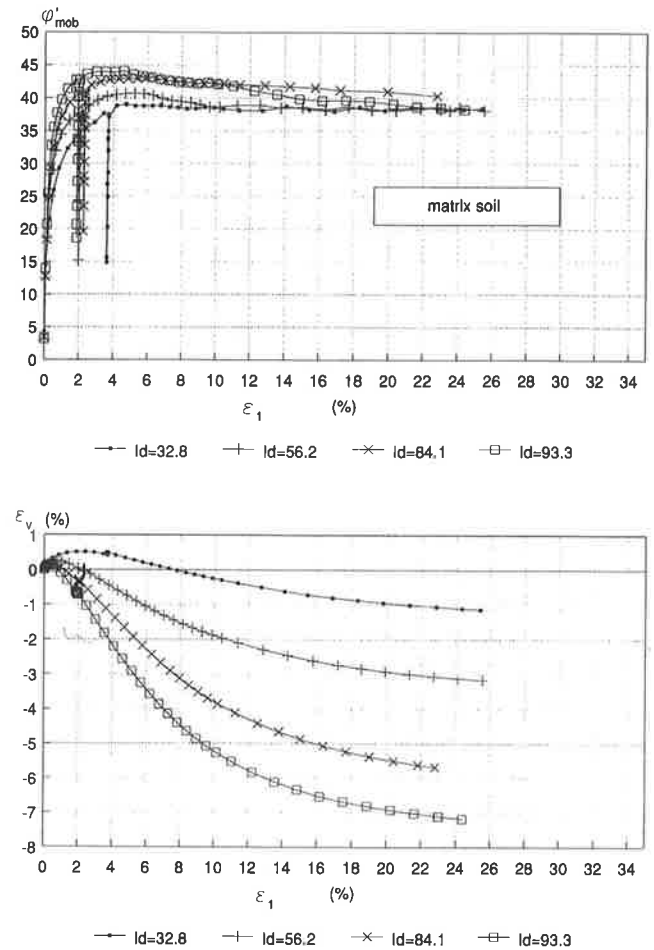


FIGURE 5 Axial strain versus mobilized strength (top) and volumetric strain (bottom) for matrix.

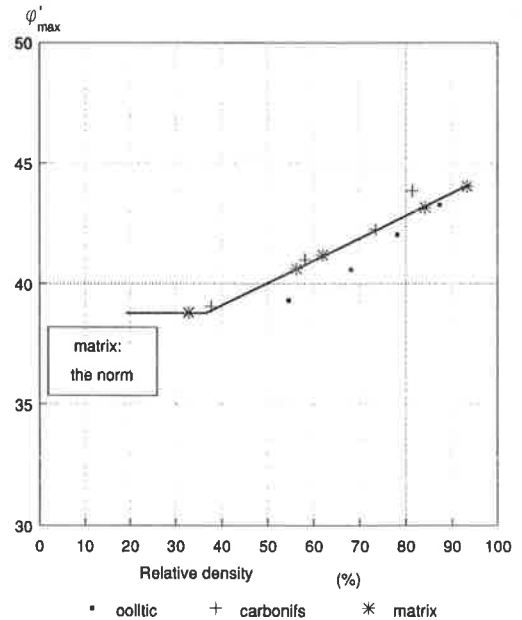


FIGURE 6 Strength versus relative density for fills A and B.

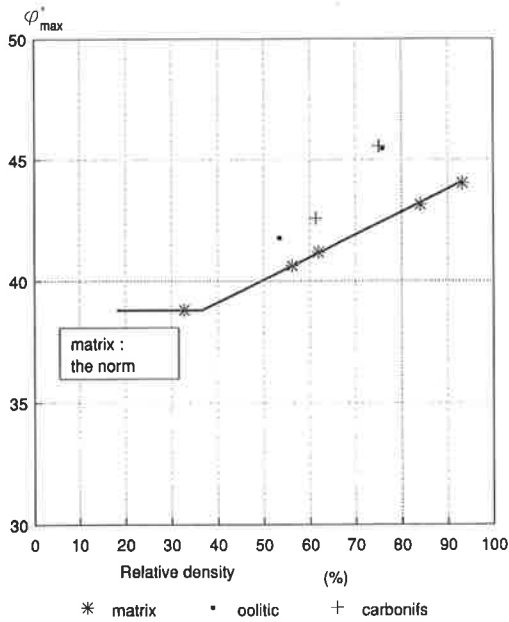


FIGURE 7 Strength versus relative density for fills C and D.

will diminish fairly rapidly as particles are further away from each other on average, leaving the strength equal to that of the matrix. Figure 6 actually shows that for Fill A, which contains 15 percent of oolitic limestone in the matrix, the strength falls approximately 2° below that of the corresponding matrix at a corresponding relative density. However, this deviation might be explicable in terms of the loss of sliding resistance on or over the surfaces of occasional large particles. Each surface facet might be regarded either as inherently smoother than the matrix ($\delta < \phi'$), or as providing a zone of disturbed packing that reduces ϕ' in the near field of the matrix. It is believed that as the peak strength approaches, a rupture surface could develop in such an orientation as to entrain as many large particle facets as possible while avoiding significant intersections through the particle bodies and maintaining an angle of approximately $45 - \phi'_{max}/2$ to the major principal stress direction. The variation in relative strength is summarized in Figure 8, where $\Delta\phi'$ represents the strength of a fill in excess of that of the matrix at $I_D = 70$ percent.

In the following two sections, attempts are made to investigate the possible magnitudes of strengthening and weakening mechanisms arising from these two hypotheses.

THE DISTURBANCE MECHANISM

The situation is idealized in Figure 9 by considering a single, large cubic particle of Side D enclosed in a cubic cell of Side L , which contains a matrix of smaller particles. The volumetric proportion of large particles is:

$$R = P/(1 + e) \tag{5}$$

where P is the mass proportion of cubic particles and e is the overall void ratio.

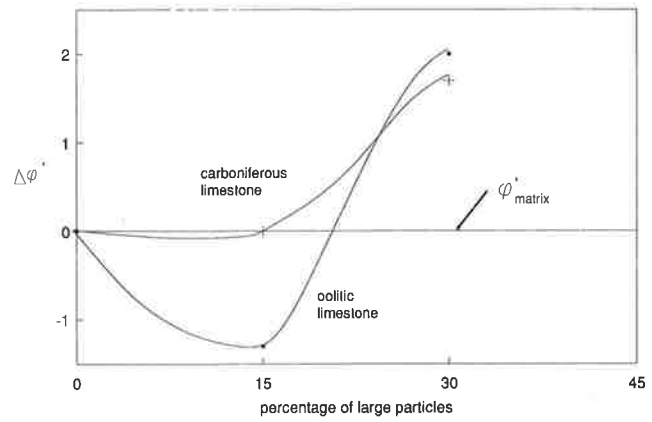


FIGURE 8 Comparison of strength at 70 percent relative density.

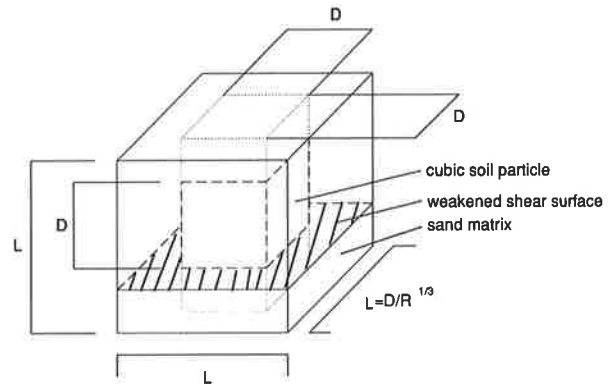


FIGURE 9 Unit cell for the disturbance mechanism model.

Then the volume of the cell is

$$L^3 = D^3/R \tag{6}$$

The proportional area of a possible shear passing through the plane face of the particle is

$$A_R = D^2/L^2 = R^{2/3} \tag{7}$$

Taking ϕ' in the matrix and reduced ϕ'_s on the surface of the cube, the operational strength of the weakened shear surface could be written

$$\phi'_s = A_R\phi'_s + (1 - A_R)\phi' \tag{8}$$

This must represent the largest possible strength reduction, because it refers to coplaner particle facets.

If $\phi' = 45^\circ$ and $\phi'_s = 30^\circ$, then for $R = 0.15$, $A_R = 0.28$ so that $\phi'_s = 40.8^\circ$ ($\Delta\phi' = 4.2^\circ$). It is assumed that a rupture surface could avoid intersecting particles while passing close to the surfaces of a representative proportion of them. This calculated reduction exceeds that inferred in Figure 8 by a factor of perhaps 3. This might be taken to reflect the statistical nature of the real soil inclusions, with their random po-

sitioning. A higher proportion of large inclusions would certainly make it impossible for any such slip surface to exist.

THE REINFORCEMENT MECHANISM

Figure 10 shows a different view of the unit cell shown earlier in Figure 9, in which it is clarified that a zone of soil $D \times D \times H$ is considered to be trapped between opposing faces of large particles, considered here to be cubes in a regular array. For this sub-cell, the strength enhancement would be similar to that of soil tested in a triaxial compression between rough platens.

The following equation is derived from Equation 6:

$$H = L - D = D(1/R^{1/3} - 1) \tag{9}$$

Figure 11 shows, in a central cross section, the equilibrium of the central zone of matrix material. The magnitude of end friction can be taken to be $\mu\sigma'_1$, but allowing for its radial orientation, the mean net lateral friction can be shown to be

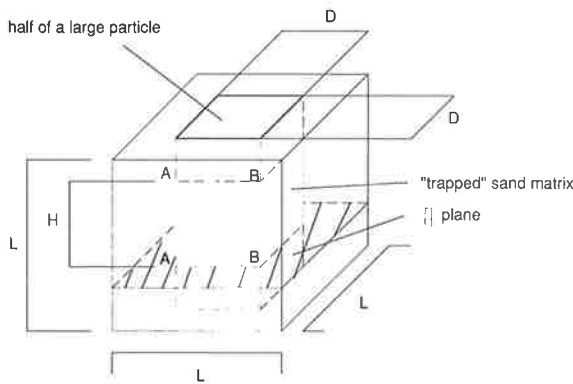


FIGURE 10 Unit cell for the strengthening effect.

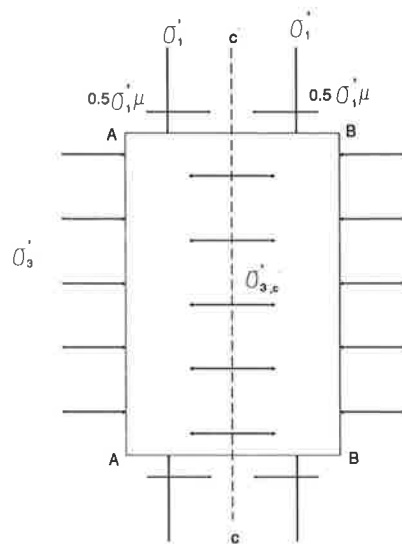


FIGURE 11 Equilibrium of unit cell across central cross section of matrix soil.

approximately $0.5 \mu\sigma'_1$. Then for equilibrium with a central lateral stress $\sigma'_{3,c}$:

$$\begin{aligned} \sigma'_{3,c} H \cdot D &= \sigma'_3 H \cdot D + 0.5 \mu\sigma'_1 \cdot D^2/2 \cdot 2 \\ \therefore \sigma'_{3,c} &= \sigma'_3 (1 + 0.5 \mu K_p D/H) \end{aligned} \tag{10}$$

The central axial stress is therefore

$$\sigma'_{1,c} = \sigma'_3 K_p (1 + 0.5 \mu K_p D/H) \tag{11}$$

Figure 12 shows the expected variation of axial stress across the whole unit cell. Allowing for the respective areas on which these stresses act, the mean axial stress is given by

$$\sigma'_1 = K_p \cdot \sigma'_3 + 0.5 \mu K_p^2 D/H \sigma'_3 \cdot 1/2 \cdot A_R \tag{12}$$

or substituting for A_R from Equation 7:

$$\frac{\sigma'_1}{\sigma'_3} = K_p \cdot [1 + (0.25 \mu K_p R)/(1 - R^{1/3})] \tag{13}$$

where the failure stress-ratio is enhanced, due to the large particles, by the factor in the brackets. This should represent the largest possible enhancement of strength, because the particles have been given ideally flat surfaces, parallel to each other.

Substituting $K_p = 4$, $\mu = 0.5$, $R = 0.21$ (relevant to $P = 30$ percent large particles at $e = 0.4$), the enhancement factor in Equation 13 estimated to be 1.26. This would indicate a new value $\phi' = 42^\circ$, with an enhancement $\Delta\phi' = 5^\circ$. If this is about double the effect shown in Figure 8, it might be taken to represent a statistical discrepancy due to the irregular shape of the actual large particles and their disposition.

CONCLUSION

An investigation has been carried out into the effects on shear strength of soil including a proportion of large particles in an otherwise conventional sound fill. It was found that some

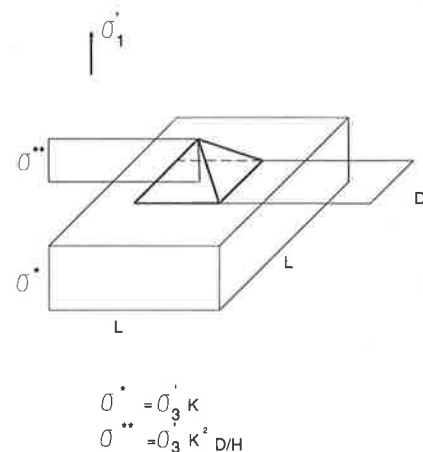


FIGURE 12 Distribution of major principal stress.

small variation occurred in the angle of shearing resistance (ϕ') when the various soils were compacted to target relative densities. A well-compacted mixture with 15 percent of large particles could lose 1.5° in ϕ' , whereas with 30 percent of large particles a gain of about 3° was available. These effects were explained by reference on one hand to disturbance of packing in the vicinity of sparse inclusions, and on the other to an internal reinforcement of matrix soil trapped between large inclusions, analogous to that found in triaxial tests with rough platens.

Similar effects were found (at low stress levels appropriate to road embankments) irrespective of whether the large inclusions were as strong as the matrix, or were five times more friable. This raises the question of the potential use of inexpensive or waste materials at a proportion of 30 percent to a good fill, which might result in a composite backfill even stronger than that of the 100 percent high-quality fill. More work on field compaction, specification, and control would be necessary before such advantage could be realized in practice.

ACKNOWLEDGMENT

The work reported in this paper was supported by the Transport and Road Research Laboratory of Great Britain. Additional support was provided by the U.S. National Science Foundation.

REFERENCES

1. *Specification of Highway Works*. Part 2. Department of Transport, Her Majesty's Stationery Office, London, United Kingdom, 1986.
2. M. D. Bolton. The Strength and Dilatancy of Sands. *Geotechnique* 36, No. 1, 1986, pp. 65-78.
3. A. J. Brown. Use of Soft Rockfill at Evretou Dam, Cyprus. *Geotechnique* 38, No. 3, 1988, pp. 333-354.
4. A. A. Griffith. The Phenomena of Rupture and Flow in Solid. *Phil. Tran. Roy. Soc. (London)* A221, 1920, pp. 163-198.
5. W. C. Krumbain. Measurement and Geologic Significance of Shape and Roundness of Sedimentary Particles. *Journal of Sedimentary Petrology*, Vol. 11, 1941, pp. 64-72.
6. G. Rittenhouse. A Visual Method of Estimating Two-Dimensional Sphericity. *Journal of Sedimentary Petrology*, Vol. 13, 1943, pp. 79-81.
7. A. W. Bishop and D. J. Henkel. *The Measurement of Soil Properties in the Triaxial Test*. Edward Arnold, 1957.
8. F. H. Siddiqi. *Strength Evaluation of Cohesionless Soils with Oversize Particles*. Ph.D. thesis. University of California, Davis, 1984.
9. N. D. Marachi, C. K. Chan, and H. B. Seed. Evaluation of Properties of Rockfill Materials. *J. SMFE Div., ASCE*, Vol. 98: SMI, pp. 95-114.
10. M. Al-Hussaini. Effect of Particle Size and Strain Conditions on the Strength of Crushed Basalt. *Canadian Geotechnical Journal*, Vol. 20, 1983.
11. W. Su. *Static Strength Evaluation of Cohesionless Soil with Oversize Particles*. Ph.D. thesis. Washington State University, 1989.
12. G. T. Houlsby. *A Study of Plasticity Theories and Their Applicability to Soils*. Ph.D. thesis. University of Cambridge, Cambridge, England, 1981.
13. R. J. Frigaszy, W. Su, and F. H. Siddiqi. Effects of Oversize Particles on Density of Clean Granular Soils. *Geotechnical Testing Journal*, ASTM, Philadelphia, Pa. Vol. 12, No.2, pp. 106-114.

Publication of this paper sponsored by Committee on Transportation Earthworks.

Application of Continuous Dynamic Compaction Control for Earthworks in Railroad Construction

ARIS A. SAMARAS, RÜDIGER LAMM, AND JOSEPH TREITERER

Continuous dynamic compaction control (CDCC) has been under development by the Federal German Railroad Authorities since 1985. The method can be used with vibrating compaction rollers of varying size and weight by measuring and recording the vertical acceleration pulses at the vibrating drum of the roller. The data are fed into a computer unit that combines the readings at the drum with other test data as the roller proceeds along the compaction area, and a continuous record of compaction data will be provided along the path of the compaction unit. Presented in this paper are the state of the art and first experiences in applying the CDCC method to the earthworks of a section of the new high-speed railroad track to be constructed between Mannheim and Stuttgart, West Germany. The following advantages are expected to be realized from the use of the new compaction control method: (a) previously used sampling methods could not provide full coverage of the construction area, and failures have occurred because of insufficient compaction data; (b) previously used spot measurements interrupted the flow of construction work extensively, thus limiting the number of samples that could be taken economically; and (c) CDCC provides a continuous compaction record, avoiding the repetition of unnecessary compaction passes and providing a more uniform compaction of the area at lower costs.

With the continuous improvement of ground transportation systems in Europe, the Federal German Railroad Authorities (FGRA) have been engaged in a program to upgrade mainlines for a speed of up to 250 km/hr (156 mph). Basic requirements of the program are extensive earthworks with uniform compaction of the subsoil and subgrade layers. It was found that the risk factor associated with random sampling was too high with fewer samples, and increasing the number of samples slowed the progress of the earthworks. New methods of continuous evaluation of compaction performance were therefore developed (1-7).

FGRA have developed standards for the degree of compaction and the resulting load bearing capacities in *Specifications for Earthworks* (8). The procedures and frequency of tests are given in the *Supplementary Technical Specifications and Guidelines for Earthworks in Highway Engineering* (9,10). The most frequently applied test methods are field density measurements to determine the degree of compaction and plate bearing tests to determine the deformation behavior.

Continuous dynamic compaction control (CDCC) has not yet been included in the above regulations because the method is still in the development stage, and more data and research are required. Preliminary results, however, indicate that the method is reliable and successful in controlling and evaluating the compaction process with contractors.

REQUIREMENTS FOR THE CONTROL OF COMPACTION

Earthworks for FGRA must be carried out in agreement with the previously listed specifications (8,9). The quality of compaction is determined by four factors:

1. Degree of compaction (D_{Pr}),
2. Modulus of deformation, first loading (E_{v1}),
3. Modulus of deformation, second loading (E_{v2}), and
4. Ratio of E_{v2} to E_{v1} .

The moduli of deformation are determined by plate bearing tests in accordance with the German standard DIN 18 134 (11). E_{v1} is calculated by the first loading and unloading of the plate, which is intended to measure permanent settlement of the ground, which can be regarded as the plastic portion of the deflection. E_{v2} is determined by the second loading of the plate, which can be regarded as an elastic response. The modulus of subgrade reaction (k) is normally calculated for a mean plate deflection of 1,25 mm during the first and the subsequent unloading of the plate. Table 1 presents the minimum requirements for layers of the subgrade and the embankment.

In addition, it is required to determine the ratio E_{v2}/E_{v1} , which is introduced as an auxiliary criterion for the elastic behavior of the compacted ground. The limits of the ratio are given elsewhere (9), and the following requirements must be met for noncohesive soils: D_{Pr} , greater than 103 percent, E_{v2}/E_{v1} less than 2.2; and D_{Pr} , less than 103 percent, E_{v2}/E_{v1} less than 2.5.

The number of required tests by the conventional method (9) is presented in Table 2. The requirements for tests by the conventional method given in specification (9) are quite high, and it is hoped that CDCC will permit a reduction in the number of samples, resulting in considerable savings by simplifying compaction work for contractors. It is also hoped that considerable improvement of the standard tests results can be realized by combining the currently required sampling method with the CDCC method.

A. A. Samaras, German Railroad Administration Karlsruhe, D-7500 Karlsruhe 1, Bahnhofstrasse 5, Germany. R. Lamm, Institute of Highway and Railroad Engineering, University of Karlsruhe, D-7500 Karlsruhe 1, Kaiserstrasse 12, Germany. J. Treiterer, 171 Medick Way, Worthington, Ohio 43085.

TABLE 1 MINIMUM REQUIREMENTS FOR SUBGRADE AND EMBANKMENT LAYERS (8)

SUBGRADE LAYERS	E_{v2} (MN/m ²)	D_{Pr} (%)
Top of 1. Layer	120	1.03
Top of 2. Layer	80	1.00
Top of Embankment	60	0.97

Legend: E_{v2} = Modulus of Deformation (MN/m²)
 $D_{Pr} = \frac{\rho_d}{\rho_{Pr}} =$ Degree of Compaction (%)
 ρ_d = Field Dry Density (t/m³)
 ρ_{Pr} = Maximum Dry Density (t/m³)

CDCC METHOD

Measurement techniques for compaction control have been studied by FGRA since 1985 (5). The newly designed high-speed railroad section from Mannheim to Stuttgart has been selected for the first field application and test of CDCC, which

TABLE 2 MINIMUM REQUIRED DEGREE OF COMPACTION OR PLATE BEARING TESTS FOR THE INTERNAL QUALITY CONTROL OF THE CONTRACTOR (9)

TESTING ZONE	TEST POINTS		
	No. of Tests	Distance per Layer	Area per Layer
Subgrade	1	≤ 200 m	≤ 2500 m ²
Subsoil	1	≤ 200 m	≤ 5000 m ²

has been combined with the standard sampling method for the evaluation and verification of data. Vibrating rollers have been equipped accordingly, and Figure 1 shows the setup. The vertical acceleration pulses of the roller drum are registered by an acceleration recorder and processed by a computer for the display and permanent record of data. The time-dependent sequence of vertical accelerations generated by the vibrating drum (referred to as dynamic values) can be plotted by an X-Y recorder (Figure 2) and can also be presented by a computer plot, as shown in Figure 3. The output of the measuring system is installed in the cabin of the vibratory

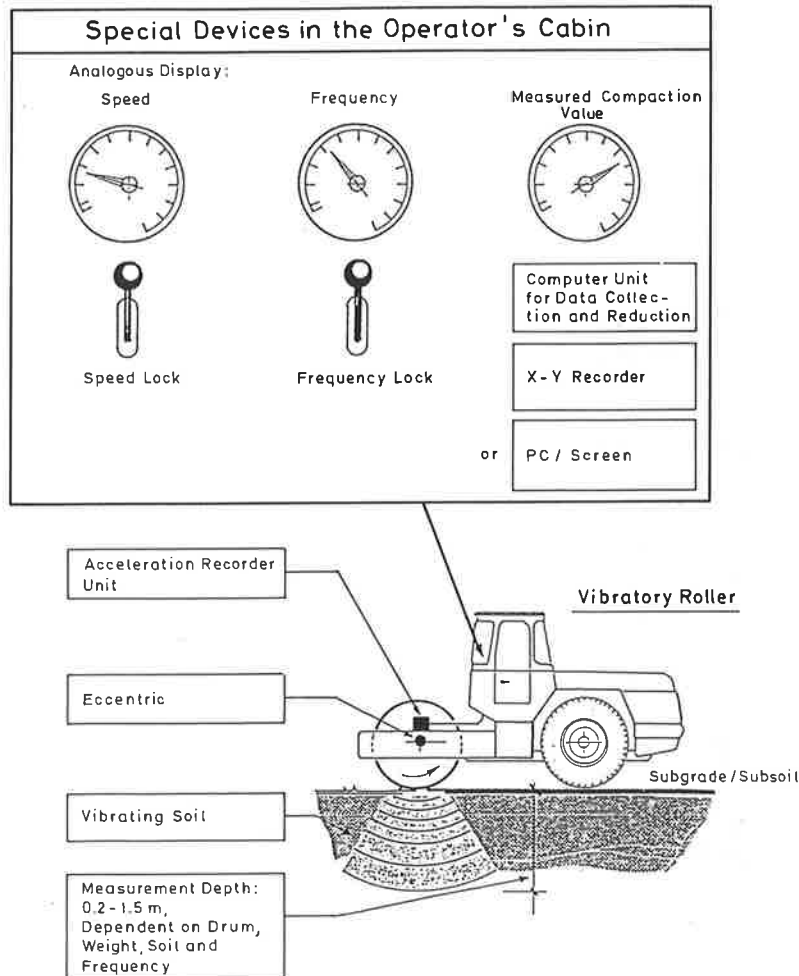


FIGURE 1 Systematic sketch of dynamic compaction measurement plant.

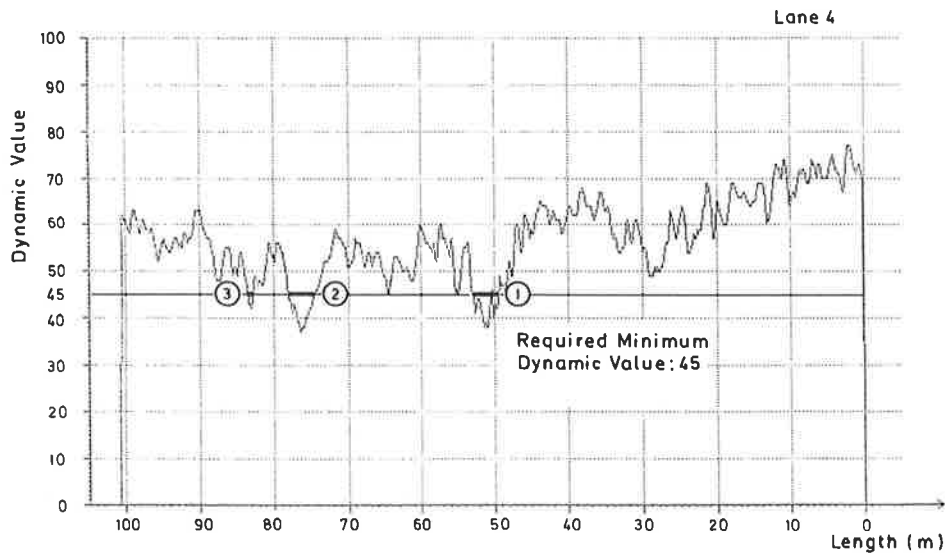


FIGURE 2 Example of lane-related X-Y recorded plot for dynamic value and length of the investigated section.

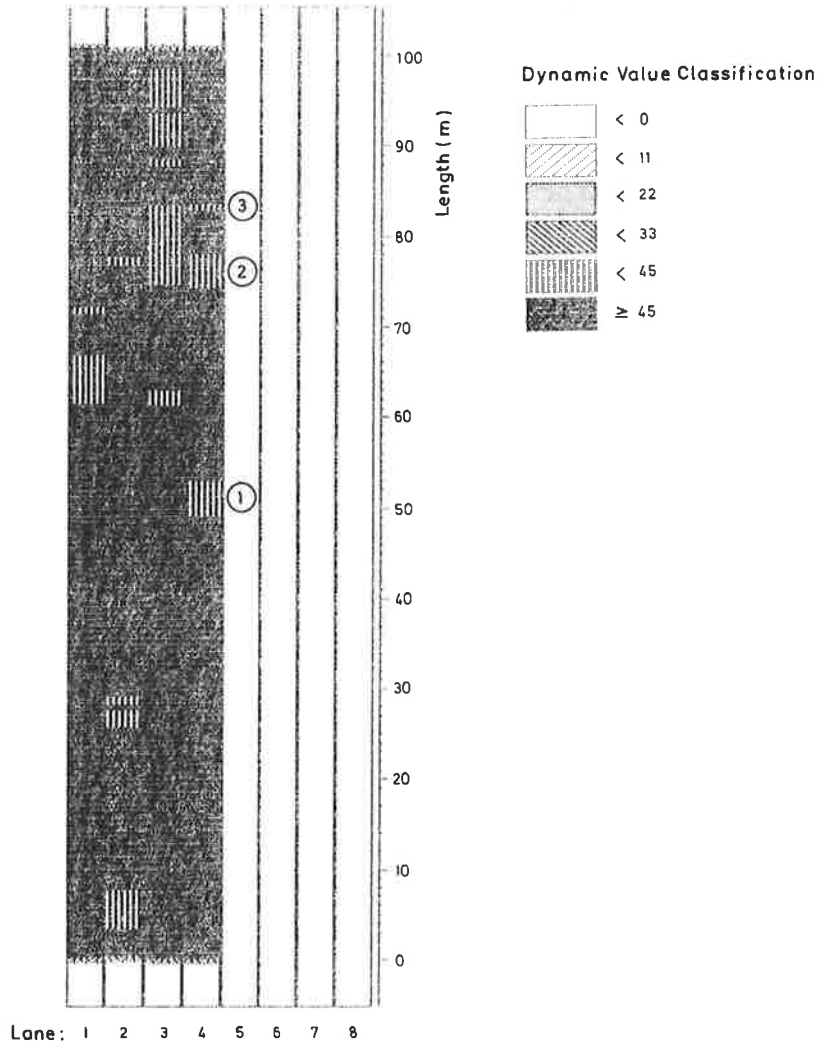


FIGURE 3 Example of computerized area plot for different dynamic value classes for length of the investigated section.

roller to aid the operator in meeting the required standard and to produce uniform compaction. No detailed description of the measuring ring system is currently available. The X-Y graph and the computerized area plot are used to supervise the compaction process and to provide evidence for the acceptance of compaction work carried out by the contractor. Figure 1 shows the display of operational settings, and Figures 2 and 3 reveal the measured and recorded compaction (dynamic) values, which enable the operator to adjust the passes to obtain the required uniform compaction of the area efficiently. Corresponding to the described principle, zones 1, 2, and 3 can be recognized as weak sections in meeting a required minimum dynamic value of 45, for example.

EVALUATION OF MEASUREMENTS AND INTERPRETATION

The measuring and recording system of the CDCC method presents a measured compaction value, a dynamic value considered to be a qualitative measure for the bearing capacity of the subsoil and subgrade. The dynamic measurements are influenced by the gradation of the soil, the density, and, with an increasing portion of the fines, by the moisture content of the soil. Contrary to the determination of the density, the dynamic CDCC value is not related to a constant volume but presents a qualitative value of the dynamically excited ground under the drum of the vibratory roller. The depth of influence is variable and depends on the weight and width of the drum, the power of the dynamic excitation, and the properties of the soil. Depending on the soil properties and the type of vibrating roller, the test was found to reach to a maximum depth of about 1.5 meters, covering a thickness of layers that is beyond the range of conventional soil-testing methods. The relationship between the CDCC test and the results of penetration and density tests is doubtful because of the difference in volume covered by the tests. The plate test, with an influence depth of 1.5 times the plate diameter, appears to be more suitable for comparison.

The comparative evaluation of dynamic measurements and supplementary field and laboratory tests lead to characteristic ranges of validity. Figure 4 shows these ranges for noncohesive soils, which have been determined from numerous individual tests of modulus of deformation and density and the dynamic values at corresponding test locations. It appears that the plate bearing test and the corresponding modulus of deformation, E_{v2} , is of special interest in comparison with the dynamic value. The regression curve in Figure 4 represents, as an example, the relationship between the E_{v2} values and the dynamic values for a granular soil used for frost protection.

The modulus of deformation should exceed 80 MN/m² according to the specified requirements in Table 1. The regression curve of Figure 4 shows a dynamic value of 32 MN/m². However, it was found from previous experience that the reading from the regression curve should be increased by a safety margin of 10 percent because the available data from samples have not yet been established statistically. It was found, however, that the density tests and the requirements for the ratio E_{v2}/E_{v1} are met if the regression curve is covered by the range of valid E_{v2} values.

To obtain reliable results with the CDCC method the following conditions must be met:

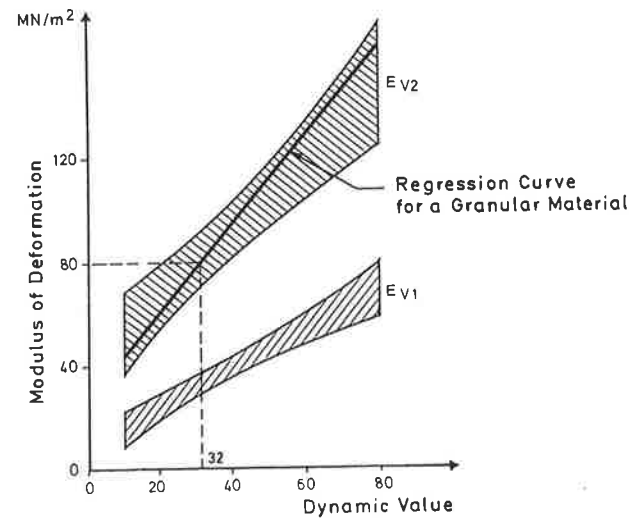
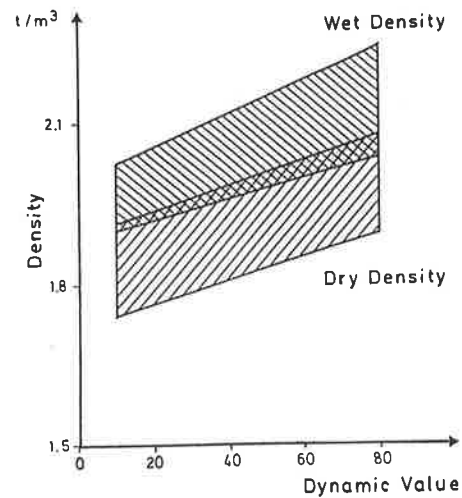


FIGURE 4 Ranges of validity between dynamic value and modulus of deformation and density for investigated noncohesive soils.

- The drum of the vibrating roller must have good, continuous contact with the ground, and the variation of a flat surface should not exceed 5 cm within a range of 4 m.
- Soft surfaces should be avoided because they can cause slippage of the drum and unreliable data.
- Hard surfaces should be avoided because they can cause bouncing of the drum, which will result in bad measurements.
- The rotational direction of the eccentric will be changed during reverse operation of the roller, resulting in less efficient compaction. Test passes should therefore be conducted in the forward motion only.
- The energy input to the dynamically excited soil is influenced by the speed of the roller and the frequency of the vibration. Both factors must therefore be kept constant for test passages.

CONCLUSION

The CDCC method offers substantial improvement in uniform soil compaction and in the control and record keeping

for contracts with earthwork. This paper is based on the methods and experience of a single construction project carried out by the FGRA covering noncohesive soils only. More data and research are needed to develop CDCC to its full advantage for field applications, and it is hoped that this paper will provide some incentive for further exploration and research.

ACKNOWLEDGMENT

The authors wish to thank A. Dengiz for his assistance in preparing and translating this paper.

REFERENCES

1. R. Floss, N. Gruber, and J. Obermayer. A Dynamical Test Method for Continuous Compaction Control. *Proc., Improvement of Ground*, Vol. 1, Helsinki, Finland, 1983, pp. 25–30.
2. R. Floss. Dynamic Compaction Control in Earthworks. *International Technical Journal: Road and Autobahn*, Vol. 2, 1985, pp. 52–57.
3. R. Floss and W. Kroeber. *Continuous Dynamic Compaction Method for Quality Control in Earthworks*. Conference on Foundation Engineering, German Foundation Engineering Association, Federal Republic of Germany, 1988, pp. 193–204.
4. N. Gruber, J. Obermayer, and R. Floss. Acceleration Measurements of Vibratory Rollers as Control for Compaction. *Symposium for Measuring Techniques in Earthworks and Foundation Engineering*, Munich, Federal Republic of Germany, 1983, pp. 71–77.
5. A. Samaras, and G. Spata. New Railroad Section Mannheim-Stuttgart: Improvement of Quality in Earthworks with the Continuous Dynamic Compaction Control—Tests and Applications. *Journal: The Federal Railways*, Vol. 5, 1987, pp. 465–471.
6. R. Kirschner. Dynamic Control of Compaction in Earthworks. *International Technical Journal: Road and Construction*, Vol. 6, 1986, pp. 18–23.
7. W. Kroeber. *Dynamic Analysis of Vibratory Compaction in Earthworks*. Publications of the Institute for Foundation Engineering, Soil and Rock Mechanics, Technical University of Munich, Vol. 11, Federal Republic of Germany, 1988.
8. *Specifications for Earthworks* (1985 ed.). DS 836. German Federal Railways, 1985.
9. Supplementary Technical Specifications and Guidelines for Earthworks in Highway Engineering (1978 ed.). ZTVE-StB 76/78. Minister of Transportation, Division of Road Construction, Federal Republic of Germany, 1978.
10. R. Floss. *Comments to the Supplementary Technical Specifications and Guidelines for Earthworks in Highway Engineering*. ZTVE-StB 76/78. Kirschbaum Publishers, Bonn-Bad Godesberg, Federal Republic of Germany, 1979.
11. *DIN 18 134—The Plate Bearing Test*. Werner Publishers Inc., Düsseldorf, P.O. Box 8529, Federal Republic of Germany.

This paper is not a final report on CDCC. It is intended to present a description of the method, which is still in development, and a summary of the experience obtained thus far from an FGRA construction project.

Publication of this paper sponsored by Committee on Transportation Earthworks.

Decision Support System for Evaluation and Treatment of Earth Slope Instability

DIMITRI A. GRIVAS AND JOHN C. REAGAN

Movements of earth slopes are common and often costly occurrences. The development of a decision aid to provide appropriate remedial actions and to restore slopes to acceptable degrees of safety is of considerable practical importance. Achievements to date in developing a decision support system for the evaluation and treatment of slope instability are presented. The conceptual design, applicability and functions of the system are established through a combination of techniques, including the use of an expert panel. The three main components for the system are knowledge base, supporting data bases, and analytical program support. Initial implementation has produced a personal computer-based prototype system, which is described and illustrated with an example. Conclusions drawn from this study include the following: (a) the domain of landslide analysis and treatment is well suited to the expert-system approach because it involves reasoning processes and data interpretations that are based on experience; (b) knowledge acquisition is a critical and involved activity in the system development effort, and simple techniques (interviews and questionnaires) appear to be inadequate for the creation of a robust knowledge base; (c) a fully implemented system requires a powerful computer environment with multi-tasking capabilities.

The selection of appropriate actions to control the movement of earth slopes and secure their safety represents an important activity in geotechnical engineering. Available expertise is typically scattered among the many facets of the problem, making it difficult to achieve decisions, especially under pressing or urgent conditions.

Delays or poor decisions in effectively controlling slope instability can have devastating effects. The damage is more acute for slopes located in urban settings. In such cases a potential slope instability may result in a major slide, which can cause economic and life losses. Estimates of direct and indirect damage to buildings and other structures due to slope failure in the United States alone are on the order of hundreds of millions of dollars a year. FHWA has estimated that an amount in excess of \$50 million is spent annually for the repair of slope-related damage on the federally financed component of the U.S. highway network (1). The total number of fatalities due to all types of slope instability exceeds 25 a year nationwide (2). These figures can explain the continued interest in the study of the factors that trigger the movements of slope-forming materials and help justify the practical need for the development of aids for better and faster decisions in controlling such movements.

Recent developments in the use of expert systems in civil engineering have demonstrated the ability of such systems to aid in decision making and solution of complex problems. Expert systems are basically computer programs that imitate the performance of human experts. They embody factual, empirical, and procedural knowledge to address specific aspects of particular problems and to manipulate relevant knowledge expressed in symbolic description. Their success is due mainly to their ability to solve difficult problems in specific areas at least as well as human experts.

The paper presents the initial research effort on a project aiming at the development of a decision methodology for the evaluation and treatment of earth slope instability. The project is conducted jointly by personnel of Rensselaer Polytechnic Institute (RPI) and the Soil Mechanics Bureau of the New York State Department of Transportation (NYSDOT). The latter is the state agency responsible for the safety of all man-made or natural slopes in the transportation infrastructure of New York. The overall goal of the project is to collect, synthesize, and validate the knowledge available on the subject and encode it in a decision support system (DSS) (3) to provide uniform, consistent, and cost-effective decisions in selecting and implementing rehabilitative solutions to problems caused by slope instability. At the core of the DSS is an expert system which stores the knowledge base. Analytical and data base components supplement the knowledge base to form the complete system.

CONTROL OF MOVEMENT AND INSTABILITY OF EARTH SLOPES

The task of determining feasible alternative options to control movement and instability of earth slopes represents an involved process. Each slope, whether natural or man-made, is a unique structure, the performance of which is influenced by local conditions (e.g., geology, materials, loads, etc.). To make an informed decision, one must be knowledgeable about these conditions, be familiar with available options, and have experience about their effectiveness in achieving a desirable objective (e.g., reduction in driving forces, increase in shear strength, etc.). Cost and other constraints (e.g. unavailability of materials, inappropriate field conditions, etc.) often eliminate some options, but the basic objective of making a final recommendation for the solution of a diagnosed problem remains valid.

If an intelligent aid were available to achieve the above task, it would embody available factual and empirical knowledge and would imitate the thinking process of human experts.

D. A. Grivas, Department of Civil Engineering, Rensselaer Polytechnic Institute, Troy, N.Y. 12180-3190. J. C. Reagan, New York State Department of Transportation, Soil Mechanics Bureau, State Campus Building 7, Room 114, Albany, N.Y. 12232.

The user of such an aid would then be able to arrive at a decision on the appropriate treatment, which would be supported by available data and experience.

Figure 1 shows the stages typically involved in arriving at a recommended solution. Each block in the figure represents a main activity, and the numbers show the order in which activities are typically pursued. A description of each main activity is given next.

Problem Identification

Problem detection and identification is typically based on observations of slope movement. The type of incurred movement is characterized according to specific attributes. One such attribute is the depth of the slope mass involved (i.e., whether the slope movement is deep seated or shallow). Additional attributes include type of material, rate of movement, geometry of the area affected, possible causes, degree of disruption of displaced mass, relation to geologic structure, and state of movement activity. There are several ways to classify slope movement, each having its own distinct advantages in the manner in which it utilizes pertinent features. In a synthesis on the subject (4) the type of movement and type of material were used to represent the primary and secondary criterion, respectively, for classification purposes. This is the classification system that is also followed in the present study.

Of practical importance during early stages of problem identification is the decision whether immediate action is necessary (e.g., closing a roadway, establishing a detour, initiating monitoring of the movement, etc.). This and other early decisions typically set the course of action to be followed during subsequent investigation.

Data Collection

This stage represents a fact-gathering activity. Several types of data are generally available to the person investigating a slope movement. Although the amount of data varies from

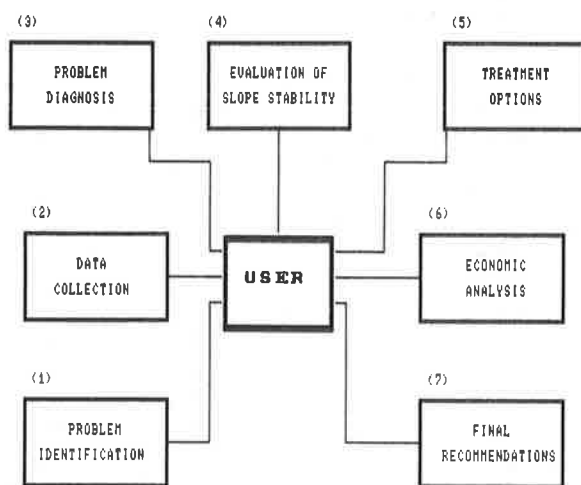


FIGURE 1 Schematic illustration of the activities involved in arriving at a final recommendation.

one case to another, some typical data types include the following:

- Geology of the region surrounding the slope site, available usually through maps, surveys, air photos, and field investigations;
- Boring log data;
- Test data on boring samples or in situ tests;
- Well data depicting groundwater fluctuation;
- Rainfall records; and
- Instrumentation data from slope indicators and the like.

The amount of data that is available at a given site is constantly changing. Thus, an important activity in investigating slope movements is the continuous updating and expanding of data files.

Problem Diagnosis

Problem diagnosis involves assessing the probable causes of slope movement. It is based on local experience and movement characteristics exhibited by certain types of materials.

Some primary causes are typically established during the data collection process (e.g., water-related problems, possible weak shear strength, etc.). They represent hypotheses that must be thoroughly examined during the problem diagnosis stage. In order to accept or reject a hypothesis, it may be necessary to conduct field tests, obtain drill holes, perform laboratory tests, review construction histories and other records in the area, and so forth. Although the task to precisely determine causes of instability is a challenging one, dominant factors can be identified reliably.

Evaluation of Slope Stability

This stage involves the use of analytical techniques to evaluate the safety of a slope. In the case of soil slopes, such methods are typically formulated on the assumption of limit equilibrium. If the analysis is based on a deterministic approach, the safety of a slope in terms of the commonly used "factor of safety" is assessed. If the analysis is based on a probabilistic approach that accommodates relevant uncertainties, the safety of a slope in terms of a "probability of failure" is assessed (5).

The finite element method (FEM) can also be used to provide stresses and deformations within soil masses. It requires, however, input data that is not always readily available or easy to obtain. Furthermore, a quantitative interpretation of results from finite element analysis requires some form of limit equilibrium calculation (6,7). These limitations are the primary reasons for the continued popularity of limit equilibrium methods for stability analysis of embankments and slopes (8).

Shown in Figure 2 is a classification of material conditions for the purpose of slope stability analysis. For natural slopes, the material may be broadly characterized as either coarse grained or fine grained. In the case of coarse-grained soils, a major distinction is given by density (i.e., loose or dense state); in the case of fine-grained soils, the distinction is be-

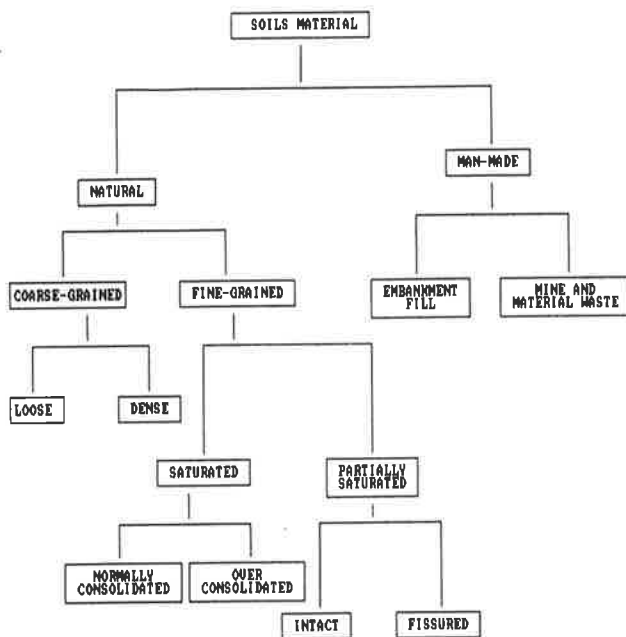


FIGURE 2 Classification of soil material conditions for stability analysis purposes.

tween saturated or partially saturated state. Further distinctions may also be made as shown in the Figure 2.

Once a failure model is adopted and a method of stability analysis is established, parametric studies can be conducted to determine the relative importance of the various factors and lead the way to the treatment selection.

Treatment Options

Selection of appropriate treatments follows a pattern that is generally directed from the results of the problem diagnosis, failure model development, and stability analysis. The goal of each treatment option is to halt slope movement and secure the overall safety of the slope. There are several ways of achieving this goal (e.g., reducing the driving forces, increasing resistance, etc.). Certain treatment options place special constraints on the solution of the problem. For example, slope flattening or use of berms requires that adequate space is available. Ease of construction and overall cost are additional considerations.

Economic Analysis

Once a set of alternative treatments has been identified, designed, and verified, a cost analysis for each treatment is conducted. NYSDOT cost estimates are based on earthwork items and other required engineering activities (e.g., control of traffic, etc.). Some treatments may necessitate the acquisition of additional rights-of-way, the cost of which must be incorporated in the economic analysis. Typically no benefit-cost analysis is undertaken on stabilization projects because treatments are expected to secure slope stability permanently. In cases in which controlled failure concepts are applied, an economic analysis includes estimated annual maintenance costs.

Final Recommendations

The final selection from the set of eligible treatment options is generally based on the minimum overall cost. Other factors include the urgency of the problem, availability of contractors to perform the work, the timing of the construction, and the ever-present political considerations.

SLOPE MOVEMENT AND STABILITY CONSULTANT

The DSS under development is expected to serve as an intelligent slope stability consultant (STABCON). In this capacity, its mission is to offer guidance in pursuing the tasks involved in the evaluation and treatment of slope instability problems. The initial implementation of STABCON is in a prototype that incorporates knowledge on significant aspects of the problem. Limitations are mainly in reference to types of slope failure mechanisms and number of treatments considered. The complete system is expected to expand the domain of applicability of STABCON without altering its architecture.

Problem Solving

A variety of problem-solving strategies may be followed using expert system techniques. Most applications can be formulated on the basis of a derivation or formation approach (9). In the derivation approach, a list of appropriate solutions for a problem is placed in the knowledge base, and the problem conditions produce the final recommendation. In contrast, in the formation approach only important aspects of the solution are placed in the knowledge base, and the final recommendation is synthesized from those aspects that are rendered valid by the problem conditions. Depending on the nature and overall complexity of the problem under investigation, the design of an expert system may use either the derivation approach, the formation approach, or both.

The implementation of STABCON was done through the use of the expert system tool Insight II+. In addition to meeting the requirement for a personal computer-based solution, Insight II+ has a number of features that make programming easy. Examples of such features include the ability to provide explanations for the reasoning process and built-in interfaces to external analysis programs and databases. Its control structure is based on a backward chaining methodology that falls in the category of the derivation approach described above. Thus, a goal state is selected and the system checks to establish whether supporting conditions are met. If this is not the case, the system pursues the state under consideration as a subgoal. This process is repeated until the original goal state is acceptable or disqualified.

Functions Pursued by STABCON

A functional overview of STABCON designed to support the landslide investigation and treatment methodology is shown in Figure 3. The first function involves the selection by the

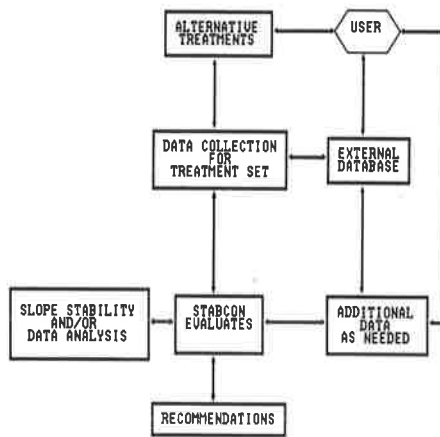


FIGURE 3 Schematic illustration of functions pursued by STABCON.

user of a goal, or set of goals, to be achieved. This function involves the identification of one or several alternative treatments for the slope movement or instability problem at hand. In using STABCON, it is also possible not to select a specific treatment at the goal identification stage. In such a case the system pursues its reasoning by considering all feasible goals (treatments) in accordance with the specified problem conditions. This feature may be desirable in practice for conditions under which no obvious treatment alternative is identifiable at the outset.

Depending on the goal selected, STABCON initiates the data collection activity to obtain data required to evaluate the selected goal. This represents the second phase in the search for the validation of a selected goal (or identification of feasible goals, if none was selected).

Once data collection is completed, STABCON uses an inference strategy, in which the viability of the selected treat-

ments in controlling the movement or instability of the slope under investigation is evaluated. This represents the third phase in the search process during which, in addition to evaluating the rules stored in its knowledge base, STABCON may need additional data on which to base its judgment. Thus, in the functional structure of the system (Figure 3), a branch is created to request user input, extract information from the data base, or, if necessary, access external programs to pursue slope stability calculations and data analysis.

The last function of STABCON involves an evaluation of the various treatment alternatives. In cases in which required information is not available, no final recommendation is offered. Instead, STABCON provides a list of data that must be obtained in order to complete the evaluation. In all other cases STABCON produces viable final recommendations.

IMPLEMENTATION OF STABCON

Knowledge Base

Once the conceptual design was defined and the knowledge structure for the system was acquired the next phase of the study was focused on the implementation of the prototype. Figure 4 shows the three principal functional components of the STABCON system: knowledge base, data bases, and analytical functions.

The knowledge acquisition process aimed to identify the critical elements of landslide investigation and treatment recommendations. To this end, a panel of experts was formed, the membership of which included representatives from the Soil Mechanics Bureau of NYSDOT. The initial focus of the panel was on the features and architecture of the proposed STABCON model (10). Also addressed were the principal methods used for correcting landslide areas.

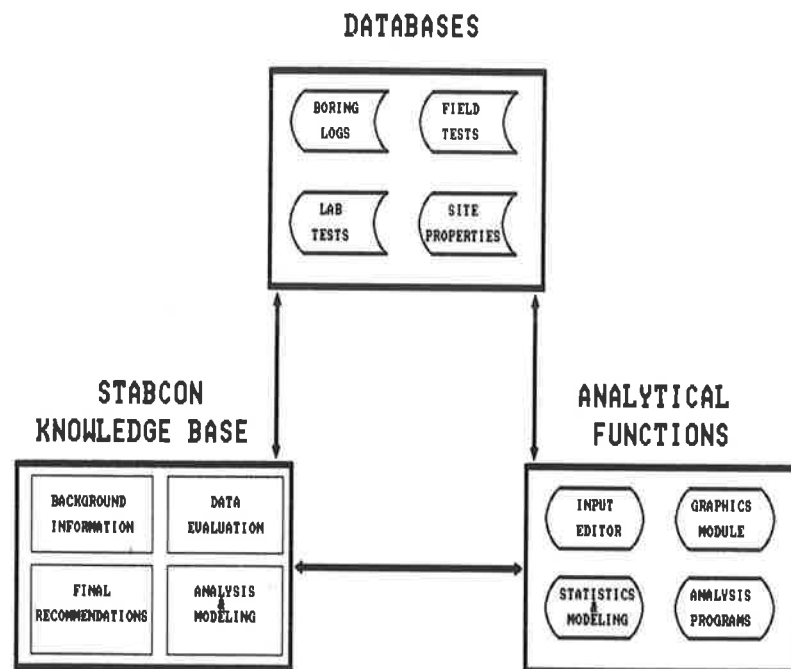


FIGURE 4 STABCON's primary functional components.

Once a general consensus was reached concerning the scope and domain of the system, a description of the approach to knowledge acquisition and of procedures to conduct the detailed design of the system was distributed to the panel. Factors important to landslides that were identified by the panel are as follows:

1. Artesian water pressure,
2. Type of roadway cross section,
3. Type of slide,
4. Average inclination of existing slope,
5. Field observations,
6. Shear strength parameters,
7. Old failures,
8. Recent construction activity,
9. Streams and creeks,
10. Rainfall,
11. Soil stratigraphy,
12. Creep (deep and shallow),
13. Leaching,
14. Surface water infiltration,
15. Progressive failure,
16. Strength softening,
17. Clay mineral,
18. Anisotropy,
19. Rate of movement,
20. Type of clay (fissure, intact, etc),
21. Number and shape of soil layers,
22. Number and value of water tables,
23. Slope of possible failure plane,
24. Relative permeability of strata,
25. Surface water,
26. Subsurface water,
27. History of area, and
28. Geology and topography.

Information on each of the factors was recorded on a knowledge acquisition form. A special form was created to collect information for the knowledge base as well as to clarify the relative importance of each factor in the landslide analysis process. It also addressed the manner in which missing or incomplete information could be generated. The information gathered was vital for developing the knowledge base and constructing the consultation paradigm.

After factors that influence landslides were identified, the system development process was focused on describing the landslide investigation process from each panelist's perspective. This resulted in the process summary shown in Figure 5. This process was consistent with NYSDOT's past practices and guidelines for slope maintenance and restoration in a related FHWA report (11).

Further interaction with the panel examined how geotechnical engineers approach a typical landslide investigation. The generated information served as background for describing the reasoning followed by experts and the manner in which they deal with the numerous factors that are associated with each landslide site. It was relatively easy for the panel to describe in detail an expert's approach to site familiarization, field investigation and preliminary analysis. However, it was not easy to describe in a rigorous manner the process of detailed investigation and the criteria for accepting a final treat-



FIGURE 5 Landslide investigation process.

ment recommendation, areas in need of additional studies and research.

KNOWLEDGE REPRESENTATION

The acquired knowledge was used to formulate the knowledge base and process structure of the system. The prototype was created in a PC-based environment using Insight II+ as the software development tool. Main features of this tool include the Production Rule Based language (PRL), interfaces to DBII and DBIII databases, an internal database (DBPAS), and an explanation facility. A typical rule from the knowledge base is as follows:

```

CONF (the water conditions ARE artesian) = -2
THEN water conditions unknown
AND DISPLAY unknown water conditions
  
```

Rules similar to the above were derived on the basis of the knowledge retrieved from the expert panel. They were then formulated in a forward chaining inference mechanism used by STABCON, and input screens and supporting explanation screens were constructed.

EXTERNAL DATABASES

Boring Logs

Borings taken at failure sites aid in determining possible causes for incurred failures and in establishing additional investigative paths. The importance to landslides of the information generated through borings requires that STABCON be able to call on it on an as-needed basis. To achieve this system objective, data are maintained in a PC-based ORACLE relational data base system. Programmatic interfaces are required to recall the data in conjunction with the knowledge

base. An example of a boring log used at NYSDOT is shown in Figure 6.

An examination of the boring log suggests that the data structure of the boring log can be decomposed into a group of common categories. This decomposition represents the normal form for the relational data base design. The principal divisions are as follows:

1. Boring data: general information on boring location and details,
2. Boring sample: data on each sample in the boring,

DEPTH SURFACE		BLOWB CASING	SAMPLE NO.	BLOWS ON SAMPLER					DESCRIPTION OF SOIL AND ROCK	MOIST. CONT. %
0	5			10	15	20	25			
0.0	b	J-1	2						Br. Ang. Gravelly SILT., Sandy With Roots (M-NP)	11
	9									
	19									
	29									
5.0	75	J-2	19						Br. Coarse Sandy GRAVEL Silty (M-NP)	7
	635									
	540								Rock Run 3.0" Diamond Bit N-1403 (U-NP)	
	750									
	659									
10.0	265	J-3	12						Gr. Coarse Sandy GRAVEL Silty (U-NP)	9
	147									
	37									
	74									
	56									
15.0	40	J-4	12						Gr. Silty Coarse SAND With Gravel (M-PLW)	11
	67									
	28									
	100									
	323									
20.0	221	J-5	26						Gr. Ang. Gravelly SILT., Sandy (U-NP)	12
	109									
	72									
	127									
	266									
25.0									AST Run 1.0" Diamond N-1403 (U-NP)	

THE SUBSURFACE INFORMATION SHOWN HEREON WAS OBTAINED FOR STATE DESIGN AND ESTIMATE PURPOSES. IT IS MADE AVAILABLE TO AUTHORIZED USERS ONLY THAT THEY MAY HAVE ACCESS TO THE SAME INFORMATION AVAILABLE TO THE STATE. IT IS PRESENTED IN GOOD FAITH, BUT IS NOT INTENDED AS A SUBSTITUTE FOR INVESTIGATIONS, INTERPRETATION OR JUDGEMENT OF SUCH AUTHORIZED USERS.

CONTRACT _____ INSPECTOR _____

DRILL RIG OPERATOR D. J. BISHOP
 SOIL & ROCK DESCRIPTION J. D. SAXTON
 REGIONAL SOILS ENGINEER _____
 STRUCTURE NAME _____
 B. I. N. _____

SHEET 1 OF 2 HOLE DA-B-8888

FIGURE 6 Typical boring log.

- 3. Boring visual: visual description of major subdivisions within the boring (interpreted by driller), and
- 4. Water readings: data describing water readings during boring.

The boring log data entry application is currently in prototype mode on an IBM 4381 system. Plans call for porting the application to the PC-based ORACLE products to support the STABCON system.

Earth and Rock Slope Evaluation System

Information of importance to STABCON is available in the existing Earth and Rock Slope Evaluation System (EARSSES). EARSSES is a data base that contains ratings of all critical rock and earth slopes in New York State. EARSSES currently operates on an IBM 4381 and is not directly accessible by the STABCON prototype system. Future developments will include the creation of an interface between STABCON and EARSSES that will eliminate the present redundancy in entering site data and will contribute toward automation of slope evaluation.

Field Instrumentation

A field instrumentation data base is also important to the STABCON system. At a failure site, measurements of displacement and pore water pressure are often essential to evaluating stability. Rates and magnitudes of movements are of extreme importance when critical stability decisions, which impact the safety of the traveling public, are made. The implementation of a complete field instrumentation data base is among future developments of the system.

Analytical Functions

Certain functions of STABCON require interfaces with analytical programs. Two significant analytical programs were identified for STABCON. One was the infinite slope analysis, which is used by engineers investigating landslides for preliminary analysis of failure sites. A goal of the STABCON system was to simplify the analytical interface and provide a means to use the analytical programs with minimal training.

Infinite slope analysis, structured as a separate module, has been placed in the knowledge base of STABCON in the form of rules and checks. Many other programs are available that perform stability analysis for geotechnical investigators. Among them is the commonly used STABL program, a version of which provides graphical screen output (GEOSLOPE). This makes it easy for the user to quickly review the cross section for obvious input errors. The screen output does not allow users to review soil properties associated with soil stratigraphy. Instead, users must compare data maintained in a data input file.

The use of this program in the STABCON environment led to creation of an improved input editor that eliminates the need for highly specialized skills to utilize the STABL program. The normal data structure of the input data was mod-

ified to include a soil type attribute. This enabled the knowledge base to perform checks and compare values of similar soil types. It also facilitated the creation of screen output, which reveals soil stratigraphy and properties in a straightforward manner.

Application of STABCON

When STABCON is initiated, it begins pursuing the process shown in Figure 7. To provide consultation, the system monitors the assertions in the knowledge base and, when conditions necessitate it, an advisory screen is automatically invoked. Help screens are available to assist users by supplying required background information.

A user may select as many geotechnical factors as considered applicable to the failure site. The user may also press a dedicated function key to bring up a detailed screen that explains each of the factors to be displayed. In this case, the user is also requested to state his confidence in his answer by entering a numerical value between 0 and 100 percent. A value of 0 means the answer is not certain, whereas a value

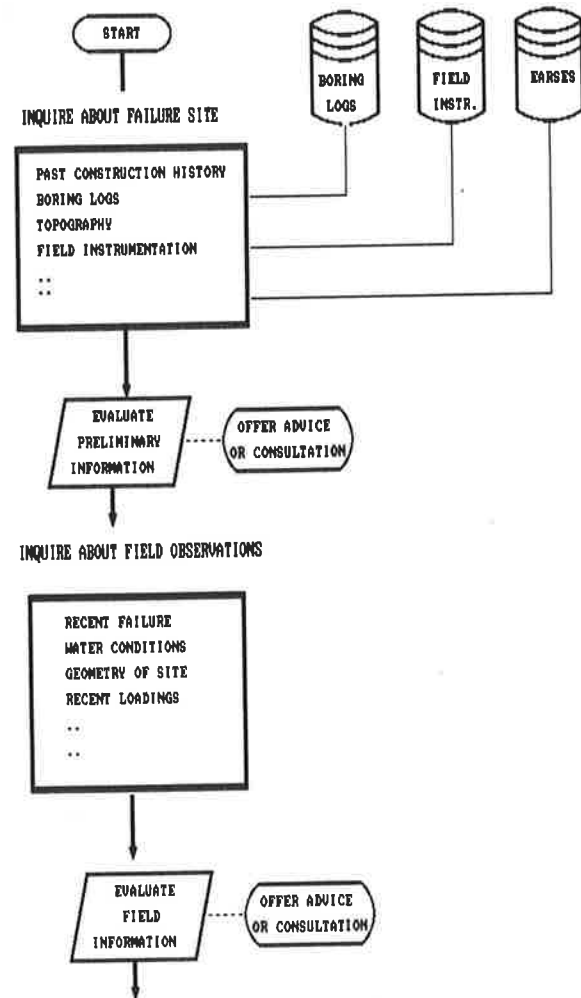


FIGURE 7 Sequence of activities in applying STABCON.

of 100 declares the answer to be known with certainty. Confidence factors are used by the system to evaluate additional investigation is required to reach a conclusion. After progressing through the general problem description screens, STABCON arrives at the preliminary analysis phase. STABCON asks whether a preliminary factor of safety has been established at the site. If the factor of safety has already been determined, STABCON pursues an additional check by invoking an infinite slope analysis.

The next assessment made by the system is the influence of water at the failure site. If water conditions are not known, STABCON offers some advice on how to establish them and provides guidelines for estimating their influence. In some instances, more detailed stability analysis is needed to interpret the sensitivity of the site to variable water conditions. To facilitate this analysis, an input editor to the GEOSLOPE stability program is used. The user invokes the input editor from the main menu of Insight II+ and is guided through a series of screens to describe the failure site. When completed, the input editor creates an input data file in a format that is accepted by the GEOSLOPE program. After the analysis is completed, the results are passed to the STABCON knowledge base, where the system performs a series of checks and makes further recommendations concerning the site. Possible alternatives at this stage include a request for additional field surveys or other investigations to better define the site and additional computer runs.

DISCUSSION OF RESULTS

The approach to knowledge acquisition followed in this study generated a broad background from which to develop rules for the knowledge base. Difficulty was experienced in the attempt to identify specific requirements for various treatment options, and relationships in the domain were not readily apparent. The knowledge acquired was focused on procedures and supporting data, which are represented in the system by analytical programs and data bases. In this respect, the domain under study was intensive in its requirements for programmatic and data base interfaces. The interface to the stability program is an essential attribute of STABCON because it enables an independent verification of the stability analyses performed by users.

The use of Insight II+ as a development tool made the creation of input and output screens an easy task. Knowledge representation formats provided by the tool were adequate for knowledge base development at the prototype level. A challenging task in developing the system was consideration of the alternatives that exist when information is unknown or incomplete. These decision paths made debugging the system cumbersome because tracing the process flow can often be obscure. The main drawback in the selected tool was in the area of programmatic interfaces, namely, the lack of computer memory to keep the development tool resident and concurrently run the STAB computer program.

SUMMARY AND CONCLUSIONS

The objective of the study was to create a prototype system that could evaluate the application of knowledge based sys-

tems to the landslide treatment domain. In the initial phase of this study, an exhaustive review of factors that influence active landslides was conducted. This was followed by the conceptual design that defined the processes and performance of the system. Emphasis was placed on failures occurring through soil masses along circular or wedge-type surfaces. An expert panel from the NYSDOT Soil Mechanics Bureau was formed to review the conceptual design and assist in the knowledge base development for the prototype. STABCON was developed using the Insight II+ tool and was successful in implementing the early phases of the conceptual design.

Future development is expected to include studies and interviews with domain experts to expand and better define the knowledge base. Furthermore, data base and program interfacing will be added to support a more robust system. Moving the prototype to a larger development environment will allow an integration of the system with data bases and analytical programs.

On the basis of the development effort to date, the following conclusions may be drawn:

1. Landslide analysis and treatment is a domain well suited to an expert system approach. Reasons for this include (a) the reasoning commonly used and the interpretation of available data are based on experience; (b) decisions are often made on incomplete or missing information; and (c) the expertise of the limited number of experts on this subject is scattered over a broad field.
2. Extracting knowledge from experts on specific components of the domain is a difficult task. An alternative (to questionnaires) approach of acquiring knowledge from experts is needed to create a production level (as opposed to prototype) knowledge base.
3. It is essential that the decision methodology be supported by a comprehensive data base management system and analytical techniques in order to encompass all aspects of the landslide domain.
4. The Insight II+ development tool does not possess sufficient memory to enable concurrent use of knowledge base and stability analysis programs. A production system requires additional computer resources.

REFERENCES

1. R. G. Chassie and R. D. Goughnour. National Highway Landslide Experience. *Highway Focus*, Vol. 8, No. 1, 1979, pp. 1-9.
2. J. P. Kohn and J. E. Slasson. Landslide Potential in the United States. *California Geology*, Vol. 29, No. 10, 1976, pp. 224-231.
3. R. H. Sprague, Jr., and E. D. Carlson. *Building Effective Decision Support Systems*. Prentice-Hall Inc., Englewood Cliffs, N.J., 1982.
4. R. L. Schuster and R. J. Krizek (eds.). Special Report 176: Landslides: Analysis and Control. TRB, National Research Council, Washington, D.C., 1978, 234 pp.
5. D. A. Grivas. Probabilistic Evaluation of Safety of Soil Structures. *Journal of Geotechnical Engineering Division, ASCE*, Vol. 105, No. GT9 Sept. 1979, pp. 1091-1095.
6. C. B. Brown and I. P. King. Automatic Embankment Analysis-Equilibrium and Instability Conditions. *Geotechnique*, Vol. 16, No. 3, Jan. 1966, pp. 209-219.
7. K. Y. Lo and C. F. Lee. Stress Analysis and Slope Stability in

- Strain-Softening Materials. *Geotechnique*, Vol. 23, No. 1, March 1973, pp. 1-11.
8. S. K. Sarma. Stability Analysis of Embankments and Slopes. *Journal of Geotechnical Engineering Division, ASCE*, Vol. 105, No. GT12, Dec. 1979, pp. 1511-1524.
 9. M. L. Maher (ed.). Problem Solving Using Expert System Techniques. *Proc., Expert Systems in Civil Engineering*, ASCE, New York, N.Y., 1987, pp. 7-17.
 10. D. A. Grivas and J. C. Reagan. An Expert System for the Evaluation and Treatment of Earth Slope Instability. *Vth International Symposium on Landslides*, Balkema Publishers, Lausanne, Switzerland, July 1988, Vol. 1., pp. 649-654.
 11. G. Kleindinst, A. Munoz, and C. W. Niessener. *Guidelines for Slope Maintenance and Slide Restoration*. Report TS-85-231. FHWA, U.S. Department of Transportation, 1986.

Publication of this paper sponsored by Committee on Transportation Earthworks.

Correlating Resilient Moduli from Pressuremeter Tests to Laboratory California Bearing Ratio Tests

PAUL J. COSENTINO AND YANGTING CHEN

In order to increase the usefulness of the pressuremeter (PMT) in the area of pavement design and evaluation, resilient moduli, determined from a special PMT test, were correlated to California Bearing Ratio (CBR) test results. The PMT resilient moduli-CBR correlations developed compared well with existing resilient moduli-CBR correlations. The special PMT test, called the resilient modulus PMT test, was developed to enable six resilient moduli to be determined from six unload-reload cycles conducted for various load durations along the linear portion of the in situ stress-strain response. The various cycle lengths enabled resilient moduli to be determined as a function of the load durations typically encountered during the traffic loading of a pavement. The cycle lengths used were 10, 20, 30, 60, 120, and 240 sec. The PMT used was the monocell TEXAM pressuremeter built by Rocrest, Inc. It was concluded that the current TEXAM PMT cannot be used to accurately conduct 10-sec unload-reload loops to determine resilient moduli, but can be used to accurately determine resilient moduli for the remaining cycle lengths and that the resilient moduli from these cycles are reasonable for use in design.

In an attempt to increase the usefulness of the pressuremeter (PMT) (Figure 1) in the field of pavement design, simple correlations were developed between PMT resilient moduli and PMT limit pressures and laboratory California Bearing Ratio (CBR) values. The PMT resilient moduli were correlated to the CBR values using the empirical relationship $M_r = B \times \text{CBR}$, where the constant B has a published range of 200 to 3,000, depending on the soil type, with a recommended value of 1,500 for design (1). Pavement designers have been attempting to determine reasonable values of resilient moduli for design since the 1986 AASHTO *Guide for the Design of Pavement Structures* (2) presented pavement design procedures based on resilient moduli. Cosentino (3) showed the usefulness of the pavement pressuremeter in predicting resilient moduli for airport pavements. The pavement pressuremeter is a scaled-down version of the PMT shown in Figure 1, with a probe length of 10 in. (25.4 cm), and a probe diameter of 1.30 in. (3.30 cm) (3). One major conclusion of the pavement PMT (1987) study was that all PMT models could be used to determine the stress-strain of soils subjected to various loading rates or durations. Because the pavement PMT was not available at Texas Tech University, where the study was conducted, the TEXAM PMT owned by the civil engineering department was used.

P. J. Cosentino, Civil Engineering Department, Florida Institute of Technology, 150 West University Boulevard, Melbourne, Fla. 32901-6988. Y. Chen, Department of Civil Engineering, University of Texas, Austin, Texas 78713.

Resilient moduli are typically found from either cyclic triaxial tests or nondestructive pavement evaluation tests, such as falling weight deflectometer or dynaflect tests. The resilient modulus is defined as the modulus associated with the elastic rebound, or resiliency, of the paving materials. It can be more simply described as the unload stress-strain slope developed during the impulse loading that occurs as vehicles pass over the pavement. The resilient modulus for one vehicle load is depicted in Figure 2 as

$$M_r = \sigma_d / \epsilon_r$$

where

M_r = resilient modulus,
 σ_d = deviator stress or applied stress, and
 ϵ_r = is the resilient or elastic rebound strain.

The current PMT models are only capable of yielding stress-strain data at points A , B , and C in Figure 2. Determining resilient moduli from cyclic triaxial tests appears to be the most logical approach from an engineering standpoint. During cyclic triaxial testing, samples of the base, subbase, or subgrade are placed in a triaxial chamber, subjected to appropriate confining pressures, and loaded by impulse loads, by pulsing the axial load at rates and magnitudes similar to those encountered on the pavement. Stress-strain plots are used to determine the design resilient modulus. The major drawbacks of cyclic triaxial tests are the time requirements of a single test (2 to 8 hr, depending on the material), the initial equipment costs (\$20,000 to \$100,000, depending on system chosen), and the expertise required to conduct cyclic triaxial tests on representative samples. These drawbacks have prevented the industry from easily adopting the cyclic triaxial test as a standard.

Nondestructive testing (NDT) is used to backcalculate resilient moduli of the individual pavement layers, and have proven useful for determining the existing structural capacity of large sections of pavement. The major drawback of backcalculating moduli from NDT is the requirement that the layer thickness be precisely known. Thus, even though NDT of pavements is an efficient approach for determining layer moduli, the moduli found can be highly questionable simply because of the uncertainty of the layer thicknesses. Pavement practitioners who use NDT have difficulty determining design resilient moduli values for input into overlay design procedures.

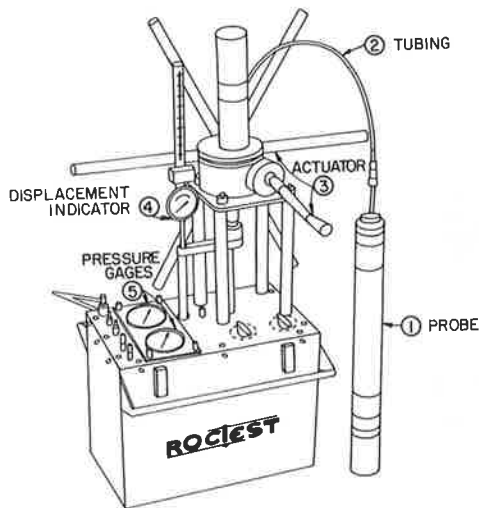


FIGURE 1 TEXAM PMT.

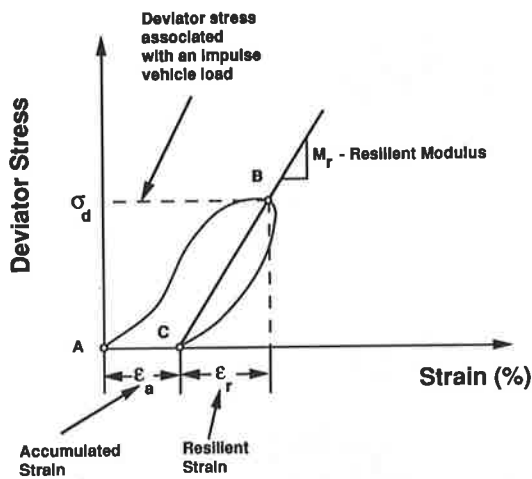


FIGURE 2 Representation of resilient modulus.

TESTING EQUIPMENT DESCRIPTION

The equipment used for this research is the TEXAM PMT (Figure 1) and the standard CBR equipment typically used in pavement design (Figure 3).

Pressuremeter

The PMT, originally developed in 1956 by Ménard (4) is an in situ testing device that has a rubber membrane that expands cylindrically in a test hole when pressurized with a fluid (Figure 1). Because PMT tests can be conducted in any type of soil or rock and can be used to run either stress-controlled or strain-controlled tests, they have become a useful geotechnical engineering tool. The TEXAM monocell PMT, manufactured by Roctest, Inc., Plattsburg, New York (Figure 1), consists of a control unit, a 50-ft (15 m) section of nylon tubing, and an expandable probe. The PMT shown costs about \$10,500. Tests are conducted once the PMT is placed at the required depth in a 3-in. (7.62 cm) diameter borehole. During testing,

the 18-in.-long (46 cm), 2.94-in. (7.5 cm) diameter cylindrical probe, covered with a flexible membrane, is inflated with water by moving a piston with the manual actuator. The inflation creates pressure against the wall of the borehole, which is the radial stress (σ_{rr}). Throughout the test, the pressure is recorded from a pressure gauge, and the increase in volume of the probe ΔV is recorded from the displacement indicator. A calibration that determines the initial volume (V_o) allows for the volumetric increase ($\Delta V/V_o$) to be obtained. This volumetric increase is converted to the hoop strain $\epsilon_{\theta\theta}$ (5) and an in situ stress-strain curve is obtained. Figure 4 shows a typical in situ stress-strain curve from a pressuremeter test. Assuming the length to diameter ratio of the PMT is of sufficient length to simulate an expansion of an infinitely long cylindrical cavity, soil moduli can be determined from the theory of elasticity. Baguelin et al. (4) developed the following equation for determining elastic moduli between any two points on the stress-strain curve (Figure 4):

$$E = 2(1 + \nu) \left(\frac{\Delta p}{\Delta V} \right) V_m \tag{1}$$

where

- E = soil modulus,
- ν = Poisson's ratio,
- Δp = change in pressure on the cavity wall ($\Delta\sigma_{rr}$)
- ΔV = change in volume of the PMT, and
- V_m = the volume midway through the pressure increment.

Equation 1 was revised as follows to enable calculation of elastic moduli based on the hoop strain (5).

$$E = (1 + \nu) \left[\left(1 + \frac{\Delta R_1}{R_o} \right)^2 + \left(1 + \frac{\Delta R_2}{R_o} \right)^2 \right] \left[\frac{\sigma_{rr2} - \sigma_{rr1}}{\left(1 + \frac{\Delta R_2}{R_o} \right)^2 - \left(1 + \frac{\Delta R_1}{R_o} \right)^2} \right] \tag{2}$$

where

- ΔR_1 = increase in probe radii at the beginning of the pressure increment,
- ΔR_2 = increase in probe radii at the end of the pressure increment,
- σ_{rr1} = radial stress at the cavity wall at the beginning of the pressure increment,
- σ_{rr2} = radial stress at the cavity wall at the end of the pressure increment, and
- R_o = initial radius of the probe.

This revised calculation makes it possible to compare results from various size PMTs, because the reduced data is plotted as radial stress versus hoop strain instead of radial stress versus volumetric increase ($\Delta V/V_o$). A single PMT test like the one shown in Figure 4 involves increasing the initial volume of the probe from V_o to $1.5V_o$ during 10 min in order to simulate undrained soil behavior. The initial volume of the TEXAM PMT is 108 in.³ (1770 cc), and a test is completed when 73 in.³ (1200 cc) of water is added in 3.7 in.³ (60 cc) increments,

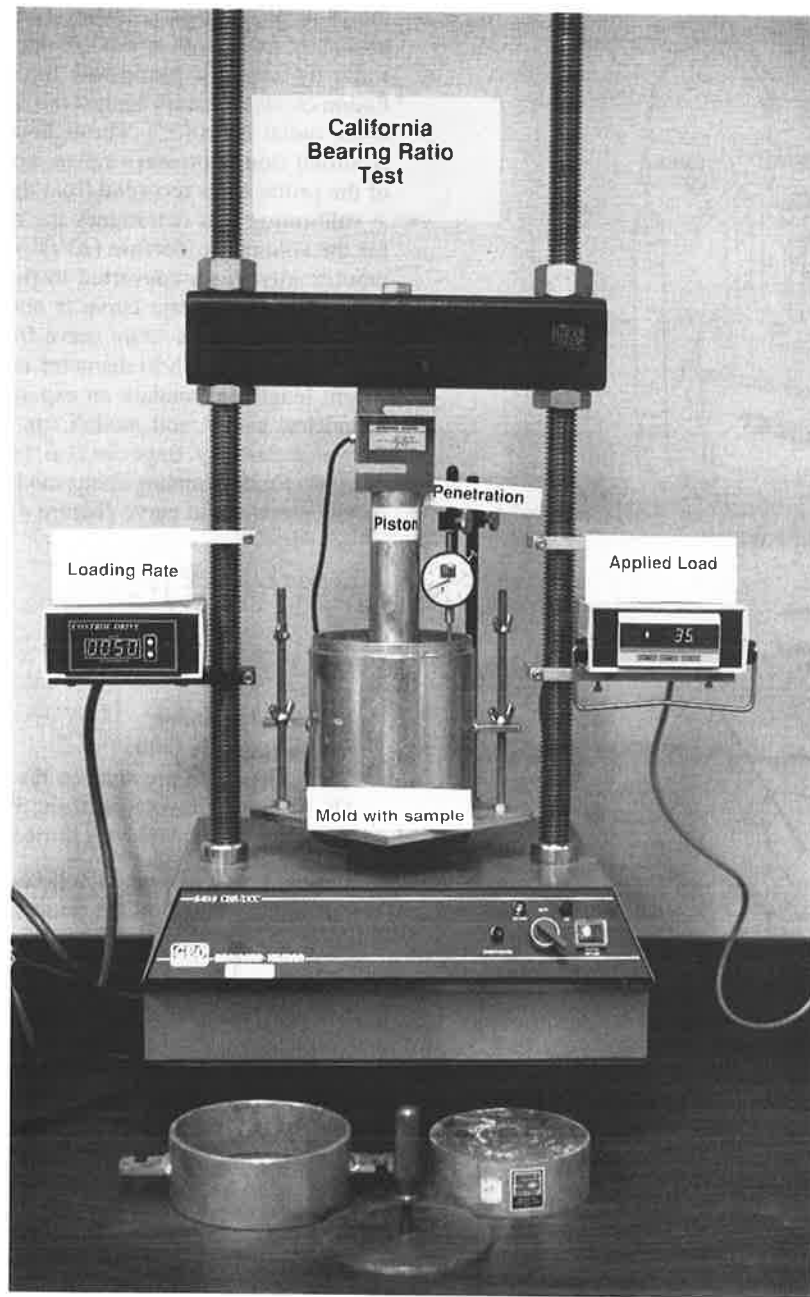


FIGURE 3 Standard CBR equipment.

which are each held constant for 30 sec. Each PMT test requires calibrations for membrane resistance, system expansion, and hydrostatic pressure. The membrane and system expansion calibrations are conducted with the PMT in the field, whereas the hydrostatic correction is simply applied to the recorded pressures. Details of the calibration techniques can be found elsewhere (6).

The California Bearing Ratio

The standard CBR equipment as required by ASTM D1883-73 (Figure 3) was used for this research (7). CBR tests were

conducted in a triaxial load frame on unsoaked samples, which were compacted to in situ moisture-density conditions.

FIELD TESTING SITES

Five testing locations were used during the research. An initial PMT testing phase was conducted at three sites in Lubbock County Texas (Figure 5) such that a resilient modulus PMT test (Figure 6) could be developed for the PMT-CBR correlations. Site 1 was the Texas Tech University (TTU) National Science Foundation (NSF) Wind Research site. Site 2 was the grass-covered area near the east entrance of the TTU

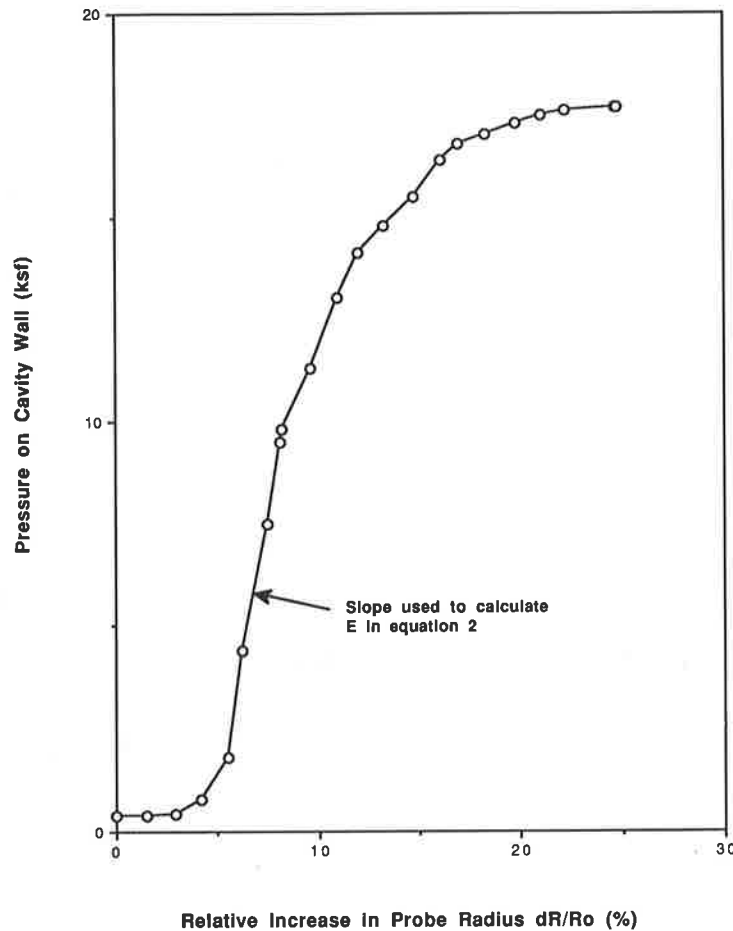


FIGURE 4 Stress-strain curve from a standard PMT test.

civil engineering building. Site 3 was located at Tech Tracer Park, on Boston and 29th streets in the city of Lubbock (Figure 5). Problems were encountered at sites 1, 2, and 3; therefore, once the resilient modulus PMT test was developed, 2 new test sites (4 and 5) (Figure 5) in Lubbock County were used to perform tests for the PMT-CBR correlations. Problems during the testing program are described in the Testing Program section. Site 4 during the final testing phase for the PMT-CBR correlations was the off-base recreational area near the tennis courts at Reese Air Force Base (AFB). Site 5 was the playa used by the TTU Water Resources Center in Shallowater, Texas (Figure 5).

SOIL CONDITIONS

In geologic terms the three sites used for development of the resilient modulus PMT test are part of the Acuff soils formed during the Pleistocene age. These soils are eolian materials that were deposited during dry periods of high winds. They originated in the southwestern regions of the United States and are commonly referred to as cover sands. They vary from clayey sands in the southern portions of Lubbock County to sandy clays in the northern portions of Lubbock County. Two different soil deposits were encountered during testing for the PMT-CBR correlations. The soil encountered at Reese AFB

is an eolian clayey sand from the Acuff formation, whereas the soil in the playa at Shallowater is an organic Randall series clay. The Randall clays formed along with the Acuff soils during the Pleistocene age at the bottom of the playa lakes.

From an engineering standpoint, the soil at Site 1 was a medium dense reddish brown, cemented sandy clay (Table 1). These soils commonly exhibit angles of internal friction from 40 to 45 degrees when dry; however, if they become wet, a significant loss of shear strength occurs. The soils at sites 2 and 3 are a loose reddish brown, cemented sandy clay (Table 1), which exhibit the same loss of shear strength during wetting. The soils at Site 4 are a loose grayish brown cemented sandy clay. Their cementitious properties also affect shear strength upon wetting. The soil at Site 5 is a soft dark gray organic clay. The typical soil properties for the five sites are summarized in Table 1. In the Acuff soils, sites 1 through 4, the unit weight ranged from 105 to about 115 pcf (16.5 to about 18.0 kN/m³), with water contents ranging from 6.4 to 14.2 percent. In the organic clay at Site 5, the unit weights ranged from 79.8 to 94 pcf (12.5 to 14.7 kN/m³), with water contents ranging from 22.7 to 30.3 percent.

TESTING PROGRAM

The testing program consisted of 29 PMT tests, 32 CBR tests, 9 standard penetration tests (SPTs), 21 troxler nuclear

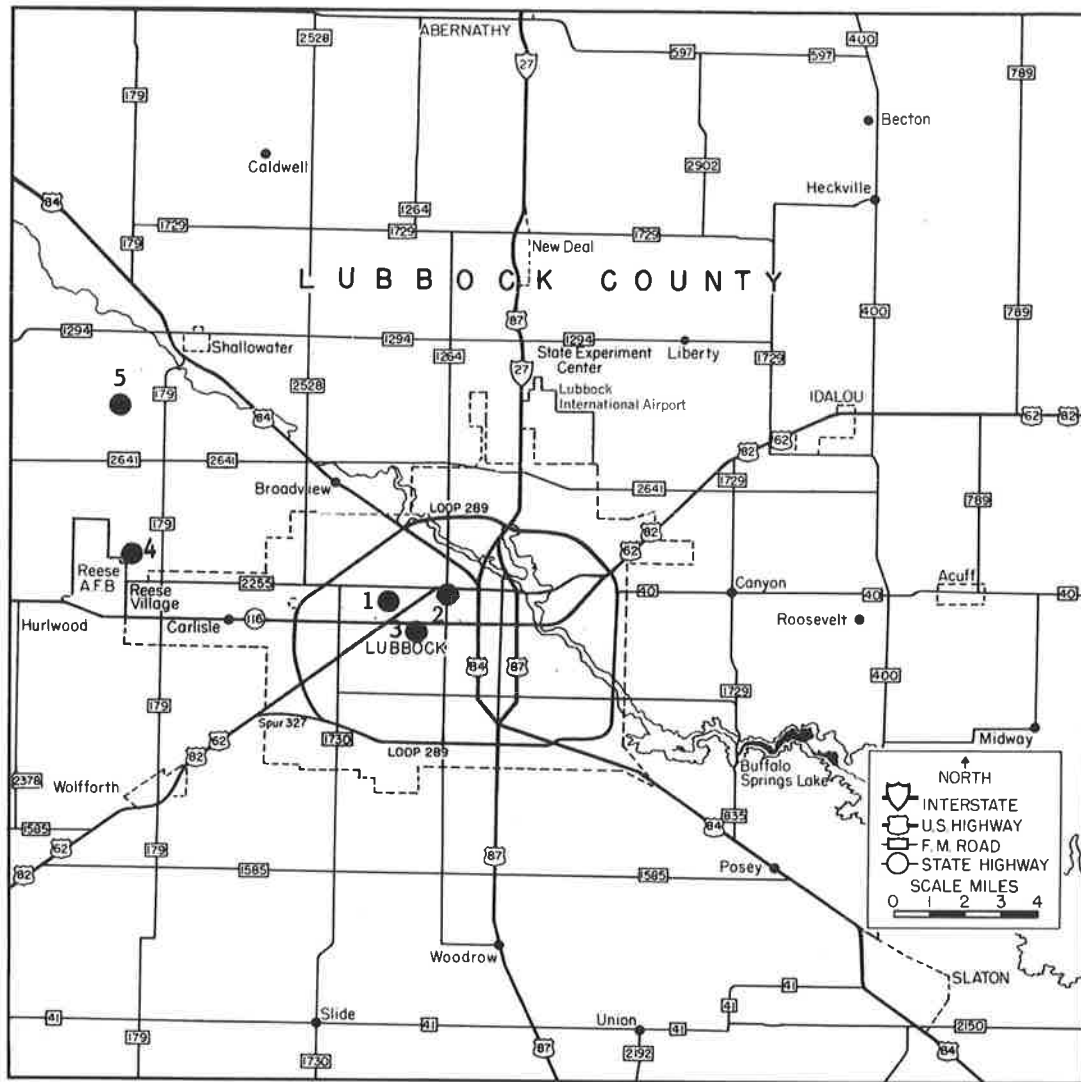


FIGURE 5 Test sites: 1, NSF Wind Research site; 2, TTU; 3, Tech Tracer Park; 4, Reese AFB; and 5, Shallowater.

moisture-density tests, 33 laboratory water content determinations, and 2 grain size analyses. During the initial phase at sites 1, 2, and 3, 11 PMT tests, 5 troxler tests, and 9 laboratory moisture content tests were conducted. During the PMT-CBR correlation phase at sites 4 and 5, 18 PMT tests, 32 CBR tests, 9 SPTs, 16 troxler tests, 24 laboratory moisture content tests, and 2 grain size analyses tests were conducted. PMT tests were typically conducted in hand-augered test holes about 4 ft deep.

Three different sites were considered during the initial testing phase to enable the various site specific testing problems encountered during this research to be alleviated. Only one PMT test was conducted at Site 1 because of difficulties encountered during hand-augering the borehole for PMT testing. The medium dense cemented sandy clay at site 1 required nearly 4 hr of hand-augering. At Site 2, 6 PMT tests were conducted. The soil types encountered during these tests were similar to those at Site 1. The main difference in the soils was that the top 18 in. (46 cm) at Site 2 was a recompacted sandy clay. This recompacted zone allowed hand-augering to be accomplished; however, due to the cemented nature of the

sandy clay, the remaining portion of the hand-augering for the 4-ft (1.2 m) deep PMT hole was difficult. The total time required to hand-auger a single PMT hole at Site 2 was about 2 hr. Site 3, at Tech Tracer Park, was a cemented sandy clay that was also difficult to hand-auger. Only 1 PMT test was conducted at Site 3 because the hand-augering process again required 4 hr. The purpose of the initial testing phase was to establish the procedure for the resilient modulus PMT test. Because this was accomplished with the 8 PMT tests at sites 1, 2, and 3, Phase 1 of the PMT testing was halted.

The final testing phase for the PMT-CBR correlations took place at Reese AFB and at the playa test site in Shallowater, Texas (Figure 5). On the basis of SPT blow counts, the soil at Reese AFB was identified as a loose cemented clayey silty sand, and visual identification techniques indicated that the soil at Shallowater was a soft organic clay (Table 1).

During the testing at Reese AFB, PMT boreholes were advanced with a drill rig, which enabled fast augering of the four PMT boreholes and made it possible to conduct nine SPTs above and below the PMT tests. Six resilient modulus PMT tests were conducted at Reese; 15 samples were taken

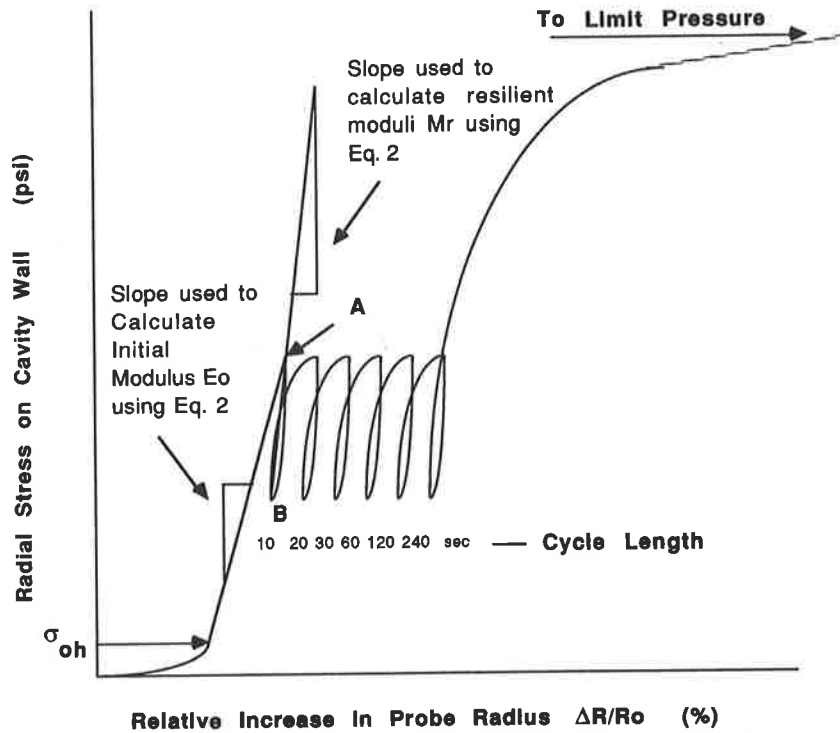


FIGURE 6 Stress-strain curve for a resilient modulus PMT test.

TABLE 1 SITE INFORMATION

Test Site	Soil Description	Average Density (pcf)	Range of Densities (pcf)	Average Water Content (%)	Range of Water Contents (%)
NSF ¹	Med. Dense Reddish brown sandy clay, trace of caliche	115 ⁶	115 ⁶	7.6	7.5 - 7.8
TTU CAE ²	Loose Reddish brown sandy clay, some caliche, trace of gravel	108.6	108.5 - 108.7	8.1	6.4 - 10.3
TTPark ³	Loose grayish brown silty clay, trace of sand	106.4	104.9 - 110.3	13.7	8.6 - 14.2
Reese AFB ⁴	Loose Reddish brown sandy clay, trace of gravel and caliche (SC-Cl)	110.8	107.4 - 113.1	11.6	9.1 - 12.9
Shallowater ⁵	Very soft dark gray clay (OH)	89.7	79.8 - 94.0	28.6	22.7 - 30.3

1. National Science Foundation Wind Research Site, Texas Tech University, Lubbock, Texas
2. Civil/Agricultural Engineering Building, Texas Tech University
3. Tech Tracer Park, Lubbock, Texas
4. Reese Air Force Base, Lubbock, Texas
5. Texas Tech University Water Resources Center Site, Shallowater, Texas
6. Assumed unit weight for site 1

Note: 1 pcf = 0.1572 kN/m³

for CBR testing; 8 troxler moisture-density tests were performed; and 10 samples were taken for water content determinations.

The testing conducted at Shallowater included 14 resilient modulus PMT tests, 20 CBR tests, and 8 troxler moisture-density tests. Hand-augering at this site was simple because the clay soil was soft. Typically 15 min or less was required to auger a 4 ft (1.2 m) deep borehole.

Development of the Resilient Modulus Pressuremeter Test

In order to correlate PMT moduli to CBR values in a manner similar to those published (8), it was determined that several resilient moduli should be found with a single PMT test such that the cycle lengths simulated during testing corresponded to various ranges of pavement vehicle loading rates. On the

basis of work with the pavement pressuremeter, the principal author (3) determined that resilient moduli could be determined from four types of pavement pressuremeter loading sequences. The sequences are variation of stress level, strain level, loading rate, and number of cycles. This knowledge was used to develop a PMT test that would show how the PMT predicts resilient moduli, which vary with cycle length. The PMT test developed (Figure 6) included 6 unload-reload cycles conducted at a predetermined stress level during the linear portion of the soil's stress-strain response, with cycle lengths of 10, 20, 30, 60, 120, and 240 sec. These cycle lengths were chosen because it was assumed that they could be easily conducted with the TEXAM PMT (Figure 1). The inclusion of the cycles resulted in a 17.5-min PMT test. Details of the entire PMT test procedure can be found in work by Chen (6).

Development of the CBR Test

The purpose of the CBR test was to accurately simulate field CBR conditions in the laboratory. Field CBR tests could not be conducted because of funding constraints. In order to simulate field conditions, in situ moisture and density values were determined for each site using a Troxler 3401B moisture-density gauge. The moisture content of the soil augered during PMT testing was then determined and laboratory CBR samples were compacted at the PMT moisture content with a 5-lb (22.2 N) hammer using 25 blows per layer in 3 layers. This procedure enabled in situ densities to be accurately established in the CBR mold (Figure 3). The laboratory CBR tests were conducted in accordance with ASTM D1883-73 (7) on samples obtained from Reese AFB and Shallowater.

DATA ANALYSIS

The data analysis made it possible to compare moduli and limit pressures from PMT tests with CBR values found from laboratory CBR tests.

Analyzing PMT Data

From one resilient modulus PMT test, six resilient moduli values were determined using Equation 2, and a soil limit pressure was determined by extrapolating the resulting stress-strain curve (Figure 6) to a hoop strain $\Delta R/R_o$ of about 41 percent. It was concluded that the PMT moduli determined during the 10-sec cycle were not reliable because of the difficulty encountered while controlling the cycle pressures and volumes during the 5-sec loading and 5-sec unloading sequence. The 5 remaining resilient moduli values from each test were normalized using the resilient modulus associated with the 20-sec cycle length and plotted versus cycle length on a log-log plot (Figure 6). This procedure allowed Riggins' power law model (9), which was originally developed for time dependent behavior of soils subjected to creep loadings, to be modified to account for cyclic loading. Riggins' original model (9) related increase in undrained shear strength S_u to the time of failure as

$$\frac{S_{u1}}{S_{u2}} = \left(\frac{t_2}{t_1} \right)^{n_c} \quad (3)$$

where S_{u1} and S_{u2} are the undrained shear strengths measured at times to failure t_1 and t_2 , respectively, and n_c is the viscous exponent, which can be determined from the slope of a log-log plot of S_{u1}/S_{u2} versus t_2/t_1 . Based on 76 n_c values obtained from 152 laboratory tests on undrained clays Briaud and Garland (10) determined that n_c has typical values from 0.02 to 0.10 and an average value of 0.061. Riggins' model (9) was used by Cosentino to account for the variation in secant moduli with time from pavement pressuremeter tests (3). Using secant moduli the viscous model can be written as follows:

$$\frac{E_{t2}}{E_{t1}} = \left(\frac{t_2}{t_1} \right)^{n_c} \quad (4)$$

where E_{t1} and E_{t2} are the secant moduli determined from PMT tests at times t_1 to t_2 , respectively, and n_c is the viscous exponent, which is negative for a negative slope on the log-log plot of E_{t2}/E_{t1} versus time. In order to model the change in resilient moduli with cycle length, the secant moduli values in Equation 4 were replaced with resilient moduli values to yield the following:

$$\frac{M_{r12}}{M_{r1}} = \left(\frac{t_2}{t_1} \right)^{n_r} \quad (5)$$

where M_{r1} and M_{r2} are the resilient moduli determined from PMT tests over cycle lengths t_1 and t_2 , respectively, and n_r is the associated exponent relating cycle length to resilient modulus (Figure 7).

Analyzing CBR Data

The procedure in ASTM D1883-73 (7) requires the determination of empirical CBR values at piston penetrations of 0.1 (0.25 cm) and 0.2 in. (0.51 cm); and if the CBR value determined at 0.2 in. (0.51 cm) is larger than the value at 0.1 in. (0.25 cm), the test must be rerun. The CBR value is determined by comparing the load developed by the soil tested to the load developed by a standard crushed stone using a 3 in.² (19.4 cm²) piston penetrating the sample at a loading rate of 0.05 in./min. The standard crushed stone develops 3,000 lb (13350 N) of resistance at 0.1 in. (0.25 cm) of penetration and 4,500 lb (20020 N) of resistance at 0.2 in. (0.51 cm) of penetration. Therefore, for example, if the soil tested was able to develop a load of 300 (1335 N) lb at 0.1 in. of penetration and less than 450 lb (2000 N) at 0.2 in. (0.51 cm) of penetration, the CBR value would be 10. ASTM requires corrections to the CBR values based on the shape of the load versus deflection curve.

DISCUSSION OF TEST RESULTS

From the use of the resilient moduli and the limit pressures from the 29 PMT tests and the CBR values from the 32 CBR tests at sites 4 and 5 (Table 1), the following results were

Boring No : TB-15
 Test Site : Reese AFB
 Test Depth : 2.33 ft

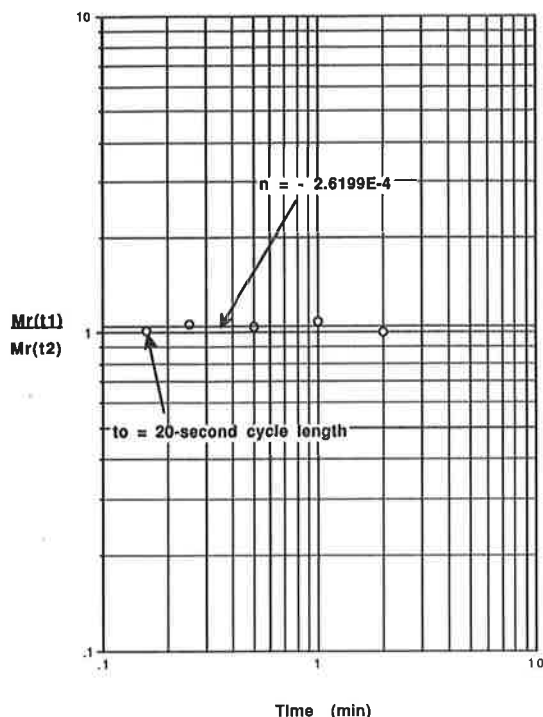


FIGURE 7 Typical normalized resilient modulus versus cycle length plot.

obtained. Values of the resilient moduli for all 29 PMT tests at the 5 sites are presented in Table 2. As can be seen from the table, the resilient modulus generally decreases with increasing cycle length. Additionally, the cemented Acuff soils tests at sites 1, 2, 3, and 4 would be considered good quality subgrade materials, whereas the Randall clay tested at Site 5 would be considered a poor quality subgrade material.

Effects of Loading Rate Variation

The variation of loading rate was studied using Equation 5. The slope of the log-log plot of resilient modulus versus time, n_r , was determined for each set of resilient modulus PMT test results. During this portion of the study, PMT tests from all five sites were used because the PMT testing procedure used for the resilient modulus PMT test was constant throughout the study. Careful examination of the log-log plots representing Equation 5 (Figure 7) indicated that more consistent values for n_r could be obtained if resilient moduli from the 20-sec cycle were excluded. Table 3 presents a summary of the power law exponents considering both the 30-, 60-, 120-, 240-sec and 20-, 30-, 60-, 120-, 240-sec approaches. The values of n_r for the 29 PMT tests ranged from -0.328 to 0.165 if four cycles were used and from -0.126 to 127 if five cycles were used. Because the soils tested ranged from a soft clay to medium dense cemented sands, finding both positive and negative values for n_r could result from a combination of reasons. Negative n_r values indicate that the resilient modulus is decreasing with increasing cycle length. This would be the result expected if sufficient rest time was allowed between successive cycles; however, because cycles were conducted without any rest period, a residual effect should have occurred after each cycle was conducted. The residual effect most likely would result in locked in residual strains, which may or may not affect the remaining cyclic responses. Positive n_r values indicate that the resilient modulus is increasing with increasing cycle length. Although this increase seems unusual, it is indeed possible for the loose to medium dense cemented soils found at sites 1 through 4, because they may simply be experiencing a compaction or strain-hardening process during each cycle due to the absence of the appropriate rest period. There is also a logical reason for the positive n_r values found in the soft clay at Shallowater. In soft clays the TEXAM PMT does not have the precision required to accurately determine elastic moduli values. The TEXAM PMT is only capable of determining moduli values with an accuracy of ± 100 psi (690 kPa). This accuracy range results from the errors accumulat-

TABLE 2 SUMMARY OF RESILIENT MODULUS PMT TEST DATA

Test Site	Resilient Modulus (psi)				
	Range (Average)				
	10 sec	15 sec	30 sec	60 sec	120 sec
NSF	7380 (7380)	7824 (7824)	6819 (6819)	7622 (7622)	6838 (6838)
TTCamp	9237 - 27054 (16915)	9874 - 22660 (15851)	9238 - 19026 (15543)	8931 - 22674 (16856)	9253 - 21655 (16198)
TTPark	8985 (8985)	9874 (9874)	9416 (9416)	9888 (9888)	10073 (10073)
Reese	11926 - 22007 (17086)	12853 - 22755 (18274)	5953 - 22774 (16085)	13121 - 22795 (18696)	11341 - 28330 (19722)
SHWTR	658 - 2290 (1456)	735 - 3052 (1600)	656 - 3439 (1472)	663 - 2503 (1598)	633 - 2057 (1479)

1. National Science Foundation Wind Research Site, Lubbock, Texas
2. Civil/Agricultural Engineering Building, Texas Tech University
3. Tech Tracer Park, Lubbock, Texas
4. Reese Air Force Base, Lubbock, Texas
5. Texas Tech University Water Resources Center Site, Shallowater, Texas

Note: 1 psi = 6.985 kPa

TABLE 3 SUMMARY OF POWER LAW EXPONENTS

PMT Test No.	Test Site	n_R 4 pts ¹	n_R 5 pts ²
TB-01	NSF	-0.042	-0.039
TB-02	TTCamp	0.006	-0.111
TB-03	TTCamp	0.085	-0.081
TB-05	TTCamp	0.030	0.128
TB-08	TTPark	0.016	0.201
TB-09	TTCamp	0.057	0.137
TB-10	TTCamp	-0.077	0.050
TB-11	TTCamp	-0.024	0.137
TB-15 (2.42 ft.)	Reese	-0.049	0.075
TB-15 (7.25 ft.)	Reese	-0.039	0.012
TB-16	Reese	0.063	0.146
TB-17	Reese	0.095	0.125
TB-12	Shallowater	-0.044	0.016
TB-13	Shallowater	-0.071	0.037
TB-22	Shallowater	-0.009	0.071
TB-23	Shallowater	-0.063	-0.031
TB-24	Shallowater	0.025	0.082
TB-25	Shallowater	0.009	0.144
TB-26	Shallowater	0.165	0.153
TB-27	Shallowater	-0.024	0.073
TB-28	Shallowater	-0.328	0.168
TB-29	Shallowater	0.069	0.259

1. Determined using the 30-, 60-, 120-, and 240-second cycles
 2. Determined using the 20-, 30-, 60-, 120-, and 240-second cycles
- Note: 1 ft = .3048 m.

ing due to the precision limitations of the pressure gauge, the volume recording gage, and the membrane, volume and hydrostatic corrections required for each PMT test (6). The combination of residual effects and the lack of precision from the data make it difficult to give precise reasons for the variation of resilient modulus with various cycle lengths. The current TEXAM PMT is not equipped to aid in solving this problem.

Inspection of the Shallowater n_r values shown in Table 3 indicates the sensitivity of the exponent: three positive n_r values become negative when only four cycles were used. Based on the n_r values shown in Table 3, it would be possible to predict resilient moduli associated with a large range of loading rates. Typical loading rates on the order of 0.1 sec are encountered on pavements. The falling weight deflectometer (FWD) applies impulse loads during a 0.2-sec period, although AASHTO recommends that a 0.1-sec loading rate be achieved during cyclic triaxial testing (8).

Correlations Between Pressuremeter Resilient Moduli and CBR Values

Correlations between resilient moduli and CBR values were established by calculating PMT resilient modulus values for the 30-, 60-, and 120-sec cycles from the Reese and Shallowater sites and comparing them directly with CBR values (Table 4). To ensure that the correlations were valid, PMT resilient moduli and CBR values were compared for soils at the same density and moisture content (Table 4). Also shown

TABLE 4 RESILIENT MODULUS-CBR CORRELATION ($M_r = B \times \text{CBR}$)

Test Site	Modulus used	B_{ave}	$B_{min} - B_{max}$
Reese AFB ¹	E_o^2	172	123 - 288
	$Mr_{0.1}^3$	1516	1386 - 1748
	Mr_{30}^4	1324	1013 - 1941
	Mr_{60}^5	1633	1504 - 2006
	Mr_{120}^6	1954	1300 - 2149
Shallowater ⁷	E_o	24	12 - 41
	$Mr_{0.1}$	186	75 - 382
	Mr_{30}	144	71 - 438
	Mr_{60}	159	69 - 288
	Mr_{120}	149	69 - 246

1. Reese Air Force Base, Lubbock, Texas
2. Elastic Modulus associated with linear portion of PMT curve (Fig. 6)
3. M_r of 0.1-second cycle length
4. M_r of 30-second cycle length
5. M_r of 60-second cycle length
6. M_r of 120-second cycle length
7. Texas Tech University Water Resources Center Site, Shallowater, Texas

in Table 4 is a correlation between M_r and CBR values for resilient moduli found for 0.1-sec cycle lengths using Equations 5. All of the B values found for Reese AFB (Table 4) compare well with the published correlations between resilient moduli and CBR values (1,8,11,12). Published ranges of B for pavement materials vary depending on the pavement layer analyzed. The values of B for subgrade soils range from 700 to 3,000; for granular base courses, B ranges from 300 to 9,000; and for granular subbase courses, B ranges from 200 to 1,100. The values for B for the soft clay at Shallowater are on the low end of the published values (Table 4). These low values may be attributed to the precision errors associated with using the TEXAM PMT in soft soils. The percent error possible for resilient moduli varying from 633 to 3469 psi (4360 to 23290 kPa), as is the case for the Shallowater data, ranges from approximately 3 to 16 percent. If an average error of 8 percent is assumed applicable and applied to the B values determined from resilient moduli (Table 4), then the average B values fall within the 200 to 1,100 range published for granular subbases, but not within the 300 to 9,000 range for subgrade soils. The only explanation possible for this discrepancy is that the soft clays may not have been included in the data base used for the subgrade correlations because they are not suitable roadbed soil; therefore, the Shallowater correlations may indeed be reasonable for soft clays.

CONCLUSIONS AND RECOMMENDATIONS

The major goal of this research—to increase the usefulness of the PMT—was achieved. The correlations developed between the PMT and the CBR tests are a clear indication of the use the PMT does have in the pavements field. The obvious next step is to develop a standard PMT test procedure

that can reliably be used to determine resilient moduli. The main problem facing researchers who understand the PMT is which resilient modulus is correct for design purposes. The researchers in the pavement industry need to clearly define the proper loading rates for resilient moduli on various roadways.

Conclusions from this study are as follows:

- A resilient modulus PMT test was developed that allows resilient moduli as a function of unload-reload cycle length to be found. This PMT test requires about 17 min to conduct once the PMT hole is augered (Figure 6).

- Correlations between the resilient moduli values from PMT tests and CBR values are similar to the published values (Table 4).

- Because this research was not sponsored, the amount of data formulated was limited. This problem should be studied further, using field CBR tests and pavement PMT tests. The pavement PMT is capable of testing layers 10 in. (25.4 cm) in thickness or less and would be more versatile than the TEXAM PMT. Field CBR tests would be more accurate for direct correlations of CBR values to PMT resilient moduli.

- The effects on the stress-strain response, of conducting 6 cycles without soil healing allowed between cycles is not understood. A study of these effects would be helpful in determining the proper resilient modulus for use in pavement design.

ACKNOWLEDGMENTS

The authors wish to acknowledge TTU and the Florida Institute of Technology for their resources and facilities and Warren K. Wray of TTU for his funding assistance. The authors are also grateful to Jean-Louis Briaud, professor at Texas A&M University, for his consultation during this study.

REFERENCES

1. E. J. Yoder and M. W. Witzak. *Principles of Pavement Design*, John Wiley & Sons, Inc., New York, N.Y., 1972.
2. *Guide for Design of Pavement Structures*. AASHTO, Washington, D.C., 1986.
3. P. J. Cosentino. *Pressuremeter Moduli for Airport Pavement Design*. Ph.D. dissertation. Texas A&M University, College Station, Tex., 1987.
4. F. Baguelin, J. F. J'ez'equel, and D. H. Shields. *The Pressuremeter and Foundation Engineering*. Trans Tech Publication, Clausthal, Germany, 1978.
5. J.-L. Briaud, T. A. Terry, P. J. Cosentino, L. M. Tucker, and R. L. Lytton. *Influence of Stress, Strain, Creep and Cycles on Moduli from Preboring and Driven Pressuremeters*. Department of Civil Engineering, Texas A&M University, College Station, Tex., 1986.
6. Y. T. Chen. *Correlating the Pressuremeter with the California Bearing Ratio*. M.S. thesis. Texas Tech University, Lubbock, Tex., 1990.
7. Soil and Rock: Building Stones. *Annual Book of ASTM Standards*, Section 4, Construction, Vol. 04.08, Philadelphia, Pa., 1984.
8. *Standard Specifications for Transportation Materials and Method of Sampling and Testing*. AASHTO, Washington, D.C., Part II, 1986, pp. 1198-1218.
9. M. Riggins. *Viscoelastic Characterization of Marine Sediment in Large Scale Simple Shear*. Ph.D. dissertation. Texas A&M University, College Station, Tex., 1981.
10. J.-L. Briaud and E. Garland. Loading Rate Method for Pile Response in Clay. *Journal of Geotechnical Engineering*, ASCE, Vol. 111, No. 3, 1985.
11. W. Heukelom and C. R. Foster. Dynamic Testing of Pavements. *Journal of the Soil Mechanics and Foundation Division*, Proceedings of the American Society of Civil Engineers, Vol. 86, No. SM1, 1960.
12. C. J. Van Til, B. F. McCullough, B. A. Vallergera, and R. G. Hicks. *NCHRP Report 128: Evaluation of AASHTO Interim Guides for Design of Pavement Structures*. HRB, National Research Council, Washington, D.C., 1972.

Publication of this paper sponsored by Committee on Soil and Rock Properties.

Laboratory Correlation Study of Near-Surface Response Parameters

DAVID C. KRAFT, RAYMOND K. MOORE, AND J. DEAN GROB

A laboratory study was performed to investigate the correlations between the Clegg Impact Value (CIV), California Bearing Ratio (CBR), and Cone Index (CI). CIV values were obtained using a Clegg Impact Soil Tester. A prototype automated cone penetrometer (30° right circular cone with base diameter of 5/8 in.) was used to develop CI data. The correlation data were obtained using soil specimens constructed in a 19.25-in.-diameter by 22-in.-deep laboratory compaction mold. Three levels of soil type, moisture content, and compactive effort were used to develop soils with a range of CBR from approximately 1 to 30. Satisfactory simple linear correlation (adjusted R^2 values ranged from 0.94 to 0.98) were developed between CIV values and the square root of CBR. Correlations between CIV and CBR were less satisfactory with adjusted R^2 values between 0.63 and 0.75. Useful correlations (adjusted R^2 values ranged from 0.58 to 0.82) were also developed between the CI values at 2 and 6 in. of penetration depth and CIV. All statistical relationships were significant at an alpha level of 0.0005.

Advances in digital electronics and instrumentation technology have created a developmental opportunity for innovative soil and pavement materials testing equipment. Improved cost-effective field measurements amenable to statistically based quality assurance programs continue to be an applied research priority. Consequently, new equipment incorporating state-of-the-art electronics for near-surface data acquisition and analysis has become commercially available.

One recently developed dynamic response device for soil and pavement materials evaluation is the Clegg Impact Soil Tester. Described as a "soil compaction tester," (1) the instrument resembles a laboratory compaction hammer. A 10 lb weight free-falls through a PVC plastic guide tube. The height of vertical drop is 18 in. An accelerometer measures the deceleration of the weight as it impacts and penetrates the soil surface. The maximum deceleration, measured in gravitational units, is multiplied by 10 and digitally displayed. This value is referred to as "Impact Value" or "Clegg Impact Value." Extensive research conducted in Australia (2-4) by Clegg, the inventor of the instrument, has suggested that useful correlations exist between the Clegg Impact Value (CIV) and California Bearing Ratio (CBR), elastic modulus, and percent compaction. In effect, the CIV value evaluates the stiffness of the surface being impacted.

An experimental laboratory research program was designed to further evaluate the statistical correlations between CIV

and CBR. In addition, Cone Index Values (CI) developed using a prototype automated cone penetrometer, developed by Khedr et al. (5) were also obtained for new correlations with the Clegg Impact Soil Tester.

EXPERIMENT DESIGN

The laboratory testing program was designed to generate sufficient data for a study of the correlations among CIV, CBR and CI. Three soil types, 3 compaction water contents, and 3 compactive efforts were used to develop 27 treatment combinations for the correlation study.

The soil types were a low plasticity clayey sand [SP-SC by the Unified Soil Classification System (USCS), A-2-4 by AASHTO], a gravelly silty sand (SM by USCS, A-1-b by AASHTO), and a highly plastic inorganic clay (CH by USCS; A-7-6, GI=34 by AASHTO). Different compactive efforts were achieved by using three different sizes of plates as base-mounted feet on an air-pressure operated vibratory hammer. Low compactive effort used a 9-in.-diameter plate and 2 coverages per compactive lift. High compactive effort used a 5.2-in.-diameter plate and 6 coverages per lift. Compaction moisture contents were based on the standard proctor compaction test. Nominal water contents were minus 2 percent of optimum and plus 2 percent of optimum moisture content. The combination of factors produced a satisfactory range of CBR values generally less than 30.

In order to prepare compacted specimens for testing, a cylindrical mold (19.25-in. diameter and 22-in. depth) was designed and fabricated. The compaction process was based on a procedure reported by Moore and Haliburton (6) used to prepare large laboratory soil samples for the calibration of nuclear moisture-density equipment. Each test was prepared using a selected soil type, a predetermined moisture content, and an estimated amount of dry soil based on target values of compacted dry unit weight. After uniformly combining the pulverized dry soil and water, the mixture was placed in the mold for four compacted lifts using one of three levels of compactive efforts. Each lift was approximately 4 in. thick after compaction.

TEST PROCEDURES

Clegg Impact Soil Tester

The Clegg Impact Soil Tester was the focus of the correlation study. Two CIV values were studied. The instrument instruc-

D. C. Kraft, University of Kansas, Engineering Management, Regents Center, Overland Park, Kans. 66206. R. K. Moore, University of Kansas, Department of Civil Engineering, Lawrence, Kans. 66045. J. D. Grob, Black and Veatch, P.O. Box 8405, Kansas City, Mo. 64114.

tions stipulate that the hammer be dropped four times to determine the CIV values for a test location. The instrumentation measured the deceleration for each drop, but only the maximum value is stored and used as the output value after the four drops. This value will be called CIVHI. However, the research was conducted by recording the individual CIV values for each drop at each location on the compacted soil specimen. The average of the first four drops (CIV4) was also used as correlates. This average was used to determine if better correlations could be developed than by using CIVHI and if the penetration of hammer in successive drops was an important influence given that soil densification and deformation takes place.

Each CIV value shown in the correlation represents the average value of three tests taken within 6 in. of each other. The CIV value does not represent a fundamental soil property, but is a measurement of dynamic soil response. It appears probable that the precision of the CIV parameter is limited, and reliance on a single value at a given test location is imprudent. Operation of the equipment is simple, and the use of three observations will not burden field personnel. From a statistical standpoint, the use of means reduces the inherent variation in the correlate.

California Bearing Ratio

A conventional, manually operated test set-up mounted in a steel frame was used for the CBR laboratory test. The basic vertical deformation data were obtained with a dial gauge, and the soil penetration resistance was monitored using proving ring deformations. The CBR data are also the average of three tests taken within 6 in. of each other on the surface of the compacted specimens. A 10 lb surcharge was used in each CBR test.

Automated Cone Penetrometer

The automated cone penetrometer used a 30° right circular cone with a base diameter of $\frac{5}{8}$ in. As the cone penetrates the soil, a recorder prints the penetration resistance in pounds along with the penetrometer depth in inches. The CI is the tip penetration resistance divided by the cone base area (psi).

The CI values used in the correlations are not averages. Three penetrometer tests were conducted on each compacted specimen. The data from all three tests were conducted on each compacted specimen. The data from all three tests were plotted as shown in Figure 1. A simple linear regression was placed through the plot of cone penetration resistance and penetration depth using data to a depth of 8 in. Cone penetration resistance was estimated using this regression at depths of 2 in. (CI2) and 6 in. (CI6).

STATISTICAL CONSIDERATIONS

The significance level of the sample Pearson correlation coefficient for all regressions shown in this paper is less than 0.0005 (Type I error in rejecting the hypothesis that the population correlation coefficient between the correlates is zero). An

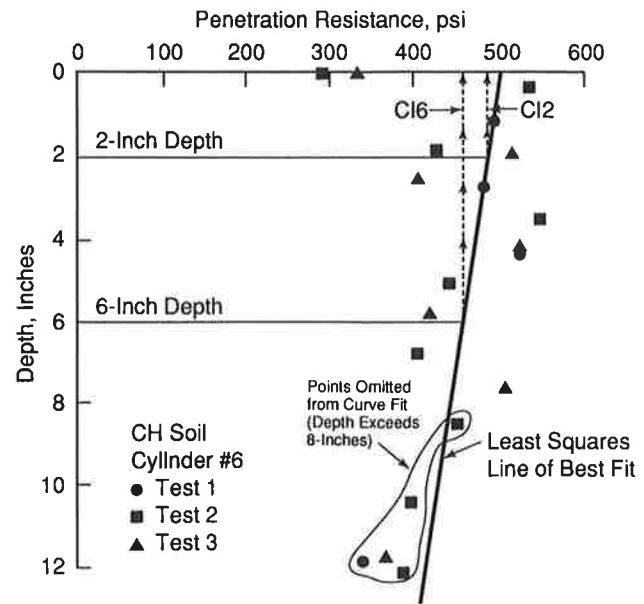


FIGURE 1 Cone Index estimation.

“adjusted R^2 ” coefficient is reported because the square of Pearson’s correlation coefficient is usually an overly optimistic estimate of how well the linear model based on the sample actually fits the population (7). The R_a^2 statistic for a simple linear regression is defined as

$$R_a^2 = R^2 - [(1 - R^2)/(N - 1)]$$

where N is the number of data pairs and R is the Pearson correlation coefficient.

DISCUSSION OF RESULTS

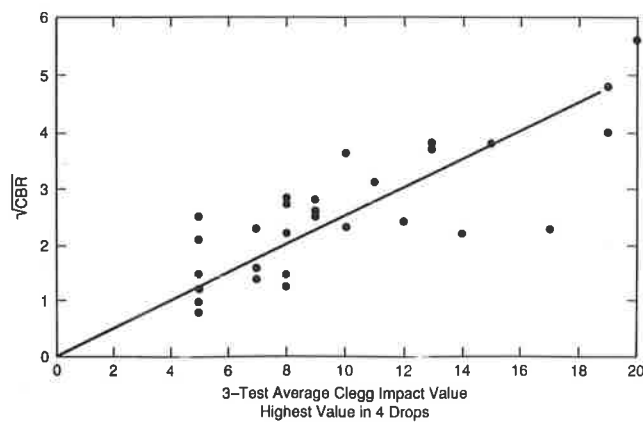
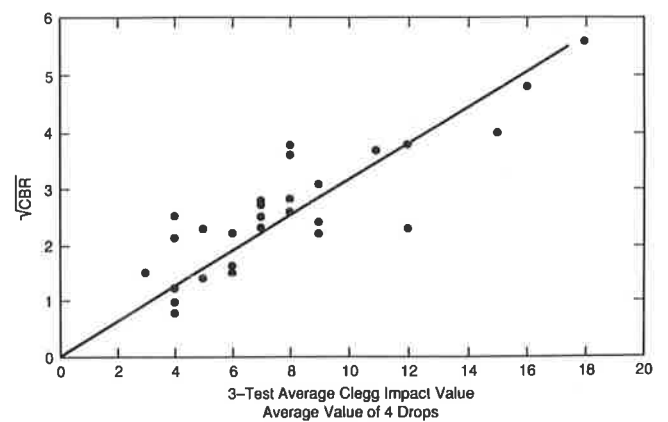
Table 1 presents a summary of the correlation and regression results for 14 cases. Detailed data summaries and other correlations between the automated cone penetrometer and CBR can be obtained elsewhere (8).

The statistical results for the individual soils are given for the square root curve fits to illustrate the similarity. Clegg (3) published a model using Australian soils that is quite similar $[(\text{CBR})^{1/2} = 0.26\text{CIVHI}]$. The combined soils data plots are given in Figures 2 and 3 for the square root models. The adjusted R^2 value and standard error are slightly better using the average of four drops instead of CIVHI. Although the practical significance of this difference may be trivial, the instrumentation could be easily modified to display both the CIVHI and CIV4 if this trend proves to be important as experience increases using the instrument for quality control.

Figures 4 and 5 illustrate the simple linear regression between CBR and the Clegg output values using the combined data sets. These illustrate the variation associated with the CBR data for a given Clegg Impact Value. A comparison of the plots clearly demonstrates that the quantitative effect of averaging is a reduction in CIV parameter by one or two units.

TABLE 1 CORRELATION AND REGRESSION SUMMARY

Regression	Adjusted R^2	Standard Error	Data Set
Sqr (CBR) = 0.20 (CIVHI)	0.94	0.58	SP-SC Soil n=11
Sqr (CBR) = 0.27 (CIVHI)	0.98	0.40	SM Soil n=9
Sqr (CBR) = 0.30 (CIVHI)	0.98	0.58	CH Soil n=9
Sqr (CBR) = 0.25 (CIVHI) Figure 2	0.94	0.70	All Soils n=29
Sqr (CBR) = 0.27 (CIV4)	0.96	0.46	SP-SC Soil n=11
Sqr (CBR) = 0.33 (CIV4)	0.97	0.53	SM Soil n=9
Sqr (CBR) = 0.36 (CIV4)	0.95	0.67	CH Soil n=9
Sqr (CBR) = 0.32 (CIV4) Figure 3	0.95	0.63	All Soils n=29
CBR = -4.40 + 1.23 (CIVHI) Figure 4	0.63	4.21	All Soils n=29
CBR = -4.71 + 1.61 (CIV4) Figure 5	0.75	3.48	All Soils n=29
CI2 = 45.19 (CIVHI) Figure 6	0.82	235.08 psi	All Soils n=29
CI2 = -188.48 + 77.48 (CIV4) Figure 7	0.68	202.95 psi	All Soils n=29
CI6 = 59.21 (CIVHI) Figure 8	0.70	428.55 psi	All Soils n=30
CI6 = -384.45 + 116.16 (CIV4) Figure 9	0.58	374.07 psi	All Soils n=30

FIGURE 2 $(\text{CBR})^{1/2}$ -CIVHI regression (all soils).FIGURE 3 $(\text{CBR})^{1/2}$ -CIV4 regression (all soils).

Figures 6–9 illustrate the relationship between CI2, CI6, and the Clegg parameters. Two lines are shown in Figures 6 and 8. In these cases, the intercept of the regression (shown by the solid line) was not statistically significant at an alpha level of 5 percent. Therefore, the regressions given in Table 1 represent the dashed lines in Figures 6 and 8. These rela-

tionships were developed by forcing the regression through the origin.

The cone penetrometer relationships using CIVHI have higher adjusted R^2 values but larger standard errors than the regressions using the average of four drops. Because these relationships appear to be the first reported in the technical

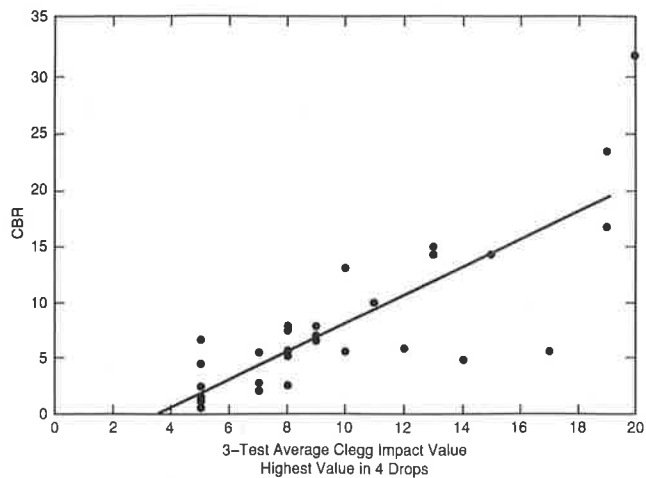


FIGURE 4 CBR-CIVHI regression (all soils).

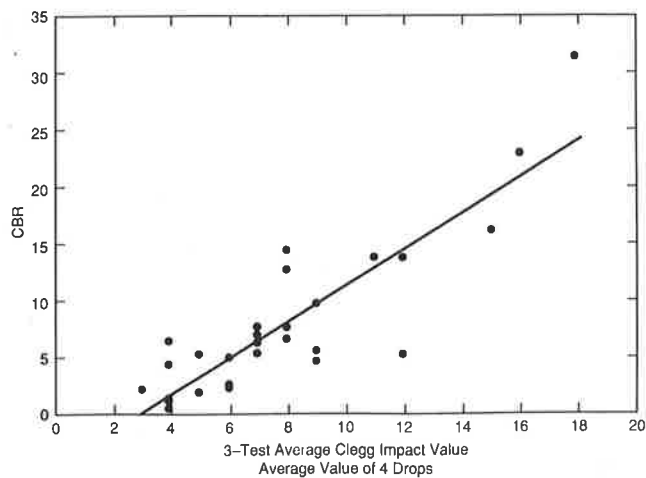


FIGURE 5 CBR-CIV4 regression (all soils).

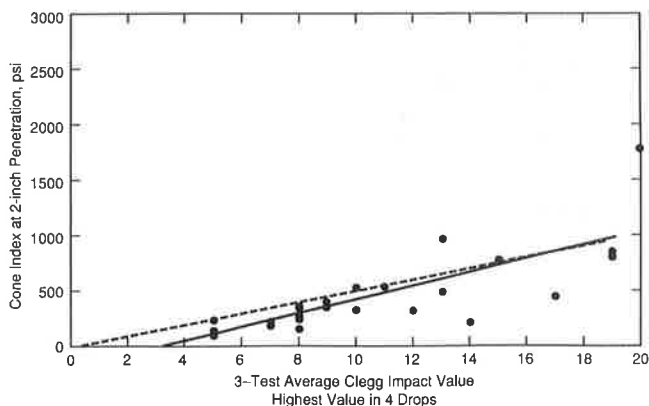


FIGURE 6 CI2-CIVHI regression (all soils).

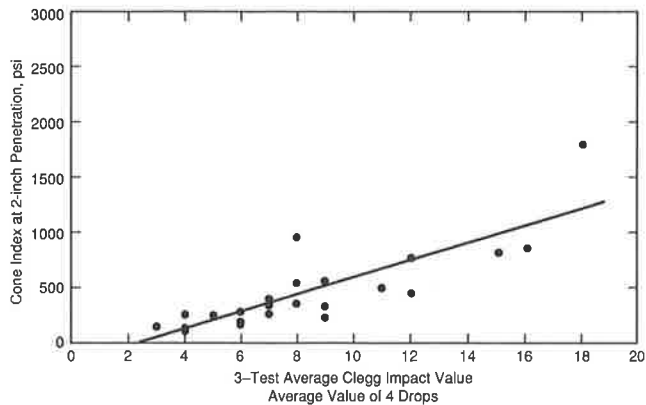


FIGURE 7 CI2-CIV4 regression (all soils).

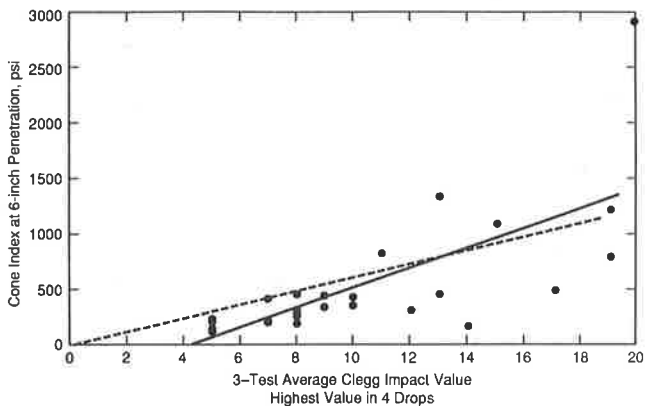


FIGURE 8 CI6-CIVHI regression (all soils).

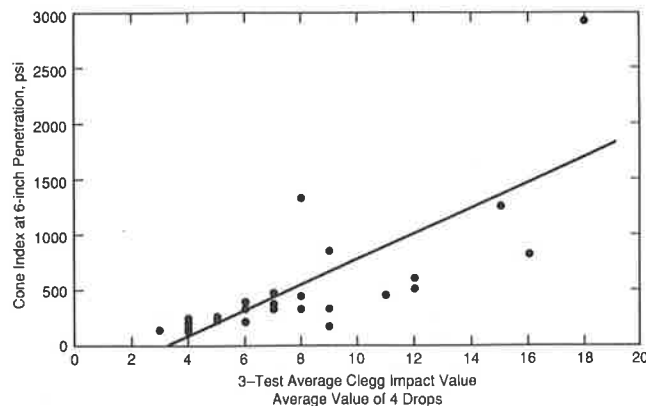


FIGURE 9 CI6-CIV4 regression (all soils).

literature, no comparisons with previous work are possible. However, research with the automated cone penetrometer suggests that the confidence levels, and hence the standard error, about estimated cone index values may be useful.

Two cone index values were studied to determine if the effect of depth on the sensitivity of the Clegg instrument could

be subjectively evaluated. Because soil penetration is limited to less than 2.4 in., its ability as a soil condition inference instrument should diminish quickly with depth. The adjusted R^2 and standard error statistics for the 2-in. cone index equations are better than their 6-in. cone index counterparts. Although this gives only a limited insight, the data appear to be consistent with the stated hypothesis. However, additional research should be conducted to quantitatively define the depth of confidence associated with the Clegg Impact Soil Tester in relatively homogeneous conditions. Clearly, the instrument

may not be appropriate for the "hard over soft" condition when the softer underlayer will control the behavior of the soil surface under the action of traffic.

BOUNDARY CONDITION EFFECTS

The experimental procedure used here may impose boundary condition effects on the data that would not be present in the field. The steel compaction mold creates a near-field rigid boundary that may affect correlation results in two ways.

The impact of the Clegg Impact Hammer on the soil surface will create a dynamic wave that will return to the test location within the time interval needed to define the maximum deceleration of the impact hammer. Oscilloscope measurements for individual hammer drops indicate that the peak CIV value occurs in about 1 mS for stiff soils (CIV greater than 35) and in about 3.5 mS for soils with CIV values of 8. The return times for either compression or shear waves in moist soil would generally be less than 1 mS. The presence of these reflected dynamic waves is not apparent in oscilloscope data; hence, their effect on CIV values may be negligible. However, this condition would normally not be present in the field.

A near-field rigid boundary can influence cone penetration values developed in laboratory calibration studies using sands (9). The rigid boundary creates an artificial constraint not consistent with field conditions. This influence appears to be a function of overconsolidation ratio and the ratio of the diameter of the calibration mold and cone diameter. Whereas the soil in the field is confined by adjacent soil, the effects of a steel ring within 8.5-in. of a cone penetration test are different. For fine-grained soils, this problem may be more complex than for sand because moisture content directly affects the soil stiffness and lateral deformation properties. The overconsolidation and diameter ratios may also be important, as has been documented for sand.

The effect of these factors has not clearly been defined. Laboratory calibration and correlation studies are needed to continue to investigate the quantitative influence of these two boundary condition effects on the instrument responses.

CONCLUSIONS

The Clegg Impact Soil Tester was evaluated in a correlation study to better define its capability to assess soil response behavior. Regression relationships were developed using correlations between the maximum and average Clegg Impact Values obtained in four drops, CBR, and Cone Index (using the automated cone penetrometer). Statistically significant and

useful correlations between CIV and CBR were developed that were similar to expressions published for Australian soils. The correlation between CIV and CI values appears to be statistically significant, but more research is needed to determine if the precision is adequate for engineering applications.

ACKNOWLEDGMENTS

The research reported herein was sponsored by the U.S. Army Corps of Engineers Waterways Experiment Station, Vicksburg, Mississippi, through the University of Kansas Center for Research, Inc. The authors wish to acknowledge the contributions of Victor C. Barber, Research Civil Engineer, Waterways Experiment Station, in the development of the research concept and experiment design. Ron Hurst, Electronics Technologist, Department of Civil Engineering, designed the static test stand for the automated cone penetrometer. Keele Lee Maison, undergraduate research assistant, assisted in the preparation of the soil specimens, acquisition of data, and statistical data analysis.

REFERENCES

1. *Clegg Impact Test Guidelines*. Lafayette Instrument Company, Lafayette, Ind., 1985.
2. B. Clegg. An Impact Testing Device for In Situ Base Course Evaluation. *Proc., Australian Road Research Board*, Vol. 8, 1976.
3. B. Clegg. An Impact Soil Test as Alternative to California Bearing Ratio. *Proc., Third Annual Conference of Soil Mechanics and Foundation Engineering*, Wellington, Australia, 1981.
4. B. Clegg. Design Compatible Control of Basecourse Construction. *Australian Road Research*, Vol. 13, No. 2, June 1983.
5. S. A. Khedr, D. C. Kraft, and J. L. Jenkins. Automated Cone Penetrometer: A Non-Destructive Field Test for Subgrade Evaluation. In *Transportation Research Record 1022*, TRB, National Research Council, Washington, D.C., 1985.
6. R. K. Moore and T. A. Haliburton. *Suggested Nuclear Depth Gage Calibration Procedures*. Interim Report IV, Subgrade Moisture Variations Study. School of Civil Engineering, Oklahoma State University, 1968.
7. M. J. Norusis. *SPSS² Introductory Statistics Guide*. SPSS Inc., McGraw Hill, 1983.
8. D. C. Kraft and R. K. Moore. *Unsurfaced Soil Strength Evaluation (USE)*. U.S. Corps of Engineers Waterways Experiment Station Project report. University of Kansas Center for Research, Inc., Lawrence, Sept. 1986.
9. A. K. Parkin. The Calibration of Cone Penetrometers. *Penetration Testing 1988, ISOPT-1*, De Ruiter (ed.), Balkema, Rotterdam, Netherlands, 1988, pp. 221-243.

Publication of this paper sponsored by Committee on Soil and Rock Properties.

Prototype Geotechnical Information System

REDA M. BAKEER, TARIK HADJ-HAMOU, AND JOHN L. NIKLAUS

The concept of a geotechnical information system (GTIS) that integrates the geotechnical data base of a particular area into a geographical information system is discussed in this paper. The geotechnical data base is obtained from earlier soil investigations and is continuously updated by adding the results of new investigations. The GTIS can be used to estimate soil properties at a specified location within a geographical area that may have not yet been explored. A "synthetic" soil boring log and profile can be generated for a particular site within the geographical area using the existing information in the data base of neighboring boring logs in addition to other subjective information about the area such as its deposition history. The feasibility of this concept is demonstrated by a prototype GTIS developed along these lines for part of Jefferson Parish County in New Orleans.

A flow chart for a typical geotechnical investigation is shown in Figure 1. For a given site under consideration for development, the engineer first identifies its location on topographic, geological, and local street maps to assess the general soil conditions. The engineer then refers to the archives of his firm or agency to survey geotechnical investigations performed earlier in the vicinity of the site before designing a final exploration program. The quality and availability of such a geotechnical data base may prove to be a decisive factor in designing an optimal soil exploration program or in winning the contract. The soil exploration program is then designed, which involves drilling and logging of boring holes at the site, obtaining soil samples for laboratory testing, and possibly performing some in situ soil testing. Shallow and deep soil borings are the most important components of any geotechnical investigation; they reveal subsurface conditions and provide disturbed or undisturbed samples for laboratory testing. Results from the laboratory testing programs define characteristics and the mechanical properties of the soil such as grain size composition, strength, permeability, and deformation potential. These parameters form the basis for the selection of the soil as a construction material or its suitability as a foundation material. The results of a geotechnical investigation are usually summarized in a detailed log such as that shown in Figure 2.

The quality of a technical soil report in many cases depends on the experience of the person writing it. For example, a field boring log form completed by a geologist may contain data on color, consistency, presence of organics, as well as a thorough visual classification. By contrast, a form filled out by an inexperienced technician may only provide a simple visual description, such as "sand" or "gravel." Weather conditions, human errors, and insufficient documentation may

produce incomplete or erroneous data. Human errors are also possible in the office during reading, interpreting, or rewriting of the field data. The same types of problems may also arise in the laboratory, where some details of test procedures may be omitted. These errors may result in an ill-planned investigation culminating in underestimated or overestimated critical soil properties. The first consequence may prove to be disastrous and the second to be costly.

Based on the results of the exploration program, the designer proceeds to produce a final structural design of the project. In few instances, it may become necessary to acquire additional information about the subsoil properties before commencing the structural design. As outlined in Figure 1, five different tasks are conducted at the office that involve human resources and manipulation of data collected from different sources that may not always be compatible. Although standard techniques to be used in the field and the laboratory are discussed in published guidelines, ample room exists for personal interpretation. These tasks can be automated and standardized by an organization or firm to optimize efficiency and reduce the associated uncertainties.

Discussed in this paper is the concept of a computerized geotechnical information system (GTIS) that integrates tasks 1, 2, 4, and 5 using a geographical information system (GIS), relational data base management, expert system technology, and conventional computer programming. The general strategy of the GTIS will be presented first, followed by an overview of a prototype GTIS developed for part of Jefferson Parish County in the greater New Orleans area.

GENERAL STRATEGY OF GTIS

A GTIS designed to operate on a personal computer or a workstation using commercial or locally developed software could function as (a) a predictor of subsoil conditions at an unknown location, or (b) a repository of information about previous investigations conducted in the area.

In order to assess the prevailing conditions at an unknown location, the user would access first a library of electronic GIS maps on which the site location is identified. An area of influence would be specified, with the unknown site at its center, to identify any previous soil borings and their associated soil investigations, which may help in determining the prevailing conditions at the unknown site. Based on the identification prompted by the GIS, the geotechnical data base would then be accessed, and a summary report of previous investigations would be prepared, along with a probable synthetic stratigraphy for the site. The information contained in

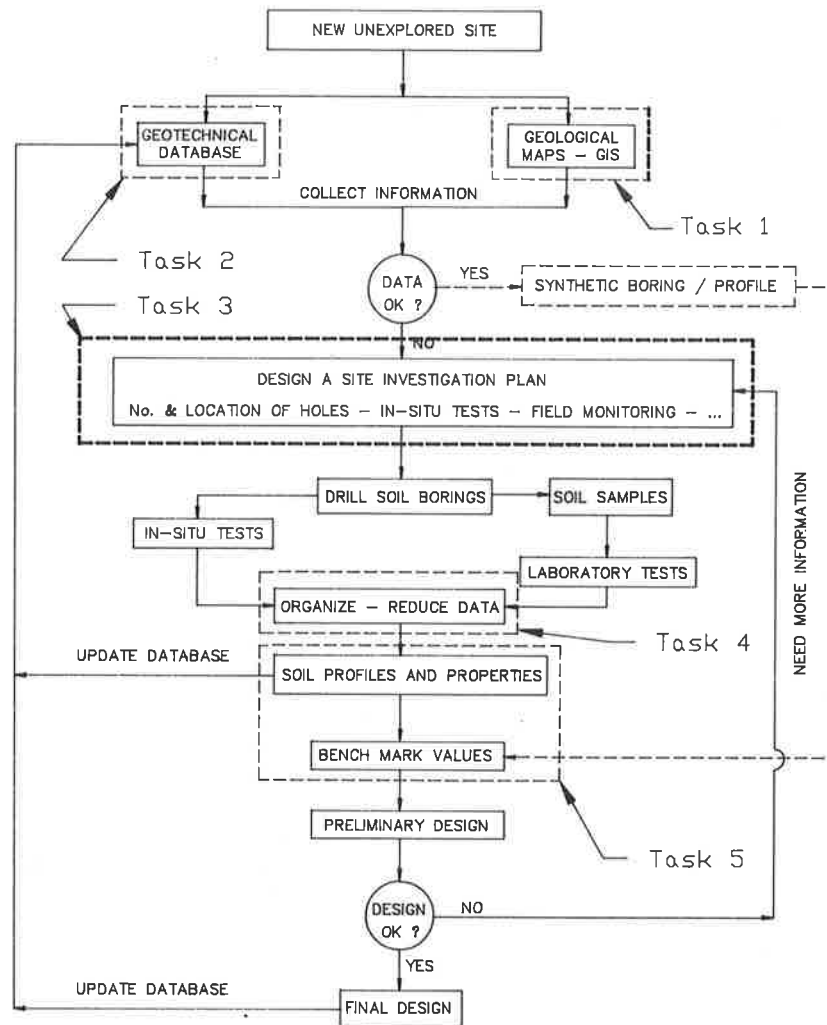


FIGURE 1 Flow chart of a geotechnical investigation.

the data base would be formulated by transferring old archives into computer records or through continuous updates with new data from ongoing exploration programs. The software packages to be used in the GTIS must be compatible to ensure full automation of the process. In addition to offering higher efficiency and better time management, software compatibility would also reduce the possible human errors associated with entering the data more than once.

A GTIS package would consist primarily of four basic modules implemented to perform the tasks of the flow chart indicated in Figure 3. They should be able to run as independent entities or in a fully interactive environment, depending on the application and the preference of the user. The four modules are detailed in the following sections.

Electronic Maps

The electronic computer maps (Module M-1) of the geographical area under consideration are the major feature in a GTIS system. These electronic maps could be purchased from a GIS vendor or digitized or scanned directly by the user from prints

using a commercial CAD software or a scanner. Several vendors produce GIS maps for many parts of the United States either for personal computers or workstations. An ideal electronic map library would contain sets, or layers, of geological, topographical, and street maps of the geographical area. In order to expand these GIS maps into a GTIS, the map library would have to be customized further by adding maps, or layers, showing the exact locations of previous soil investigations conducted in the area. These GTIS maps would be updated continuously by appending any new investigations as they become available. Ease of use, price, flexibility, and the offered features should all be considered in the selection of a CAD system for a GTIS. Zooming, panning, layering, and the capability of exchanging data with other software are some of the required features in such a CAD system. The different maps in the GTIS should all share a common reference to allow for exchanging information among the different modules. A standard coordinate system, such as the Coast and Geodetic Survey State Coordinates System (CGSSCS), and unique identification codes should be used on all maps for that purpose. For a given site, the GTIS maps would be searched, and a file containing the identification codes and

Sample No.	SAMPLE Depth - Feet		STRATUM Depth In Feet	VISUAL CLASSIFICATION	Blows per Foot	Symbol Log	Scale feet	QU (lbs./sq.ft.)	WATER CONTENT (percent)	UNIT WEIGHT (lbs./cu. ft.)		ATTERBERG LIMITS		
	From	To								DRY	WET	LL	PL	PI
			0.0	ASPHALT										
			0.1	SHELLS										
1	3.5	4.0	1.5	MEDIUM STIFF TO STIFF TAN AND GRAY CLAY W/SILT AND WOOD			10	2425	33.8	84.7	113.3			
2	6.5	7.0	8.0	SOFT GRAY CLAY W/SPECKS OF WOOD				1150	60.2	64.2	102.9	93		
3	10.0	10.5	11.0	VERY SOFT GRAY CLAY W/ORGANIC CLAY LAYERS AND WOOD				880	66.0	60.9	101.1			
4	14.0	14.5	15.5	MEDIUM STIFF GRAY SILTY CLAY W/CLAY LAYERS				350	99.5	45.7	91.2			
5	19.0	19.5	20.0	VERY SOFT GRAY CLAY W/FEW SHELL FRAGMENTS				440	63.3	63.1	103.0			
6	21.5	22.0	23.0					490	67.5	60.6	101.5			
7	23.0	23.5	24.0											
8	24.0	25.5		DENSE TO VERY DENSE GRAY FINE SAND	30=0.8'	Symbol Log	Scale feet							
9	26.5	28.0			30=0.6'									
10	28.5	30.0			30=0.7'									
11	33.5	35.0			30=0.4'									
12	38.5	40.0			30=0.9'									
13	43.5	45.0	42.5	MEDIUM DENSE GRAY FINE SAND	20									
14	47.5	48.0	47.0	SOFT TO MEDIUM STIFF GRAY CLAY W/SAND, POCKETS & SHELL FRGMTS.				845	45.6	74.9	109.1	45		
15	49.5	50.0	50.0											

CLAY
Predominant type bold. Modifying type light.

SILT

SAND

ORGANIC

* 140 lb. hammer dropped 30in. on 2in. split spoon sampler after first being seated 6in.

REMARKS:

FIGURE 2 Typical geotechnical exploration boring log.

coordinates of earlier soils investigations at the vicinity of the site would be prepared for analysis by the other modules of the GTIS.

Geotechnical Data Bases

This module (M-2) would consist of the data bases and tailored programs written in the data base management software environment to manage the data bases and perform the required searches. In order to limit the size of the data base file for a particular geographical area, a series of data base files should be created instead. Each record in the first data base set (DB-1) would correspond to one particular soil boring hole drilled in the geographical area. A typical record in DB-1 would contain a unique identification code of the hole, its location according to the coordinate system used in the electronic map, its maximum depth, whether or not soil samples were recovered, and a list of the in situ tests conducted at the hole, if any. The second data base set (DB-2) would

contain the results of the laboratory tests performed on the soil samples recovered from a hole, along with identification codes. Consequently, several records in DB-2 will be associated to one hole and be related to one record in the DB-2 file. A third set of data base files (DB-3) would be required to describe any information about the in situ tests performed at the location of a hole. Records of DB-3 files would contain references to other electronic or printed files depending on the nature of the conducted test. Records in any of the three data base files can be easily related to each other and to the boring through the unique identification code and the coordinates.

The data base module M-2 would be accessed by the other modules in the system to furnish the required information pertaining to the particular holes selected for estimating the synthetic borings and soil properties. When a particular boring hole in DB-1 is included in the estimation analysis, the other data bases (DB-2 and DB-3) are scanned to retrieve the specific information about the soil conditions.

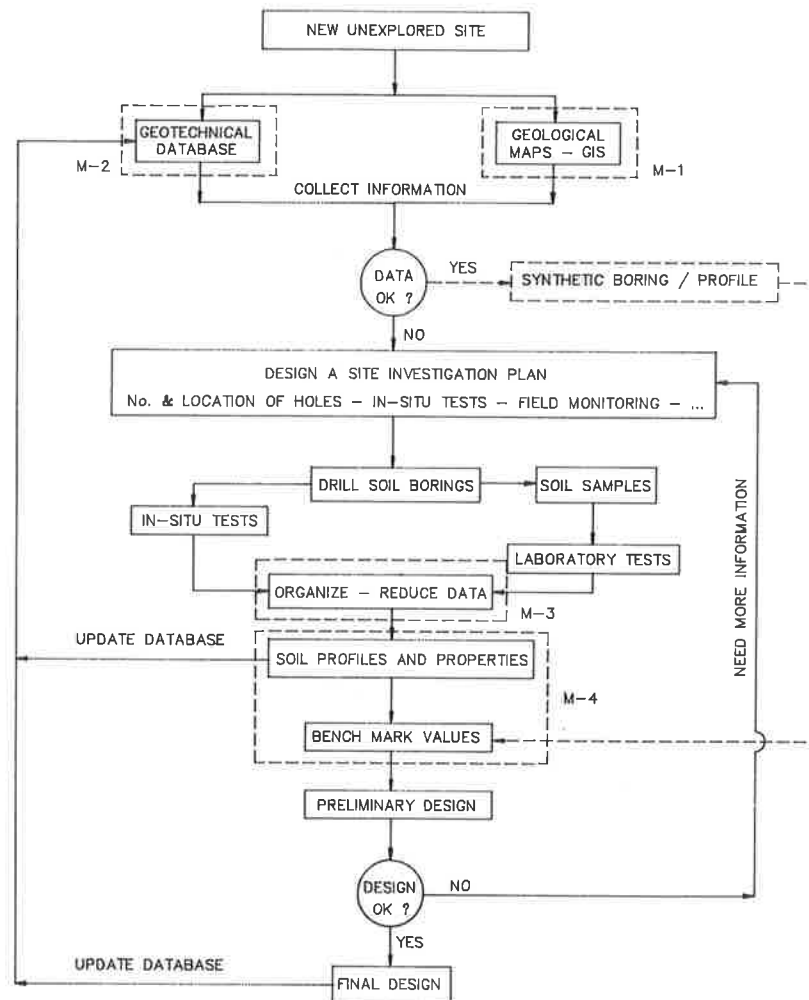


FIGURE 3 Modules of GTIS.

Data Acquisition and Management

Module M-3 consists of a comprehensive package, or a group of programs, that manages both field and laboratory data and upgrades the data bases in M-2 and the electronic maps in M-1. This module has no specific structure; it should be specifically tailored to meet the needs of the agency using it and the sources of information. The software recommended for this module may include commercial packages such as spread sheets or data base management programs, specialized commercial software for soil investigation, or programs developed locally by the agency in a conventional programming language.

Estimator/Predictor

In this module (M-4), soil conditions at an unexplored site are estimated using the data generated by the first three modules. Module M-4 would prepare a summary report listing all the existing boring holes in the vicinity of the site within a specified distance of influence. An expert system program would be required to combine the available objective information, such as distances and data from previous holes, with the subjective information, such as the known geological trends,

special soil formations in the area, and local engineering experience. The information provided by the expert system would be used to produce a "most likely" synthetic boring at the location of the unexplored site. This synthetic boring would be used along with data from the other soil investigation to construct soil profiles across that particular site. The provided information could be used by the agency to design an efficient soil exploration program, to perform feasibility studies, or for contract bidding purposes. Following the full soil exploration, the newly acquired data would be appended to the data bases and the electronic maps for future use.

The four modules (M-1, M-2, M-3, and M-4) could be fully interactive or independent of one another. For example, it may not be necessary to identify the information regarding previous investigations from the electronic maps because the user may search the data base directly by specifying a set of limiting coordinates to extrude the existing boring holes within these limits. The modules could be fully developed locally by an agency or a combination of commercial and developed software. To demonstrate the philosophy of a GTIS system, the prototype system TU-DIRT was developed at Tulane University following the above strategy. This prototype is presented in the following sections.

GTIS PROTOTYPE TU-DIRT

The prototype system is targeted toward a specific portion of Jefferson Parish in the New Orleans metropolitan area. Such a small area was selected to control the massive data base size required for a particular geographical area. Although the electronic maps and data bases created for this project are site specific, the other programs that perform computations, searches, and data management are all generic and can be used for other geographical areas with minor modifications. A combination of commercial software packages and programs written in conventional languages developed at the Department of Civil Engineering at Tulane were used to develop the four modules of the GTIS. It should be noted that the commercial packages were selected from the software library available at Tulane, but other computer packages could be used to develop similar GTIS systems.

TU-DIRT Electronic Maps

The geology of the prototype area is dominated by the continuous migration of the Mississippi River over the past 15,000 years (1). During this era, fine grained alluvial deposits advanced to the gulf in the form of river deltas created by the many shifts in the river course. Each time the river created a new alluvial fan, it would abandon one course in favor of a shorter and more direct route to the gulf. During the last 5,000 years several major delta complexes have formed, resulting in a complex subsurface geology dominated by the Pleistocene formations and the Holocene deposits. The Pleistocene formations consist of interbedded strata of clays, silts, and sands. High strength deposits are encountered in the overconsolidated crust and are sometimes labeled "local bedrock" (2). These deposits form the foundation strata for most heavy structures in the New Orleans area. The soft sediments of the Holocene epoch are typically divided into natural levees, point bars, and backswamp deposits. The natural levees are the slightly elevated ridges that occur on both sides of a water stream. Point bar deposits are the direct result of the lateral migrations of the river when erosion of the banks occurs, and the coarser materials are redeposited immediately downstream at the convex side of the river bank. Backswamp deposits are formed by the deposition of fine sediments in the shallow ponded areas of overbank flows. Backswamp deposits consist primarily of thinly laminated clays and silts, which sometimes exhibit a high organic content. The geological nature of the subsurface deposits governs the selection of foundation systems of a structure. Shallow footings are common on natural levees but are not feasible on backswamp deposits. The depth of the Pleistocene formations is also a strong factor for the selection of a deep foundation type and geometry.

A library of maps was established for the prototype system TU-DIRT showing the main geological features of the subsurface and a schematic of the city streets. Because of the large area covered and the amount of information on city street maps, a series of layers and blocks with varying details was created in the prototype. Figure 4 shows a general view of the region included in the prototype. This particular map was digitized using AutoCAD (3) and a digitizing tablet.

CGSSCS was used as the standard reference to digitize the details shown on the maps.

TU-DIRT Geotechnical Data Bases

The data base management software dBase III-plus (4) was used to organize and manage the prototype data bases. A total of 54 boring holes was coded in the data base, representing more than 650 soil samples tested. The data base information was provided by two local geotechnical engineering firms and the U.S. Army Corps of Engineers, New Orleans District. A typical record in the first data base (JP-LOC.DBF) contains the unique identification of a boring hole, its location, whether soil samples were recovered and tested, and if in situ tests were conducted. The data entry screen of JP-LOC.DBF is shown on Figure 5. Logical variables T or Y for True or Yes, and F or N for False or No are used to indicate the type of tests performed on each hole to provide faster screening of the massive data. The coordinates of each hole are specified in CGSSC to guarantee compatibility with the electronic maps. The second data base (JP-PROP.DBF) contains results of the tests performed on the samples recovered from each hole, as shown on the sample data entry screen on Figure 6. New information and additional holes can be coded into the data base files either directly from the interactive entry screens or by retrieving output files created in the field or the laboratory. Reading data files is more efficient because it eliminates the possible human errors associated with reentering the data, whereas the screen entry is more suited for the gradual transfer of existing data in the archives.

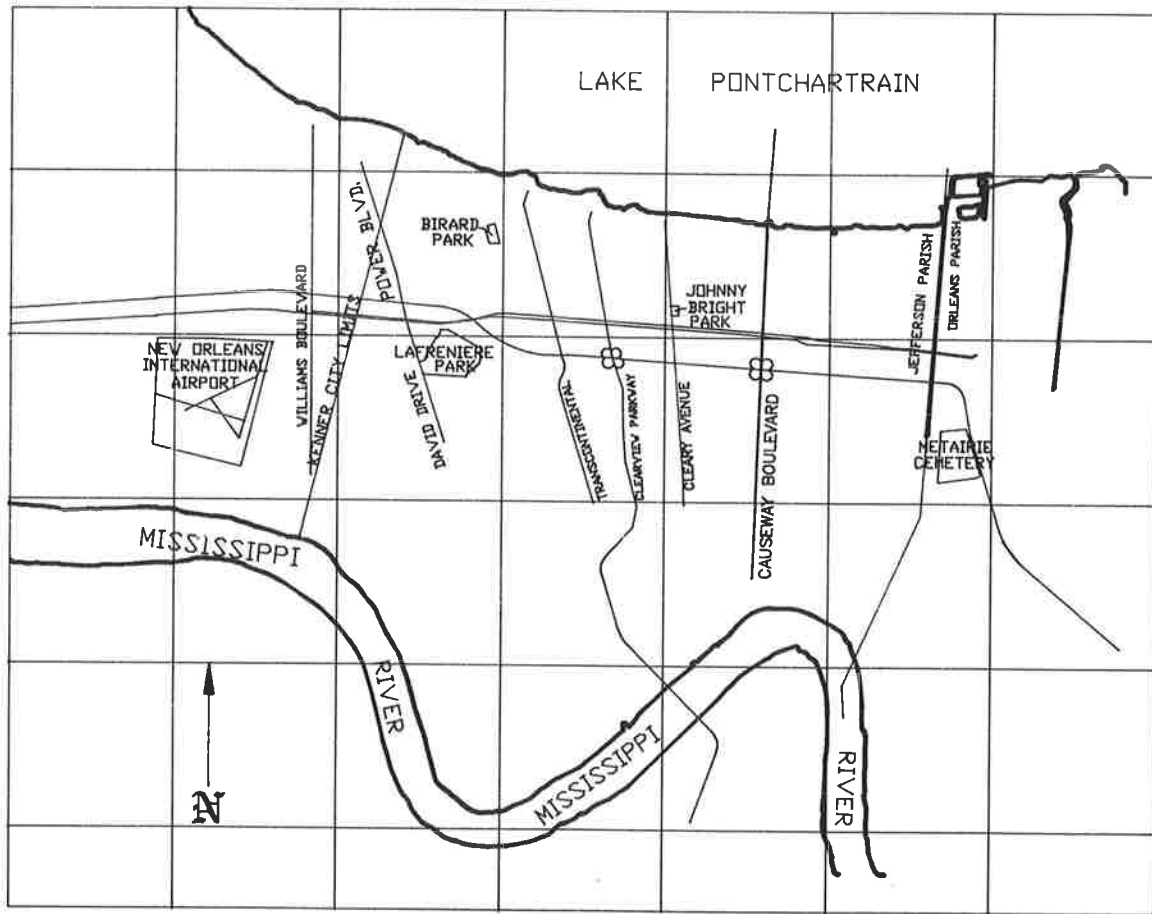
Two programs were written in the dBase III environment to access and manage the data base files. The first program is strictly for data input and editing of the existing data base files. The second program searches the database for previous borings within a specified radius of influence and provides a summary report of the findings. The summary report lists all of the holes within the search area specifying the distance and angle in the X-Y plane from the unknown site as well as the stored values of the requested soil properties. This information is used to produce a synthetic boring for the site.

Field and Laboratory Data Management

Two computer programs, BORLOG and LABLOG, were developed at Tulane for the acquisition and reduction of the field and laboratory data according to standard ASTM formats compatible with the GTIS. The programs were written in BASIC for use on IBM personal computers.

BORLOG

All pertinent information about the site conditions, weather, and working conditions should be recorded by the drilling crew or a supervisor during drilling of a soil boring. Because it is not feasible to obtain samples at every foot along the depth of a boring, the technician at the site is required to monitor the drilling carefully. This information is usually recorded on paper forms and transcribed at the office.



Scale: 1.0 in = 2.76 mi

○- Boring Location

FIGURE 4 General view of Jefferson Parish, Louisiana.

TULANE UNIVERSITY DEPARTMENT OF CIVIL ENGINEERING GENERAL BOREHOLE DATA SHEET	
Date: 08/30/89	Boring Identification: HEBERT-B1
Location: X= -1298452.00000 Y= -3498763.00000	
Bottom Depth of Hole: 100.00	
Were Samples Recovered ? Y	
Were Lab Tests Performed ? Y	
SHEAR: UCT Y Triax Test Y Direct Shear N	
GENERAL: Consolid Y Permeability Y	
Alterberg Y	
Were In-Situ Tests Performed ? N	
SPT N	CPT N PMT N FVT N

FIGURE 5 Data entry screen for JP-LOC.DBF.

TULANE UNIVERSITY DEPARTMENT OF CIVIL ENGINEERING SOIL SAMPLE INPUT FORM		
SAMPLE SOURCE: US-COE	LOCATION: JP LEVEE 41-U	ZONE: 2-F
NORTH COORD: 1258.33	EAST COORD: -3025.0	
DEPTH: 41.9	DATUM: NGVD	DEPTH WT: 0.0 GS: 5.7
USCS CLASSF: CH	VISUAL CLASSF: PLASTIC CLAY, GRAY, SHELLS	
SAMPLE TYPE: UNDIST	DRY WT: 58.3	WET WT: 98.0
WATER CONT: 72.6	LL: 80	PL: 24 LI: 0 PI: 56
TESTS PERFORMED ON SAMPLE: TRIAX CONFIDENCE: NA		
SHEAR TEST: Q-TEST Qu: NA C: 448.0 C': NA		
CLAY FRACTION: NA PHI: 0.0 PHI': NA GRAIN SIZE: NA		
PERMEAB: NA COMPR INDEX: NA PENETROM: NA		
COMMENTS:		

FIGURE 6 Data entry screen for JP-PROP.DBF.

The computerized boring log program BORLOG was developed to provide a unified format for recording boring logs according to the ASTM standards (5). The program simplifies documenting soil boring logs and provides the data base files required for the GTIS system. BORLOG is interactive and user-friendly software that provides on-line data error checks, instructions, and assistance. The input data for BORLOG can

be entered directly at the site via a portable computer, or indirectly by transcribing written data forms at the office. Both methods follow the format shown in Figures 7 and 8 and yield identical output files (6).

Direct Entry Mode Direct entry is performed at the site with a DOS-type portable computer installed on the drilling rigs. The information required for the program is based on the visual and field tests specified by ASTM, such as the

GEOTECHNICAL EXPLORATION, Inc.
SOIL BORING LOG - GENERAL FORM

PROJECT NAME : _____

LOCATION : _____

PROJECT No. : _____ BORING No. : _____

TYPE OF DRILL RIG : _____

START DATE : _____ FINISH DATE : _____

START TIME : _____ FINISH TIME : _____

GROUND SURFACE : _____ WATER TABLE : _____

BORING DEPTH : _____

CREW : _____

REMARKS : _____

HIGH WATER SEASON	YES		NO		N/A				
TYPE OF SAMPLES	DISTURBED		UNDISTURBED		N/A				
SAMPLING DEVICE	SHELBY TUBE		SPLIT SPOON		N/A				
SAMPLE SIZE	3 INCHES		5 INCHES		N/A				
IN-SITU TESTS	SPT	CPT	DMT	PMT/VANE	UC	REPEAT	N/A		
WEATHER CONDITIONS	SUN	PCD	CLD	YR	RAINS	SNOW	WIND	REPEAT	N/A
TEMPERATURE (C°)	-10	0	10	20	30	40	50	+5	N/A

PREPARED BY : _____

PAGE 1 OF _____

1

2

3

4

5

6

7

8

9

0

*

ENTER

CANCEL

FIGURE 7 General form for soil boring logs.

approximate grain size distribution. However, this data can be updated later by LABLOG to include the more accurate results from detailed laboratory tests, such as the exact grain size distribution. A series of screens similar in format to Figures 7 and 8 are used in BORLOG to acquire information. Details of these screens are explained later.

Indirect Entry Mode For indirect entry, the drilling crew fills out a general form, Figure 7, per boring per day at the start of drilling. The first nine lines of the general form contain the information necessary to identify the exploration program (project name, location, crew, equipment, weather conditions, time, and date). It is written by the crew on the paper form. The next five lines on the form are for the crew to include their remarks, such as the use of special equipment, site condition, or weather changes. Starting from line 15, the crew enters the responses by checking the appropriate box or








boxes on the form. The N/A entry is used when the entry is not applicable or when no data is available.

Figure 8 shows the form accompanying each sample recovered during the investigation. On that form, the crew defines the elevations of the core and indicates if any changes occur in a soil layer. The quality of the core can be described by indicating its length and the location of any observed cracks on the two scales representing a standard 3-ft-long sampling tube. Other information on the recovered core will be described in the subsequent lines, including its color, odor, and moisture content. Some of the information on the form can be obtained in the field by performing in situ tests described by ASTM (D-2488). The remaining information is entered by checking the appropriate box or boxes on the form for indirect entry option. The shapes and sizes of the soil particles are required to classify coarse grained soils and to determine their engineering properties. The crew can use the grain shapes plotted on the form to identify the shape of soil particles. The

GEO TECHNICAL EXPLORATION, Inc.

SOIL BORING LOG - FIELD LOG

PROJECT No. 1 _____ BORING No. 1 _____

ELEVATION (ft)	TOP :	BOTTOM :	N/A	
STRATUM CHANGE	(feet)		N/A	
RECOVERED CORE	TOP	BOT	N/A	
CRACKS LOCATION	TOP	BOT	N/A	
CORE STRUCTURE	STRATF	LAMINTD	FISSRD	
	ROCKY	LENSED	HOMOGNS	
COLOR	Bk Bl Bn Gn Gy Dr	DARK		
	Pk Pr Rd Tn Wh Yw	LIGHT		
ODOR	STRONG	MODERATE	FAINT	
FIBROUS MATTER	YES		NO	
MOISTURE	DRY	MOIST	WET	
DILATANCY	NONE	SLOW	RAPID	
TOUGHNESS	LOW	MEDIUM	HIGH	
CEMENTATION	WEAK	MODERATE	STRONG	
COARSE GRAINED SOIL	YES		NO	
PERCENTAGE GRAVEL	COARSE	FINE	%	
			N/A	
PERCENTAGE SAND	COARSE	FINE	%	
			N/A	
PERCENTAGE FINES	SILT	CLAY	%	
MAX PARTICLE SIZE	< 305	76	19	
ANGULARITY				
	ROUNDED	SUBROUNDED	SUBANGULAR	
				
				ANGULAR
PARTICLE SHAPE			FLAT	
			ELONGATED	
			FLAT & ELONG	
FINE GRAINED SOIL	YES		NO	
MANUAL UCT (tsf)			N/A	
DRY STRENGTH	NONE	LOW	MEDIUM	
CONSISTENCY	V SOFT	SOFT	FIRM	
	HARD	V HARD	N/A	

PREPARED BY : _____

PAGE _____ OF _____

1
2
3
4
5
6
7
8
9
0
.

ENTER

CANCEL

PARTICLE SIZE:

(mm)

19

O 4.75

o 2

. 0.42

POWDER

FIGURE 8 Form for details of boring logs.

circles on the right side of the form on Figure 8 represent the standard ASTM sizes of soil particles. These circles are plotted to scale on the production version of the form for use in the field for measuring the size of soil particles. In a direct entry in the field, consecutive screens, identical to the paper form on Figure 8, will be displayed on the monitor of the portable

computer. Particle shapes and sizes will also be displayed on the computer screen in the direct entry option.

Information Retrieval The data recorded on the special paper forms, or as a file on the computer disk, is transferred

back by BORLOG to a computer at the office. This task does not require engineering background and needs minimal computer skills. For indirect entry, data will be entered via an electronic transducer. The current version of BORLOG uses a Summagraphics MM 1201 digitizing tablet with four cursor buttons to read the forms into a computer. The four buttons on the cursor pad execute the functions pick, enter, cancel, and quit. The information collected on the forms, or by BORLOG, is used for classifying the soils and to expand the geotechnical data base of the GTIS system. The keyboard of the office computer is used to enter the first lines written on the general form. The form can then be affixed to the digitizing tablet, and the tablet is calibrated using the two small circles at the top and lower corners of the paper form. The remaining data on the forms will be read by placing the tablet cursor anywhere within the boundaries of the marked box at the field and pressing the pick button on the pad. Numerical values can be entered using the numerical boxes on the top right corner of the forms or the keyboard. Entries can be canceled by picking the cancel box or pressing the cancel button on the pad. The enter box, or enter button on the pad,

is used to enter numeric entries. The quit button is used to abort the session. During the session the computer displays the form on the screen showing the questions, possible answers and the selected responses in three different colors. The user is asked at the end of each screen to check the data before it is written to the data files. BORLOG creates two data files: a standard ASCII file and a GTIS file to be read by dBase III.

LABLOG

A series of forms was developed for most of the standard laboratory tests frequently performed in soils investigations. These laboratory forms are also available in both paper as well as a computer format for direct or indirect entry mode. Figure 9 shows the form pertaining to the triaxial test. The computer version of the forms is the program LABLOG. LABLOG acquires the information and prepares output reports and files for automatic upgrades of the data bases according to a format similar to that used by BORLOG.

TRIAxIAL COMPRESSION TEST

SPECIMEN NO.					
INITIAL	WATER CONTENT, %	W_o			
	DRY DENSITY, pcf	γ_{dc}			
	SATURATION, %	S_o			
	VOID RATIO	e_o			
BEFORE SHEAR	WATER CONTENT, %	W_c			
	DRY DENSITY, pcf	γ_{dc}			
	SATURATION, %	S_c			
	VOID RATIO	e_c			
FINAL BACK PRESSURE, TSF		U_o			
MINOR PRINCIPAL STRESS, TSF		σ_3			
MAXIMUM DEVIATOR STRESS, TSF					
TIME TO $(\sigma_1 - \sigma_3)_{max}^{min}$		t_f			
ULTIMATE DEVIATOR STRESS, TSF					
INITIAL DIAMETER, IN.					
INITIAL HEIGHT, IN.					
DESCRIPTION OF SPECIMENS					
LL	PL	PI	G_s		
TYPE OF SPECIMEN :			TYPE OF TEST :		
PROJECT :					
BORING No. :			SAMPLE No. :		
DEPTH ELEVATION :			DATE :		
GEOTECHNICAL LABORATORY CIVIL ENGINEERING DEPARTMENT TULANE UNIVERSITY					

1
2
3
4
5
6
7
8
9
0
.

PAGE — OF —

FIGURE 9 LABLOG form for triaxial tests.

Synthetic Soil Estimator

A synthetic boring can be produced by the expert system BORPROF, which combines objective and subjective information in the analysis. The objective information consists of the summary reports extracted from the data bases. Meanwhile, the subjective information consists of descriptive knowledge of the geographical area, including geological trends such as a point bar, special soil conditions such as a hydraulic fill, and information supplied by experts and local engineers. The expert system and the external routines were built using Turbo Pascal version 4.0 and BASIC. The system combines the data obtained from the holes neighboring the proposed site through a weighing algorithm to develop a synthetic boring. The weighing algorithm adopted in the current version of BORPROF is a power formula of the distance (R_i) multiplied by a function of the difference in azimuth $F(\text{ALPHA}_i)$ between the required synthetic boring and each of the actual borings. Each property of the soil obtained from Boring i is assigned a weight in the calculations that expresses its "closeness" to the proposed site. The following formula is currently used to obtain the weight factor W_i , multiplier for each hole:

$$W_i = 1/R_i^a * F(\text{ALPHA}_i) \quad (1)$$

The exponent a of the power function and the nature of the function $F(\text{ALPHA}_i)$ are specified by the expert system by combining the distinctive trend in the data along with the subjective information retrieved from the knowledge base. The information from the knowledge base is extracted through a consultation with the expert system. The system first queries the user for the location of the site and the trend observed in the data. It then consults its knowledge base to identify the distinctive features of the area under consideration and proposes weighing factors along with their associated confidence. For the particular application discussed in this paper, some geological features are important. Sand ridges, old tributaries, and backswamp deposits produce a complex variation in stratification with different levels of homogeneity. Sand ridges are typically elongated and curved, resembling a moon crescent. Accordingly, properties of a hole centered in a sand ridge will be approximated better by the average of the holes following the longitudinal axis of the sand ridge than by the average of those following the transversal axis, which may lay beyond the width of the ridge. The knowledge of the extent of the ridge combined with the inclinations of its axes will be used to specify weighing factors for the data obtained from the different holes. This procedure is still under development, and further refinement will be made to the statistical model to improve its predictions.

APPLICATION

General

The GTIS TU-DIRT is used herein to simulate a soil boring in Jefferson Parish, Louisiana. The programs BORLOG and LABLOG were used earlier to prepare the data base files in the GTIS. Locations of the borings are entered on the LOCATION layer of the AutoCAD map of the area. The

boring location is indicated by inserting a BLOCK entity with an attribute label. The BLOCK insertion point defines the coordinates of the soil boring, and the attribute tag is an identification name for the boring, which is used to link to the dBase III records containing the soil boring data.

The procedure to generate a synthetic boring is as follows:

1. The desired location of the boring is indicated on the map by a symbol.
2. A radius of influence is selected to draw a circle that surrounds the holes in the data base that will be used. Note that the analysis can be performed more than once. Using the Selection Set capabilities of AutoCAD, the holes within the circle are selected.
3. With the selection set defined, an AutoLISP routine is invoked to execute the ATTEXT (Attribute Extraction) command of AutoCAD to produce a CDF-Format file, which can be transported to dBase III for further processing. This file contains the coordinates and identification code of all borings within the circle of influence.
4. Using the CDF-Format files, the data base files are searched for full information on the holes, and a summary report is prepared.
5. The summary report is sent to the EXPERT system BORPROF, which then produces the synthetic boring.

Example

From Figure 4 a site identified for exploration, which is near Johnny Bright Park, in square 4-E, is shown in Figure 10, with all the layers turned on, showing all the streets. Using the ZOOM command the area was enlarged, as shown on Figure 11. The site, at the intersection of 19th Street and Neyrey Drive, is indicated by a dot. Two analyses were performed, with a radius of influence of 400 yd shown by the inner circle on Figure 11 and a radius of influence of 530 yd shown by the outer circle. Three and five previous holes are covered by the circles. Their characteristics are extracted and sent out to two files and are listed in Tables 1 and 2. This area consists mostly of backswamp deposit, and the Pleistocene formation is found at a depth of a 100 ft. The depth of the boring was set at 75 ft with increments of 5 ft. No particular features exist around the site, and the weighing function was set to $1/R$ with no account for angle effect. Based on the above information BORPROF searched the data bases and produced the synthetic boring presented in Table 3. The table shows a possible stratification along with benchmark values for the soil properties. The synthetic hole obtained using five holes is presented in Table 4. Little difference exists between the two synthetic borings, indicative of the relative homogeneity of the area.

CONCLUSIONS

The concept of a GTIS that combines the geotechnical data base of a geographical area with its GIS maps was introduced. The system could be developed and tailored to meet the needs of a specific agency using either commercial packages or lo-

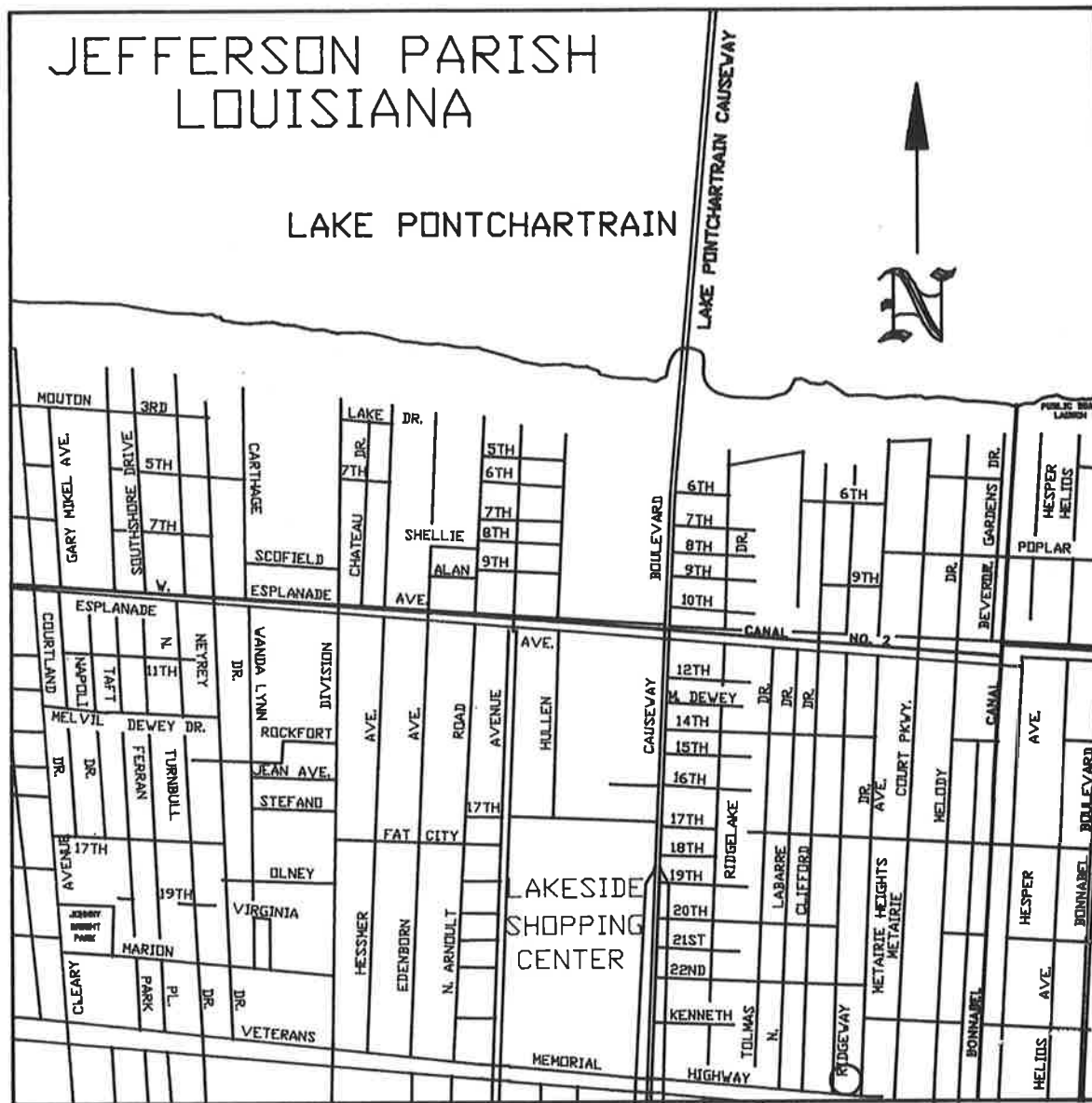


FIGURE 10 Example of application (Square 4-E).

TABLE 1 LIST OF HOLES FOR USE IN GENERATING SYNTHETIC BORING IN BORPROF WITH RADIUS OF 400 yd

Identification	Coordinate	
	East	North
JP-8-N68	-2850.00	-1683.30
JP-8-N63	-2716.70	-1791.70
JP-8-N117	-2633.30	-1108.30

TABLE 2 LIST OF HOLES FOR USE IN GENERATING SYNTHETIC BORING IN BORPROF WITH RADIUS OF 530 yd

Identification	Coordinate	
	East	North
JP-8-N117	-2633.30	-1108.30
JP-8-N111	-3058.30	-1191.70
JP-8-N94	3141.70	-1650.00
JP-8-N68	-2850.00	-1683.30
JP-8-N63	-2716.70	-1791.70

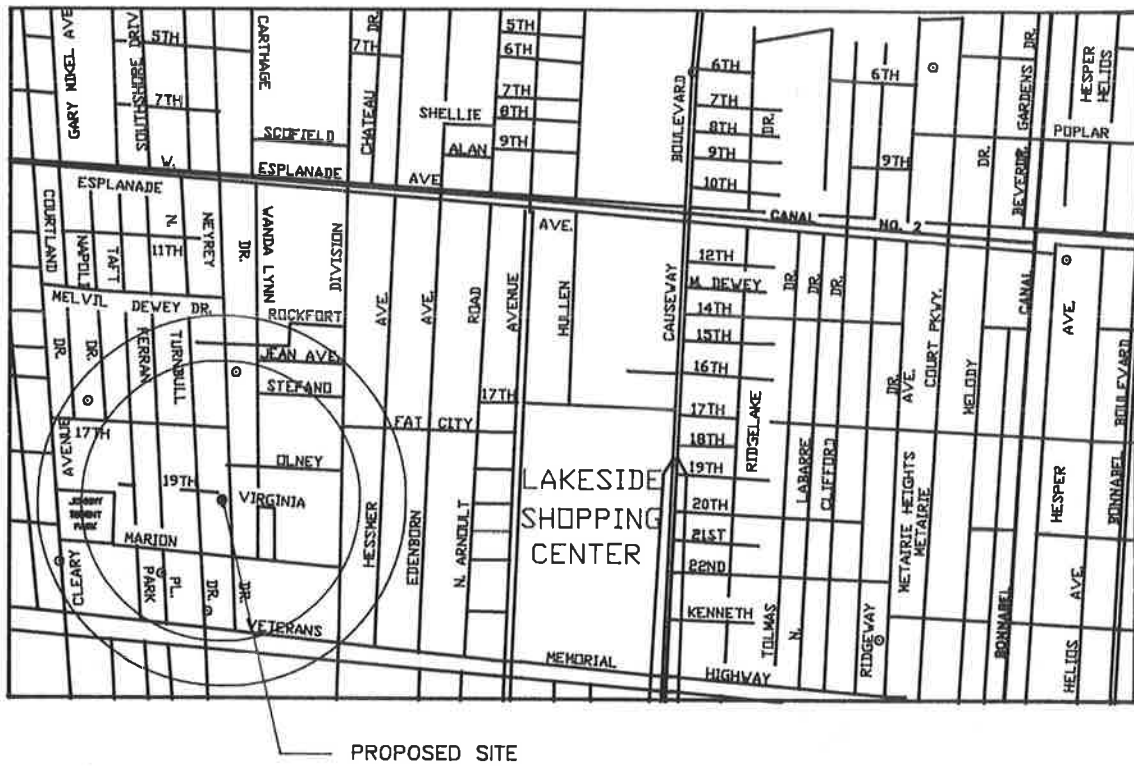


FIGURE 11 Close-up view of site.

TABLE 3 SUMMARY REPORT FOR SYNTHETIC BORING (400-ft RADIUS)

BORING DEPTH (ft)	SOIL TYPE USCS	WEIGHTED AVERAGES				
		Q _u (psf)	LL	PL	PI	SPT
5.00	PT	381.61	0	0	0	0
10.00	CH	235.15	0	0	0	0
15.00	CH	330.00	0	0	0	0
20.00	CH	269.10	0	0	0	0
25.00	SC/CH	170.00	0	0	0	26
30.00	SW	560.00	0	0	0	31
35.00	SW	0.00	0	0	0	17
40.00	CH	550.00	0	0	0	0
45.00	CH	797.31	96	26	70	0
50.00	CH	725.60	0	0	0	0
55.00	CH	1060.00	67	22	45	0
60.00	CH	2690.00	0	0	0	0
65.00	CL	3220.00	34	22	12	0
70.00	CL	2995.00	0	0	0	0
75.00	SC	785.00	24	19	5	30

TABLE 4 SUMMARY REPORT FOR SYNTHETIC BORING (530-ft RADIUS)

BORING DEPTH (ft)	SOIL TYPE USCS	WEIGHTED AVERAGES				
		Q _u (psf)	LL	PL	PI	SPT
5.00	Pt	381.61	0	0	0	0
10.00	CH	278.18	0	0	0	0
15.00	CH	385.27	0	0	0	0
20.00	CH	297.39	0	0	0	0
25.00	CH	312.07	0	0	0	0
30.00	SW	557.82	0	0	0	31
35.00	SW	0.00	0	0	0	17
40.00	CH	550.00	0	0	0	0
45.00	CH	843.31	88	22	66	0
50.00	CH	725.60	0	0	0	0
55.00	CH	1056.17	67	22	45	0
60.00	CH	2690.00	0	0	0	0
65.00	CL	3220.00	34	22	12	0
70.00	CL	2995.00	0	0	0	0
75.00	SC	785.00	24	19	5	30

cally developed software. The geotechnical information to be included in the GTIS is acquired from previous soil investigations and would be updated continuously. The system is capable of estimating soil properties of an unexplored site within the geographical area or to create synthetic soil boring logs and profiles for that site. Data bases from neighboring boring logs and subjective information about the area are used to generate the synthetic data. A prototype GTIS, TU-DIRT, was developed along these lines. The advantages of the computerized format of the GTIS are many and include standardized format for documenting soil investigations, consistency in the information supplied by technicians, reduction in bias, preservation of data, and full interaction with the other components.

ACKNOWLEDGMENTS

The authors are indebted to J. W. Winford and N. Marianos, graduate students in the Department of Civil Engineering who digitized the maps, used the application, and coded the data in the data bases. L. Gilbert of Gore Engineering, R. Eustis

of Eustis Engineering, and F. Duarte of the U.S. Corps of Engineers, New Orleans District, provided the data for the data bases. Their interest in the work and collaboration is gratefully acknowledged.

REFERENCES

1. H. N. Fisk. *Geological Investigation of the Alluvial Valley of the Lower Mississippi River*. War Department, Corps of Engineers, U.S. Army, Mississippi River Commission, Vicksburg, 1944.
2. C. R. Kolb and R. T. Saucier. Engineering Geology of New Orleans. Geology Under Cities (R. F. Leggett, ed.). *Reviews in Engineering Geology*, Vol. V, Geological Society of America, 1982.
3. *AutoCAD*. Release 10.0 c5. Autodesk, Inc., Sausalito, Calif., 1989.
4. *dBase III Plus*. Ashton-Tate, Torrance, Calif., 1987.
5. ASTM. Soil and Rock, Building Stones; Geotextile. *Annual Book of ASTM Standards*, Volume 04.08. Philadelphia, Pa., 1989.
6. R. M. Bakeer, M. D. Morse, and T. Hadj-Hamou. An Integrated Computer Package for Geotechnical Investigation. In *Proc., ISMM International Conference*, Microcomputer Applications, Los Angeles, Calif., 1989.

Publication of this paper sponsored by Committee on Soil and Rock Properties.

Seismic Spectra for Highway Bridges in Washington State

GEORGE TSIATAS, KAREN KORNER, AND CARLTON HO

A base spectrum and soil amplification spectra are developed and are intended to replace the seismic response spectrum and site coefficients presented in the AASHTO guidelines for highway bridge design in Washington State. The base spectrum is constructed using available data on ground motion from subduction zone earthquakes similar to those that occur in Washington State. These earthquakes generally have larger high-frequency components than shallow-focus earthquakes. Because the existing codes are based primarily on data from shallow-focus earthquakes, the base spectrum developed has a larger high-frequency content than the existing base spectrum. The soil amplification spectra are derived using 123 boring logs from actual bridge sites in Washington. Data from the boring logs are correlated to dynamic soil properties, which are used in the computer program SHAKE to find the frequency-dependent amplification properties of the soil profiles. The profiles are grouped by depth and type of soils. Nine groups are identified, and mean amplification spectra are developed for each group. The design spectra are compared with results from other site-dependent studies as well as to the responses of the 1949 and 1965 Puget Sound earthquakes.

Washington State is one of the major centers of earthquake activity in the country. Two recent earthquakes (in 1949, with a magnitude of 7.1 and in 1965, with a magnitude of 6.5) caused considerable structural damage in the highly populated Puget Sound basin. The estimated recurrence interval of magnitude 6 earthquakes in this area is between 5 and 10 years (1,2). The possible occurrence of an earthquake with a magnitude greater than 8 has been suggested (3).

The Washington State Department of Transportation (WSDOT) is currently using AASHTO's 1983 seismic guidelines (4). These guidelines were originally developed by the Applied Technology Council as seismic guidelines for buildings (5) and were later modified for bridges (6). The guidelines were developed for general U.S. use and are based on research relying largely on data from California earthquakes. Earthquakes occurring in Washington differ significantly from those in California in terms of source characteristics, wave propagation paths, and site geology. The differences become obvious when the unique geology and seismicity of Washington are studied.

The landmass of the western U.S. is a result of the activity along a convergent plate boundary parallel to the Rocky Mountains over the past 300 million years (7). The subduction of the Juan de Fuca plate appears to be currently active (3), and the largest earthquakes occurring in the area are deep-

focus events associated with this subduction process (7). Many smaller earthquakes that occur at shallower depths are believed to be associated with active north-south compression in this area. The reader is referred to Hopper et al. (8) for a more complete description of these tectonic processes. Much of the geology in the Puget Sound basin is dominated by the effects of the various advances and retreats of the Puget Lobe of the Cordillerian Ice Sheet. This ice sheet is associated with periods of global glaciation beginning more than 40,000 years ago. During this period, the area was sometimes covered with up to 5,000 ft of ice. As the ice retreated, thick layers of till were deposited and lakes and rivers formed. As the ice again advanced, these deposits were overridden, reworked, and re-deposited. These multiple periods of glaciation resulted in deep layers of heavily over-consolidated till interspersed with glaciofluvial and glaciolacustrine deposits in most of the Puget Sound basin. These deposits hide much of the underlying bedrock structure in this area, making it difficult to identify active faults or understand their movements.

EXISTING GUIDELINES

Figure 1 shows the AASHTO zoning map for Washington State (4). The map depicts contours of effective ground acceleration, which is an Acceleration Coefficient developed, by the Applied Technology Council, specifically as a response spectrum scaling factor. The mapping is based on the work of Algermissen and Perkins (9), who mapped peak ground accelerations in the contiguous United States. The difference is that whereas the work of Algermissen and Perkins depicts contours of peak ground acceleration, the AASHTO guidelines show contours of expected ground acceleration, which is an acceleration coefficient developed specifically as a response spectrum scaling factor.

Perkins et al. in 1980 developed new zoning maps for Washington State, which are an improvement over the 1976 study by Algermissen and Perkins because geologic factors were considered along with historic seismicity (10). Perkins et al. used attenuation factors from Schnabel and Seed's 1973 study of California earthquakes (11). The maps developed by Perkins et al. in 1980 depict contours of expected peak ground acceleration and not of the Acceleration Coefficient used in the AASHTO guidelines. The zoning maps were recalculated by Higgins et al. (12) in 1986. Their work is based on the 1980 study by Perkins et al. the difference being that Higgins et al. modified the acceleration data to account for velocity attenuation effects so the resulting velocity-related acceleration coefficients would be more nearly like the Acceleration

G. Tsiatas, Department of Civil and Environmental Engineering, University of Rhode Island, Kingston, R.I. 02881. K. Kornher, CH₂M Hill Corporation, 777 108th Avenue, N.E., Bellevue, Wash. 98009-2050. C. Ho, Department of Civil and Environmental Engineering, Washington State University, Pullman, Wash. 99164-2910.



FIGURE 1 Seismic map of Washington State by AASHTO.

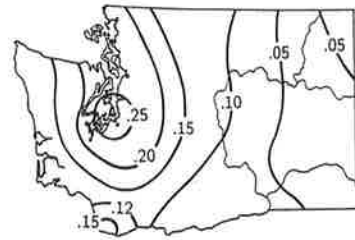


FIGURE 2 Seismic map of Washington State by Higgins et al. (12).

Coefficient used in the AASHTO codes. Figure 2 shows the map developed by Higgins. The study of Perkins et al., and hence the report of Higgins et al., may not represent the best estimate of relative ground shaking in light of recent developments in the understanding of subduction zone earthquake ground motion. Recent studies on subduction zone ground motion indicate definite differences in attenuation properties between shallow-focus and deep-focus earthquakes (13). Distinct differences also exist in frequency content. Because of these recent developments, it is anticipated that the zoning may need to be reconsidered in the near future.

The base spectrum and modification factors for local soil conditions in AASHTO were developed using a study by Seed et al. (14), who found significant differences in spectral shapes for four different generalized soil conditions: (a) rock, (b) stiff soil, (c) deep cohesionless soil, and (d) soft to medium clays and sands. An ensemble of 104 strong-motion records were used in this analysis, the majority from California earthquakes. The rock and stiff soil categories were combined into one category and simplified to represent the base spectrum in the AASHTO guidelines. For other site conditions, the base spectrum is multiplied by a scaling factor (1.2 for stiff clays and deep cohesionless soils and 1.5 for soft to medium-stiff clays and sands) to duplicate the general effects of these soils as indicated by Seed et al. The curves developed by Seed et al. and the corresponding AASHTO curves are shown in Figures 3 and 4. The resulting response values are then used to obtain either an elastic seismic response coefficient, which is used to find an equivalent static force, or an elastic seismic response spectrum, which can be used in a dynamic modal analysis.

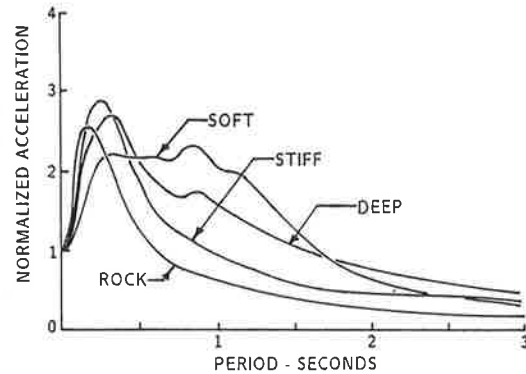


FIGURE 3 Site-dependent spectra developed by Seed et al. (14).

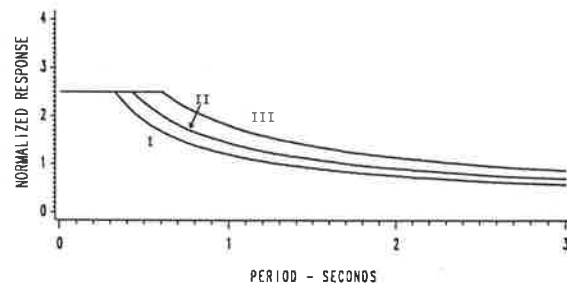


FIGURE 4 AASHTO curves for three soil conditions.

DEVELOPMENT OF DESIGN RESPONSE SPECTRA

Input Motion

The computer program SHAKE (15) was used for the determination of the soil amplification spectra. SHAKE models vertical propagation of shear waves through a linear, viscoelastic system of horizontal soil layers. Required program input consists of a soil profile (with depths and types of soil layers), strain-dependent damping and moduli curves for the types of soils, and an acceleration time history used as input at the base of the profile. The nonlinear behavior of the soil is approximated using an iterative procedure to obtain strain compatible moduli and damping values for each layer.

This is a simplified model, but for a study of this magnitude it appears to be an appropriate calculation tool. Studies comparing down-hole data with analytic response using SHAKE show that near surface motions may contain components not predicted with this simple model (16). Wave theory predicts that shear waves become more vertical as they pass through increasingly less dense materials on their way to the surface (17). For deep-focus earthquakes, this assumption of vertical shear waves seems reasonable. Non-horizontally layered bedrock can affect the propagation of earthquake waves through reflection and refraction and result in non-vertical propagation near the ground surface. Focusing effects in sedimentary basins can produce long-period surface waves (18) that may be critical in terms of differential movement between bridge piers (19). These long-period effects are accounted for in the AASHTO guidelines in a general way by increasing the base spectrum ordinates at longer periods. Although the effects of focusing can be large, they are very much site- and earthquake-specific and will not affect most sites. Not accounting for them

appears consistent with the AASHTO philosophy. The assumption of horizontal soil layers is not unreasonable. Softer soils, which have a greater impact on attenuation and amplification of base motion, are typically horizontally (or nearly horizontally) layered. Finally, SHAKE has been used extensively in similar studies and its limitations are known and can be accounted for.

One of the first questions to be answered is what kind of input motion should be used for the calculation of the amplification spectra. Several possibilities can be employed. The first possibility is the use of SHAKE to deconvolute existing records from earthquakes in Washington. There are two problems with this approach. First, few records from strong motion earthquakes are available in this area. Use of such a limited number could introduce bias in the resulting spectra. Second, it is known that SHAKE tends to attenuate high frequency components and conversely, during deconvolution high frequency components would appear at the base. The second possibility is the use of actual records from subduction zone earthquakes. The problem here is that soil properties and earthquake characteristics must be matched exactly. Such properties though, are not usually available in detail, especially for earthquakes occurring abroad, and it would be difficult to factor them out from the records. A third possibility is to use predictive equations, which give average response spectra as functions of magnitude and distance. The average spectra can then be used as target spectra for the development of simulated records.

This last approach based on predictive equations was followed in this study. Several predictive equations, along with appropriate modifications, were used to develop a target spectrum (20). It was found that the resulting shape resembles closely the spectral shape developed by Seed et al. (14) for stiff soil conditions. This curve scaled by 0.1, 0.2, and 0.3 was used as target spectra in the program SIMQUAKE (21) to produce four acceleration time histories, which were used for the determination of the soil amplification factors. The four records were used in order to eliminate any possible bias introduced by use of only one record. The scaling factors were selected based on the current level of seismicity in the area, as shown in the contours of expected ground acceleration developed by Higgins et al. (12). Results for other scaling factors can be approximately found by interpolation or can be exactly determined by repeating the present calculations with the new scaling factors.

Base Spectrum

The base spectrum was determined by appropriately modifying the target spectrum. At least two modifications need to be considered, both in conjunction with the simplifications made in constructing the AASHTO curves. In these guidelines (6), the response is simplified so that a single equation can be used to represent the response spectrum:

$$C_s = (1.2AS)/T^{2/3} \leq 2.5 A \quad (1)$$

where

- C_s = seismic response coefficient,
- A = acceleration coefficient,

- S = soil coefficient, and
- T = the period.

When $S = 1.5$ and $A \geq 0.3$, C_s need not exceed $2.0 A$. Plotting C_s versus T will generate the associated response spectrum.

The development of the soil amplification spectra complicates using this type of simplified analysis. The base times the amplification spectrum would also have to be treated in a simplified manner. The effect of doing this would essentially reduce the spectra back to the form of the AASHTO curves. This would not then be a significant improvement over the existing guidelines. Because of these considerations, it was decided that this simplification is not justified. This, of course, means that it will no longer be possible to use a simple equation to find the appropriate seismic factor, but it will be necessary to choose appropriate numbers from the spectral curves.

The second modification deals with increasing the response spectrum ordinates at longer periods because of concerns with inelastic response of longer period bridges. Recommendations in the AASHTO guidelines state that the spectra should be about 50 percent greater at a period of 2 sec. This conservatism was applied to the spectrum in this study to maintain consistency with the AASHTO philosophy.

Another possible modification is lengthening the period of the peak response. This would incorporate changes in the spectral shapes for earthquakes at larger distances from source zones. This, however, makes the spectrum overly conservative in regions of high seismic risk (closer to source zones), where seismic forces may control the design. It would be more appropriate to use a slightly higher scaling factor for regions far from source zones that encompass the longer period motion expected because the seismic forces in these regions are less critical in design. Because of SHAKE's tendency to attenuate high frequency motions, the soil amplification spectra reduce the base spectrum unrealistically at that end of the spectrum. Because of this, it is appropriate to increase the spectral values at those periods to compensate for that reduction.

The base spectrum developed by modifying the Seed stiff spectrum is shown in Figure 5. In the same figure, the AASHTO base (soil group I) is shown for comparison. Ordinates for the base spectrum curve can be found elsewhere (22).

Soil Amplification Spectra

The soil profiles used were developed from 123 boring holes from bridge sites in Washington State. This large study group

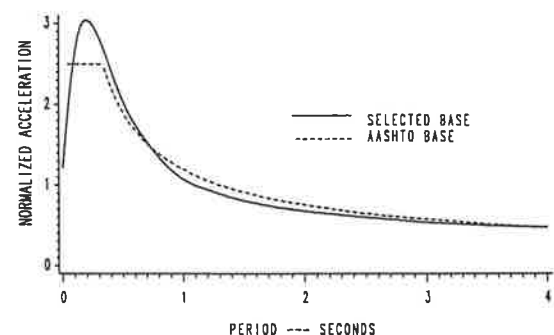


FIGURE 5 Selected base spectrum and AASHTO Soil Type I curve.

was used in an attempt to include the range of soil types and variations encountered in this area. The properties of all these profiles can be found elsewhere (22).

Input requirements for SHAKE include strain versus shear modulus and strain versus damping curves. For cohesionless soils, curves developed by Seed and Idriss (23) were used (Figure 6). The shear modulus relates to the K_2 parameter given in Figure 6 according to the following:

$$G = 1,000K_2(\sigma_m)^{0.5} \quad (2)$$

where K_2 is a function of the void ratio and strain amplitude, and σ_m is the effective mean principal stress. For the case of clays, shear modulus and damping curves developed by Seed and Idriss (23) were also used (Figure 7). This figure indicates that the shear modulus is normalized with respect to undrained shear strength.

The soils were categorized as clays or sand depending on their predominant behavior, as required for the input to SHAKE. Because the type of information available on the logs is limited, it was necessary to use empirical relations between the available data [usually Standard Penetration Tests (SPT) and undrained shear strength] and dynamic properties of the soil. The following relationship for uncorrected blow counts from work by Ohsaki and Iwasaki (24), was chosen because it is correlated to down-hole velocity studies, the correlation coefficient is high, and the results are intermediate when compared with the results of other researchers.

$$G_{max} = 1.47N^{.68} (tsf) \quad (3)$$

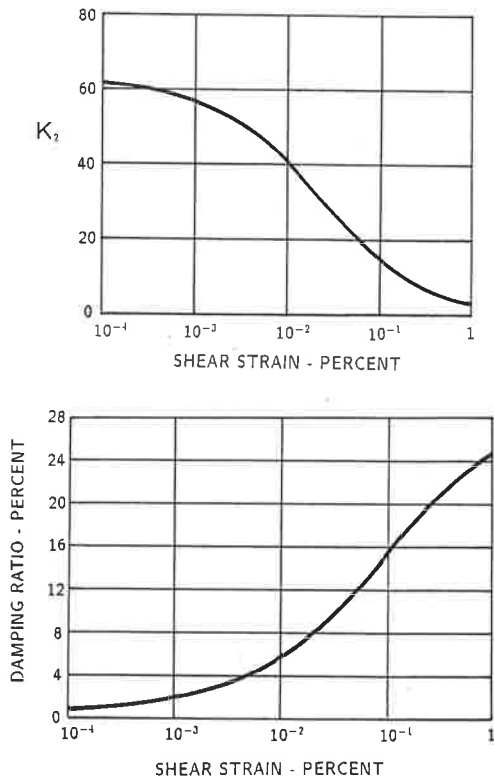


FIGURE 6 Shear modulus for sands (top); damping ratio for sands (bottom).

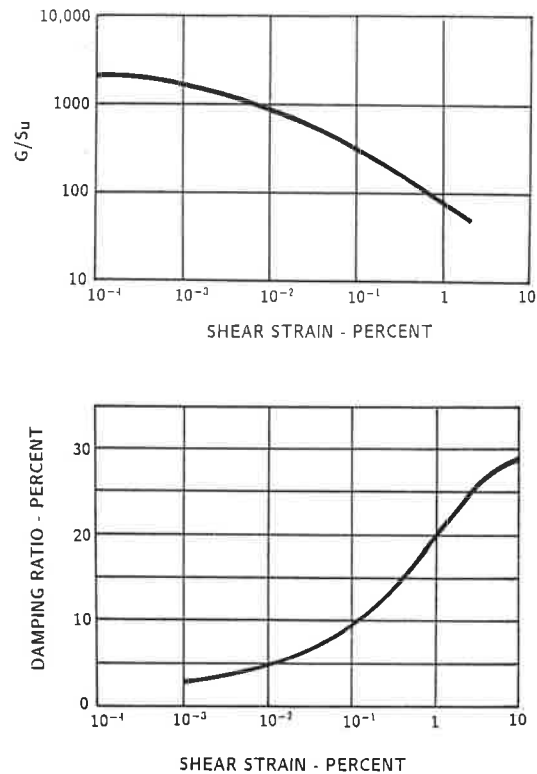


FIGURE 7 Shear modulus for saturated clays (top); damping ratio for saturated clays (bottom).

It should be noted that using such empirical correlations requires caution. Many factors can affect the blow counts recorded and undrained shear strength test results. The values seen in the boring logs exhibited significant variability, even in apparently homogeneous deposits. Sensitivity studies were performed in an attempt to bracket the possible response, and it appears that the profile responses are not sensitive to minor variations in calculated shear modulus values except at soft sites. These soft sites fall into groups that incorporate a wide range of frequency amplification, accounting for this greater variation.

The four simulated records scaled by 0.1, 0.2, and 0.3 were used with SHAKE to determine the 5 percent damped acceleration response of the soil profiles. This response was divided by the response of the time history at a rock outcropping. The result is a soil amplification spectrum that shows the amplification (or attenuation) effects of the profile on the underlying base motion. The spectra developed with the 0.2 scaled simulation were used to determine groupings. The assumption made was that groupings obtained using the 0.1 and 0.3 scaled records would be the same as those developed using the 0.2 records. Peak spectral amplification for each site was plotted as a function of period, and preliminary groupings were made. Sites within each group were analyzed for similarities. The results appeared to be primarily functions of depth and types of soils in the profiles. Some slight shifting between the preliminary groups allowed categorization by easily identifiable traits. The final groups are presented in Table 1. Figures 8 and 9 show peak amplification versus period for sites in each group.

TABLE 1 SOIL GROUPS

Group	Description
1	20-50 ft to blow counts of 100 or greater of medium to dense cohesionless soils with up to 5 ft of loose soils (blow counts less than or equal to 10) at the surface. Variable layers of medium and dense soils, with no layers of loose soils beneath the top 5 ft.
2	51-100 ft to blow counts of 100 or greater of medium to dense cohesionless soils with up to 20 ft of loose soils at the surface. Variable layers of medium and dense soils, with no layers of loose soil beneath the top 20 ft.
3	100-300 ft to blow counts of 100 or greater of medium to dense cohesionless soils with up to 30 ft of loose soils at the surface. Variable layers of medium and dense soils, with no layers of loose soil beneath the top 30 ft.
4	10-50 ft to blow counts of 100 or greater of all other soils not in group 1.
5	50-100 ft to blow counts of 100 or greater of all other soils not in group 2.
6	100-300 ft to blow counts of 100 or greater of all other soils not in groups 3, 7.
7	100+ ft to blow counts of 100 or greater of soils consisting primarily of clays or clays and loose sands.
8	COAST SITES, 10-50 ft of loose silt and sand (not necessarily to SPT=100)
9	COAST SITES, 50+ ft of loose silt and sand (not necessarily to SPT=100)

Coastal sites, with loose, silty deposits, were grouped separately because of the great variability in response for minor variations in G_{max} values calculated from blow counts. Because of the small number of coastal sites available, sites with variations in depths and G_{max} values were simulated to find a probable range of responses. Sites on rock or hard soil deposits (blow counts greater than 100 within the top 20 ft) would be represented by the base spectrum alone (no soil amplification effects).

For each of the 9 soil groups, soil amplification spectra were developed corresponding to values 0.1, 0.2, and 0.3 of the severity coefficient (acceleration coefficient). The amplifica-

tions were analyzed statistically at 38 periods. Finally, the mean amplification spectra were determined. Figure 10 compares the mean amplification spectra for all 9 groups developed using the 0.2 scaled record. Similar curves were obtained for the 0.1 and 0.3 scaled spectra. Hard copies of the spectral ordinates can be found elsewhere (22). From Figure 10 it can be seen that Groups 1, 2 and 3 represent well-behaved sites, and conservative amplifications are allowed. The groups of the same depths with clays or loose soils or both in general show higher amplitudes and greater ranges in frequency content.

DISCUSSION OF RESULTS

The product of the base spectrum and the soil amplification spectra for the 9 soil groups results in the design response spectra. Figure 11 depicts these spectra for the case of the 0.2 scaling of the records. Superimposed on Figure 11 is the base spectrum. The design spectra were compared with the spectra developed by Seed et al., the AASHTO curves, the curves generated by predictive equations for subduction zone earthquakes, and the response from the existing strong ground-motion records from the Puget Sound area.

The derived spectra compared with the spectra developed by Seed et al. (Figure 3) have smaller high-frequency components and larger long-period components with increasing depth or softness of the deposits. These same trends can also be seen in the spectra developed by Hayashi et al. for Japanese sites (25). The earthquakes that their analysis were based on are subduction zone earthquakes, where larger high frequency content can be expected. The higher frequencies can be seen in these spectra in the stiff soil category.

Figure 12 compares the derived spectra to the predictive equations for subduction zone earthquake ground response. It can be seen that Group 3 spectra scaled by 0.30 are most similar in spectral shape to the Crouse et al. (26) and Vyas et al. (27) spectra for a magnitude 8 earthquake at a depth of 50 km.

The AASHTO curves scaled by the soil factors for three soil conditions are similar to the spectra developed in this study in terms of strengths of records (Figure 13). In that

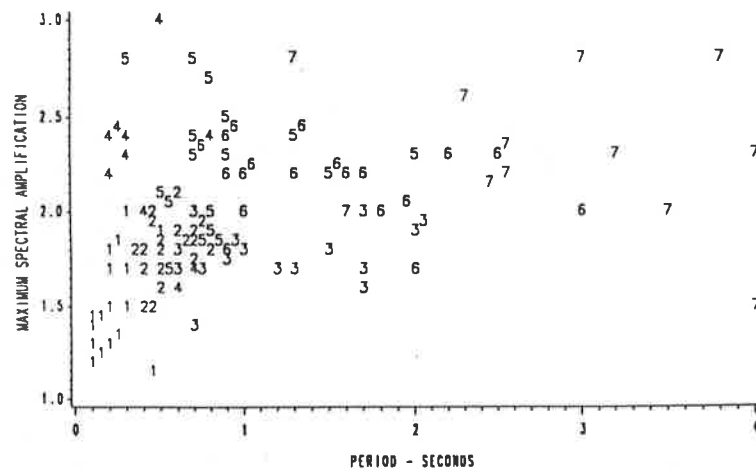


FIGURE 8 Maximum spectral amplification for soil groups 1-7.

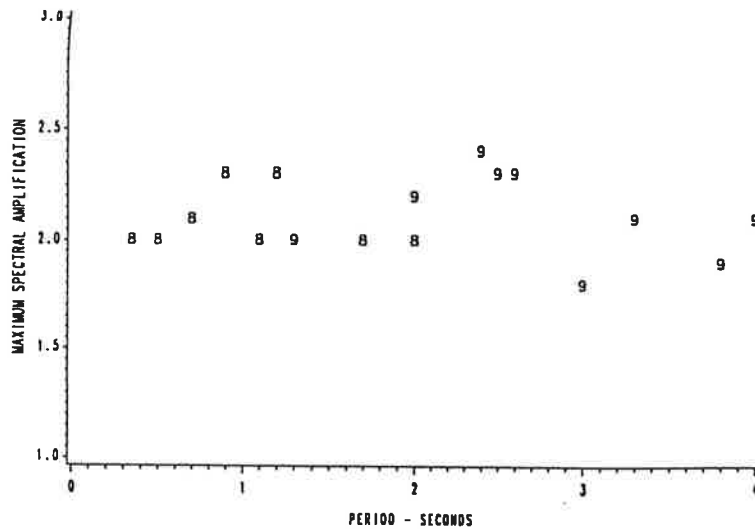
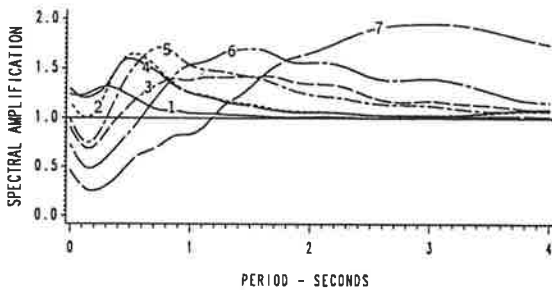
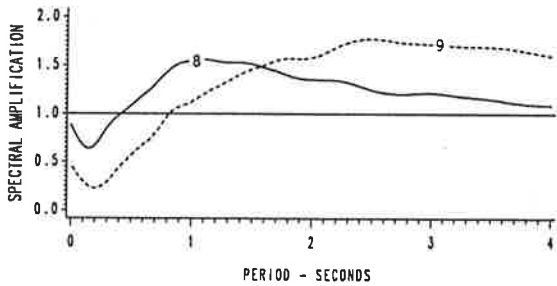


FIGURE 9 Maximum spectral amplification for soil groups 8 and 9.



(a)



(b)

FIGURE 10 Soil amplification spectra for 0.2 scaled records for (a) groups 1-7 and (b) coastal sites: groups 8 and 9.

respect, the derived spectra are consistent with the existing codes. The differences in spectral shapes are from two sources. There are differences in frequency content because deep-focus earthquakes have larger high frequency contents than shallow-focus earthquakes. There are also differences because of the unique types of soils in Washington and because of the refinement of the soil groupings. These differences should be expected because the AASHTO curves are based primarily on spectra developed using California earthquakes and Cal-

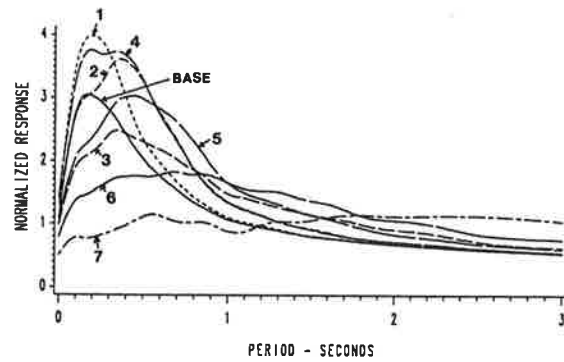


FIGURE 11 Normalized acceleration response spectra and base spectrum.

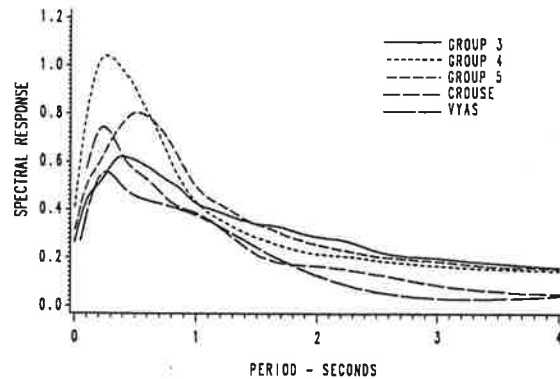


FIGURE 12 Comparison with curves developed from predictive equations.

ifornia soils, which are different from the soils and earthquakes in Washington.

When the spectra developed in this study are compared with the existing AASHTO curves, it must be noted that the depths specified in this analysis are generally to hard soils (blow counts above 100) and not to bedrock, which is the

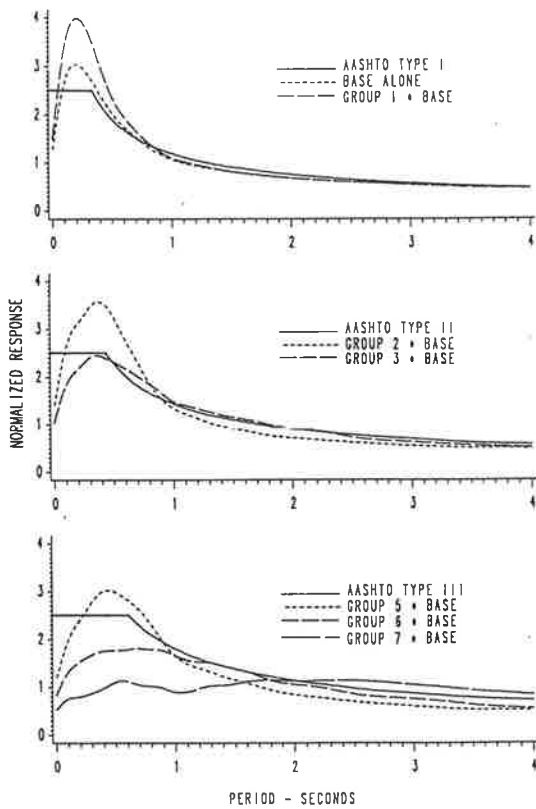


FIGURE 13 Comparison of AASHTO curves to spectra developed in this study.

depth prescribed by the AASHTO guidelines. The depth from hard soils to bedrock soils varies from zero to around 900 ft in Washington. The AASHTO spectrum for stiff soil sites (Group 1) generally corresponds to the base spectrum and Group 1 of this study. Larger high-frequency components exist in the spectra from this study. This is consistent with studies showing subduction zone ground motions having larger high frequency content. The spectra are similar above a period of about 1 sec. The AASHTO spectrum for stiff clays and deep cohesionless soils (Group II) corresponds to the groups 2 and 3 spectra in this study. These groups do not include clays, which would generally reduce the higher frequency response. The AASHTO spectrum for soft to medium-stiff clays and sands would include groups 5, 6 and 7 of this study. The average of these spectra would be close to the AASHTO guideline curves. These comparisons show that the results of this analysis are generally consistent with existing spectra in terms of strengths. They also address the soil and earthquake factors in Washington more realistically.

The spectra can also be compared with the responses of the 1949 and 1965 Puget Sound earthquakes. The recording site in Olympia for the 1949 and 1965 events can be classified as a Group 3 site (28). Scaled Group 3 spectra are compared with the responses from these two events in Figure 14. This actual response is enveloped fairly well by the Group 3 spectra except for the high frequency response of the 1965 record. This event was almost directly under the recording station. Because of this, the time history may be rich in high frequency components that would not be seen elsewhere. The recording site in Seattle for the 1965 event would be classified as a Group

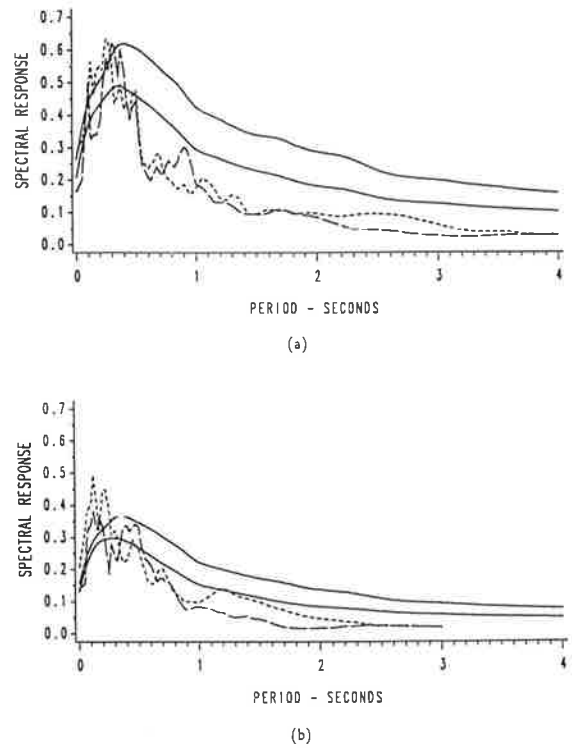


FIGURE 14 Comparison with Puget Sound earthquakes recorded in Olympia: (a) Group 3 soils scaled by 0.3 and 0.2 and the 1949 event; (b) Group 3 soils scaled by 0.1 and 0.15 and the 1965 event.

1 site. The response at this site is enveloped fairly well by the predicted spectra scaled by 0.10 as shown in Figure 15.

CONCLUSIONS

A base spectrum and soil amplification spectra are developed to be used in seismic design considerations of highway bridges in Washington State. In summary, the following steps are required to use the present results: (a) determine the soil profile and the acceleration coefficient for the site, (b) find base spectrum ordinate for period of interest, (c) find the soil amplification ordinate for period of interest from the spectrum corresponding to the selected soil profile and acceleration coefficient, and (d) the seismic coefficient used in the calculations (AASHTO) is then given by: $C_s = \text{acceleration coefficient} \times \text{base spectrum ordinate} \times \text{soil amplification ordinate}$. The appropriate severity coefficient can be taken

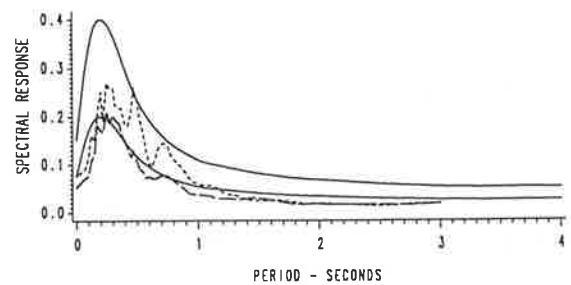


FIGURE 15 Comparison of spectra for Group 1 soils scaled by 0.10 and 0.05 to 1965 earthquake recorded in Seattle.

from the map of velocity-related accelerations developed by Higgins et al. (12) until the remapping is accomplished. When the results of the present study are used in conjunction with a computer program, such as SEISAB, for earthquake analysis of bridges, a library design response spectra must be introduced into the program. The base spectrum ordinates should be multiplied by all derived spectra. Twenty-seven design response spectra will result, which correspond to the nine soil profiles and the three severity coefficients for each soil profile. The digitized data included elsewhere in work by Tsiatas et al. (22) can be easily used for this purpose.

Although the base spectrum and soil amplification spectra developed in this study are in general agreement with the existing codes in terms of strengths of ground shaking, differences in spectral shapes are seen. These differences are consistent with expected differences in frequency content between shallow- and deep-focus earthquakes. The soils in Washington are diverse, making it logical to divide the types into more groups than those identified by the existing codes. The spectral amplification and attenuation characteristics of these soil groups, however, correspond fairly well with the site-response characteristics of less refined groupings. The most substantial differences between the existing codes and results of this study are at the higher frequencies (periods less than 0.4 sec). This means the greatest changes in design forces calculated will be to stiff structures or in the transverse direction in long-span bridges. For other periods of interest, the spectra developed here may provide a slightly higher or lower (but hopefully more reasonable) value of relative ground-shaking.

ACKNOWLEDGMENT

The work on which this report is based was supported by WSDOT and FHWA, U.S. Department of Transportation. Grateful acknowledgment is made to representatives of various departments of WSDOT, in particular to Bill Carr, planning, research, and public transportation; Dick Stoddard, bridges and structures; and Todd Harrison, geotechnical.

REFERENCES

1. R. S. Crossen. Review of Seismicity in the Puget Sound Region from 1970 through 1978. *U.S. Geological Survey Open-File Report 83-19*, 1983.
2. N. H. Rasmussen, R. C. Millard, and S. W. Smith. *Earthquake Hazard Evaluation of the Puget Sound Region*, Washington State Geophysics Program, University of Washington, Seattle, 1975.
3. T. H. Heaton and S. H. Hartzell. Source Characteristics of Hypothetical Subduction Earthquakes in the Northwestern United States. *Bulletin of the Seismological Society of America*, Vol. 71, No. 3, June 1986, pp. 675-708.
4. *Guide Specifications for Seismic Design of Highway Bridges*. AASHTO, Washington, D.C., 1983.
5. *Tentative Provisions for the Development of Seismic Regulations for Buildings*. Publication ATC 3-06. Applied Technology Council, 1978.
6. *Seismic Guidelines for Highway Bridges*. Publication ATC-6. Applied Technology Council, Redwood City, Calif., Oct. 1981.
7. J. J. Taber and S. W. Smith. Seismicity and Focal Mechanisms Associated with the Subduction of the Juan de Fuca Plate Beneath the Olympic Peninsula, Washington. *Bulletin of the Seismological Society of America*, Vol. 75, No. 1, Feb. 1985, pp. 237-249.
8. M. G. Hopper et al. A Study of Earthquake Losses in the Puget Sound, Washington Area. *U.S. Geological Survey Open-File Report 75-375*, 1975.
9. S. T. Algermissen and D. M. Perkins. A Probabilistic Estimate of Accelerations in Rock in the Contiguous United States. *U.S. Geological Survey Open-File Report 76-416*, 1976.
10. D. M. Perkins et al. Probabilistic Estimates of Maximum Seismic Horizontal Ground Motion on Rock in the Pacific Northwest and the Adjacent Outer Continental Shelf. *U.S. Geologic Survey Open-File Report 80-471*, 1980.
11. P. B. Schnabel and H. B. Seed. Accelerations in Rock for Earthquakes in the Western United States. *Bulletin of the Seismological Society of America*, Vol. 63, No. 2, April 1973, pp. 501-516.
12. J. D. Higgins, R. J. Frigaszy, and L. D. Beard. *Seismic Zonation for Highway Bridge Design in Washington*. Washington State Department of Transportation, 1988.
13. T. H. Heaton and S. H. Hartzell. Earthquake Hazards on the Cascadia Subduction Zone. *Science*, Vol 236, April 1987, pp. 162-168.
14. H. B. Seed, C. Ugas, and J. Lysmer. Site-Dependent Spectra for Earthquake Resistant Design. *Bulletin of the Seismological Society of America*, Vol. 66, No. 1, Feb. 1976, pp. 221-234.
15. P. B. Schnabel, J. Lysmer, and H. B. Seed. *SHAKE, A Computer Program for Earthquake Response Analysis of Horizontally Layered Sites*. EERC 72-12. Earthquake Engineering Research Center, University of California, Berkeley, Dec. 1972.
16. C. Y. Chang and M. S. Powers. Empirical Data on Spatial Variation of Earthquake Ground Motion. *Second International Conference on Soil Dynamics and Earthquake Engineering, The Queen Elizabeth II*, New York to Southampton, Vol. 1, June/July 1985, pp. 3-17.
17. K. Kanai. *Engineering Seismology*, University of Tokyo Press, 1983.
18. W. B. Joyner and D. M. Boore. Measurement, Characterization and Prediction of Strong Ground Motion. *Earthquake Engineering and Soil Dynamics II—Recent Advances in Ground Motion Evaluation*. Geotechnical Special Publication No. 20, ASCE, New York, N.Y., June 1988, pp. 43-102.
19. T. C. Hanks and D. A. Johnson. Geophysical Assessment of Peak Accelerations. *Bulletin of the Seismological Society of America*, Vol. 66, No. 3, June 1976, pp. 959-968.
20. C. Ho, K. Kornher, and G. Tsiatas. Ground Motion Model for Puget Sound Cohesionless Soil Sites. *Earthquake Spectra*, May 1991.
21. D. A. Gasparini and E. H. Vanmarcke. *Simulated Earthquake Motions Compatible with Prescribed Response Spectra*. Report R76-4. Massachusetts Institute of Technology, Jan. 1976.
22. G. Tsiatas, R. Fragaszy, C. Ho, and K. Kornher. *Design Response Spectra for Washington State Bridges*. Final Technical Report. Washington State Department of Transportation, May 1989.
23. H. B. Seed and I. M. Idriss. *Soil Moduli and Damping Factors for Dynamic Response Analysis*. Report No. EERC 70-10. Earthquake Engineering Research Center, University of California, Berkeley, 1970.
24. Y. Ohsaki and R. Iwasaki. On Dynamic Shear Moduli and Poisson's Ratio of Soil Deposits. *Soils and Foundations*, Japanese Society of Soil Mechanics and Foundation Engineering, Vol. 13, No. 4, Dec. 1973, pp. 61-71.
25. S. Hayashi, H. Tsuchida, and E. Kurata. *Average Response Spectra for Various Subsoil Conditions*. Third Joint Meeting, U.S.-Japan Panel on Wind and Seismic Effects, UJNR, Tokyo, Japan, May 10-12, 1971.
26. C. B. Crouse, Y. K. Vyas, and B. A. Schell. Ground Motions from Subduction Zone Earthquakes. *Bulletin of the Seismological Society of America*, Vol. 78, No. 1, Feb. 1988, pp. 1-25.
27. Y. K. Vyas, C. B. Crouse, and B. A. Schell. *Regional Design Ground Motion Criteria for the Southern Bearing Sea*. *Seventh International Conferences on Offshore Mechanics and Arctic Engineering*, Houston, Tex., Feb. 7-12, Vol. I, 1988, pp. 187-193.
28. *Geotechnical and Strong Motion Earthquake Data from U.S. Accelerograph Stations*. NUREG/CR-0985. Shannon and Wilson, Inc., and Agbajian Associates, Vol. 4.